Part I: The Synthesis and Characterization of Scorpionate Ligands for Lanthanide Complexation for Potential PARACEST Applications
Part II: The Synthesis and the Characterization of New and Old Organic Dyes

by

Emma Nicholls-Allison
BSc., University of Victoria, 2010

A Dissertation Submitted in Partial Fulfillment
of the Requirements for the Degree of

DOCTOR OF PHILOSOPHY

in the Department of Chemistry

Supervisory Committee

Part I: The Synthesis and Characterization of Scorpionate Ligands for Lanthanide Complexation for Potential PARACEST Applications
Part II: The Synthesis and the Characterization of New and Old Organic Dyes

by

Emma Nicholls-Allison
BSc., University of Victoria, 2010

Supervisory Committee

Dr. David J. Berg, (Department of Chemistry)
Co-Supervisor

Dr. Robin G. Hicks, (Department of Chemistry)
Co-Supervisor

Dr. Cornelia Bohne, (Department of Chemistry)
Departmental Member

Dr. Michel Lefebvre, (Department of Physics)
Outside Member

Abstract

Supervisory Committee
Dr. David J. Berg, (Department of Chemistry)
Co-Supervisor
Dr. Robin G. Hicks, (Department of Chemistry)
Co-Supervisor
Dr. Cornelia Bohne, (Department of Chemistry)
Departmental Member
Dr. Michel Lefebvre, (Department of Physics)
Outside Member

Reported in Chapter 2 of this thesis is the reliable and tolerant synthesis of a small library of pyrazole and triazole heterocycles. This synthesis was achieved in two steps in good yields from the reaction of acetophenone and benzamide derivatives with dimethyl formamide-dimethyl acetal followed by a cyclization with hydrazine. Also reported is the synthesis and characterization of their corresponding scorpionate ligands. Preliminary co-ordination chemistry was done with a variety of lanthanide metals and was studied by standard spectroscopic methods as well as variable temperature ^{1}H NMR, which revealed that Curie-Weiss behaviour was followed for these complexes in solution. An X-ray crystal structure of a nine co-ordinate ytterbium metal centre with eight nitrogen atom (four pyrazole, four pyridine) donors and one chloride atom was obtained, which may have been a product of decomposition during crystal growth. The bond lengths of this structure were compared with other lanthanide complexes of similar structural motifs. This comparison supported the theory of decomposition as the pyridine nitrogen atom-ytterbium bond lengths were longer than the average ytterbium-nitrogen atom bond length.

Reported in Chapter 4 of this thesis is the synthesis and partial characterization of a new organic dye named perinaphthindigo. Perinaphthindigo was synthesized with adapted

Baeyer-Drewson reaction conditions for the synthesis of indigo which involved the treatment of 1,8-nitronaphthaldehyde with acetone under basic conditions, and was found to be an intense green colour in solution. Perinaphthindigo was produced in poor yields, so efforts were undertaken to improve the yields through an alternative two-step synthesis, first between 1,8-nitronaphthaldehyde and nitromethane in a Henry reaction followed by oxidative coupling. The synthesis of perinaphindigo was adapted so as to structurally modify the final compound, either through incorporation of solubilizing *tert*-butyl groups or bromine atoms for future cross-coupling chemistry. The brominated derivatives of perinaphthindigo were also synthesized in low yields so cross-coupling conditions were scanned on model precursor compounds. The brominated perinaphthindigo compounds were found to have a bathochromically shifted absorbance maximum from the parent perinaphthindigo. This bathochromic shift was more pronounced in our compounds than in the comparison of indigo and 6.6'-dibromoindigo which indicates our compounds are more sensitive to perturbation by substitution.

Reported in Chapter 5 of this thesis is the study of the acid and base chemistry of Nindigo, a previously reported compound. The treatment of Nindigo with a series of strong acids led to an interesting "protoisomerization", or *trans* to *cis* isomerization of the central olefin, with ultimate structural determination through X-ray crystallographic methods. This isomerization was studied through absorbance stopped-flow methods which identified a probable pathway of the isomerization through a neutral, *cis* species. The investigation of neutral Nindigo was undertaken to attempt to identify two peaks which are red-shifted from the π-to-π transition at 586 nm. These two peaks appear at 657 nm and 741 nm and are present in all solvents. The preparative acid chemistry allowed us to assign the first red

shifted peak at 657 nm to the cationic species. Aggregation studies showed concentration dependent behaviour of the ratio between the peaks at 586 nm and 657 nm with little effect on the species at 741 nm. In order to probe whether an autoionization process was occurring, variable temperature NMR and UV-Vis experiments were performed which did not provide a definitive answer to the species at 741 nm.

Table of Contents

List of Tables

List of Schemes

List of Figures

List of Equations

List of Abbreviations

A	absorbance
A.U. or a.u.	absorbance units
Å	angstroms
Ar	aromatic group
BASF	Baeden Aniline and Soda Factory
BF_2	boron-difluoride
BF_4	tetrafluoroborate
BODIPY	4,4-difluoro-4-bora-3a,4a-diaza-s-indacene
nBu	n-Butyl
^oC	degrees Celsius
C	carbon atom
ca.	approximately
CEST	chemical exchange saturation transfer
CF_3COO	trifluoroacetate
CH_2Cl_2	dichloromethane
cm	centimeter
cm^{-1}	wavenumber
Cp	cyclopentadienyl
CSD	Cambridge Structure Database
CT	charge-transfer or computed topography
d	doublet
^{o}	degrees

DABCO	1,4-diazabicyclo[2.2.2]octane
DCM	dichloromethane
DIPEA	N,N-diisopropylethylamine
DOTA	1,4,7,10-tetraazacyclododecane-1,4,7,10-tetraacetic acid
δ	parts per million (chemical shift, NMR)
Δ	heat or difference
DMSO	dimethylsulfoxide
D_2O	deuterium oxide
ε	molar extinction coefficient
e-	electron
EDTA	ethylenediaminetetraacetic acid
EI	electron impact
eq	equivalents
Et	ethyl
HBF_4	tetrafluoroboric acid
HMDS	hexamethyldisiloxane
H_2O	water
HRMS	high resolution mass spectrometry
Hz	hertz
i	ipso
IR	infrared
J	coupling constant (NMR)
K	Kelvin

λ	wavelength
λmax	wavelength of maximam electronic absorption
m	multiplet (NMR)
M	molarity
Me	methyl
MeCN	acetonitrile
MeOH	methanol
mg	milligram
MHz	megahertz
min	minute(s)
mol	mole
mol^{-1}	per mole
mmol	millimole
MRI	magnetic resonance imaging
MS	mass spectrometry
m/z	mass per unit charge
NaOH	Sodium hydroxide
NIR	near infrared
Nm	nanometer (10-9 m)
NMR	nuclear magnetic resonance
OPV	organic photovoltaic cells
PARACEST	paramagnetic chemical exchange saturation transfer
PET	positron emission topography

Ph	phenyl
ppm	parts per million
q	quartet (NMR)
s	singlet (NMR)
s-	per second
SPIO	superparamagnetic iron oxide
t	triplet (NMR) or time
T	temperature
THF	tetrahydrofuran
TLC	thin layer chromatography
TTC	tetratetracontane
USPIO	ultrasmall superparamagnetic iron oxide
UV	ultraviolet
vis	visible
vs.	versus

List of Numbered Compounds

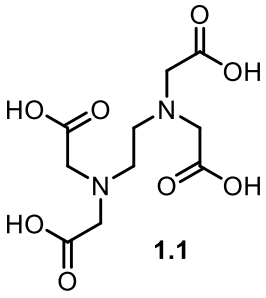

1.1

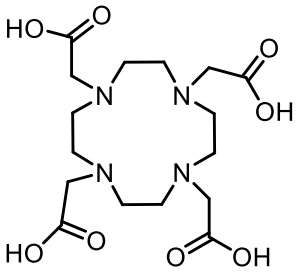

1.2

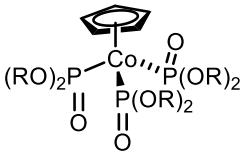

2.1

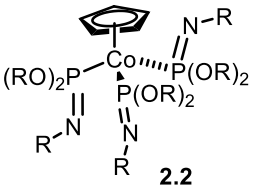

2.2

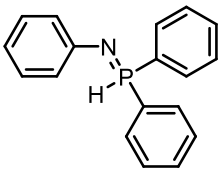

2.3a

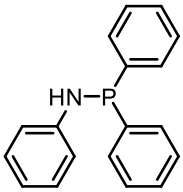

2.3b

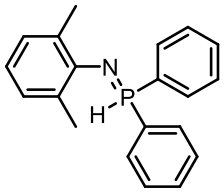

2.4a

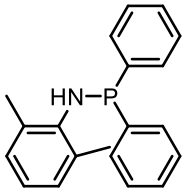

2.4b

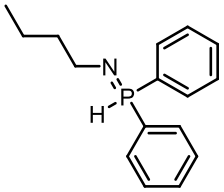

2.5a

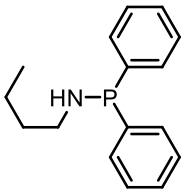

2.5b

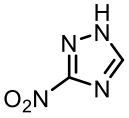

2.6

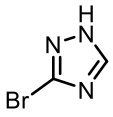

2.7

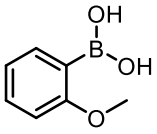

2.8

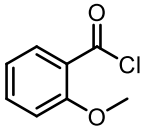

2.9

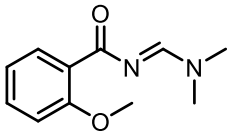

2.10a

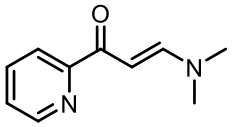

2.11a

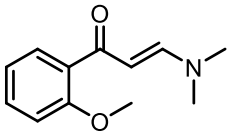

2.12a

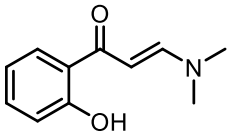

2.13a

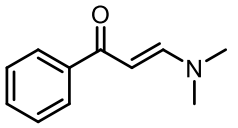

2.14a

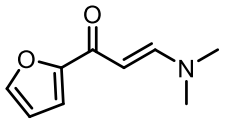

2.15a

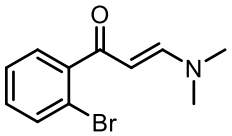

2.16a

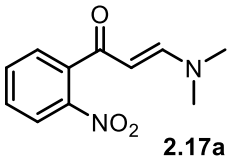

2.17a

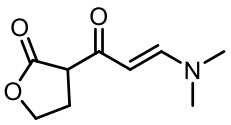

2.18a

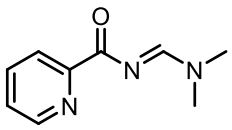

2.19a

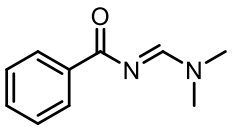

2.20a

2.10b

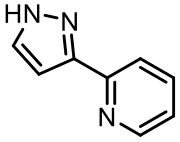

2.11b

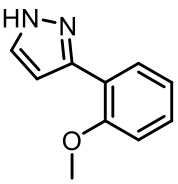

2.12b

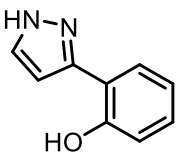

2.13b

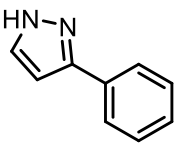

2.14b

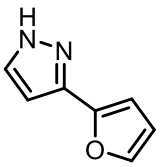

2.15b

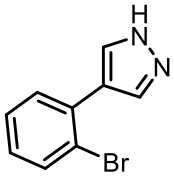

2.16b

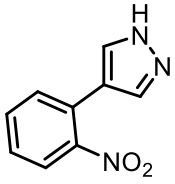

2.17b

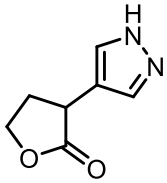

2.18b

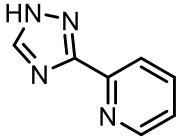

2.19b

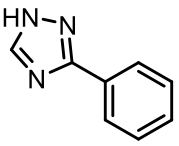

2.20b

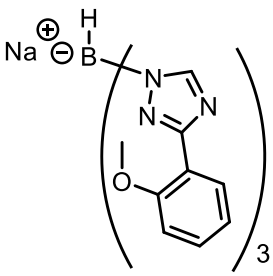

2.10c

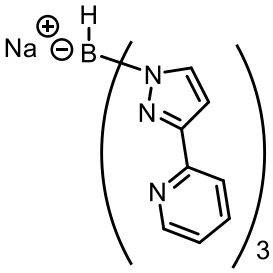

2.11c

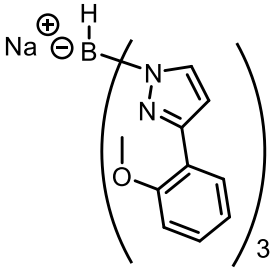

2.12c

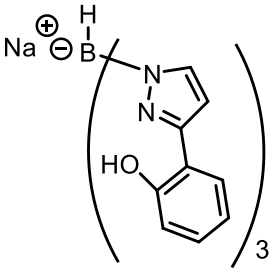

2.13c

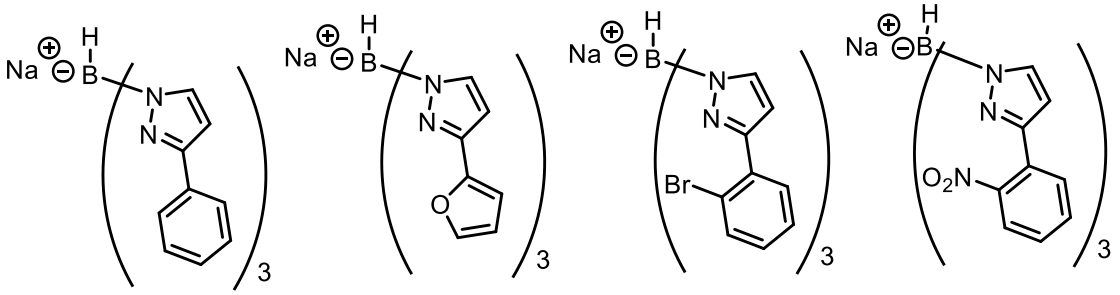

2.14c **2.15c** **2.16c** **2.17c**

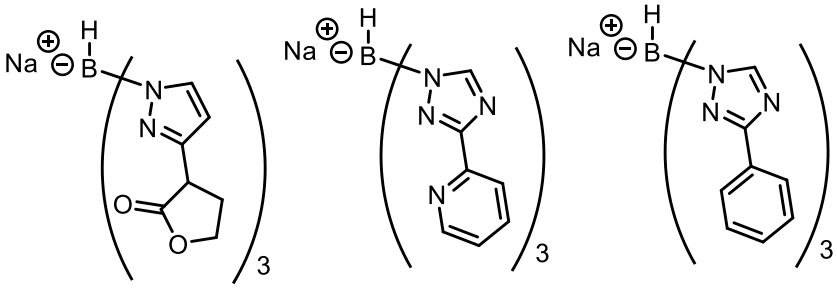

2.18c **2.19c** **2.20c**

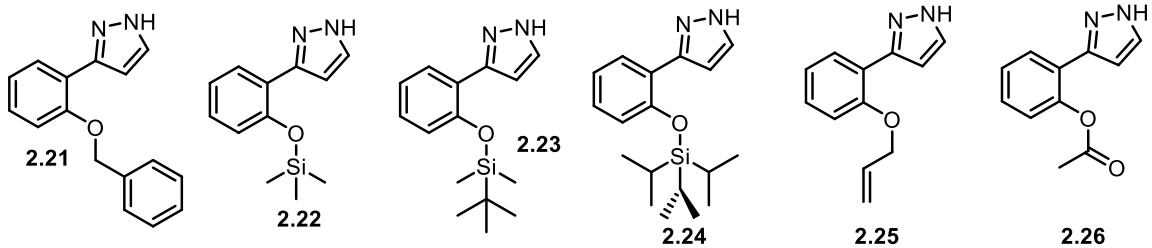

2.21 **2.22** **2.23** **2.24** **2.25** **2.26**

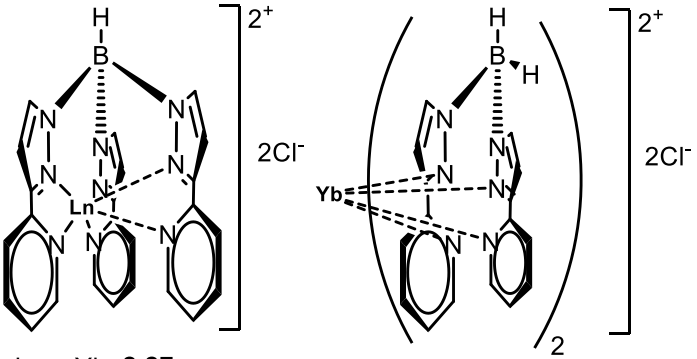

Ln = Yb **2.27**
Sm **2.29**
Nd **2.30**
Y **2.31**
Tb **2.32**
Eu **2.33**

2.28

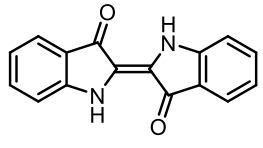

3.1

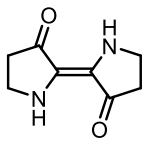

3.2

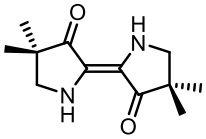

3.3

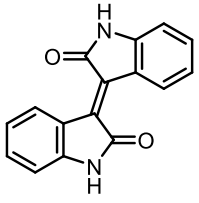

3.4

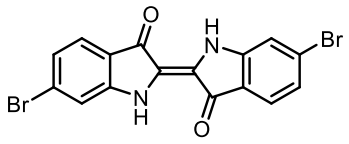

3.5

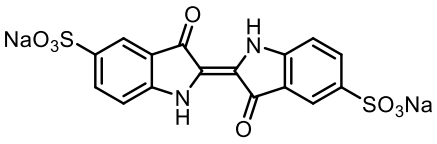

3.6

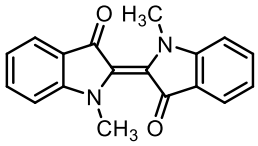

3.7

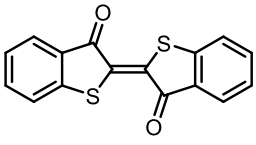

3.8

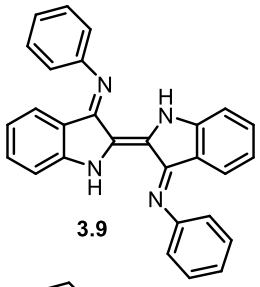

3.9

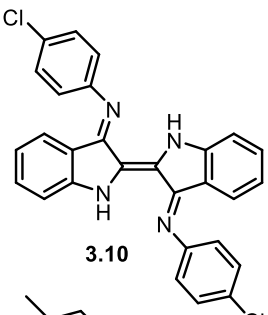

3.10

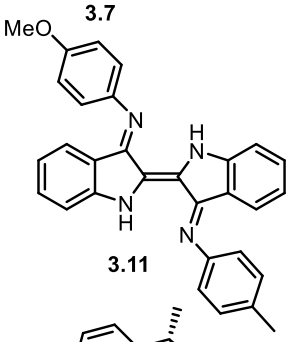

3.11

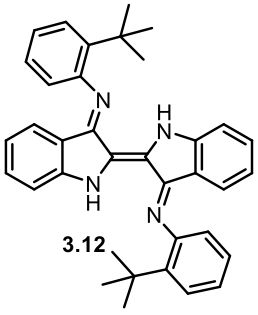

3.12

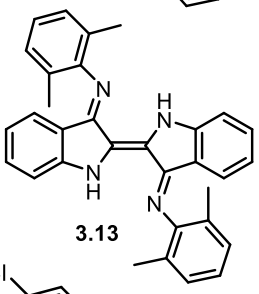

3.13

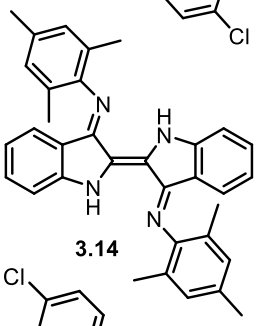

3.14

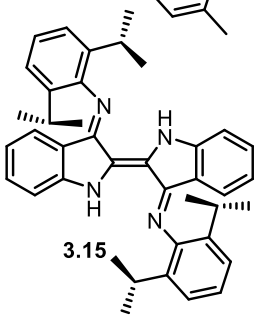

3.15

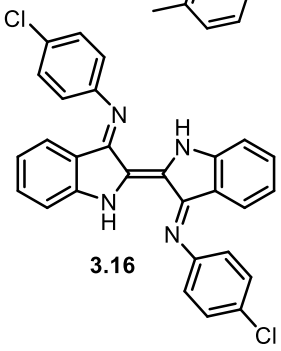

3.16

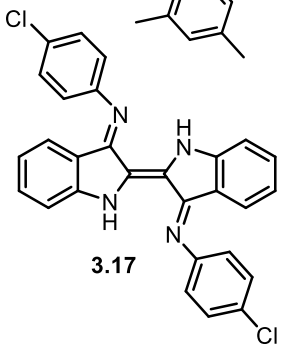

3.17

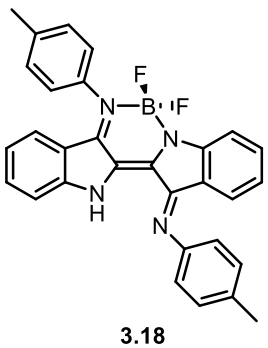

3.18

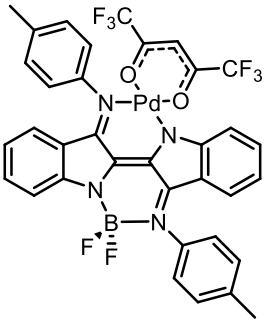

3.19

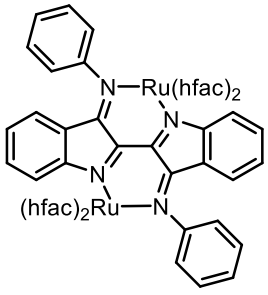

3.20

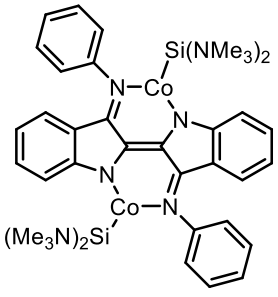

3.21

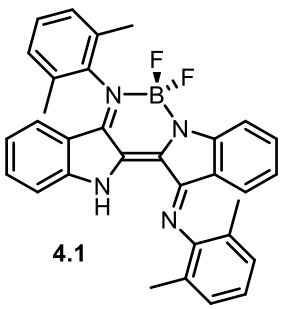

4.1

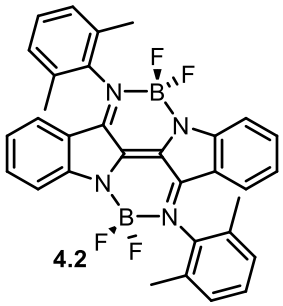

4.2

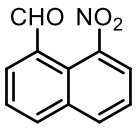

4.3a

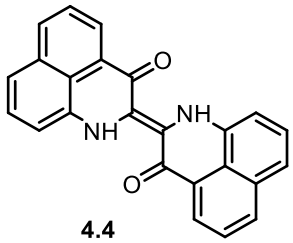

4.4

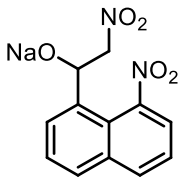

4.5

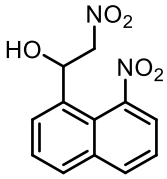

4.6

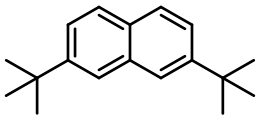

4.7b

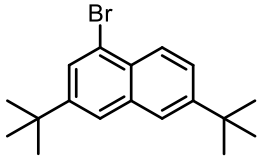

4.8

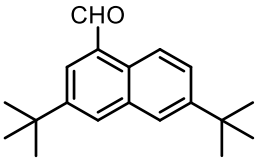

4.9

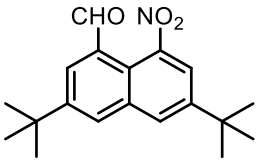

4.10

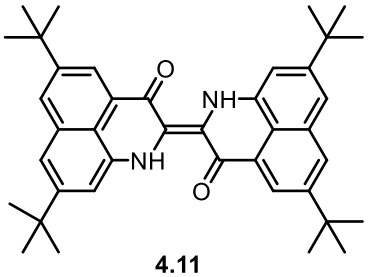

4.11

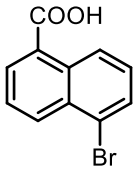

4.12

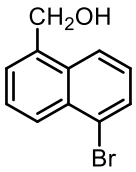

4.13

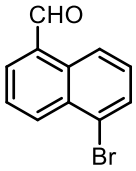

4.14

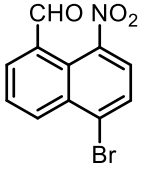

4.15a

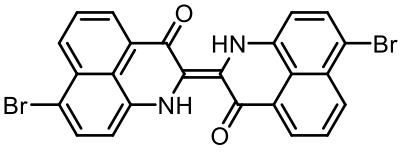

4.16

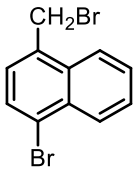

4.17

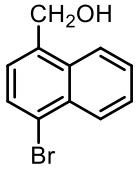

4.18

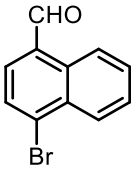

4.19

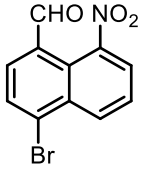

4.20a

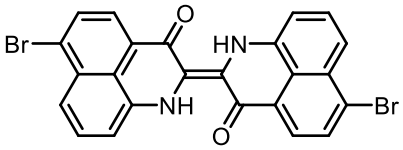

4.21

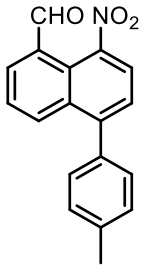

4.22

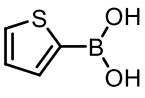

4.23

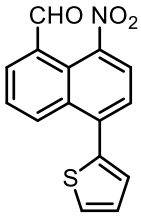

4.25

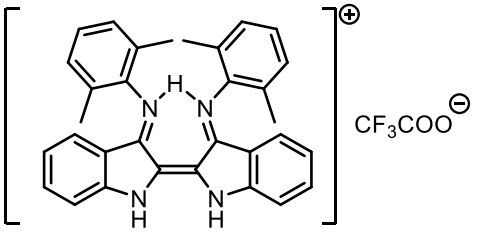

5.1aCF$_3$COO

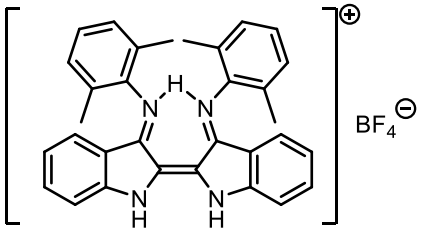

5.1aBF$_4$

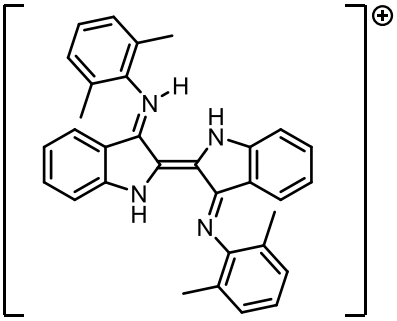

5.1b

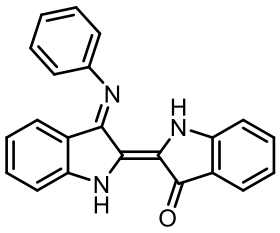

5.2

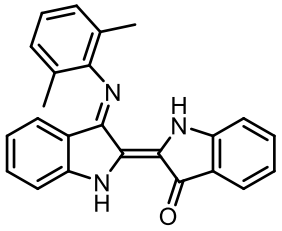

5.3

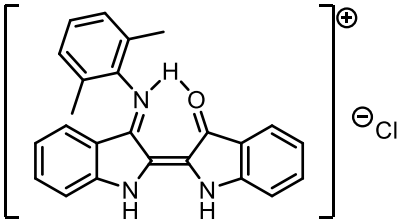

5.4aCl

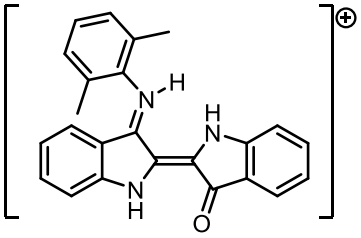

5.4b

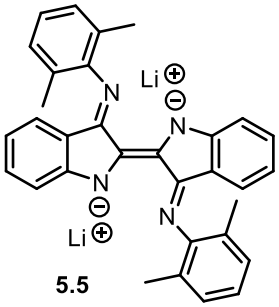

5.5

Acknowledgments

First and foremost I would like to acknowledge the supervision of two outstanding individuals: Dr. David Berg and Dr. Robin Hicks. Dave inspired me to do chemistry in 2007 in Chemistry 222, and it was then that I decided that I would pursue research. Robin gave me a chemistry home when I needed one in 2012. Both have been such amazing role models and I don't think I can ever express my gratitude fully for how much they have done for me. I also gratefully acknowledge Dr. Cornelia Bohne, both for serving as a member of my supervisory committee and for allowing me to use her instruments as well as for many helpful discussions. Dr. Scott McIndoe, although no longer a member of my supervisory committee, served as a member for the first two years of my degree and filled in for Dr. Bohne for my candidacy exam while she was on sabbatical. I would like to thank Dr. Michel Lefebvre from the Department of Physics for reading this thesis and for always saying hello in the hallway. Finally, I would like to acknowledge my external examiner Dr. Tim Storr for making the trip to the island.

It was at UVic Chemistry that I realized that my true love was teaching chemistry. This passion of mine was fostered by the unbelievable teaching staff at UVic, especially Dr. Dave Berry for his guidance and all the time he took to support me and Kelli Fawkes for being so kind to me and being such a good example of a teaching professional.

The Department of Chemistry at UVic is lucky to have a wonderful staff maintaining all the facilities. I am indebted to the work of Ms. Shubha Hosali and Mr. Andrew MacDonald in the electronics shop for their fast work whenever it was needed. Mr. Shawn Adams in the glassware shop somehow manages to keep up with how clumsy I am. Dr. Ori Granot at UVic and Dr. Yun Ling at UBC acquired all accurate mass spectra. Finally, Mr.

Christopher Barr has served as not only an amazing NMR manager but also a fantastic mentor who always took the time to teach me something new.

I've worked with some fantastic people in the two groups that I have called home: first, Dr. Kevin Allen (who taught me everything I know), Dr. Jin Zou, and Dr. Pengrong Zhang from the Berg group. Second, the former members of the Hicks group who paved the way on the Nindigo project, Mr. Simon Oakley and Dr. Graeme Nawn for their high-quality work. Third, the past and current members of the Hicks group: Mr. Cooper Johnson who was always good for a laugh, Mr. Corey Sanz for being the lab muscle, Ms. Genevieve Boice for being an ear to bend, Mr. Dillon Hofsommer for being the next member of team Nindigo, Ms. Erica Hong for her hard work, and Mr. Shaun MacLean, a new member who has served as the computational guru. I am greatly indebted to Ms. Suma Susan Thomas for all of her help with the stopped-flow studies as well as for helpful discussions afterwards. I have had the pleasure of working with many talented undergraduate students including: Mr. Hector Cortes, Ms. Bryony McAllister, Ms. Clara MacDonald, Mr. James Kirkpatrick, Mr. Patrick Ferguson, and Mr. Tyler Tuck. I am also indebted to Dr. Jeremy Wulff and Dr. Natia Frank and their groups: Dr. Katherine Davies, Dr. Caleb Bromba, Dr. Natasha O'Rourke, Mr. Micheal Brant (my teaching buddy for the last four years), and Ms. Aiko Kurimoto.

Finally, I want to acknowledge my "little" brother for always being there for me and Dr. Jason Davy for being my best friend and champion for the last two and a half years.

Dedication

For my Jason, the best "bond" I have ever made…

Chapter 1: Introduction to Part 1

1.1 Metals in medicine

The use of transition and rare earth metals in a variety of medicinal settings has become more important in recent years with applications ranging widely. Some prominent examples include cisplatin and ruthenium complexes for the treatment of cancer,[1-2] gold complexes in the treatment of arthritis,[3] and ferrocene for the treatment of malaria.[4-5] These metal complexes show a tremendous amount of structural diversity as illustrated in the small subset presented in **Figure 1.** A common example of metals in medicine is that of diagnostic applications[6-8] where imaging agents are used for the *in vivo* diagnosis of abnormal tissues (such as tumours) or to inspect organs, such as the heart or liver, for abnormalities. In order for an imaging agent to be considered for clinical use, it needs to meet stringent safety standards, have minimal side effects, and, for toxic metals, must be completely eliminated from the body in a reasonable time.

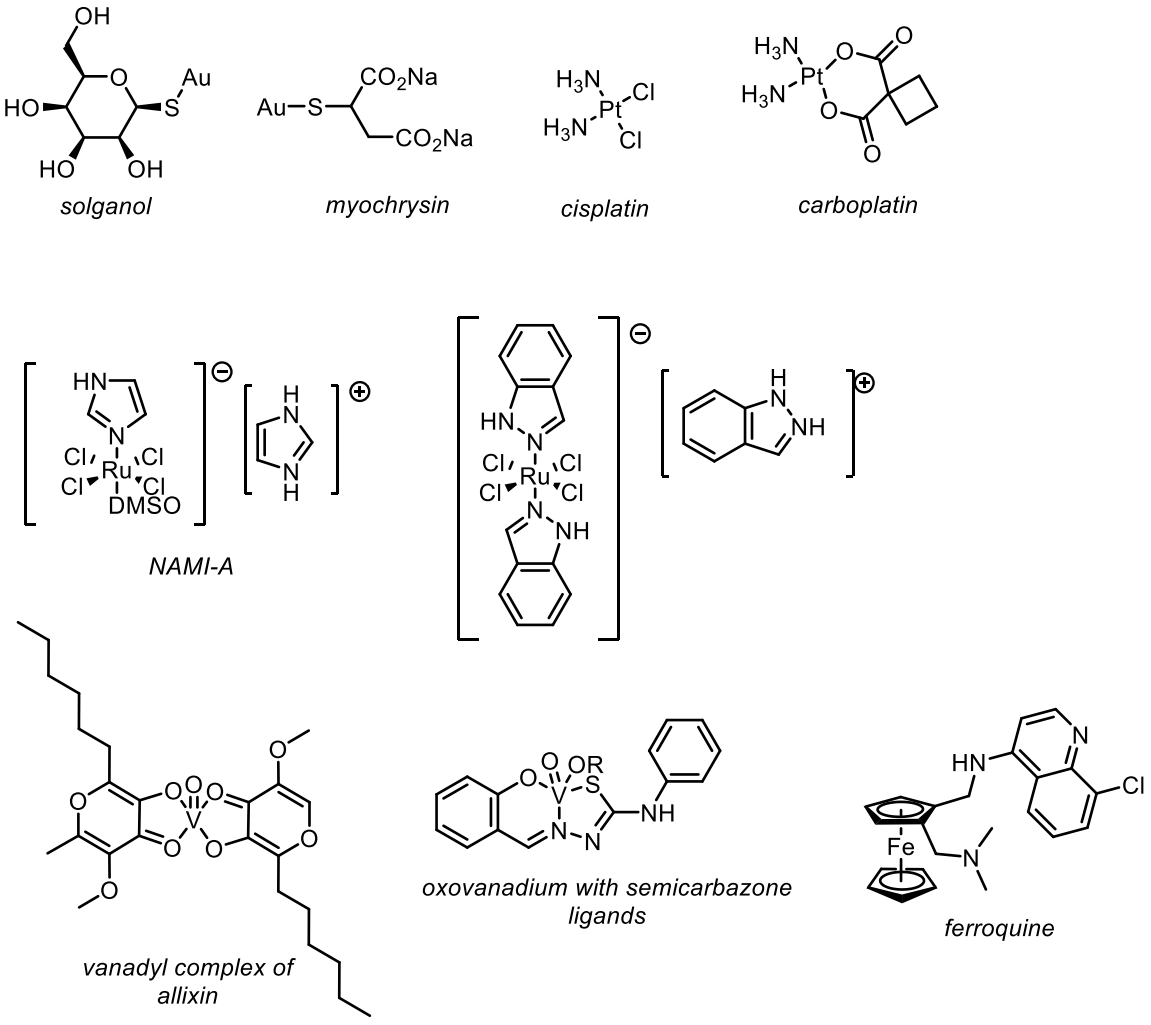

Figure 1. Examples of bioinorganic systems used for medical applications.

1.2 Other diagnostic medicine techniques

There are a variety of imaging techniques used in the diagnostic field: some that use an additional imaging agent and some that do not. One technique that does not use an additional contrast agent is X-ray imaging which relies on the heavier elements in bone such as phosphorus and calcium to diffract and scatter the X-rays. Computed Tomography

(CT) is an extension of X-ray imaging as it also uses X-ray radiation but utilizes a contrast agent.[6] However, in this technique, the dosages of both the radiation and external imaging agent are high and the contrast is poor.

Positron Emission Tomography (PET) utilizes a radiopharmaceutical labelled radionucleotide such as an ^{18}F labelled glucose molecule (molecular structure shown below).[6] The radionucleotide is distributed through the blood stream and collects in tissues where it will be metabolized. The radionucleotide is a positron emitter and, after emission, the collision of the positron with a nearby electron results in annihilation, producing two photons. The angle between these two photons is 180^{o} and this helps pinpoint the site of emission.

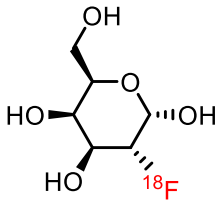

Single Photon Emission Computed Tomography (SPECT) uses a radiolabelled nucleotide which stays in the blood and emits gamma rays. This method is less expensive than PET and is more often used in pre-surgical evaluations. The commercially available SPECT imaging agents contain a metastable radioactive isotope of ^{99m}Tc selected for its high nuclear energy (140keV), ideal half-life (6 hours) and its relatively easy production from stable molybdenum.[9] Some common technetium SPECT agents are shown in **Figure 2.**

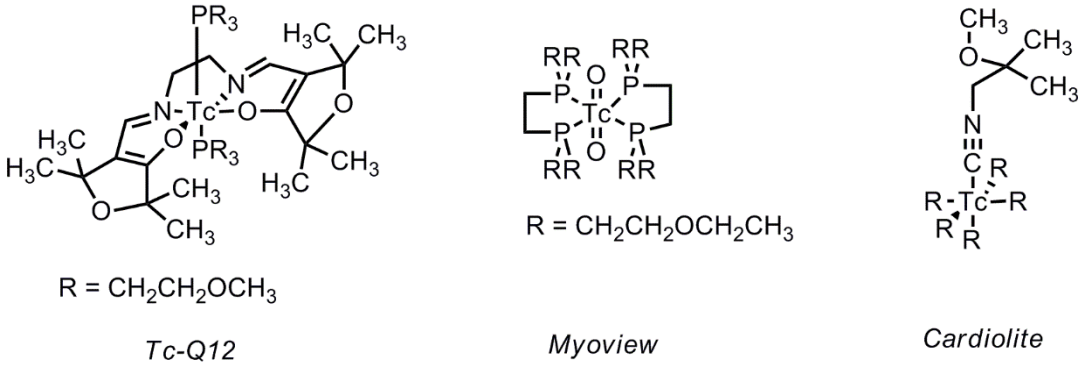

Figure 2. Technetium containing drugs for SPECT imaging.[9]

1.3 Magnetic Resonance Imaging (MRI) in diagnostic medicine

X-ray, SPECT, and PET imaging are all useful imaging techniques for conformational diagnostics. Magnetic Resonance Imaging (MRI) is another important and highly utilized diagnostic technique. The mechanism of traditional T_1 relaxation agents, Chemical Exchange Saturation Transfer (CEST) and Paramagnetic Chemical Exchange Saturation Transfer (PARACEST) agents are outlined in the following sections.[10]

1.3.1 MRI and traditional T_1 relaxation agents

Magnetic Resonance Imaging (MRI), was first introduced in 1978 by P.C. Lauterbur and has become a very powerful technique to image abnormal masses in tissues and organs.[11] The spatial distribution of water protons in the body is investigated by applying a non-invasive radio-frequency pulse to perturb the spin of those protons.[8, 11-13] Traditionally, a contrast agent containing the lanthanide metal gadolinium (although other agents are known and approved) is administered because gadolinium is highly paramagnetic and

alters both the T_1 (spin-lattice) and T_2 (spin-spin) relaxation times of the bulk water protons leading to positive contrast (and thus, image brightening) between the point of localization of the imaging agent and the surrounding tissues.[12] Of the two relaxation times altered, the T_1 relaxation time experiences the largest effect so these agents are commonly called T_1 agents.

Currently, there are nine gadolinium contrast agents (with the three top sellers for 2009 shown in **Figure 3**) approved for administration in the United States as well as a paramagnetic manganese complex, a superparamagnetic iron oxide (SPIO) and ultrasmall superparamagnetic iron oxide (USPIO) nanoparticles.[14] While gadolinium contrast agents are effective, there are multiple disadvantages to them. The first disadvantage is the large dose of imaging agent needed as the MRI experiment has poor contrast because image brightening in the region of contrast agent accumulation is diminished by minor image brightening of the bulk water protons.[6] This makes a higher dosage to achieve sufficient contrast a requirement. The second disadvantage of the large dosage is that since it is excreted by the renal system it can be especially wasteful. Finally, the inherent toxicity of the agents themselves are a concern for these heavy metal reagents. In fact, 5% of patients dosed with gadolinium contrast agents report adverse health effects.[15] There are also special concerns with gadolinium agents when it comes to patient with previously existing kidney disease. Any patient with pre-existing kidney concerns cannot be administered the gadolinium agents as nephrogenic systemic fibrosis (NSF), or hardening of the tissues in the kidneys, can occur.[16-17]

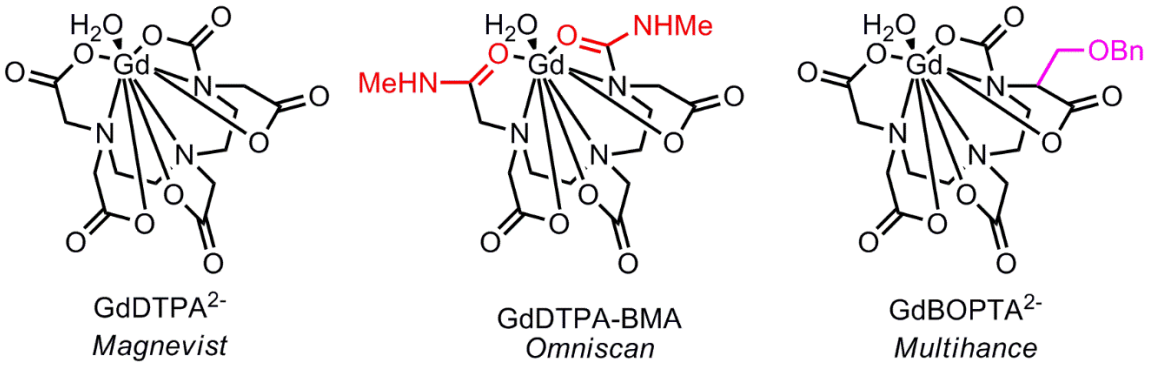

Figure 3. Gadolinium containing drugs for MRI imaging.

Because MRI exams are so necessary to diagnostic medicine, the current contrast agents are considered acceptable, even with all these concerns. However, the current imaging methods leave much be desired and improvements are important and necessary. It was with this in mind that a new and different design and mode of contrast is being explored.[8]

1.3.2 CEST and PARACEST agents for imaging

Nuclear Magnetic Resonance (NMR) Spectroscopy is a common technique used in chemistry to gain structural information about a sample that contains at least one spin active nucleus. When placed in a magnetic field, the sample at equilibrium will have nuclear spins that are aligned with the external magnetic field (lower energy α) and spins that are opposed to the external magnetic field (higher energy β), with a slight preference for the low energy state (**Figure 5A**). This results in a net magnetization of the sample along the *z*-axis in the positive direction (spins aligned with the applied field).[18] It is this net magnetization that is perturbed with radiofrequency pulses to acquire an NMR spectrum (not unlike the acquisition of an MRI scan). If we consider an imaging agent in bulk water,

the net magnetization can be disrupted by applying an on-resonance radiofrequency pulse (with respect to the imaging agent) to promote some of the lower lying spins into the higher energy level. This, in turn, disrupts the bulk magnetization by reducing (or even eliminating) the signal generated. This process, called saturation, is illustrated in both **Figure 4B** (which shows the even distribution of spins in both energy states in the imaging agent) and **Figure 5** where the signal for the imaging agent (red) has disappeared after saturation.[19-20]

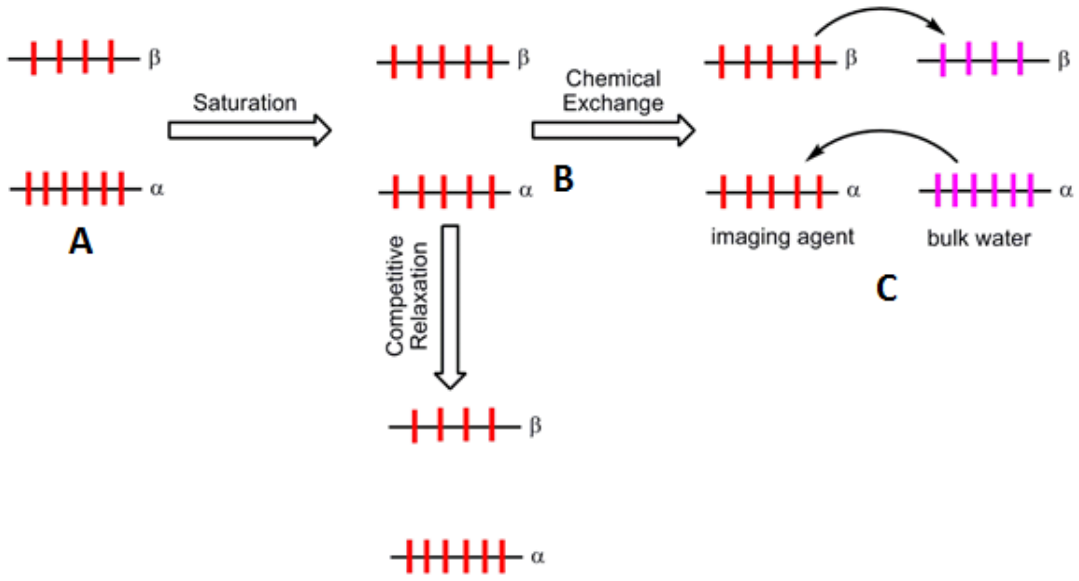

Figure 4. Spin states for the Saturation (B), Chemical Exchange (C), and Competitive Relaxation for the imaging agent (red) and bulk water (pink).[20]

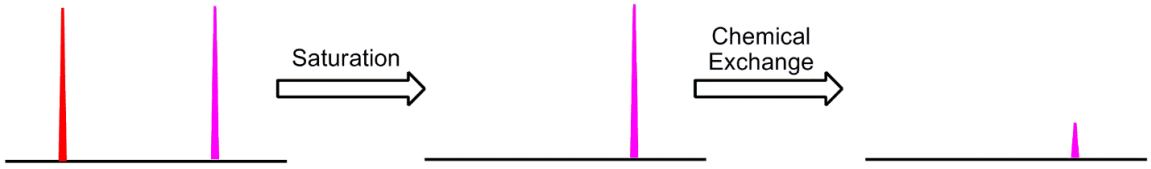

Figure 5. Chemical Shift changes with PARACEST exchange for the imaging agent (red) and bulk water (pink).

Chemical Exchange Saturation Transfer (CEST) involves magnetization transfer (either through dipolar interaction or chemical exchange) between the bulk water protons and chemically unique protons (that are part of the imaging agent).[18] When the imaging agent protons are first irradiated with an on-resonance radiofrequency pulse (with respect to the imaging agent protons) (**Figure 4B**) magnetization transfer to the bulk water protons occurs due to chemical exchange, altering the spin states and diminishing the signal intensity of the bulk water (**Figure 4C** and **Figure 5**). This means that the presence of the imaging agent in the organs and tissues results in *darkening* of the signal from this region that can be detected.

There are limitations to this technique that lie largely in the competitive relaxation from the high energy state (β) to the low energy state (α) before exchange can occur (**Figure 4**). If the relaxation process occurs before the chemical exchange process can happen then there will be no difference in the signal intensity for the bulk water signal (and thus, no imaging of the organs and tissues). It is important that the chemical shift of the imaging agent is different enough from bulk water signal so that a pre-saturation pulse can be applied to a distinct signal belonging to the imaging agent. It is also important that magnetization transfer is fast in order to achieve the best possible contrast. This means that exchange needs to be as fast as possible without coalescence between the protons of

the contrast agent and bulk water. At coalescence, the rate of exchange is just equal to the difference in chemical shift between the two coalescing pools of protons so an exchange rate just below that required for coalescence is optimal to achieve maximum contrast (**Equation 1**). The larger we can make Δω the larger the contrast we can achieve.

$$k_{ex} \leq \Delta\omega$$

Equation 1. Allowable rate of exchange between two proton pools compared to the difference in chemical shift of those two pools.

Diamagnetic Chemical Exchange Saturation Transfer (CEST) agents have exchangeable protons with chemical shifts close to that of bulk water (both in the 0-15 ppm range). This can be a problem because irradiation of the imaging agent can lead to "leakage" of magnetization to the bulk water leading to poorer contrast. Paramagnetic Chemical Exchange Saturation Transfer (PARACEST) complexes have emerged recently as a potential solution to this problem.[21-24] PARACEST complexes function in the same way as the CEST agents but the paramagnetic metal centre shifts the exchangeable proton signal much further from the bulk water signal. This allows for much greater exchange rates for the exchange process and the competitive rate of relaxation is to be less of an issue.

Currently, PARACEST contrast agent design is centred about the EDTA (**1.1**)-like 1,4,7,10-tetraazacyclodecane-1,4,7,10-tetraacetate (DOTA, **1.2**) ligand and its modified versions.[6, 12, 20] DOTA (**1.2**) is a desirable candidate due to its many lanthanide co-ordination sites (eight), strong ligand-metal binding due to the chelate effect, exchangeable protons in the form of carboxylic acids, and good water solubility. A more detailed analysis

of ligand design for contrast agents and other bioinorganic applications is provided in the following section.

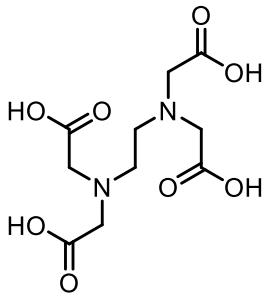

EDTA
1.1

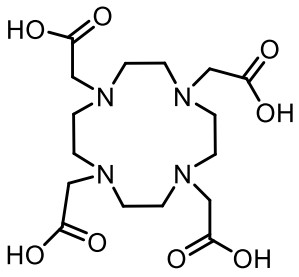

DOTA
1.2

1.4 Bioinorganic ligand design for MRI contrast agents

There are many factors which make a ligand-metal system a good candidate as a contrast agent including: low toxicity, exchangeable protons on the periphery to exchange with bulk water, good water solubility at physiological pH, and strong ligand metal co-ordination (usually by taking advantage of the chelate effect). Other factors contributing to suitability of a contrast agent is the number of open co-ordination sites for water to bind to the lanthanide metal (where the number of inner sphere water molecules is defined by the hydration number *q*) as well as the tumbling rate in solution (**Figure 6**).[25-27]

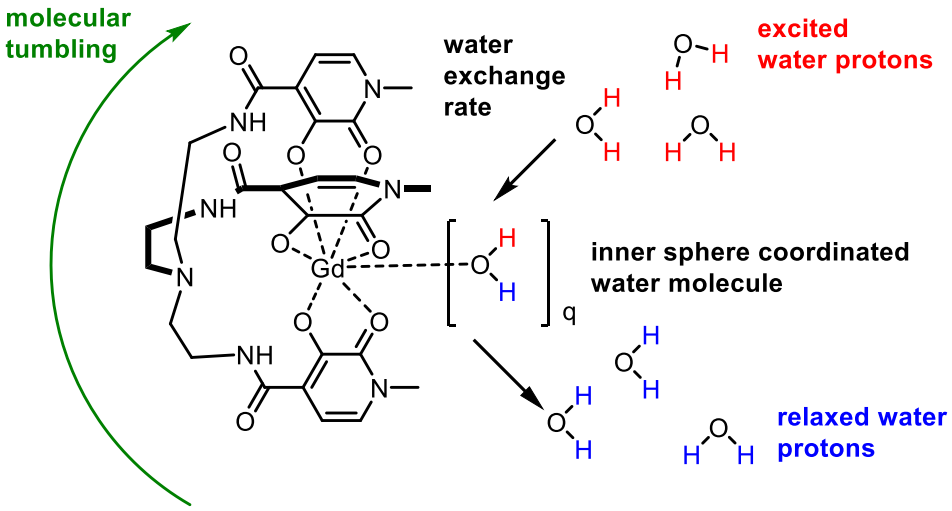

Figure 6. Depiction of parameters that determine viability of a contrast agent.[26-27]

Toxicity concerns can arise from the metal-ligand system or just the ligand or metal by itself. Toxicity from the ligand itself can often be avoided by selecting starting materials that are known to be non-toxic and making modifications to these systems which improve other properties. Most metals (gadolinium included) are toxic which is why it is especially important that the metal centre is tightly bound to the ligand system, normally through multiple chelation sites. The incorporation of functional groups such as alcohols, amines, and carboxylic acids serves many purposes: first, they have exchangeable protons which can exchange with the bulk water intensifying the signal and second, they typically serve to improve the water solubility.

1.5 Objectives of this work

Previously, the Berg group has investigated lanthanide complexes of the Klaüi metalloligand system as potential MRI contrast agents. The Klaüi ligand system is a cobalt

metalloligand which adopts a tripodal orientation with oxygen donors acting as lanthanide binding sites. These ligand systems demonstrated exceptional stability towards oxidizing agents, water, and aqueous acids (all excellent qualities in ligands being considered for biological applications). Also of note, the phosphite portion of this ligand system is open to structural modification which allows for the incorporation of new chelation sites as well as exchangeable protons.

Lanthanide complexes of the Klaüi metalloligand have been reported in the literature.[28] In order to assess the viability of Klaüi complexes as potential contrast agents, the lanthanide-Klaüi ligand complexes of neodymium, europium, terbium, and ytterbium as well as yttrium were prepared (**Figure 7**). Ligand lability was investigated by ESI-MS using deuterated and non-deuterated versions of the ligands as shown in **Figure 8**, using terbium as a representative complex.[29]

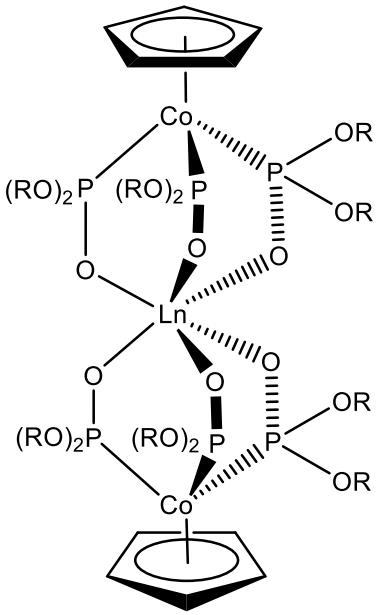

Figure 7. The Klaüi ligand system as part of a lanthanide metal complex.

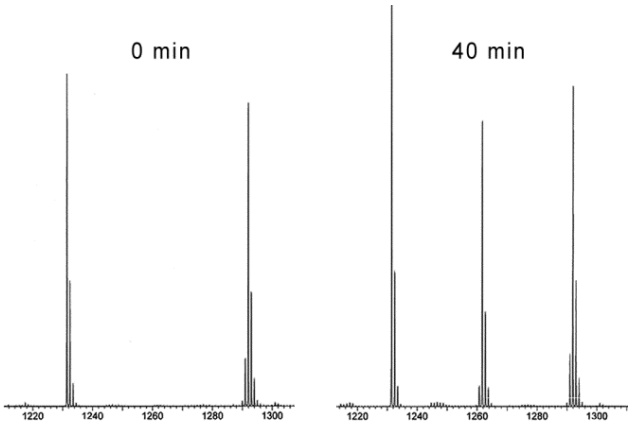

Figure 8. The evolution of the d_{30} species over time from the d_0 and the d_{60} species of the Klaùi ligand-terbium species, $Tb[\{O=P(OEt)_2\}_3CoCp]_2$.[29]

Mass spectroscopic results revealed that the Klaùi metalloligand was not a good candidate for lanthanide based PARACEST applications because it underwent ligand exchange too rapidly in solution. The purpose of this work is to make improvements to the Klaùi ligand system by seeing if we could incorporate phosphinimine arms for additional chelation sites. When it became clear this route was not viable, the synthesis and investigation of new hexadentate ligands based on the scorpionate system (shown below in **Figure 9**) was undertaken.

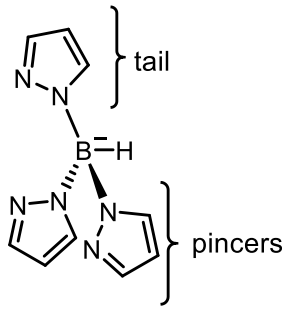

Figure 9. A representative scorpionate ligand showing the "tail" and "pincers".

Chapter 2: Ligand Design for Lanthanide Co-ordination Chemistry for PARACEST Applications

2.0 Introduction

As described in the introduction, previous work in the group has centred about the Klaüi ligand system. However, this ligand system exhibited some problems when it came to viability as an MRI contrast agent. One member of the research group (Dr. Kevin Allen) continued work to modify the Klaüi ligand incorporating phosphites. However, we postulated that it would also be a good strategy to incorporate more sites of chelation by changing the phosphite units for phosphinimines (as shown in **Figure 10**) where the R-groups on the nitrogen contain additional chelation sites. There were a few approaches to this ligand system, which are outlined here.

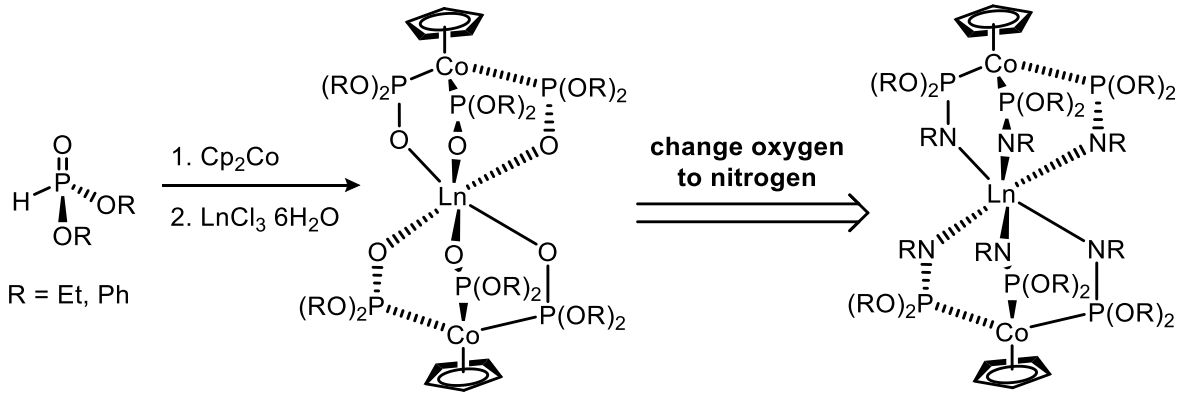

Figure 10. Substitution of oxygen atoms by an "NR" unit on the Klaüi ligand.

2.1 Results of the phosphinimine chemistry

The first reaction to consider was the condensation of either the Klaùi metalloligand (compound **2.1**) or the phosphite precursor with a primary amine. First attempted was the reaction of the Klaùi metalloligand with a primary amine (aniline in this case, with the reaction shown in **Scheme 1**) in a variety of conditions shown in **Table 1**.

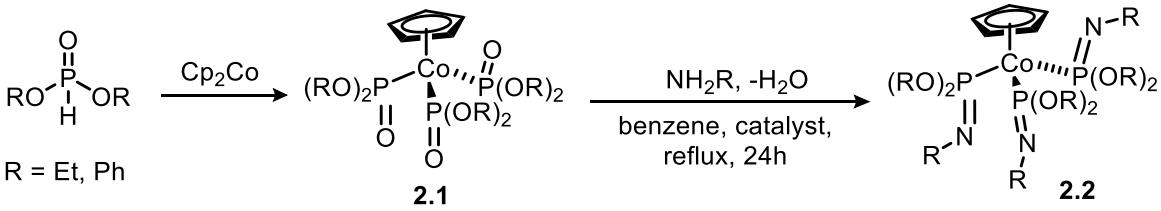

Scheme 1. Synthesis of the Klaùi ligand from the phosphite precursor followed by attempted condensation reaction of the Klaùi ligand with a primary amine.

Primary Amine	**Catalyst**	**Result**
Aniline	None	No reaction
Aniline	Sulfuric acid (three drops)	No reaction
Aniline	Aluminum (III) chloride (20 mol %)	No reaction

Table 1. Results of the condensation of aniline and compound **2.1** with R = Et and different catalysts

Since conversion of the Klaùi ligand to the phosphinimine analogue failed, the next option was to attempt the condensation reaction with the phosphites themselves (both the ethyl and phenyl derivatives previously reported),[28-29] again using aniline as the primary

amine. With no catalyst present, this reaction was unsuccessful so the same catalysts as **Table 1** were added but this also led to no reaction. At this point, it was necessary to probe other reaction conditions to investigate if the desired product could be made.

The next pathway to be explored was that of reacting chlorodiphenylphosphine with aniline under an inert atmosphere with base to hopefully generate compound **2.3a** (**Scheme 2**).

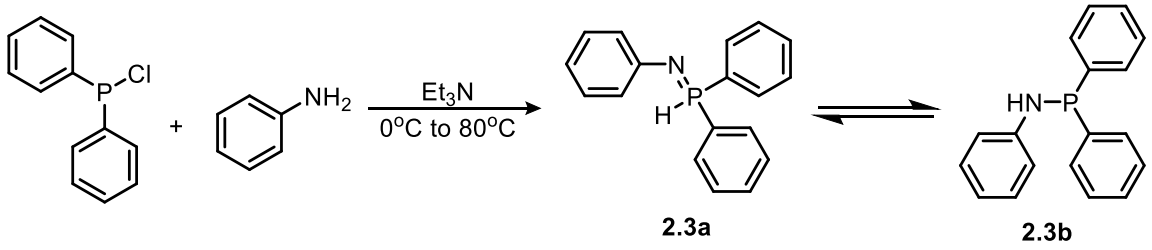

Scheme 2. Reaction to form **2.3a**.

After work-up, it was found that there were actually two different compounds present, as revealed by the ^{31}P NMR, consistent with compounds **2.3a** and **2.3b.** These two structures are representative of a tautomeric equilibrium between the two valencies of phosphorus with structure **2.3a** being pentavalent phosphorus and compound **2.3b** being trivalent phosphorus This mixture was carried forward and used in two different Klaüi ligand synthesis conditions.

The first was the reaction of the phosphinimine mixture with in-house synthesized cobaltocene (**Scheme 3**). This route repeats the synthetic procedure previously used in the group to synthesize the Klaüi ligand. Despite repetition and elongated reaction time, this reaction never proved successful.

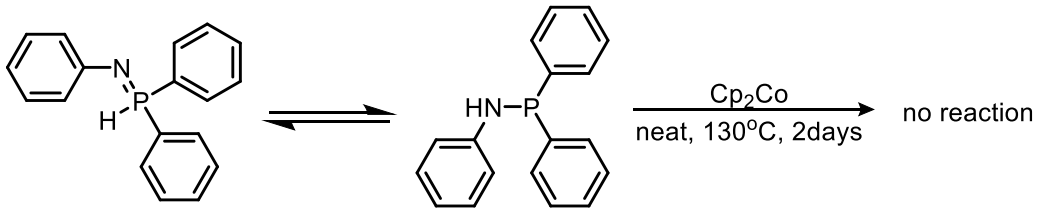

Scheme 3. Proposed synthesis of modified Klaüi ligand.

The second method of synthesis involved the deprotonation of the phosphinimine species with sodium hydride, followed by reaction with cyclopentadienyl cobalt diiodide (**Scheme 4**). This method had proven successful in the past in our research group to synthesize the Klaüi ligand. Disappointingly, this chemistry also proved unsuccessful.

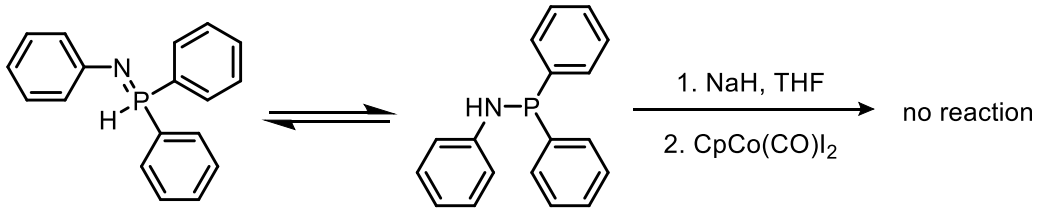

Scheme 4. Second attempted synthesis of modified Klaüi ligand.

At this point, it was postulated that perhaps the nature of the phosphinimine was the source of synthetic problems. It was with this in mind that we attempted to synthesize phosphinimines that would be more likely to adopt the five co-ordinate valency. For this, we explored building up steric bulk at the 2- and 6-positions of the aromatic ring on nitrogen as well as investigating alkyl amines to change the electronic nature of the system.

The first synthesis used 2,6-dimethylaniline as the source of primary amine and used the same synthetic protocol as earlier reported (**Scheme 5**). Again, the same tautomeric

equilibrium was observed between the two phosphorus tautomers (**2.4a** and **2.4b**). Both traditional Klaùi ligand syntheses were attempted, but again to no avail.

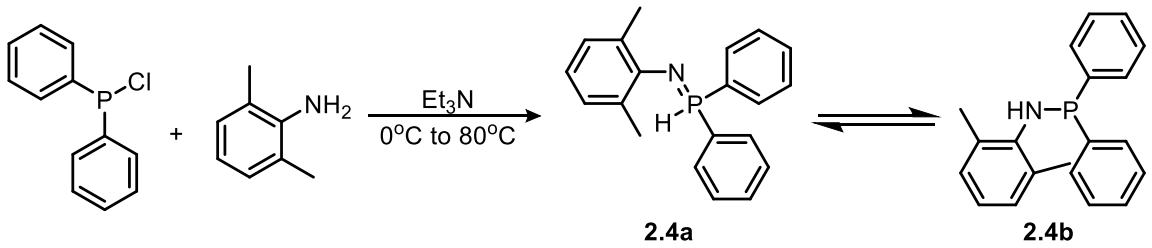

2.4a **2.4b**

Scheme 5. Reaction to form compounds **2.4a** and **2.4b**.

Finally, an alkyl amine (in our case, butylamine) was used as the source of the primary amine in the synthesis of the phosphinimine (**Scheme 6**). The rationale for this was that the alkyl group would be more electron-donating that the aromatic ring in aniline, which would stabilize the pentavalent species better. Again, the tautomeric equilibrium persisted between compounds **2.5a** and **2.5b** and the reaction to synthesize the Klaùi ligand from the mixture proved unsuccessful.

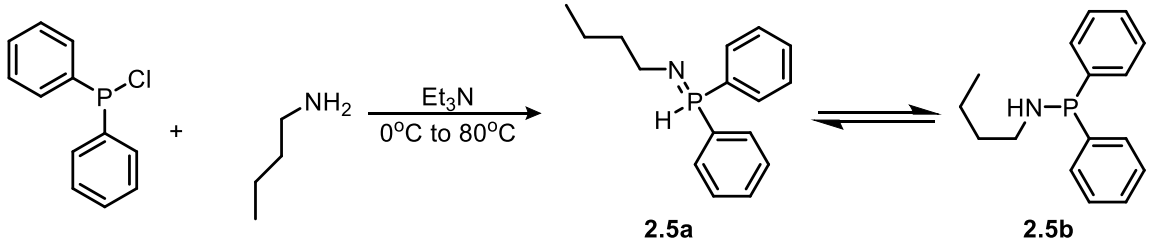

2.5a **2.5b**

Scheme 6. Synthesis of compounds **2.5a** and **2.5b**.

It was at this point that it was assessed that this chemistry was unlikely to produce the desired results. However, this ligand design did suggest that any new ligand system for lanthanide metal co-ordination should include hexadentate (or more) co-ordination to the

metal centre and the opportunity for modifications to include exchangeable hydrogens for PARACEST purposes and improved water solubility. With these ideas in mind, it was decided that an excellent class of ligand to explore would be based on the scorpionate ligands, developed by Trofimenko in the 1960's (a metal bound scorpionate ligand is shown in **Figure 11**).

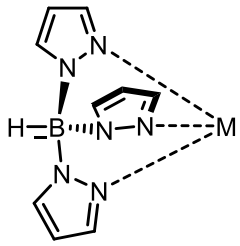

Figure 11. A metal-bound scorpionate ligand.

2.2 Introduction to scorpionate chemistry

The chemistry of the scorpionate ligands has been studied extensively since their introduction by Trofimenko in 1965.[30] Also widely studied is the co-ordination chemistry of these ligand systems with respect to both the d-block and f-block metals.[31-36] What is lacking, however, is the study of functionalized scorpionate ligands with chelation sites beyond the pyrazole and triazole nitrogen atoms. The *tris*(triazolyl)borate ligands were of greater interest than the *tris*(pyrazolyl)borate ligands for two reasons. The first is that the additional nitrogen atom in the heteroaromatic ring can serve to improve the water solubility of both the ligand and the potential lanthanide complexes. The second reason is that there are far less reports of the *tris*(triazolyl)borate ligand systems and their complexes which means there is more potential for novel work. Our design is intended to introduce as many chelation sites for the lanthanide metal as possible. As part of this work, we

wanted to investigate the general co-ordination chemistry of these ligand systems with different lanthanide metals. An important aspect of the ligand design is that it be as efficient and convenient as possible to ensure high overall yields and wide functional group tolerance.

2.3 Triazole synthesis by Suzuki cross coupling

In order to synthesize the *tris*(triazolyl)borate ligands, the functionalized triazoles must first be synthesized. Originally, it was proposed to develop cross-coupling conditions to link together an in-house synthesized compound (**2.7**, synthesized in **Scheme 7**) and a suitable cross-coupling partner – in particular, a boronic acid (**Scheme 8**).[37] The 3-amino-1H-1,2,4-triazole was a convenient starting point because it could be purchased. Upon treatment with sodium nitrite in water to yield compound **2.6** followed by heating in 35% HBr (and quenching with sodium carbonate), the bromo-substituted triazole (**2.7**) was generated in good yield.

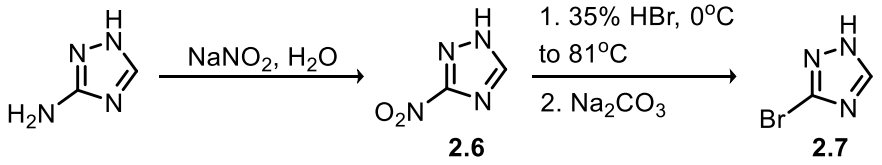

Scheme 7. Synthesis of the 3-bromo-1,2,4-triazole (**2.7**).

The Suzuki cross-coupling protocol between a boronic acid and an sp^2 carbon halide was selected as the palladium cross-coupling route of choice due to the mild conditions in terms

of solvent (typically mixtures of water and THF), temperature (could be done at room temperature), and base (cesium carbonate or triethylamine). The catalytic cycle of the Suzuki cross-coupling reaction is shown in **Figure 12**.[38]

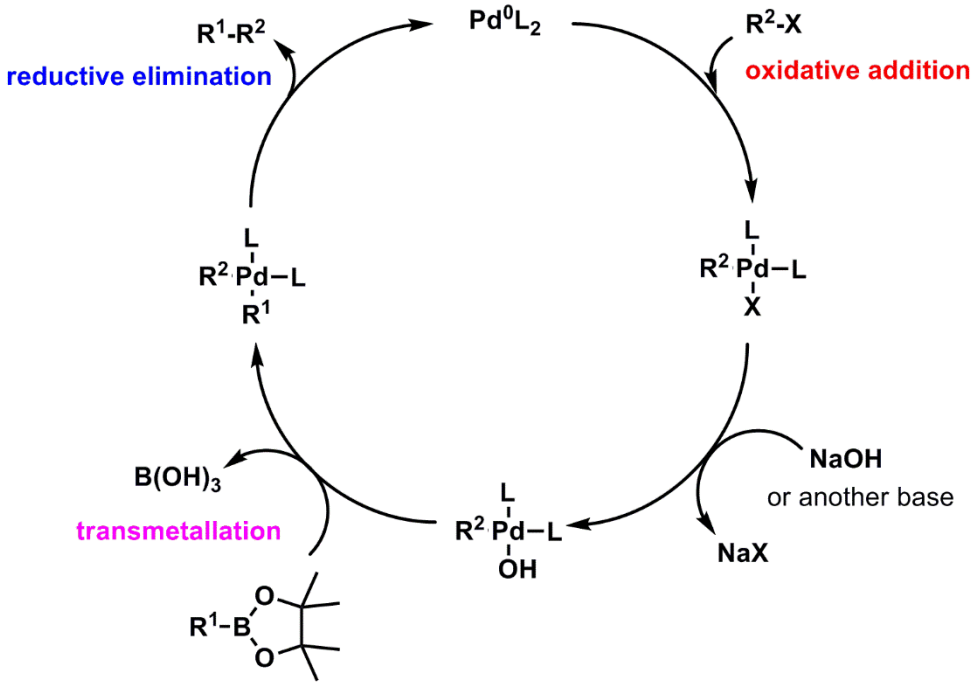

Figure 12. The catalytic cycle of the palladium catalyzed Suzuki cross-coupling.

It was with this in mind that the boronic acid (compound **2.8**) necessary for the coupling needed to be generated (**Scheme 8**).[39] The general procedure for the synthesis of the boronic acid coupling partner proceeded from a brominated species via lithium-halogen exchange (using butyl lithium), boration with trimethylborate followed by a quench with hydrochloric acid. Recrystallization with ether and hexanes typically yielded clean boronic acid.[39] General Suzuki coupling conditions use palladium metal, a phosphine ligand, aqueous solvent conditions (mixtures of water and THF), a mild base, and the boronic acid and halogenated coupling partners. For these reactions, the following palladium catalysts

were explored: tetrakis(triphenylphosphine) palladium (0), bis(triphenylphosphine) palladium dichloride (II), palladium dichloride (II), and bis(acetonitrile) palladium dichloride. The phosphine ligands explored were triphenylphosphine and *o-(*di-*tert*-butylphosphino)biphenyl. In addition to the exploration of different metal/phosphine catalyst systems, different solvent systems and temperatures were also investigated.

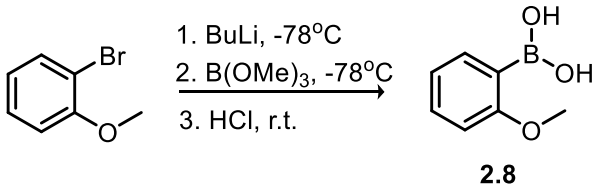

2.8

Scheme 8. Synthesis of the compound **2.8**.

Unfortunately, this reaction did not meet with success even after attempting multiple permutations of temperature, solvent, metal, and phosphine ligand. It was then proposed that the coupling partners could be reversed so that the 3-bromo-1H-1,2,4-triazole (**2.7**) was transformed into the boronic acid and this could be used to couple with a substituted bromophenyl partner. The conversion of the of the 3-bromo-1H-1,2,4-triazole (**2.7**) to the boronic acid was successful, however, the coupling reaction using different catalyst systems, solvents and temperature was not successful so another route was undertaken to generate the triazoles.

2.4 Triazole synthesis using the Ferrence method

The Ferrence group had successfully prepared 1,2,4-triazoles using a multistep approach shown below in **Scheme 9**.[40] We adopted this synthesis to contain an aromatic substituent as shown in **Scheme 10**. However, in our case this reaction failed to give the desired triazoles. We believe this may be because the electron donating methoxy substituent deactivated the carbonyl group of the acid chloride. In the systems explored by Ferrence, alkyl acid chlorides were used so the switch to electron rich aryl substituents apparently shuts down the reaction. This route was not ideal as it included more steps than desired (including the synthesis of an acid chloride), although it was successful for the Ferrence Group.

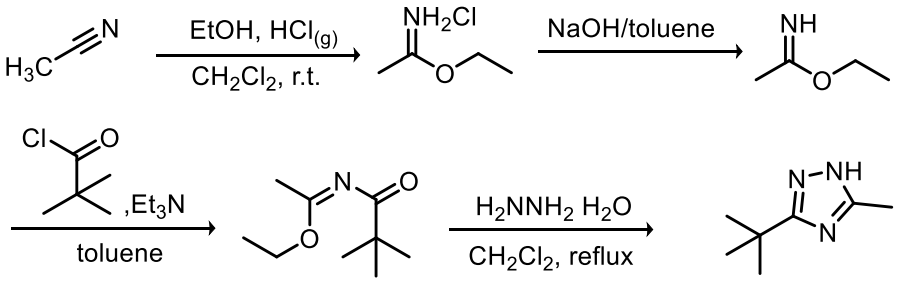

Scheme 9. Synthesis of 3-tert-butyl-5-methyl-1,2,4-triazole by the Ferrence group.

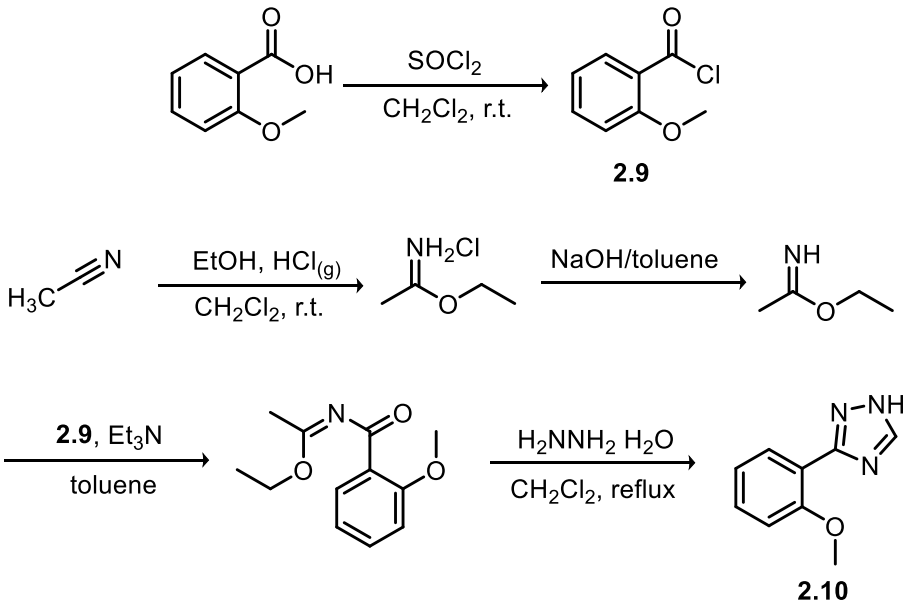

Scheme 10. Synthesis of the **2.10** through intermediate **2.9** using protocols developed by the Ferrence group.

2.5 Successful and highly tolerant scorpionate synthesis

After investigation of the Ferrence method as a means to access the triazole precursor, it was deemed necessary to explore chemistry that allowed for a more diverse structural architecture. Detailed below is the developed synthesis for pyrazole and triazole precursors which proved high-yielding with good functional group tolerance.

2.5.1 Pyrazole and triazole synthesis

It was clear that a different method was necessary in order to achieve the desired goals of a convenient and efficient synthesis of the scorpionate ligands. The next approach undertaken was the reaction of dimethylformamide-dimethylacetal with acetophenone derivatives at elevated temperature resulting in the generation of an isolable amino α,β-unsaturated ketone intermediate (**2.11a**-**2.15a**) that could then be cyclized with hydrazine to the desired pyrazoles (**Scheme 11**).[41-42]

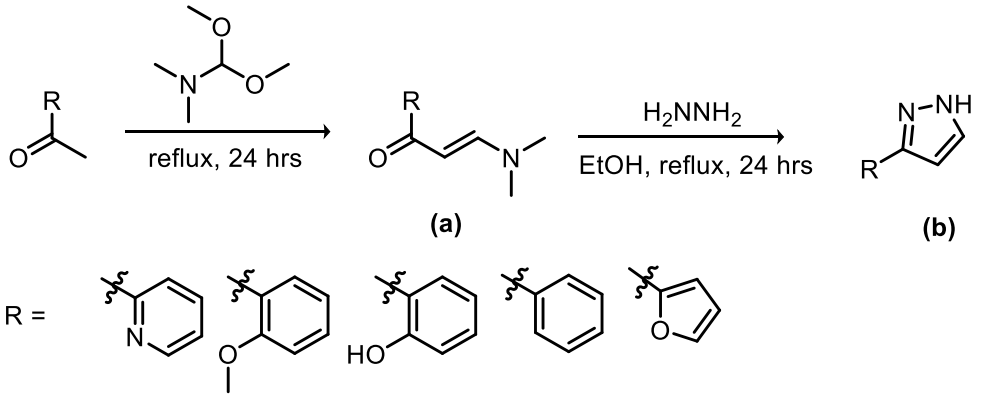

	2.11	**2.12**	**2.13**	**2.14**	**2.15**
% yield **(a)**	69	48	95	48	59
% yield **(b)**	79	71	54	95	83

Scheme 11. Synthesis of the 3-substituted pyrazoles (**2.11-2.15**) using dimethylformamide-dimethylacetal.

This procedure proved to be very successful. Simple crystallization of the pyrazoles from water in the last step yielded very clean product in good yields (55-90%). This procedure also shows tolerance for different electron-donating functional groups. The most important substituents from our perspective were the rigid aromatic and heteroaromatic ring systems as these set the geometry for lanthanide metal chelation nicely.

We did find that for functional groups with stronger electron-withdrawing substituents such as the nitrophenyl, bromophenyl, and lactone, the reaction with dimethylformamide-dimethylacetal did not proceed to completion if done neat in solvent, as before. However, if the two reagents were combined in higher boiling solvent such as toluene and heated to reflux overnight the acyclic intermediate was generated in good yield (**Scheme 12**). The cyclization to the pyrazole proceeded in the same manner as before, but these products would not crystallize from water. Instead, they needed to be extracted into a polar solvent such as ethyl acetate or chloroform.

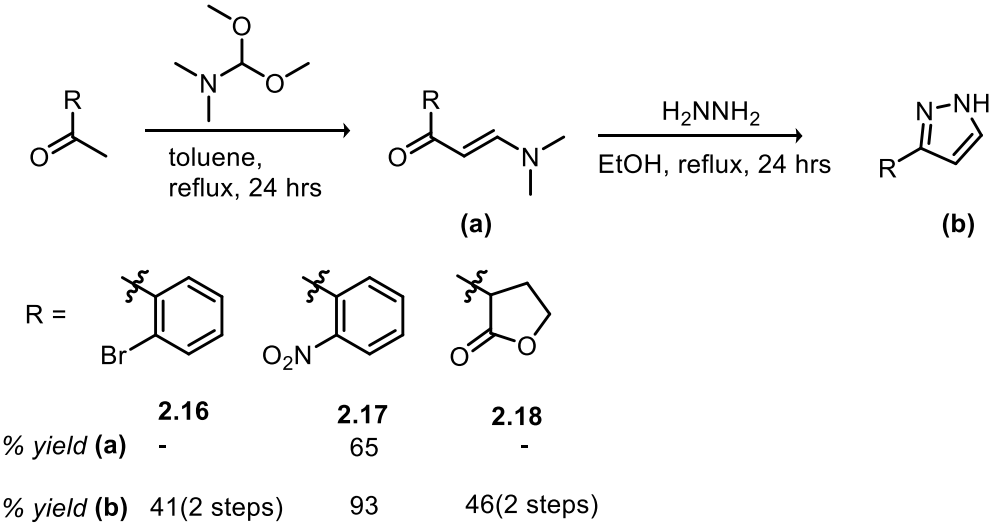

Scheme 12. Synthesis of more 3-substitued pyrazoles (**2.16-2.18**) using dimethyl-formamide dimethyl acetal.

As already stated, the *tris*(triazolyl)borate ligands were of particular interest because there are less literature reports of these ligands and the additional nitrogen atom in the 4-position can serve to improve the solubility of the ligands and complexes in water. We hoped that the same procedure used for the synthesis of the pyrazole rings could be adapted for the synthesis of the triazole system using arylamides rather than acetophenone

derivatives (**Scheme 13**).[43-44] The aryl amides were accessible in two steps from their corresponding benzoic acids.

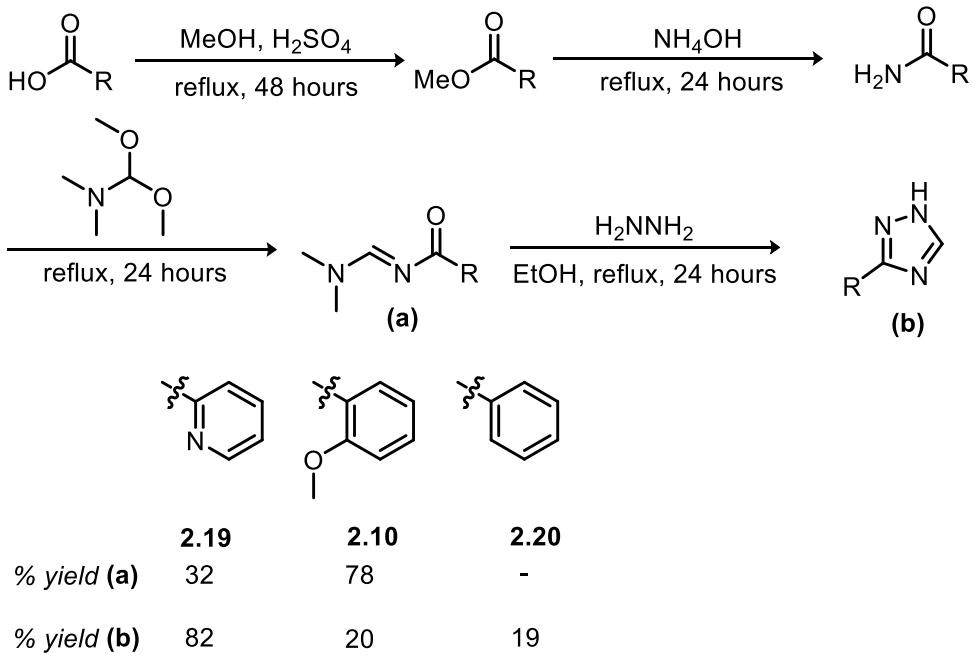

	2.19	**2.10**	**2.20**
% yield **(a)**	32	78	-
% yield **(b)**	82	20	19

Scheme 13. Synthesis of 3-substituted 1,2,4-triazoles (**2.19**, **2.10**, **2.20**) using the dimethyl-formamide dimethyl acetal method.

Fortunately, this route worked very well and showed reasonable functional group tolerance, although admittedly, the range of functional groups explored was small. Having achieved the goal of a facile and tolerant pyrazole and triazole synthesis, the next step was to synthesize the scorpionate ligands themselves.

2.5.2 Synthesis of the scorpionate ligands

The synthesis of the *tris*(pyrazolyl)borate and *tris*(triazolyl)borate ligands was carried out by a melt reaction between three equivalents of the pyrazole or triazole and one equivalent of sodium borohydride (or potassium borohydride), where evolution of hydrogen gas was measured by water displacement (**Scheme 14**).[30] A major impurity in the melt reactions was the *bis*-substituted boron product. To prevent this from happening, the stoichiometry of the reaction must be closely controlled, but this by-product was observed in nearly every case. The only concern with using an excess of the pyrazole or triazole is the possible formation of a four co-ordinate boron centre. However, this was not observed, presumably due to steric constraints. Purification of these compounds was done either by recrystallization from benzene or sublimation at 75 -95°C.

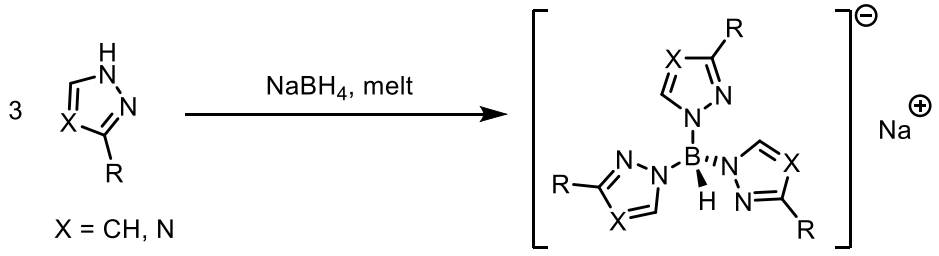

Scheme 14. Synthesis of the *tris*(pyrazolyl)borate and *tris*(triazolyl)borate ligands.

2.5.3 Characterization of the Scorpionate Complexes

^{11}B (I = 3/2, 80% natural abundance) NMR was a useful tool for determining the co-ordination number and type at the boron centre.[18] The chemical shift in the ^{11}B NMR is particularly informative for the scorpionate ligands. For instance, if the resonance occurred

at ca. 3 ppm, the boron centre of the scorpionate is *tris*-substituted, but if the resonance appeared at ca. -7ppm, then the boron centre of the scorpionate is *bis*-substituted (**Table 2**).

IR spectroscopy is also an important method of analysis for the scorpionate ligands. In the case of the *tris*-substituted scorpionate ligands, the B-H stretch occurred at ca. 2350 cm^{-1}, whereas the *bis*-substituted scorpionate showed both an asymmetric stretch (ca. 2400 cm^{-1}) and a symmetric stretch (ca. 2200 cm^{-1}).[45] All of the scorpionates synthesized here had peaks in the 2350 cm^{-1} region, consistent with *tris*-substituted boron centres (see **Table 2** for stretching frequencies).

Complex		**^{11}B NMR shift/ppm[a]**	**B-*H* stretch[b]/ cm^{-1}**
Tris(pyrazolyl)borate	R = Ph (**2.14c)**	3.25	2352
	R = *o*-OMeC$_6$H$_4$ (**2.12c**)	2.96	2364, 2263
	R = pyridine (**2.11c**)	2.82	2364, 2330, 2257
	R = *o*-NO$_2$C$_6$H$_4$ (**2.17c**)	2.80	2365, 2346
	R = lactone (**2.18c**)	3.11	2358, 2341, 2296
	R= furan (**2.15c**)	3.04	2347, 2285
	R = *o*-BrC$_6$H$_4$ (**2.16c**)	2.91	2347, 2235
Tris(triazolyl)borate	R = pyridine (**2.19c**)	3.22	2375

[a]111 Mz, relative to $BF_3 \cdot OEt_2$ [b]KBr, air background

Table 2. ^{11}B NMR chemical shifts and selected B-H IR stretches for the scorpionate ligands synthesized.

All of the scorpionate ligands were also characterized by ^{1}H and ^{13}C NMR. The resonances of the pyrazoles and triazoles did not change significantly upon formation of the scorpionate ligands. In some NMR solvents (such as $CDCl_3$ and d_6-DMSO), the acidic pyrazole and triazole N-H resonance could be observed downfield (around 10-12 ppm). The disappearance of this peak in the ^{1}H NMR was also a good indication of formation of the scorpionate complex.

2.6 Continued work towards novel ligand systems with oxygen donors

Initially, it was proposed that a 2'-hydroxyl group bound to the pyrazole of a scorpionate ligand would generate a favourable 6-membered lanthanide containing ring (**Figure 13**). Synthetically though, this ligand system presented a challenge because protecting groups needed to be used to prevent boron-oxygen bond formation rather than the desired boron-nitrogen bond formation. Indeed, if the sodium borohydride-pyrazole melt reaction is conducted with the free 2'-hydroxyphenylpyrazole, a "glass" forms in the reaction vessel which does not correspond to the desired product. Multiple routes to this target were explored. A standard method to protect the hydroxyl function is with a methyl group. The methyl group was small enough to avoid any steric concerns and stable enough to survive the melt reaction with the sodium borohydride. The required pyrazole could be made from 2'-methoxyacetophenone and the *tris*(pyrazolyl)borate complex was synthesized readily.

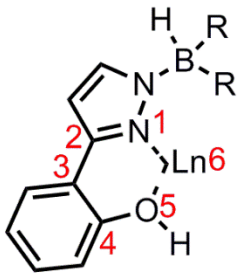

Figure 13. Lanthanide complex containing a six-membered ring with R = 3-(2-hydroxyphenyl)-pyrazole.

With this complex in hand, we then explored a range of deprotection conditions. Typically the deprotection of a methoxy group is done with boron tribromide.[46] However, when these conditions were attempted (1.0 M solution of BBr_3 in THF or neat BBr_3),

considerable decomposition was observed and the ^{11}B NMR showed a resonance corresponding only to the boron tribromide (+38 ppm).

Since these typical conditions failed, other deprotection protocols were explored including other Lewis Acids ($AlCl_3$,[47] $NdCl_5$,[48] TMS-I,[49] or $B(C_6F_5)_3$[50]) and nucleophilic conditions (PhSH[51] or NaCN[52]), all of which are shown in **Table 3**. When these conditions also failed to produce the desired 2'-hydroxyphenyl product, other protecting groups were explored.

Reaction	**Conditions**	**Result**
1	$B(C_6F_5)_3$, Et_3SiH, DCM, reflux	Decomposition
2	BBr_3, DCM, -78 ^{o}C to reflux	Decomposition
3	PhSH, K_2CO_3, NMP, reflux	Starting Material
4	TMS-I, DCM, r.t.	Starting Material
5	$AlCl_3$, DCM, 0 ^{o}C to r.t.	Starting Material
6	NaI, $AlCl_3$, DMSO, 70 ^{o}C	Starting Material
7	NaCN, DMSO, reflux	Starting Material
8	$NbCl_5$, DCM, reflux	Starting Material

Table 3. Reaction conditions for the deprotection of the methyl ether.

The next protecting groups explored were a variety of silyl ethers (**2.22** – **2.24**),[53] allyl ether (**2.25**),[54] acyl esters (**2.26**)[55] and a benzyl ether (**2.21**) (**Scheme 15**).[56]

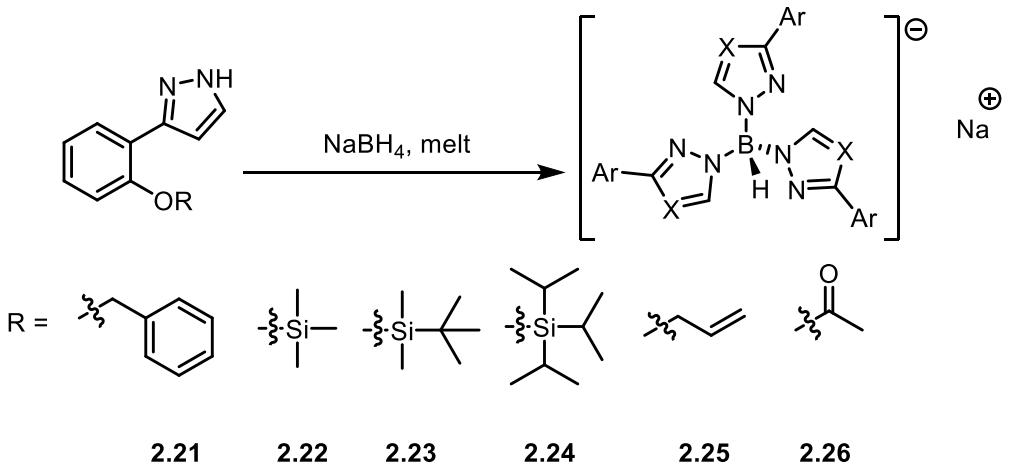

Scheme 15. Assorted protected ethers as alternatives to methyl ether protecting groups.

With silyl ether protecting groups (**2.22** – **2.24**), the bulkier the aliphatic group on the silicon, the more stable the protected compound. A variety of silyl protecting groups were explored in order to enhance the stability but all of these silyl ethers decomposed in the melt reaction under the high temperatures necessary to form the boron-nitrogen bond.

The next group explored was the benzyl ether protecting group (**2.21**). This is a less attractive option as column chromatography was generally required to remove the excess benzyl bromide after the reaction to protect the 2'-hydroxypyrazole was completed. Fortunately, the benzyl protected hydroxy compound could be collected as a crystalline product that, unlike the silyl ethers, did survive the melt reaction. However, as characterized by ^{11}B NMR, only the *bis*-substituted boron complex was formed, presumably because the larger benzyl group caused steric crowding that limited introduction of a third pyrazole group (**Scheme 16**).

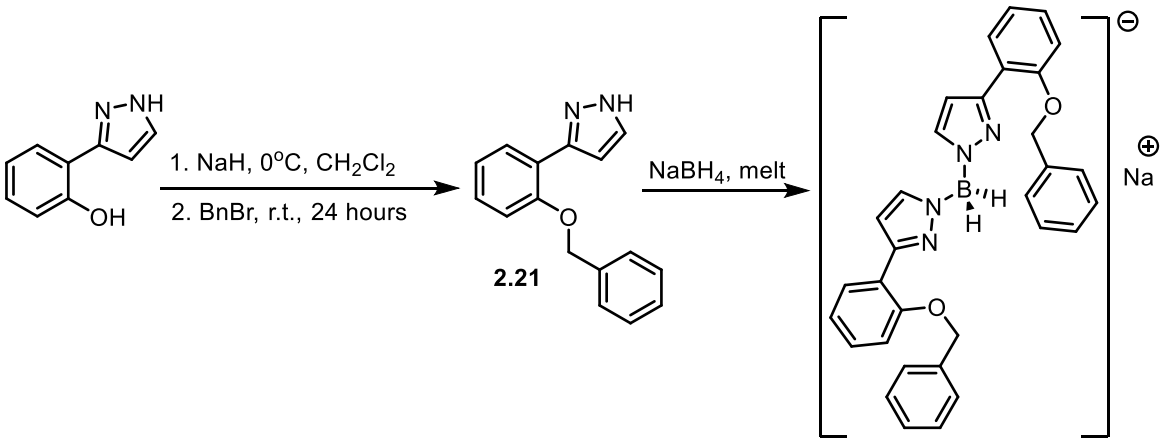

Scheme 16. Reaction with benzyl protected 2'-hydroxypyrazole.

An allyl protecting group was also explored because it was thought that it would survive the melt reaction like the benzyl group without causing the same steric concern. Despite best efforts, the allyl-protected 2'-hydroxyl species (compound **2.25**) could not be isolated as a solid. Due to the inability to collect a crystalline pyrazole, the sodium borohydride melt was not attempted for this protected pyrazole.

Finally, the methyl ester was explored as a possible protecting group. In this case, a more interesting result was observed (by both mass spectroscopy and NMR techniques). Two of the ligands substituted onto the boron centre, but instead of a third substitution, boron-oxygen bonds were formed to make the four co-ordinate species (as shown in **Scheme 17**).

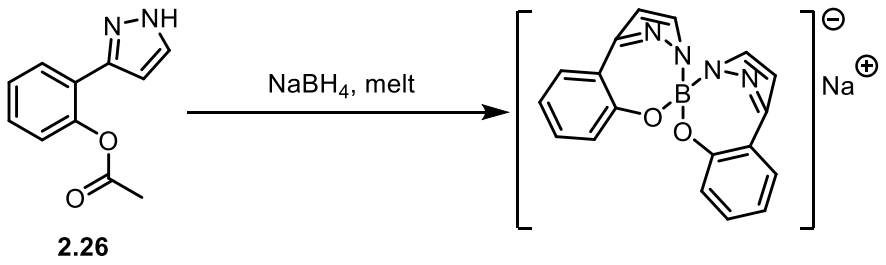

Scheme 17. Reaction with methyl ester protected pyrazole to yield a "cyclized" structure.

2.7 Continued work towards a novel ligand systems with nitrogen donors

In lieu of the hydroxyl compound, it was proposed that a nitro compound could be prepared and reduced to an amine (**Scheme 18**) to bind to a metal in the same fashion as the hydroxyl compound. The *tris*(2'-nitrophenylpyrazolyl)borate was prepared in good yield using the melt reaction.

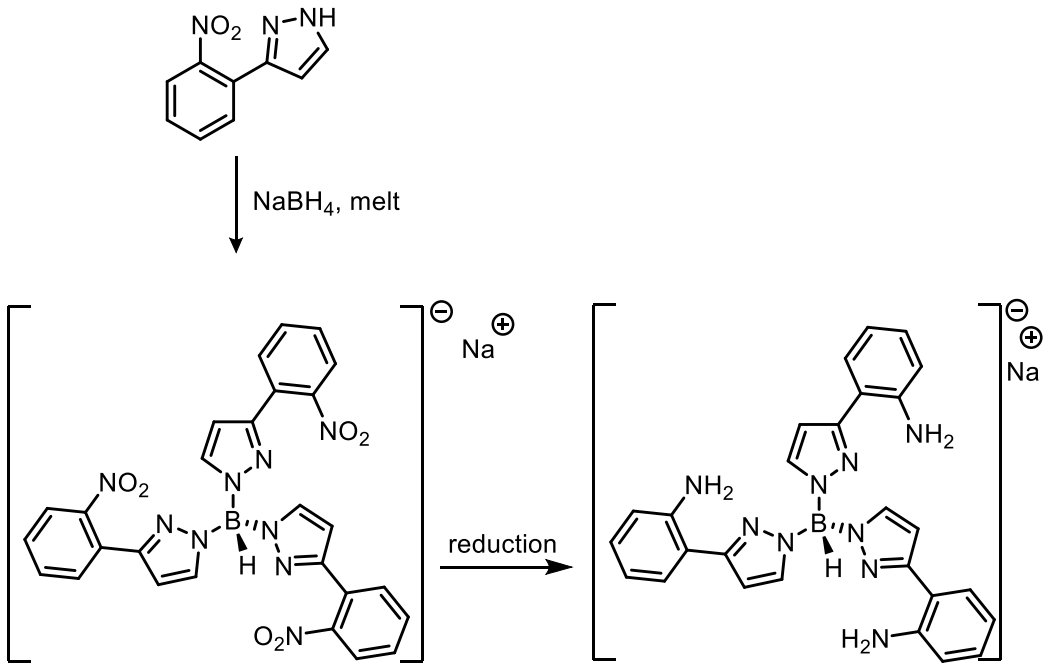

Scheme 18. Proposed reduction of nitro group to primary amine.

In this case, there were fewer conditions available for the reduction of nitro compounds to amines than for the deprotection of methyl ethers. The first reaction that was attempted was direct hydrogenation at elevated pressure (300 psi) over a 10% palladium on carbon catalyst in a high pressure Parr reactor. After this reaction, severe decomposition was noted in the ^{1}H NMR where all the pyrazole resonances were missing and only two resonances were observed in the aromatic region (between 7.5-7 ppm). The hydrogenation was

attempted a second time at low pressure (ca. 1 psi) with a hydrogen balloon.[57] Again, decomposition was noted in the ^{1}H NMR spectrum. Reduction using Raney Nickel in methanol was also attempted but due to difficulty in the work-up and the air sensitivity of the nickel, this method was abandoned.[58]

Finally, it was discovered that a reduction with a 9:1 mixture of iron:iron trichloride in acetic acid would yield the desired product.[59] This was evident by an upfield shift of the phenyl resonances in the ^{1}H NMR and the upfield shift of the *ipso* carbon bearing the amine function in the ^{13}C NMR. However, the ^{11}B NMR did not show a peak at ca. 3 ppm; instead, there was a single resonance at 18.47 ppm. A similar resonance had been observed in the ^{11}B NMR for the yttrium-pyridine substituted *tris*(pyrazolyl)borate complex which had a resonance at 18.46 ppm. This observation strongly suggested that the iron reduction proceeds to the amine but this compound then acted as a co-ordinating ligand for the excess iron in solution. What is interesting, however, is that while the ^{1}H NMR shows some broadening, the peaks are still distinct. This is relativity unexpected as high spin iron in the 3+ oxidation state should broaden the NMR spectrum considerably. However, since the iron is being used in reducing conditions, there is an excellent chance that the iron present is the low spin diamagnetic iron 2+ species.

2.8 Synthesis and Characterization of the Lanthanide Metal-Scorpionate Complexes

The synthesis of the ligand-lanthanide complexes was straightforward. Mixing one equivalent of ligand and one equivalent of lanthanide (III) chloride hexahydrate in a polar solvent such as methanol, and stirring at room temperature overnight, followed by removal

of the solvent, afforded the compounds as crystalline solids (general synthesis shown in **Scheme 19**). These solids needed to be washed extensively with water in order to remove any sodium chloride, a by-product of the reaction.

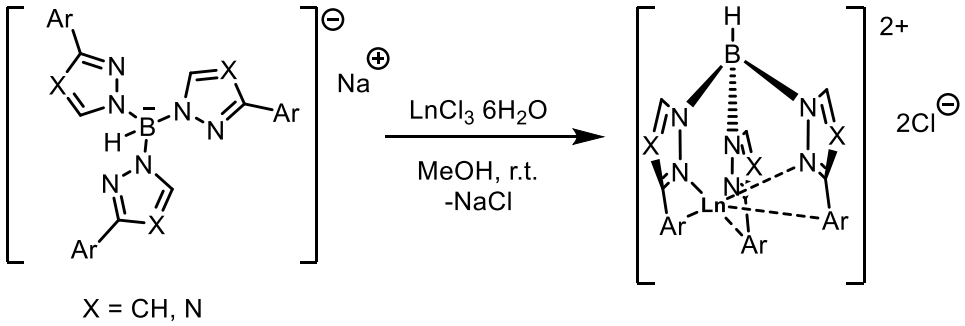

Scheme 19. General synthesis of the lanthanide metal-scorpionate ligand complexes.

Since lanthanide metals in the 3+ oxidation state are paramagnetic, ^{1}H NMR provided little information on the structure of the complexes. Other characterization methods such as colour, melting point, and X-ray crystallography provided additional information. In terms of colour, all compounds were pale colours, characteristic of the specific lanthanide metal due to weak f-f transitions.[60] All of the complexes prepared were pale yellow, pale pink, or white. The melting points collected for all compounds were higher than 300^{o}C.

The B-H stretch in the IR spectrum of the free ligand was also observed in the complexes as well. This stretch was observed at 2360 cm^{-1} for the ligand and for all of the lanthanide complexes synthesized with the pyridine-substituted *tris*(pyrazolyl)borate.

Tabulated below in **Table 4** is the B-H stretching frequency for the complexes formed in the reaction of the *tris*(2'-pyridinopyrazolyl)borate ligand (**Scheme 20**) with a variety of lanthanide metals.

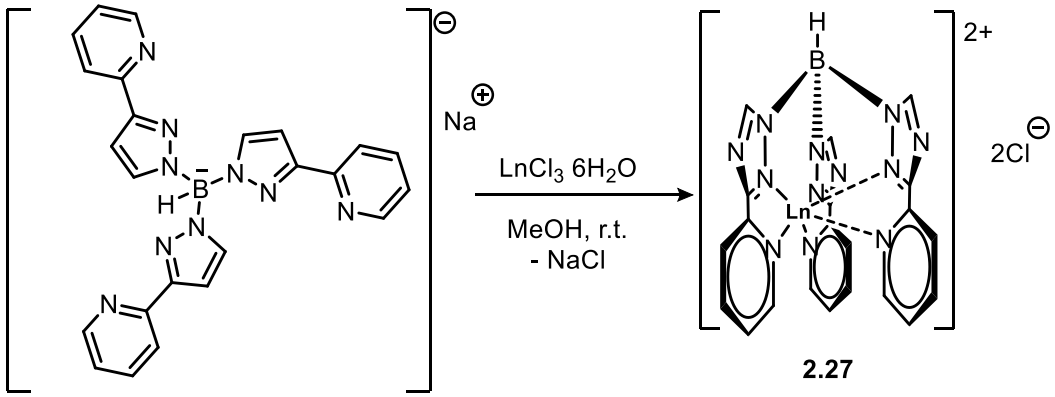

Scheme 20. Synthesis of the *tris*(2'-pyridinopyrazolyl)borate ligand-lanthanide metal complex.

Lanthanide Metal	**B-*H* stretch[b]/ cm^{-1}**
Yb **(2.27)**	2365
Tb **(2.32)**	2397
Nd **(2.30)**	2395, 2341, 2274
Y **(2.31)**	2358, 2347
Eu **(2.33)**	2364
Sm **(2.29)**	2373, 2357, 2344

[b]KBr, air background

Table 4. B-H stretching frequency of the *tris*(2'-pyridinopyrazolyl)borate ligand-lanthanide metal complex.

For all of the lanthanide complexes, paramagnetic NMR spectra were collected. All of the lanthanide metals have different numbers of unpaired electrons in the 3+ oxidation state. This means that the lanthanide metals will give different degrees of paramagnetic

shift for the ligand protons. Significant broadening of the resonances from 10-300 Hz is also observed depending on the metal ion.

Variable temperature NMR experiments were carried out in deuterated DMSO in order to gain a better understanding of the solution structure. For ions that follow Curie or Curie-Weiss paramagnetic behavior over the temperature range of the NMR experiment, plots of δ vs. 1/T are expected to follow a straight line because δ is proportional to χ. Deviation from straight line behavior usually indicates aggregation (monomer/dimer equilibria) or other temperature dependent structural changes.[61]

Shown below is the variable temperature plot for the terbium complex **2.32,** as a representative example. For the lanthanide metals studied, the Curie-Weiss law was obeyed for all distinguishable resonances. This was promising as it indicates no aggregation or unusual solution behavior at high temperature.

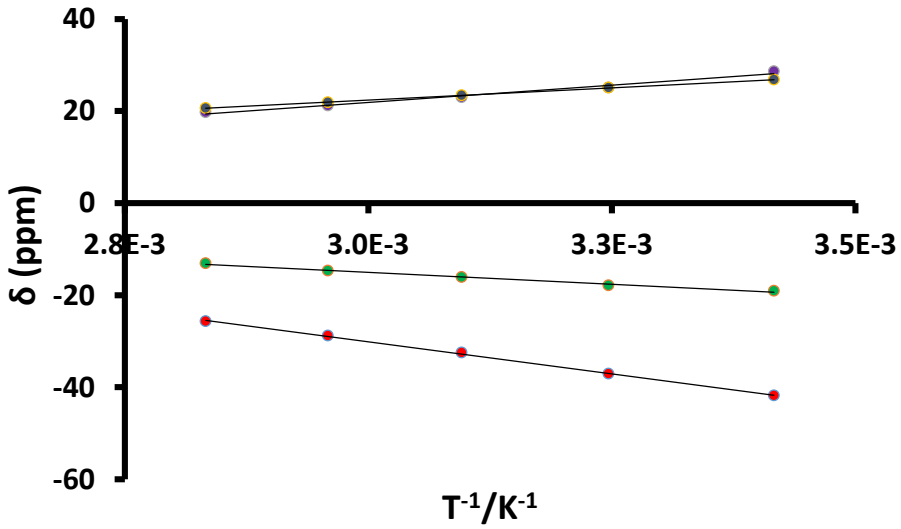

Figure 14. Variable temperature NMR for the compound **2.32** with each line corresponding to the change in chemical shift for a distinct hydrogen atom.

Crystals suitable for X-ray analysis were grown of what was assumed to be compound **2.27 (**which was synthesized in an acceptable yield of 53.5%) by slow evaporation from a 1-butanol solution. The crystals that were analyzed were large, yellow, and rhomboid in size and shape. Upon analysis, however, it was found that the solid state structure was actually compound **2.28** where the borate ligand has only two chelate arms and there are two of these ligands co-ordinated to each ytterbium metal centre.

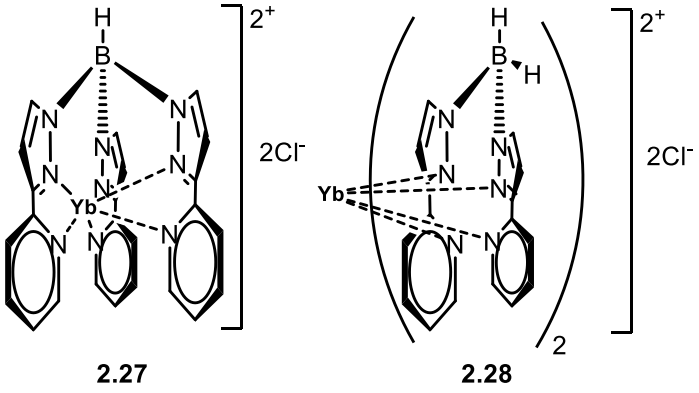

2.27 **2.28**

Figure 15. Structure of proposed compound **2.27** and actual compound **2.28**.

There are two proposals for why this compound was isolated. The first was that there was a small amount of H_2Bpz_2 present as an impurity when the ligand was mixed with ytterbium chloride and this minor impurity carried through to a ytterbium complex isolated during crystallization. Compound **2.28** would be difficult to detect at low concentrations as both the ^{1}H and ^{11}B NMR would be complicated and broadened by the presence of the paramagnetic ytterbium metal centre. The other common technique to detect the presence of the H_2Bpz_2 species is infrared spectroscopy, but if this impurity was at a low concentration then it is likely that those stretches would not be observed due to the lack of sensitivity of the technique. The H_2Bpz_2 species was not detected by either technique, but

could have been present at a concentration below the detection limits of either of these analytical methods.

Another proposal for the isolation of compound **2.28** is that compound **2.27** was initially present but one of the arms was cleaved from the boron centre during crystal growth. If this occurred, it could be due to the highly rigid nature of the ligand from the planar aromatic groups present (both the pyrazole and pyridine). The pyridine group may not be able to "reach" close enough to the ytterbium metal centre (with an average Yb-N bond distance of 2.679Å for the pyridine function compared to an average Yb-N bond distance of 2.579Å for the pyrazole group) to form a stable bonding interaction. Cleavage would afford a *bis*(2'-pyridinopyrazolyl)borate ligand where all four nitrogen donors can bind to the lanthanide centre without introducing excessive strain. Shown below is the X-ray crystals structure in both **Figure 16** and **Figure 17**, with select bond lengths tabulated in **Table 5**.

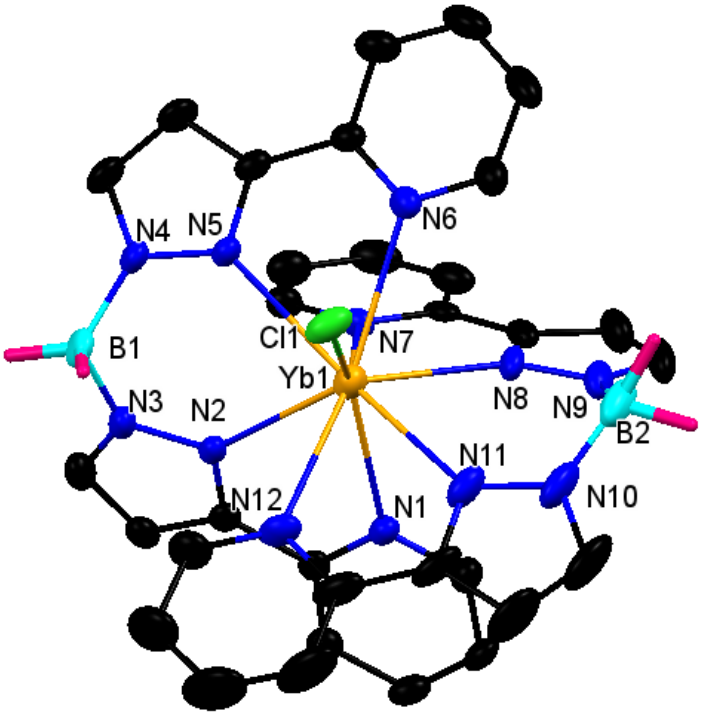

Figure 16. X-Ray structure of compound **2.28.** All hydrogen atoms removed with the exception of the B-H protons. Thermal ellipsoids shown at 50% probability level.

Bond	**Bond Length (Å)**
B1-N3	1.544(8)
B1-N4	1.541(8)
N3-N2	1.366(6)
N4-N5	1.363(6)
N2-Yb1	2.550(4)
N5-Yb1	2.610(4)
N1-Yb1	2.674(4)
N6-Yb1	2.696(4)
Yb1-Cl1	2.7056(14)
B2-N9	1.544(10)
B2-N10	1.518(11)
N9-N8	1.359(6)
N10-N11	1.354(7)
N8-Yb1	2.559(4)
N11-Yb1	2.588(4)
N7-Yb1	2.675(4)
N12-Yb1	2.673(4)

Table 5. Selected bond lengths of interest for compound **2.28**.

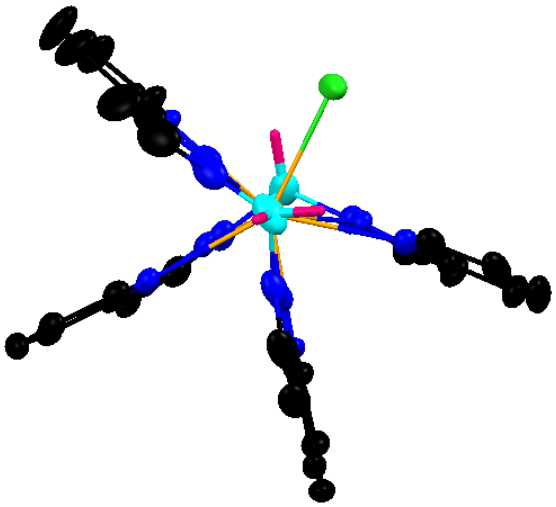

Figure 17. X-Ray structure of compound **2.28.** All hydrogen atoms removed with the exception of the B-H protons. Thermal ellipsoids shown at 50% probability level.

The ytterbium metal is nine co-ordinate with eight nitrogen donors and one chlorine donor and adopts a three-face capped trigonal prismatic geometry with two nitrogen atoms and the chlorine atom acting as the face-capping atoms. The Cambridge Structural Database (CSD) shows that there are only fourteen results with the LnN_8Cl structural motif (where Ln is any lanthanide metal). It is worth noting is none of these structures contain the lanthanide metal ytterbium. Instead there are six with europium, two with samarium, two with neodymium, two with terbium, two with lanthanum, one with cerium, and one with praseodymium.

Analysis of these structures revealed that the average lanthanide ion-nitrogen atom bond length is 2.565Å (when corrected for the difference in ionic radius by the Shannon index).[62] In the bond length analysis of compound **2.28** it was shown that the ytterbium-pyrazole nitrogen (N2, N5, N8, N11) bond had an average length of 2.576 Å (with a range of 2.550-2.610Å) (that is, very close to the average ytterbium-nitrogen bond length from the CSD).

However, the ytterbium-pyridine nitrogen atom (N1, N6, N7, N12) bond length has an average of 2.679Å (with a range of 2.673-2.696Å). The pyridine nitrogen atom-ytterbium ion bond lengths in compound **2.28** were longer than the average bond length from the CSD which supports our hypothesis that the ligand in compound **2.27** might experience exceptional crowding that could promote loss of an arm during crystal growth. This result indicated that in order to develop a stable, hexadentate scorpionate ligand the additional chelation site should project from the aromatic ring.

In the search of both *bis*(pyrazolyl)borate and *tris*(pyrazolyl)borate ligands as complexed to lanthanide metals there was only one example of a ytterbium complex. This complex was reported by the Takats *et. al.* in 2008 (**Figure 18**).[63] In this structure, two tridentate *tris*(pyrazolyl)borate ligands are co-ordinated to the ytterbium metal centre. However, due to steric constraints, one of the ligands was not bound through the three nitrogen atoms and instead was bound through two nitrogen atoms and had formed an agostic interaction (highlighted in blue on **Figure 18**) with the hydrogen atom bound to the boron atom. The geometry around this metal centre was a distorted octahedron. This agostic interaction with sterically demanding substrates supports the hypothesis that crowding around the metal centre could lead to structural modifications of the ligand.

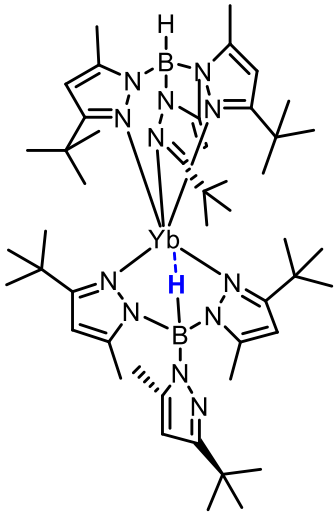

Figure 18. Ytterbium-scorpionate complex reported by the Takats *et al.*[63]

2.9 Summary

After it was realized that the phophite based Klaùi ligand system was not an appropriate candidate for the proposed PARACEST contrast agent applications, it was proposed that a phosphinimine-based Klaùi ligand systems would perhaps be better candidates as a substituent on the nitrogen atom could present another site for chelation. However, the syntheses of these ligands proved unsuccessful so this work was abandoned and the scorpionate ligand system was explored. With this chemistry, an efficient and tolerant route was developed to synthesize a variety of *tris*(pyrazolyl)borate and *tris*(triazolyl)borate ligands. This synthesis allowed for the development of a small library of compounds which incorporated electron-donating group and electron-withdrawing groups. From here, several lanthanide metal complexes were synthesized and studied using standard spectroscopic techniques. X-ray crystallography of **2.28** revealed a unique structural motif, possibly the product of cleavage of a boron-nitrogen bond during crystal

growth. Comparison of the bond lengths in this complex with other lanthanide metal containing complexes of a similar structural type supported the argument that bond cleavage during crystal growth was possible.

2.10 Experimental Section

2.10.1 Methods and Materials

All reactions and manipulations were carried out under an argon atmosphere using standard Schlenk or glovebox techniques unless otherwise stated. All reagents were purchased from Aldrich and used as received unless stated in which case they were purified or dried under appropriate conditions. NMR spectra were recorded on 300, 360 or 500 MHz instruments at room temperature unless stated otherwise. Accurate mass determination was performed at the UVic Genome BC Proteomics Centre on a Thermo Scientific LTQ Velos Orbitrap instrument. Samples (mg/mL) were diluted by a factor of 10-100 and injected by liquid infusion through a nano ESI source. X-ray diffraction data was collected on a Bruker PLATFORM/SMART 1000 CCD with a graphite-monochromatacized Mo-Kα radiation ($\lambda = 0.71073$ Å) by Dr. Allen Oliver (University of Notre Dame).

2.10.2 Experimental Data

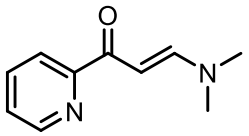

2E-*3-dimethylamino-1-pyridin-2-yl-propanone* **(2.11a)**

To an oven-dried 100 mL round bottom flask equipped with a Schlenk adaptor and stir bar was added 2-acetylpyridine (5.45 g, 0.0445 moles, 1 eq) and dimethylformamide-dimethylacetal (7.15 g, 0.0600 moles, 1.3 eq). The solution was heated at reflux overnight (21h). After this time, the flask was allowed to cool to room temperature. A minimal amount of anhydrous ethyl ether was added to precipitate olive green crystals of **2.11a**. Yield: 5.5 g (68.9%). ^{1}H NMR (300 MHz, $CDCl_3$): δ 8.62 (ddd, 1H, $^{3}J_{HH}$ = 4.8 Hz, $^{4}J_{HH}$ = 1.6 Hz, $^{5}J_{HH}$ = 0.9 Hz), 8.15 (dt, 1H, $^{3}J_{HH}$ = 7.9 Hz, $^{4}J_{HH}$ = 1.0 Hz), 7.91 (d, 1H, $^{3}J_{HH}$ = 12.7 Hz), 7.81 (td, 1H, $^{3}J_{HH}$ = 7.8 Hz, $^{4}J_{HH}$ = 1.7 Hz), 6.46 (d, 1H, $^{3}J_{HH}$ = 12.7 Hz), 3.16 (s, 3H), 2.99 (s, 3H). ^{13}C{^{1}H} NMR (75.5 MHz, $CDCl_3$): 188.9, 158.2, 156.8, 150.3, 138.7, 127.4, 124.1, 93.2, 47.2, 39.5.

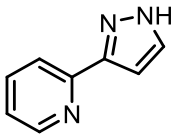

2-(1H-pyrazol-3-yl)pyridine **(2.11b)**

To a 1-neck 100 mL round bottom flask equipped with a stir bar was added **2.11a** (0.968 g, 0.00550 moles, 1 eq), an excess of hydrazine monohydrate (1.00 g, 0.0200 moles), and 25 mL anhydrous ethanol. The solution was heated at reflux overnight (19h). After this time, the flask was allowed to cool to room temperature. The solvent was evaporated under reduced pressure and **2.11b** was crystallized by addition of ice water and storage in the fridge as colourless crystals. Yield: 0.63 g (79.2%). Mp 125-127°C. ^{1}H NMR (300 MHz, $CDCl_3$): δ 8.62 (d, 1H, $^{3}J_{HH}$ = 5.0 Hz), 7.74 (d, 2H, $^{3}J_{HH}$ = 4.3 Hz), 7.65 (d, 1H $^{3}J_{HH}$ = 1.9

Hz), 7.22 fg(m, 1H), 6.80 (d, 1H, $^{3}J_{HH}$ = 1.9 Hz), NH resonance not observed. $^{13}C\{^{1}H\}$ NMR (75.5 MHz, $CDCl_3$): 149.3, 149.2, 137.6, 137.1, 122.9, 120.2, 103.4. One carbon signal not observed. LRMS ($M\text{-}H^{+}$): 144.

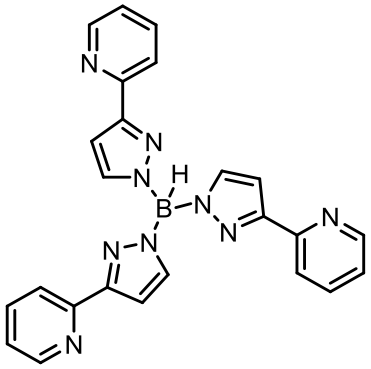

*2'-pyridyl*tris*(pyrazolyl)borate* **(2.11c)**

To an oven-dried 1-neck 25 mL round bottom flask equipped with a stir bar was adde **2.11b** (0.723 g, 0.00499 moles,1 eq) and sodium borohydride (0.0701 g, 0.00185 moles, 0.37 eq). The solid mixture was heated to melting at 200ºC for 1.5h, and the amount of hydrogen gas produced was measured by water displacement. After this time, the melt was allowed to cool to room temperature. After purification by sublimation at 75ºC or recrystallization from benzene **2.11c** was collected as white crystals. Yield: 0.51 g (62 %). Mp >300°C. Selected IR (KBr): 2364, 2330, 2257 (B*H*) cm^{-1}. ^{1}H NMR (500 MHz, MeOD) δ 8.45 (ddd, 3H, $^{3}J_{HH}$ = 4.7 Hz, $^{4}J_{HH}$ = 1.8 Hz, $^{5}J_{HH}$ = 0.7 Hz), 8.01 (dt, 3H, $^{3}J_{HH}$ = 7.7 Hz, $^{4}J_{HH}$ = 0.7 Hz), 7.78 (dt, 3H, $^{3}J_{HH}$ = 7.7, $^{4}J_{HH}$ =1.8 Hz), 7.59 (d, 3H, $^{3}J_{HH}$ = 2.2 Hz), 7.22 (ddd, 3H, $^{3}J_{HH}$ = 7.7 Hz, $^{4}J_{HH}$ = 4.7 Hz, $^{5}J_{HH}$ = 1.8 Hz), 6.71 (d, 3H, $^{3}J_{HH}$ = 2.2 Hz). $^{13}C\{^{1}H\}$ NMR (125.8 MHz, MeOD): 153.7, 151.0, 148.3, 137.2, 136.3, 121.6, 120.4, 102.7. $^{11}B\{^{1}H\}$ NMR (160.5 MHz, MeOD): 2.80. HRMS (ESI) calcd for $C_{24}H_{19}N_9B$ (M+Na): 490.1652. Found: 490.1655.

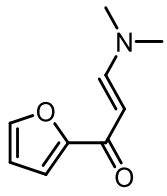

2E-*3-(dimethylamino)-1-(2-furyl)prop-2-en-1-one* **(2.15a)**

To an oven-dried 100 mL round bottom flask fitted with a Schlenk adaptor and a stir bar was added 2-furyl methyl ketone (6.37 g, 0.0579 moles, 1 eq) and dimethylformamide-dimethylacetal (8.97 g, 0.0754 moles, 1.3 eq). The solution was heated to reflux for 6h. After this time, the solution was cooled to room temperature and excess solvent was removed under reduced pressure to collect **2.15a** as brown crystals. Yield: 5.6 g (58.6%). ^{1} H NMR (300 MHz, $CDCl_3$) δ 7.78 (d, 1H, $^{3}J_{HH}$ = 12.4 Hz), 7.46 (dd, 1H, $^{3}J_{HH}$ = 1.7 Hz, $^{4}J_{HH}$ = 0.66 Hz), 7.04 (dd, 1H, $^{3}J_{HH}$ = 3.5 Hz, $^{4}J_{HH}$ = 0.7 Hz), 6.45 (dd, 1H, $^{3}J_{HH}$ = 3.5 Hz, $^{4}J_{HH}$ = 1.7 Hz), 5.66 (d, 1H, $^{3}J_{HH}$ = 12.4 Hz), 3.11 (s, 3H), 2.85 (s, 3H). $^{13}C\{^{1}H\}$ NMR (75.5 MHz, $CDCl_3$): 177.5, 154.8, 153.5, 144.1, 113.3, 111.8, 91.5, 51.2, 45.1.

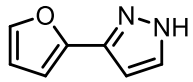

3-(2-furyl)-1H-pyrazole **(2.15b)**

To a 1-neck 250mL round bottom flask equipped with a stir bar was added **2.15a** (2.07g, 0.0126 moles, 1 eq), an excess of hydrazine monohydrate (5.00 g, 0.999 moles), and 100 mL anhydrous ethanol. The solution was heated at reflux overnight (16h). After this time, the flask was allowed to cool to room temperature. The solvent was evaporated under reduced pressure and **2.15b** was crystallized by addition of ice water and storage in the fridge as colourless crystals. Yield: 1.4 g (83%). mp: 117-120°C. ^{1} H NMR (300 MHz, $CDCl_3$) δ 7.62 (d, 1H, $^{3}J_{HH}$ = 2.3 Hz), 7.45 (dd, 1H, $^{3}J_{HH}$ = 1.8 Hz, $^{4}J_{HH}$ = 0.9 Hz), 6.64 (dd, 1H, $^{3}J_{HH}$ = 3.4 Hz, $^{4}J_{HH}$ = 0.9 Hz), 6.53 (d, 1H, $^{3}J_{HH}$ = 3.4 Hz), 6.46 (dd, 1H, $^{3}J_{HH}$ = 3.4 Hz, $^{4}J_{HH}$ = 1.8 Hz), NH resonance not observed. $^{13}C\{^{1}H\}$ NMR (75.5 MHz, $CDCl_3$): 148.5, 142.2, 141.8, 131.4, 111.4, 106.0, 102.0. LRMS ($M\text{-}H^{+}$): 133.

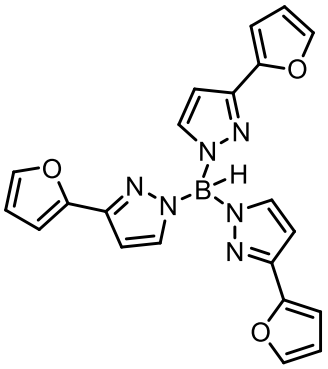

*2'-furyl*tris*(pyrazolyl)borate* (**2.15c)**

To an oven-dried 1-neck 50 mL round bottom flask equipped with a stir bar was added **2.15b** (0.759 g, 0.00566 moles, 1 eq) and sodium borohydride (0.116 g, 0.00308 moles, 0.54 eq). The solid mixture was heated to melting at 200°C for 3h, and the amount of hydrogen gas produced was measured by water displacement. After this time, the melt was allowed to cool to room temperature. Purification by sublimation at 75°C or recrystallization from benzene afforded **2.15c** as white crystals. Yield: 0.35 g (14.8%). Mp >300°C. Selected IR (KBr): 2347, 2285 (B*H*) cm^{-1}. ^{1}H NMR (500 MHz, MeOD): δ 7.50 (m, 3H), 7.42 (m, 3H), 6.61 (m, 3H), 6.41 (m, 3H), 6.31 (m, 3H), BH resonance not observed. $^{13}C\{^{1}H\}$ NMR (125.77 MHz, MeOD): 140.5, 135.7, 110.7, 103.5, 100.6. Two quaternary carbon atoms not observed. $^{11}B\{^{1}H\}$ NMR (160.46 MHz, MeOD): 3.02. HRMS (ESI) calcd for $C_{21}H_{16}N_6O_3B$ (M+H): 411.1377. Found: 411.1388.

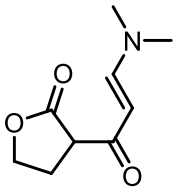

2E-*3-(dimethylamino)-1-γ-lactone-2-en-1-one* **(2.18a)**

To an oven-dried 1-neck 100mL round bottom flask equipped with a Schlenk adaptor and a stir bar was added 3-acetyl butyrolactone (4.76 g, 0.0371 moles), 1 equiv dimethylformamide-dimethylacetal (4.49 g, 0.0374 moles) and 60 mL toluene. This was heated to reflux for 48h. After this time, the flask was allowed to cool to room temperature.

The solvent was removed under reduced pressure to give **2.18a** as an orange-red oil which was carried through the next step. ^{1}H NMR (300 MHz, $CDCl_3$) δ 7.62 (d, 1H, $^{3}J_{HH}$ = 12.5 Hz), 5.24 (d, 1H, $^{3}J_{HH}$ = 12.5 Hz), 4.19 (m, 2H), 3.52 (br s, 1H), 3.08 (s, 3H), 2.84 (s, 3H), 2.75 (m, 1H), 2.27 (m, 1H). ^{13}C{^{1}H} NMR (75.5 MHz, $CDCl_3$): 187.8, 175.8, 154.0, 129.0, 93.7, 68.0, 45.1, 37.2, 25.3.

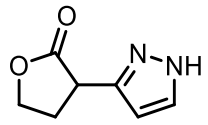

3-γ-lactone-1H-pyrazole **(2.18b)**

To a 1-neck 250 mL round bottom flask equipped with a stir bar was added crude **2.18a**, an excess of hydrazine monohydrate (8.00 g, 0.160 moles), and 100 mL anhydrous ethanol. The solution was heated at reflux at 38h. After this time, the flask was allowed to cool to room temperature. The solvent was evaporated under reduced pressure and diluted with water. The solution was extracted with 3 x 100 mL chloroform, combined, and dried over $MgSO_4$. The solvent was removed under reduced pressure and **2.18b** was isolated as a yellow solid. Yield: 2.56 g (45.8% over two steps). Mp 128-131°C. ^{1}H NMR (300 MHz, MeOD) δ 7.54 (d, 1H, $^{3}J_{HH}$ = 2.0 Hz), 6.28 (d, 1H, $^{3}J_{HH}$ = 2.0 Hz), 3.79 (t, 1H, $^{3}J_{HH}$ = 7.6 Hz), 3.52 (t, 2H, $^{3}J_{HH}$ = 6.4 Hz), 2.21 (ddd, 1H, $^{2}J_{HH}$ = 1.9 Hz, $^{3}J_{HH}$ = 6.4 Hz, $^{3}J_{HH}$ = 7.6 Hz), 2.06 (ddd, 1H, , $^{2}J_{HH}$ = 1.9 Hz, $^{3}J_{HH}$ = 6.4 Hz, $^{3}J_{HH}$ = 7.6 Hz), NH resonance not observed. ^{13}C{^{1}H} NMR (75.5 MHz, DMSO): 171.4, 154.2, 143.6, 102.8, 58.6, 48.6, 35.0. LRMS ($M\text{-}H^{+}$): 151.

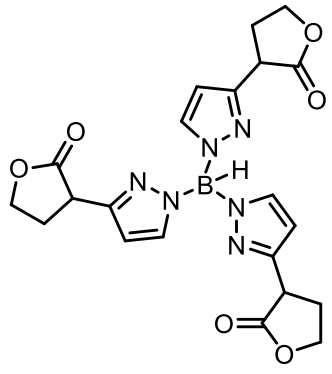

*γ-lactone*tris*(pyrazolyl)borate* **(2.18c)**

To an oven-dried 1-neck 25mL round bottom flask equipped with a stir bar was added **2.18b** (0.645 g, 0.00425 moles, 1 eq) and sodium borohydride (0.102 g, 0.00269 moles, 0.63 eq). The solid mixture was heated to melting at 150°C for 45 minutes, and the amount of hydrogen gas produced was measured by water displacement. After this time, the melt was allowed to cool to room temperature. Purification by sublimation at 95°C afforded **2.18c** as pale yellow crystals. Yield: 0.51 g (21.3 %). Mp >300°C. Selected IR (KBr): 2358, 2341, 2296 (B*H*) cm^{-1}. ^{1}H NMR (500 MHz, MeOD): δ 7.54 (d, 3H, $^{3}J_{HH}$ = 2.0 Hz), 6.23 (d, 3H, $^{3}J_{HH}$ = 2.0 Hz), 3.67 (t, 3H, $^{3}J_{HH}$ = 7.6 Hz), 3.49 (m, 6H), 2.44 (ddd, 3H, $^{2}J_{HH}$ = 1.9 Hz, $^{3}J_{HH}$ = 6.4 Hz, $^{3}J_{HH}$ = 7.6 Hz), 1.99 (ddd, 3H, $^{2}J_{HH}$ = 1.9 Hz, $^{3}J_{HH}$ = 6.4 Hz, $^{3}J_{HH}$ = 7.6 Hz). $^{13}C\{^{1}H\}$ NMR (125.8 MHz, MeOD): 173.1, 141.5, 129.4, 103.3, 59.2, 40.4, 35.1. $^{11}B\{^{1}H\}$ NMR (160.5 MHz, MeOD): 3.11. (ESI) calcd for $C_{21}H_{23}BN_6O_6Na$ (M+H): 489.1670. Found: 489.1793.

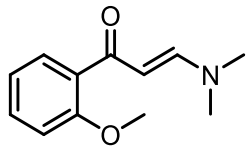

2E-*3-(dimethylamino)-1-(2-methoxyphenyl)-prop-2-en-1-one*

(**2.12a)**

To an oven-dried 250 mL round bottom flask fitted with a Schlenk adaptor and a stir bar was added 2'-methoxyacetophenone (8.72 g, 0.0581 moles, 1 eq) and dimethylformamide-

dimethylacetal (15.3 g, 0.128 moles, 2.2 eq). The solution was heated to reflux for 2 days (38h). After this time, the flask was allowed to cool to room temperature. Addition of a minimal amount of anyhydrous ethyl ether induced precipitation of **2.12a** as olive green crystals. Yield: 5.8 g (48.4%). ^{1}H NMR (300 MHz, $CDCl_3$): δ 7.39 (m, 2H), 7.24 (td, 1H, $^{3}J_{HH}$ = 7.5 Hz, $^{4}J_{HH}$ = 1.9 Hz), 6.88 (overlapping td and d: td, 1H, $^{3}J_{HH}$ = 7.5 Hz, $^{4}J_{HH}$ = 0.8 Hz; d, 1H, $^{3}J_{HH}$ = 8.6 Hz), 5.45 (d, 1H, $^{3}J_{HH}$ = 12.5 Hz), 3.75 (s, 3H), 2.94 (br s, 3H), 2.77 (br s, 3H). ^{13}C{^{1}H} NMR (75.5 MHz, $CDCl_3$): 162.5, 156.8, 154.3, 131.6, 130.5, 129.3, 120.4, 111.4, 98.0, 55.7, 37.1, 36.5.

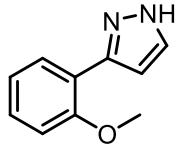

3-(2-methoxyphenyl)-1H-pyrazole **(2.12b)**

To a 1-neck 250 mL round bottom flask was added **2.12a** (5.76 g, 0.0285 moles, 1 eq), an excess of hydrazine monohydrate (12.0 g, 0.240 moles), and 100 mL anhydrous ethanol. The solution was heated to reflux for 2 days (39h). After this time, the flask was allowed to cool to room temperature. The solvent was evaporated under reduced pressure and **2.12b** was crystallized by addition of ice water and storage in the fridge as colourless crystals. Yield: 3.5 g (71.0%). Mp 89-91°C. ^{1}H NMR (300 MHz, $CDCl_3$): δ 10.13 (br s, 1H), 7.69 (dd, 1H, $^{3}J_{HH}$ = 7.6 Hz, $^{4}J_{HH}$ = 1.8 Hz), 7.60 (d, 1H, $^{3}J_{HH}$ = 1.9 Hz), 7.29 (m, 1H), 7.02 (m, 2H), 6.64 (d, 1H, $^{3}J_{HH}$ = 1.8 Hz), 3.98 (s, 3H). ^{13}C{^{1}H} NMR (75.5 MHz, $CDCl_3$): 155.8, 141.0, 138.9, 129.3, 128.0, 121.4, 117.9, 111.6, 102.9, 55.76. LRMS ($M+H^{+}$): 175.

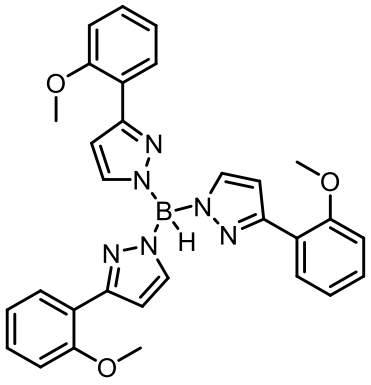

(*2-methoxyphenyl)*tris*(pyrazolyl)borate* **(2.12c)**

To an oven-dried 1-neck 50 mL round bottom flask equipped with a stir bar was added **2.12b** (1.50 g, 0.00862 moles, 1 eq) and sodium borohydride (0.109 g, 0.00287 moles, 0.33 eq). The solid mixture was heated to melting at 200°C for 1h, and the amount of hydrogen gas produced was measured by water displacement. After this time, the melt was allowed to cool to room temperature. Purification by sublimation at 75°C or recrystallization from benzene afforded **2.12c** as white crystals. Yield: 0.35 g (14.8%). Mp >300°C. Selected IR (KBr): 2364, 2263 (B*H*) cm^{-1}. ^{1}H NMR (500 MHz, MeOD): δ 7.65 (d, 3H, $^{3}J_{HH}$ = 7.5 Hz), 7.54 (d, 3H, $^{3}J_{HH}$ = 1.5 Hz), 7.27 (m, 3H), 7.03 (d, 3H, $^{3}J_{HH}$ = 8.4 Hz), 6.96 (td, 3H, $^{3}J_{HH}$ = 7.5 Hz, $^{4}J_{HH}$ = 1.0 Hz), 6.67 (d, 3H, $^{3}J_{HH}$ = 1.5 Hz), 3.86 (s, 9H), BH resonance not observed. $^{13}C\{^{1}H\}$ NMR (125.8 MHz, MeOD): 156.5, 139.4, 129.3, 128.0, 123.9, 120.7, 118.1, 111.3, 96.8, 54.8. $^{11}B\{^{1}H\}$ NMR (160.5 MHz, MeOD): 2.96. HRMS (ESI) calcd for $C_{21}H_{17}N_6O_3B$ (M+H): 411.1377. Found: 411.1388.

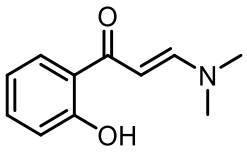

2E-*3-(dimethylamino)-1-(2-hydroxyphenyl)-prop-2-en-1-one*

(2.13a)

In a 2-neck 100 mL round bottom flask was added 2'-hydroxyacetophenone (5.66 g, 0.0415 moles, 1 eq) and dimethylformamide-dimethylacetal (5.32 g, 0.0449 moles, 1.1 eq).

This solution was heated to reflux overnight (21h). After this time, the flask was allowed to cool to room temperature. A minimal amount of pentane was added to induce precipitation of **2.13a** which was filtered, washed with ice cold methanol, and collected as yellow crystals. Yield: 7.6 g (95.4%). ^{1}H NMR (300 MHz, $CDCl_3$) δ 7.87 (s, 1H), 7.67 (dd, 1H, $^{3}J_{HH}$ = 8.2 Hz, $^{4}J_{HH}$ = 1.7 Hz), 7.33 (ddd, 1H, $^{3}J_{HH}$ = 8.4 Hz. $^{3}J_{HH}$ = 7.2 Hz, $^{4}J_{HH}$ = 1.7 Hz), 6.92 (dd, 1H, $^{3}J_{HH}$ = 8.4 Hz), 6.80 (m, 1H), 5.78 (s, 1H), 3.13 (s, 3H), 2.98 (s, 3H). $^{13}C\{^{1}H\}$c NMR (75.5 MHz, $CDCl_3$): 191.4, 162.9, 154.8, 133.9, 128.3, 120.3 118.2, 118.0, 90.0, 45.4, 37.4.

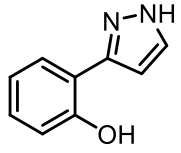

3-(2-hydroxyphenyl)-1H-pyrazole **(2.13b)**

To a 1-neck 100 mL round bottom flask equipped with a stir bar is added **2.13a** (3.08 g, 0.0161 moles, 1 eq), an excess of hydrazine monohydrate (6.00 g, 0.120 moles), and 40 mL anhydrous ethanol. The solution was heated at reflux for 2h. After this time, the flask was allowed to cool to room temperature. The solvent was evaporated under reduced pressure and **2.13b** was crystallized by addition of ice water and storage in the fridge as colourless crystals. Yield: 1.4 g (53.7%). mp: 106-108°C. ^{1}H NMR (300 MHz, $CDCl_3$) δ 10.90 (br s, 1H), 10.34 (br s, 1H), 7.61 (d, 1H, $^{3}J_{HH}$ = 2.67 Hz), 7.59 (dd, 1H, $^{3}J_{HH}$ = 7.79 Hz, $^{4}J_{HH}$ = 1.86 Hz), 7.21 (ddd, 1H, $^{3}J_{HH}$ = 8.26 Hz, $^{3}J_{HH}$ = 7.14 Hz, $^{4}J_{HH}$ = 1.86 Hz), 7.03 (dd, 1H, $^{3}J_{HH}$ = 8.31 Hz, $^{4}J_{HH}$ = 1.08 Hz), 6.91 (td, 1H, $^{3}J_{HH}$ = 7.34 Hz, $^{4}J_{HH}$ = 1.34 Hz), 6.71 (d, 1H, $^{3}J_{HH}$ = 2.59 Hz). $^{13}C\{^{1}H\}$ NMR (75.5 MHz, $CDCl_3$): 155.8, 129.3, 129.1, 126.6, 119.4, 117.0, 116.6, 102.0. LRMS ($M\text{-}H^{+}$): 159

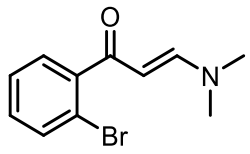

2E-*3-(dimethylamino)-1-(2-bromophenyl)-prop-2-en-1-one* **(2.16a)**

To an oven-dried 250 mL round bottom flask fitted with a Schlenk adaptor and a stir bar was added 2'-bromoacetophenone (4.43 g, 0.0222 moles, 1 eq) and dimethylformamide-dimethylacetal (5.38 g, 0.0449 moles, 2.0 eq). The solution was heated at reflux overnight (19h). After this time, the flask was allowed to cool to room temperature. Excess solvent was removed under reduced pressure to collect **2.16a** as a red-orange oil which was carried through to the next step. ^{1}H NMR (300 MHz, $CDCl_3$) δ 7.46 (d, 1H, $^{3}J_{HH}$ = 12.3 Hz), 7.31-7.09 (m, 4H), 5.18 (d, 1H, $^{3}J_{HH}$ = 12.3 Hz), 2.89 (s, 3H), 2.72 (s, 3H). ^{13}C{^{1}H} NMR (75.5 MHz, $CDCl_3$): 206.7, 162.3, 156.0, 132.8, 129.8, 128.5, 127.0, 119.1, 98.0, 45.0, 37.3.

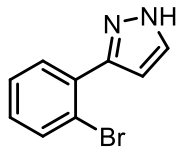

3-(2-bromophenyl)-1H-pyrazole **(2.16b)**

To a 1-neck 250 mL round bottom flask equipped with a stir bar was added **2.16a** (5.36 g, 0.0222 moles, 1 eq), an excess of hydrazine monohydrate (5.00 g, 0.100 moles), and 150 mL anhydrous ethanol. The solution was heated at reflux overnight (16h). After this time, the flask was allowed to cool to room temperature. The solvent was evaporated under reduced pressure and **2.16b** was crystallized by addition of ice water to a saturated solution in dichloromethane and storage in the fridge as pale yellow crystals. Yield: 2.0 g (41.2%). Mp 135-138°C. ^{1}H NMR (300 MHz, $CDCl_3$) δ 7.52 (td, 1H, $^{3}J_{HH}$ = 8.0 Hz, $^{4}J_{HH}$ = 1.1), 7.45 (m, 2H), 7.19 (td, 1H, $^{3}J_{HH}$ = 7.7 Hz, $^{4}J_{HH}$ = 1.3 Hz), 7.35 (td, 1H, $^{3}J_{HH}$ = 7.7 Hz, $^{4}J_{HH}$ = 1.3 Hz), 6.59 (d, 1H, $^{3}J_{HH}$ = 2.2 Hz), NH resonance not observed. ^{13}C{^{1}H} NMR (75.5

MHz, $CDCl_3$): 161.5, 147.5, 133.7, 132.0, 131.0, 129.5, 127.5, 121.8, 106.3. LRMS ($M+H^+$): 223.

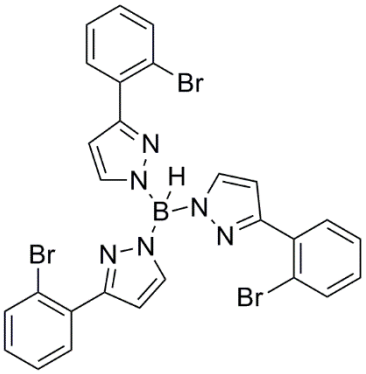

(*2-bromophenyl)*tris*(pyrazolyl)borate* **(2.16c)**

To an oven-dried 1-neck 50 mL round bottom flask equipped with a stir bar was added **2.16b** (1.81 g, 0.00814 moles, 1 eq) and sodium borohydride (0.116 g, 0.00308 moles, 0.37 eq). The solid mixture was heated to melting at 200ºC for 3h, and the amount of hydrogen gas produced was measured by water displacement. After this time, the melt was allowed to cool to room temperature. Purification by sublimation at 75ºC or recrystallization from benzene afforded **2.16c** as pale yellow crystals. Yield: 0.84 g (39.1%). Mp >300°C. Selected IR (KBr): 2364, 2341 (B*H*) cm^{-1}. ^1H NMR (500 MHz, MeOD): δ 7.67 (d, 6H, $^3J_{HH}$ = 8.5 Hz), 7.53 (d, 3H, $^3J_{HH}$ = 7.7 Hz), 7.37 (t, 3H, $^3J_{HH}$ = 7.7 Hz), 7.24 (t, 3H, 7.7 Hz), 6.63 (s, 3H), BH resonance not observed. $^{13}C\{^1H\}$ NMR (125.8 MHz, MeOD): 133.3, 131.1, 129.4, 127.3, 122.1, 105.8. One quaternary carbon not observed. ^{11}B NMR (160.5 MHz, MeOD): 2.91. MS (ESI) calcd for $C_{27}H_{19}BBr_3N_6Na_2$ ($M+Na^+$): 720.9110. Found: 720.8642.

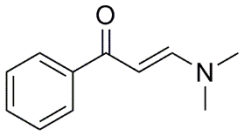

2E-*3-(dimethylamino)-1-(phenyl)-prop-2-en-1-one* **(2.14a)**

To a 250 mL round bottom flask fitted with a Schlenk adaptor and a stir bar was added acetophenone (7.21 g, 0.0600 moles, 1 eq) and dimethylformamide-dimethylacetal (8.96 g, 0.0751 moles, 1.3 eq). The solution was heated at reflux overnight (19h). After this time, the flask was allowed to cool to room temperature. A minimal amount of anhydrous ethyl ether was added to induce precipitation of **2.14a** as a yellow solid. Yield: 5.5 g (47.6 %). ^{1}H NMR (300 MHz, $CDCl_3$): δ 7.87 (m, 2H), 7.78 (d, 1H, 12.4 Hz), 7.39 (m, 3H), 5.69 (d, 1H, 12.4 Hz), 3.10 (s, 3H), 2.91 (s, 3H). $^{13}C\{^{1}H\}$ NMR (75.5 MHz, $CDCl_3$): 188.7, 154.2, 140.5, 130.9, 128.1, 127.5, 92.2, 44.8, 37.0.

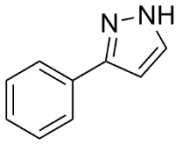

3-phenyl-1H-pyrazole **(2.14b)**

To a 1-neck 250 mL round bottom flask equipped with a stir bar was added **2.14a** (4.69 g, 0.0245 moles, 1 eq), an excess of hydrazine monohydrate (3.00 g, 0.060 moles), and 100 mL anhydrous ethanol. The solution was heated at reflux for 16h. After this time, the flask was allowed to cool to room temperature. The solvent was evaporated under reduced pressure and **2.14b** was redissolved in acetone, dried over anhydrous magnesium sulphate, filtered to remove the solid and concentrated under reduced pressure to yield **2.14b** as colourless crystals. Yield: 3.3 g (94.5 %). Mp 80-82°C. ^{1}H NMR (300 MHz, $CDCl_3$): δ 7.79 (m, 2H), 7.60 (d, 1H, $^{3}J_{HH}$ =2.3 Hz), 7.37 (m, 3H), 6.61 (d, 1H, $^{3}J_{HH}$ = 2.3 Hz), NH resonance not observed. $^{13}C\{^{1}H\}$ NMR (75.5 MHz, $CDCl_3$): 149.2, 133.3, 132.3, 128.8, 128.0, 125.9, 102.7. LRMS ($M\text{-}H^{+}$): 143.

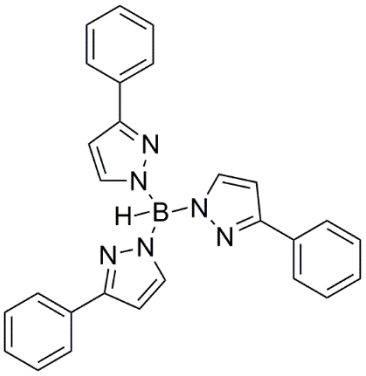

*phenyl*tris*(pyrazolyl)borate* **(2.14c)**

To a flame-dried 1-neck 25 mL round bottom flask equipped with a stir bar was added **2.14b** (4.619 g, 0.0321 moles, 1 eq) and sodium borohydride (0.463 g, 0.0122 moles, 0.38eq). The solid mixture was heated to melting at 200ºC for 2h, and the amount of hydrogen gas produced was measured by water displacement. After this time, the melt was allowed to cool to room temperature. Purification by sublimation at 75ºC or recrystallization from benzene afforded **2.14c** as white crystals. Yield: 2.1 g (39.2%). Mp >300°C. Selected IR (KBr): 2352 (B*H*) cm^{-1}. ^{1}H NMR (500 MHz, MeOD): δ 7.79 (m, 6H), 7.54 (d, 3H, $^{3}J_{HH}$ = 2.1 Hz), 7.40 (m, 6H), 7.23 (dt, 3H, $^{3}J_{HH}$ = 7.0 Hz, $^{4}J_{HH}$ = 1.1 Hz), 6.42 (d, 3H, $^{3}J_{HH}$ = 2.1 Hz). $^{13}C\{^{1}H\}$ NMR (125.8 MHz, MeOD): 152.8, 136.1, 134.7, 128.6, 128.2, 126.7, 125.7, 102.0. ^{11}B NMR (160.5 MHz, MeOD): 3.22. HRMS (ESI) calcd for: $C_{27}H_{23}BN_6Na$ ($M+H^+$): 465.1969. Found: 465.1969.

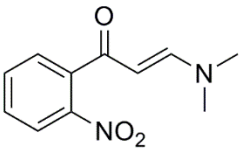

2E-*3-(dimethylamino)-1-(2-nitrophenyl)-prop-2-en-1-one* **(2.17a)**

To a 100 mL round bottom flask fitted with a Schlenk adaptor and a stir bar is added 2'-nitroacetophenone (9.91 g, 0.0600 moles) and dimethylformamide-dimethylacetal (7.27 g, 0.0601 moles, 1 eq). The solution was heated at reflux for 30h. After this time, the flask

was allowed to cool to room temperature. A minimal amount of anhydrous ethyl ether was added to induce precipitation of **2.17a** as a yellow solid. Yield: 8.4 g (64 %). ^{1}H NMR (300 MHz, $CDCl_3$): δ 7.88 (d, 1H, $^{3}J_{HH}$ = 8.1 Hz), 7.56 (td, 1H, $^{3}J_{HH}$ = 7.6 Hz, $^{4}J_{HH}$ = 1.1 Hz), 7.44 (m, 3H), 5.22 (d, 1H, $^{3}J_{HH}$ = 12.7 Hz), 3.03 (s, 3H), 2.81 (s, 3H). $^{13}C\{^{1}H\}$ NMR (75.5 MHz, $CDCl_3$): 188.8, 154.9, 147.3, 138.5, 133.0, 129.4, 128.9, 124.1, 95.6, 45.1, 37.2.

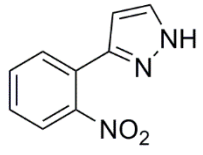

3-(2-nitrophenyl)-1H-pyrazole **(2.17b)**

To a 1-neck 500 mL round bottom flask equipped with a stir bar was added **2.17a** (8.45 g, 0.0384 moles), an excess of hydrazine monohydrate (5.00 g, 0.100 moles), and 300 mL anhydrous ethanol. The solution was heated at reflux for 38h. After this time, the flask was allowed to cool to room temperature. The solvent was evaporated under reduced pressure and **2.17b** was crystallized by addition of ice water and storage in the fridge as colourless crystals. Yield: 6.7 g (93%) mp: 100-106°C. ^{1}H NMR (300 MHz, $CDCl_3$): δ 7.69 (m, 2H), 7.57 (m, 2H), 7.44 (td, 1H, $^{3}J_{HH}$ = 7.7 Hz, $^{4}J_{HH}$ = 1.5 Hz), 6.47 (d, 1H, $^{3}J_{HH}$ = 2.4 Hz), NH resonance not observed. $^{13}C\{^{1}H\}$ NMR (75.5 MHz, $CDCl_3$): 149.2, 131.9, 130.9, 130.7, 128.6, 126.9, 123.6, 104.8. LRMS ($M\text{-}H^{+}$): 188.

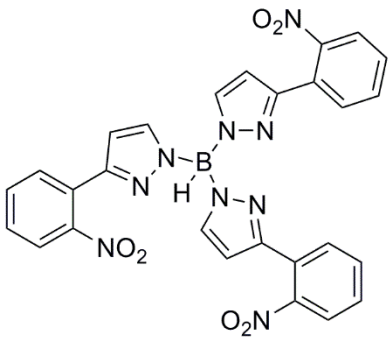

(*2-nitrophenyl)*tris*(pyrazolyl)borate* **(2.17c)**

To a flame-dried 1-neck 25 mL round bottom flask equipped with a stir bar was added **2.17b** (1.54 g, 0.00813 moles, 1 eq) and sodium borohydride (0.125 g, 0.00330 moles, 0.41 eq). The solid mixture was heated to melting at 200°C for 1h, and the amount of hydrogen gas produced was measured by water displacement. After this time, the melt was allowed to cool to room temperature. Purification by sublimation at 75°C or recrystallization from benzene afforded **2.17c** as dark red crystals. Yield: 0.74g (65%) Mp > 300°C. Selected IR (KBr): 2365, 2346 (B*H*) cm^{-1}. ^{1}H NMR (500 MHz, MeOD): 7.76 (dd, 1H, $^{3}J_{HH}$ = 8.3 Hz, $^{4}J_{HH}$ = 1.2 Hz), 7.68 (m, 4H), 7.52 (td, 1H, $^{3}J_{HH}$ = 7.9 Hz, $^{4}J_{HH}$ = 1.5 Hz), BH resonance not observed. $^{13}C\{^{1}H\}$ NMR (125.8 MHz, MeOD): 131.8, 130.9, 128.8, 128.1, 123.5, 117.5, 116.5, 104.1. $^{11}B\{^{1}H\}$ NMR (160.5 MHz, MeOD): 2.80. MS (ESI) calcd for $C_{27}H_{19}BN_9O_6Na_2$ ($M+Na^+$): 622.1347. Found: 622.0882.

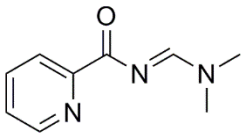

N-(dimethylamino)methylene-2-pyridinecarboxamide **(2.19a)**

In a 1-neck 100 mL round bottom flask equipped with a stir bar was added benzamide (8.76 g, 0.0789 moles, 1 eq), dimethylformamide-dimethylacetal (8.97 g, 0.0754 moles, 1 eq), and 40 mL THF. The solution was allowed to stir at room temperature overnight (21h). Removal of solvent under reduced pressure yielded **2.19a** as a yellow oil. Yield: 4.5 g (32 %). ^{1}H NMR (300 MHz, $CDCl_3$): δ 8.67 (ddd, 1H, $^{3}J_{HH}$ = 7.2 Hz, $^{4}J_{HH}$ = 1.3 Hz, $^{5}J_{HH}$ =

0.8 Hz), 8.61 (s, 1H), 8.23 (td, 1H, $^{3}J_{HH}$ = 7.2 Hz, $^{4}J_{HH}$ = 1.3 Hz), 7.71 (td, 1H, $^{3}J_{HH}$ = 7.2 Hz, $^{4}J_{HH}$ = 1.3 Hz), 7.30 (ddd, 1H, $^{3}J_{HH}$ = 7.2 Hz, $^{4}J_{HH}$ = 1.3 Hz, $^{5}J_{HH}$ = 0.8 Hz), 3.16 (s, 3H), 3.12 (s, 3H). $^{13}C\{^{1}H\}$ NMR (75.5 MHz, $CDCl_3$): 160.8, 141.4, 137.7, 123.3, 122.7, 119.7, 109.7, 34.8, 32.0.

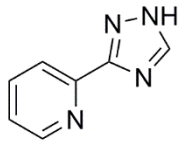

2-(1H-1,2,4-triazole-3-yl)-pyridine **(2.19b)**

In a 1-neck 250 mL round bottom flask equipped with a stir bar was added **2.19a** (4.51 g, 0.0255 moles, 1eq), an excess of hydrazine monohydrate (7.00g, 0.140 moles), and 200 mL anhydrous ethyl alcohol. The solution was heated at reflux for 6 h after which, the solution was allowed to cool to room temperature and the solvent was removed under reduced pressure. The resulting yellow oil was redissolved in water, extracted into chloroform twice (70 mL), and dried over magnesium sulphate. After filtration to remove the solid, the solvent was removed under reduced pressure to yield **2.19b** as a yellow solid. Yield: 3.1 g (82 %). Mp 95-97°C. ^{1}H NMR (300 MHz, $CDCl_3$): δ 9.03 (br s, 1H), 8.53 (ddd, 1H, $^{3}J_{HH}$ = 4.7 Hz, $^{4}J_{HH}$ = 1.7 Hz, $^{5}J_{HH}$ = 0.9 Hz), 8.14 (dt, 1H, $^{3}J_{HH}$ = 7.8 Hz, $^{4}J_{HH}$ = 1.1 Hz), 7.83 (td, 1H, $^{3}J_{HH}$ = 7.8 Hz, $^{4}J_{HH}$ = 1.7 Hz), 7.40 (m, 1H), NH resonance not observed. $^{13}C\{^{1}H\}$ NMR (75.5 MHz, $CDCl_3$): 149.0, 148.4, 148.3, 137.3, 126.5, 122.5, 122.2. LRMS ($M\text{-}H^{+}$): 145.

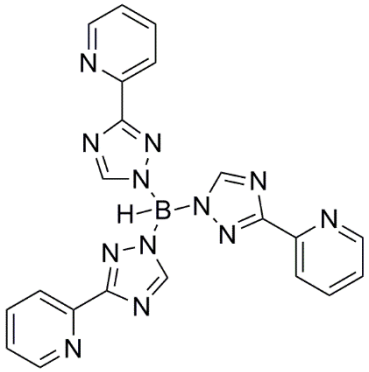

*2'-pyridyl*tris*(triazolyl)borate* **(2.19c)**

To an oven-dried 1-neck 50 mL round bottom flask equipped with a stir bar was added **2.19b** (3.32 g, 0.0228 moles, 1 eq) and sodium borohydride (0.330 g, 0.00873 moles, 0.38 eq). The solid mixture was heated to melting at 200°C for 1h, and the amount of hydrogen gas produced was measured by water displacement. After this time, the melt was allowed to cool to room temperature. Purification by sublimation at 90°C or recrystallization from benzene afforded **2.19c** as yellow crystals. Yield: 1.0 g (26.3%). Mp >300°C. Selected IR (KBr): 2375 (B*H*) cm^{-1}. ^{1}H NMR (300 MHz, MeOD): δ 8.60 (ddd, 3H, $^{3}J_{HH}$ = 4.7 Hz, $^{4}J_{HH}$ = 1.8 Hz, $^{5}J_{HH}$ = 1.2 Hz), 8.31 (dt, 1H, $^{3}J_{HH}$ = 7.9 Hz, $^{4}J_{HH}$ = 1.2 Hz), 7.90 (dd, 1H, $^{3}J_{HH}$ = 7.9 Hz, $^{4}J_{HH}$ = 1.8 Hz), 7.42 (ddd, 1H, $^{3}J_{HH}$ = 7.6 Hz, $^{3}J_{HH}$ = 4.7 Hz, $^{5}J_{HH}$ = 1.2 Hz). $^{13}C\{^{1}H\}$ NMR (75.5 MHz, MeOD): 160.4, 150.6, 150.5, 149.9, 125.2, 123.1, 122.6. ^{11}B NMR (115.5 MHz, MeOD): 5.79. HRMS (ESI) calcd for $C_{21}H_{16}N_{12}B$: 447.171393. Found: 447.17217.

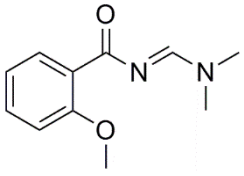

N-(dimethylamino)methylene-2-methoxy-benzamide **(2.10a)**

To a 1-neck 100 mL round bottom flask equipped with a stir bar is added 2'-methoxybenzamide (9.32 g, 0.0651 moles, 1 eq), dimethylformamide-dimethylacetal (8.16g, 0.0686 moles, 1 eq), and 60 mL THF. This is stirred at room temperature overnight

(16h). Removal of the solvent under reduced pressure yields **2.10a** as a yellow oil. Yield: 9.8 g (77.7 %). ^{1}H NMR (300 MHz, $CDCl_3$): δ 8.13 (dd, 1H, $^{3}J_{HH}$ =7.91 Hz, $^{4}J_{HH}$ = 1.91 Hz), 7.91 (s, 1H), 7.40 (ddd, 1H, $^{3}J_{HH}$ = 8.39 Hz, $^{3}J_{HH}$ = 7.91 Hz, $^{4}J_{HH}$ = 1.91 Hz), 7.01 (m, 1H), 6.15 (s, 1H), 3.89 (s, 3H), 2.87 (s, 3H), 2.80 (s, 3H). ^{13}C{^{1}H} NMR (75.5 MHz, $CDCl_3$): 178.8, 167.1, 162.5, 157.8, 133.3, 131.8, 121.2, 111.9, 55.9, 35.3, 31.4.

3-(2-methoxyphenyl)-1H-1,2,4-triazole **(2.10b)**

To a 1-neck 250mL round bottom flask equipped with a stir bar was added **2.10a** (9.82 g, 0.0477 moles, 1 eq), excess hydrazine monohydrate (7.00g, 0.140 moles), and 200 mL anhydrous ethyl alcohol. This mixture was heated to reflux for two days (38h). After this time, the solution was allowed to cool to room temperature and the solution is concentrated under reduced pressure. The resulting oil was redissolved in water, extracted into dichloromethane 2 w (150 mL) and dried over magnesium sulphate. After filtration to remove solid and concentration under reduced pressure, crude **2.10b** was collected as a pale pink solid. Purification was carried out by column chromatography, using: 90:10 chloroform:methanol. Yield: 3.8 (19.2 %). mp: 116-119°C. ^{1}H NMR (300 MHz, DMSO): δ 7.86 (dd, 1H, $^{3}J_{HH}$ =7.6 Hz, $^{4}J_{HH}$ = 1.8 Hz), 7.68 (br s, 1H), 7.52 (overlapping br s, ddd, 2H, $^{3}J_{HH}$ = 8.4 Hz, $^{3}J_{HH}$ = 7.4, $^{4}J_{HH}$ = 1.9 Hz), 7.18 (d, 1H, $^{3}J_{HH}$ =8.4 Hz), 7.08 (td, 1H, $^{3}J_{HH}$ =7.4 Hz, $^{4}J_{HH}$ = 0.9 Hz), 3.94 (s, 3H). ^{13}C{^{1}H} NMR (75.5 MHz, DMSO): 166.3, 162.3, 157.2, 132.4, 130.7, 122.7, 120.7, 111.9, 55.8. LRMS ($M+H^{+}$): 176.

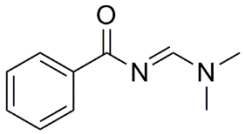

N-(dimethylamino)methylene-benzamide **(2.20a)**

To an oven-dried 1-neck 100mL round bottom flask equipped with a stir bar was added benzamide (8.76 g, 0.0789 moles, 1 eq), dimethylformamide-dimethylacetal (8.97 g, 0.0754 moles, 1 eq), and 40 mL THF. This mixture was stirred at room temperature overnight (16h). After this time, the reaction was concentrated under reduced pressure to yield **2.20a** as a pale yellow oil The crude product was carried through the next step. ^{1}H NMR (300 MHz, $CDCl_3$): δ 8.55 (s, 1H), 8.20 (d, 2H, $^{3}J_{HH}$ = 7.5 Hz), 7.37 (m, 3H), 3.11 (s, 3H), 3.07 (s, 3H). $^{13}C\{^{1}H\}$ NMR (75.5 MHz, $CDCl_3$): 177.7, 160.7, 136.8, 131.8, 129.7, 127.9, 41.3, 35.2.

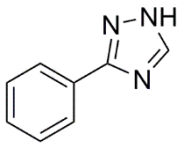

3-phenyl-1H-1,2,4-triazole **(2.20b)**

To a 250 mL 1-neck round bottom flask equipped with a stir bar was added **2.20a**, hydrazine monohydrate (6.00 g, 0.120 moles, 1 eq), and 200 mL anhydrous ethanol. This mixture was heated to reflux overnight (13.5h). After this time, the flask was allowed to cool to room temperature. The solvent was evaporated under reduced pressure and the residue was crystallized by addition of ice water and storage in the fridge to afford **2.20b** as colourless crystals. Yield: 2.23 g (19.5 % over two steps). Mp 127-130°C. ^{1}H NMR (300 MHz, DMSO): δ 7.98 (br s, 1H), 7.87 (m, 2H), 7.48 (m, 3H), 7.36 (br s, 1H). $^{13}C\{^{1}H\}$ NMR (75.5 MHz, DMSO): 168.0, 160.0, 134.2, 131.2, 128.2, 127.4. LRMS ($M\text{-}H^{+}$): 144.

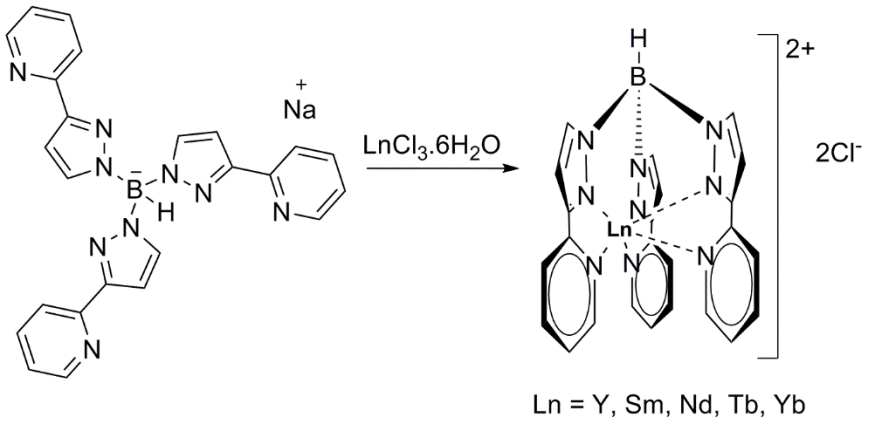

All ligand-metal complexes were prepared in the same way. To a 50 mL 1-neck round-bottom flask equipped with a stir bar was added one equivalent of lanthanide trichloride hexahydrate, one equivalent of **2.11c**, and 25 mL of methanol. This was stirred at room temperature overnight (16-22h). After this time, the solution was concentrated to a solid which was washed extensively with water to remove any excess sodium chloride and the resulting complexes were dried under vacuum.

[Yb(Tpz$^{2'py}$)]Cl$_2$ (2.27): yellow solid, Mp > 300°C, selected IR (KBr): 2365 cm^{-1}. ^{1}H NMR (298 K, 360 MHz, DMSO): δ 79.3 (br s, 3H, $\nu_{1/2}$ = 125 Hz), 61.6 (br s, 3H, $\nu_{1/2}$ = 150 Hz), 55.5 (br s, 3H, $\nu_{1/2}$ = 140 Hz), 37.7 (br s, 3H, $\nu_{1/2}$ = 100 Hz), -53.6 (br s, 3H, $\nu_{1/2}$ = 150 Hz), 108.8 (br s, 3H, $\nu_{1/2}$ = 260 Hz). LRMS: [Yb(Tpz$^{2'py}$)]Cl$_2$ · Tpz$^{2'py}$ClNa: 1143 (isotoπc match for one Yb).

[Sm(Tpz$^{2'py}$)]Cl$_2$ (2.29): pale yellow solid, Mp > 300°C, selected IR (KBr): 2373, 2357, 2344 cm^{-1}. ^{1}H NMR (298 K, 360 MHz, DMSO): δ 13.1 (s, 3H, $\nu_{1/2}$ = 15 Hz), 8.53 (s, 3H, $\nu_{1/2}$ = 10 Hz), 7.9 (s, 3H, $\nu_{1/2}$ = 5 Hz), 7.78 (s, 6H, $\nu_{1/2}$ = 15 Hz), 6.8 (s, 6H, $\nu_{1/2}$ = 10 Hz).

[Nd(Tpz$^{2'py}$)]Cl$_2$ (2.30): pale yellow solid, Mp > 300°C, selected IR (KBr): 2395, 2341, 2274 cm^{-1}. ^{1}H NMR (298 K, 360 MHz, MeOD): δ 20.2 (br s, 3H, $\nu_{1/2}$ = 360 Hz), 14.5 (br

s, 3H, $\nu_{1/2}$ = 270 Hz), 12.8 (br s, 3H, $\nu_{1/2}$ = 180 Hz), 10.8 (br s, 3H, $\nu_{1/2}$ = 180 Hz), 9.2 (br s, 3H, $\nu_{1/2}$ = 180 Hz), -1.0 (br s, 3H, $\nu_{1/2}$ = 270 Hz).

[Y(Tpz$^{2'py}$)]Cl$_2$ (2.31): pale yellow solid, Mp > 300°C, IR (KBr): 2358, 2347 cm^{-1}. ^{1}H NMR (298 K, 500 MHz, MeOD): δ 9.72 (d, 1*H*, $^3J_{HH}$ = 5.3 Hz), 7.98 (m, 2*H*), 7.73 (d, 1*H*, $^3J_{HH}$ = 1.9 Hz), 7.45 (m, 1*H*), 6.89 (d, 1*H*, $^3J_{HH}$ = 1.9 Hz). ^{13}C NMR (125.77 MHz, MeOD): 151.8, 148.9, 139.1, 137.6, 122.9, 120.7, 102.5. ^{11}B NMR (166.43 MHz, MeOD): 18.46.

[Tb(Tpz$^{2'py}$)]Cl$_2$ (2.32): colourless solid, Mp > 300°C, selected IR (KBr): 2397 cm^{-1}. ^{1}H NMR (298 K, 360 MHz, DMSO): δ 28.6, 26.8 (overlapping br s, 6H, $\nu_{1/2}$ = 65 Hz), -18.7 (br s, 6H, $\nu_{1/2}$ = 125 Hz), -41.9 (br s, 6H, $\nu_{1/2}$ = 65 Hz).

[Eu(Tpz$^{2'py}$)]Cl$_2$ (2.33): pale yellow solid, Mp > 300°C, selected IR (KBr): 2364 cm^{-1}. ^{1}H NMR (298 K, 360 MHz, MeOD): δ 6.3 (br s, 3H, $\nu_{1/2}$ = 35 Hz), 5.7 (br s, 3H, $\nu_{1/2}$ = 35 Hz), 5.4 (br s, 3H, $\nu_{1/2}$ = 35 Hz), 2.9 (br s, 3H, $\nu_{1/2}$ = 30 Hz), 2.2 (s, 3H, $\nu_{1/2}$ = 10 Hz), 1.7 (br s, 3H, $\nu_{1/2}$ = 35 Hz).

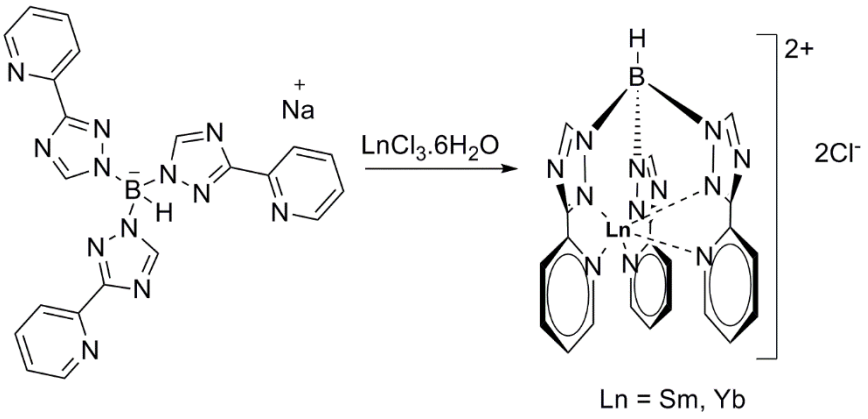

All complexes were prepared in the same way. To a 50 mL 1-neck round-bottom flask equipped with a stir bar was added one equivalent of lanthanide trichloride hexahydrate, one equivalent of **9c**, and 25 mL of methanol. This was stirred at room temperature overnight (16-22h). After this time, the solution was concentrated to a solid which was

washed extensively with water to remove any excess sodium chloride and the resulting complexes were dried under vacuum.

[Yb(Ttz$^{2'py}$)]Cl$_2$ (2.34): bright yellow solid, Mp > 300°C, selected IR (KBr): 2373, 2357, 2338 cm^{-1}.

Chapter 3: Introduction to Part II

3.1 Colour chemistry

There is a great deal of interest in chromophores that absorb strongly in visible (350-750 nm) and near-infrared region (800-3000 nm) of the electromagnetic spectrum.[64-66] The interest in these chromophores is due to a variety of applications including textiles, health applications like diagnostics and treatment, renewable energy, and electronic materials. These chromophores come in variety of forms including inorganic chromophores (metal containing), organic chromophores, and nanostructured materials.[67-69] Organic chromophores are of interest as they can be structurally modified, tuned electronically, and solubilized for organic solvents or water.[70-72] There are almost endless examples of highly coloured compounds that show outstandingly diverse structural architecture and applications. A few representative examples are in **Figure 19**.[73]

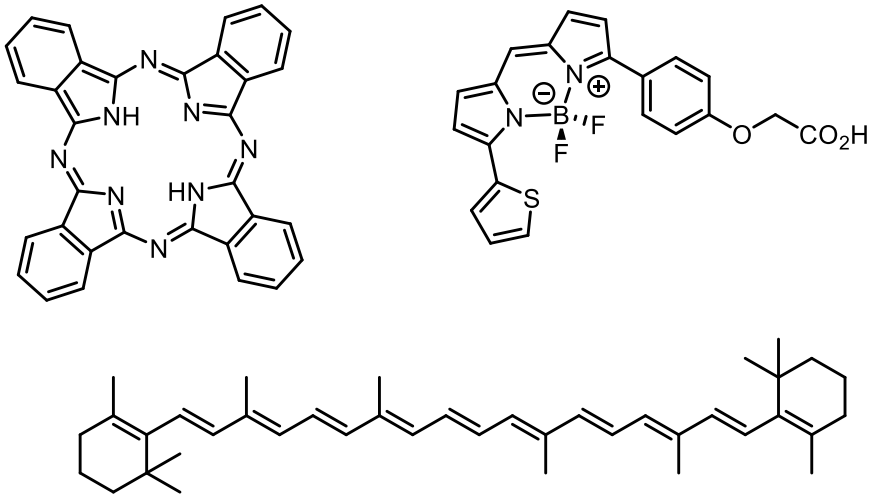

Figure 19. Examples of coloured compounds (clockwise from left): phthalocyanine, boron dipyrromethene (BoDIPY), and β-carotene.

3.2 Indigo: A brief history of discovery and synthesis

Indigo (**3.1**, molecular structure and colour in solution shown in **Figure 20**) is arguably the most famous organic pigment. It has been known for over 4000 years and was used a textile dye in China and India.[74-75] Since its discovery, indigo has become a billion dollar a year industry with thousands of tonnes manufactured annually. The high demand for indigo is in large part due to its extensive use as a colourant in the denim industry where more than one billion pairs of jeans were produced in 2010 alone.[76]

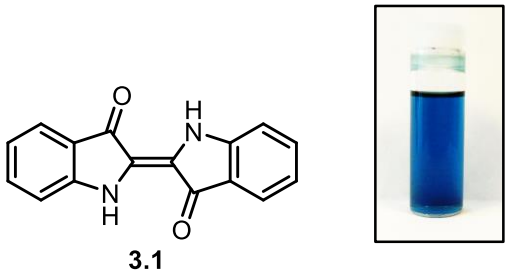

3.1

Figure 20. The molecular structure of indigo (**3.1**) (left) and a photograph of an ~100 micromolar solution of indigo in dimethylsulfoxide (right).

Natural indigo results from the decomposition of indican – a glycoside unit found in *Indigofera Tinctoria,* a shrub found in Asia and some parts of Africa. This glycoside is susceptible to hydrolysis, and upon decomposition with water will yield glucose and an indoxyl (3-hydroxyindole) monomer. This indoxyl unit is very oxygen sensitive and will rapidly dimerize under mild oxidative conditions to indigo (**Scheme 21**).[74]

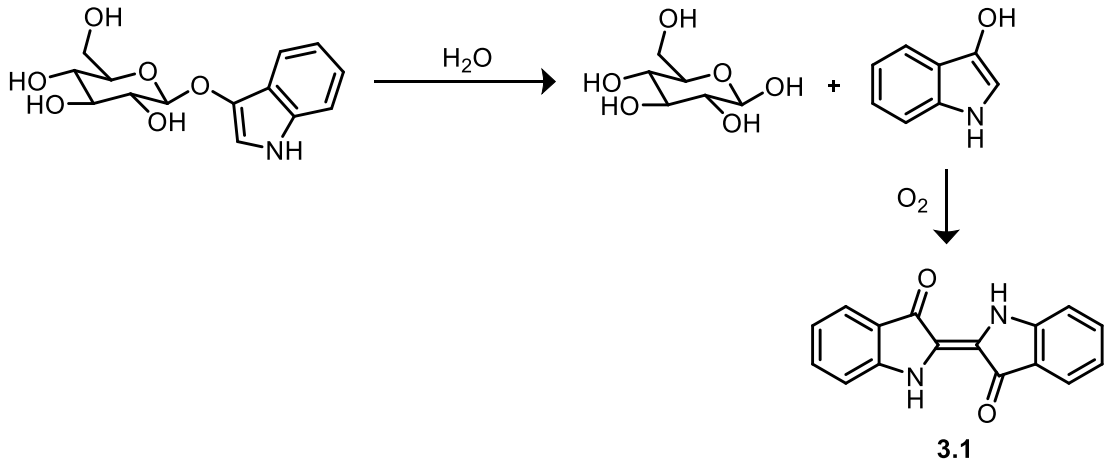

Scheme 21. The biosynthesis of indigo (**3.1**) from indican via rapid dimerization of indoxyl.

Synthetic production of indigo was initiated by Adolf von Baeyer in the late 1800's.[77] von Baeyer developed a synthesis of indigo in 1880 and determined the molecular structure in 1883. It was for his work on organic dyes that von Baeyer was awarded the Nobel Prize in Chemistry in 1905. The first company to produce synthetic indigo was the Baeden Aniline and Soda Factory (BASF) in 1897.[74] Indigo is now available commercially from a variety of chemical suppliers using a variety of synthetic routes. These routes take advantage of commercially inexpensive starting materials such as aniline or *N*-phenyl glycerine. Most protocols are two to four steps concluding with a melt reaction with either sodium hydroxide or potassium hydroxide to yield indigo in appreciable yields and purity for distribution.[74]

3.3 Properties of indigo

Indigo is desirable for use in the textile industry due to its intense blue colour. The low energy electronic absorption of indigo is a result of the donor-acceptor properties of the

amine and carbonyl moieties through the core of the molecule, and, to a lesser extent, extension of the π-framework through introduction of the benzene rings.[78-79] The core of indigo (the carbonyl, amine, and internal double bond highlighted in red on compound **3.2**) is often referred to as the H-chromophore (because of the shape) and is largely responsible for the low energy absorption of indigo. To investigate the role of the H-chromophore in the colour of indigo, the non-benzannulated indigo analogue 3-pyrrolidinone was synthesized (compound **3.3**) which lacks the outer benzene π-system and possesses only the amine and carbonyl functions.[80] This molecule has an electronic absorption at 497 nm, which is blue shifted from indigo, but is still at remarkably low energy for a compound with such a low degree of conjugation.[80-82]

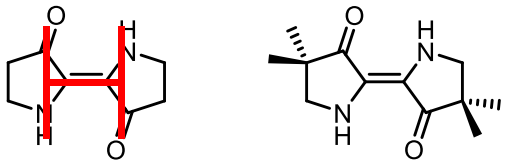

3.2 **3.3**

The photophysics of indigo have been studied extensively.[78, 83-85] Indigo does not fluoresce or phosphoresce appreciably. Instead, indigo relaxes back to its ground state through non-radiative decay.[84] The non-radiative decay was originally postulated to be from a rapid excited state proton transfer from the enol form of indigo, however, picosecond measurements have revealed that this non-radiative decay is a result of internal conversion from the S_1 to S_0 state (**Scheme 22**).[78, 85] The internal conversion has a measured quantum yield of 0.991.[86] Indigo is also photostable, which means there is no *cis-trans* isomerization in the excited state.[83] This is believed to be due to intramolecular

hydrogen bonding from the indole hydrogen atom to the carbonyl oxygen atom (shown on compound **3.1** in **Scheme 22**).

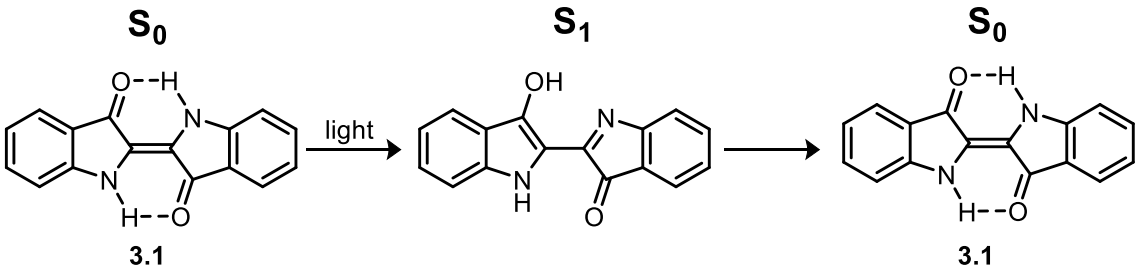

Scheme 22. Proposed tautomerization of indigo (3.1) into its enol form as mediated by light in the excited state.

Since indigo is planar, it is capable of π-stacking in solution which leads to indigo being poorly soluble in all common organic solvents and makes indigo subject to aggregation at higher concentrations. The aggregation of indigo has been studied by UV-Vis spectroscopy. At very low (micromolar) concentrations, the UV-Vis spectrum for indigo shows a single electronic transition at 599 nm (DMSO). However, at higher concentrations (high micromolar or low millimolar), a peak at 700 nm appears which was attributed to a dimer. Variable temperature and concentration studies revealed that this aggregate peak disappears as temperature increases and concentration decreases which is representative of an exothermic process.[85]

3.4 Materials properties of indigo

Indigo has some properties that are attractive for materials research such as a low HOMO-LUMO gap, a tendency to self-associate, and quasireversible two electron

oxidative and two electron reductive processes.[87] Despite this, there have only recently been reports of indigo being used in organic materials such as semi-conductors. In 2012, it was reported in *Advanced Materials* that indigo could be used in semi-conducting devices.[73, 87] Work continues on the studies of indigo as well as the structural analogues Tyrian purple (6,6'-dibromoindigo) and 6,6'-dichloroindigo.

Indigo is also being explored for use in donor-acceptor organic photovoltaic cells (OPVs). It was reported in 1986 by two independent research groups that *N,N'*-disubstituted derivatives of indigo (which have very similar electrochemical behaviour to indigo itself) participated in photoinduced electron transfer as a donor and an acceptor. It has also been reported that indigo and derivatives show promise as acceptor (n-type) for bulk heterojunction OPVs.[88-89]

Although there are only a few (recent) reports of use of indigo in organic materials, a different structural analogue called isoindigo (molecular structure shown in **Figure 21**)[90] has shown excellent potential as a component in organic materials since the first report in 2010 from the Reynolds group.[91] Isoindigo (which appears yellow in solution) and structural analogues can be synthesized easily from isatin and oxindole and are blue-shifted in their absorption as compared to indigo. As isoindigo is electron-deficient and can be coupled with electron-rich thiophene units it is used in bulk heterojunction OPVs (ad example is shown in **Figure 21**).

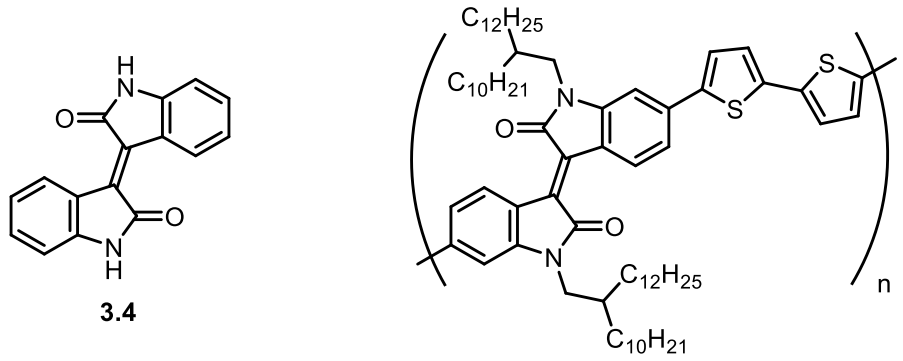

Figure 21. Molecular structure of isoindigo (**3.4**) and an example of a thiophene/isoindigo containing polymer[90]

3.5 Structural modifications to indigo

There are many ways in which indigo can be modified – at the carbon atoms on the periphery of the scaffold, by alkylation or acylation of the indole nitrogen atoms, or by complexation to transition metals or main group elements. All of these structural modifications lead to new physical characteristics and previously reported work in the area will be discussed briefly below.

One of the major challenges of working with indigo is the poor solubility in organic solvents. Solubility can be addressed through incorporation of functionality at the carbon atoms of the peripheral ring systems. Tyrian purple – arguably the most famous indigoid after indigo itself – has bromine atoms are at the 6 and 6' positions of the benzannulated rings of carbon scaffold (compound **3.5**). Tyrian purple exhibits most of the same physical properties of indigo (poorly soluble, does not fluoresce) but is a different colour in solution which is a result a slight bathochromic shift of the absorption in the electronic spectrum to 590 nm from 599 nm, respectively (DMSO).[73-74] Indigo carmine is another derivative of

indigo in which sulfonate groups have been installed, at the 5 and 5' position. These sulfonate groups render the molecule water-soluble and do not have a great effect on the colour in neutral aqueous solution but lead to a hypsochromic shift at high pH (greater than 13). The water solubility of indigo carmine is of importance as indigo carmine is approved for use as blue food colouring (FD&C Blue H2).[92] Indigo carmine is also used a superoxide indicator under physiological conditions and for ozone detection.[93]

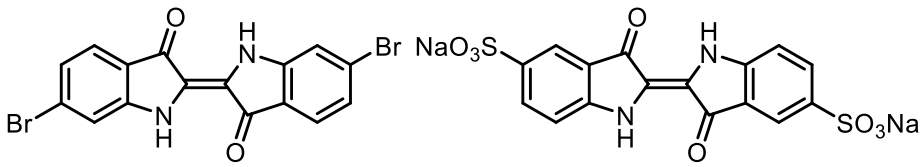

3.5 **3.6**

A variety of indigo derivatives with substituents on the indole nitrogen atom have been prepared and reported.[94-96] It has been shown that *N,N*-dimethylindigo (**3.7**) undergoes *cis-trans* isomerization as catalyzed by acid or by laser pulse experiments (**Figure 22**). *Trans N,N'*-dimethylindigo has an absorbance maximum at 644 nm in its electron spectrum (benzene) and upon isomerization to its *cis* form the absorbance maximum is observed at 588 nm (benzene).[97-99] The isomerization behaviour of N,N'-dimethylindigo is analogous to indigoid thioindigo (molecular structure shown in **Figure 23**) where *cis-trans* isomerization can be initiated with light.[100] Thioindigo also fluoresces from the excited state with a quantum yield of fluorescence of 0.7 and appears bright orange in solution.[101-102]

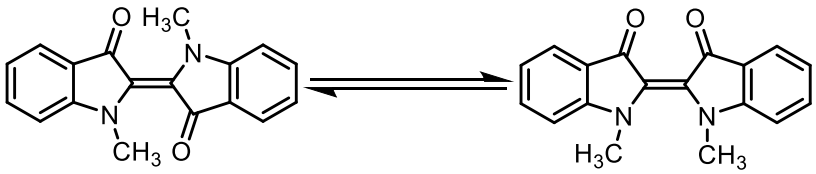

3.7

Figure 22. Cis-trans isomerization of N,N'-dimethylindigo (**3.7**).

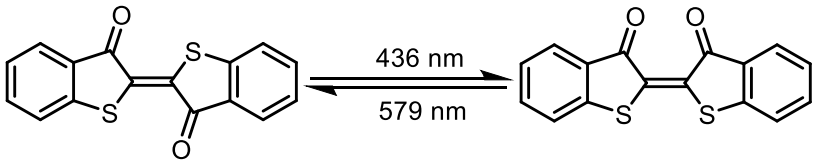

3.8

Figure 23. *Cis-trans* Isomerization of thioindigo (**3.8**) as initiated by light.[100]

Probably due to the poor solubility of indigo in organic solvents, there are very few examples of metal complexes containing indigo as a ligand. In 1989, Beck *et al.* reported palladium and platinum indigo complexes, of the ML, ML_2 and M_2L types (where L = indigo or indigo derivative), some of which have been characterized cyrstallographically (**Figure 24**).[103]

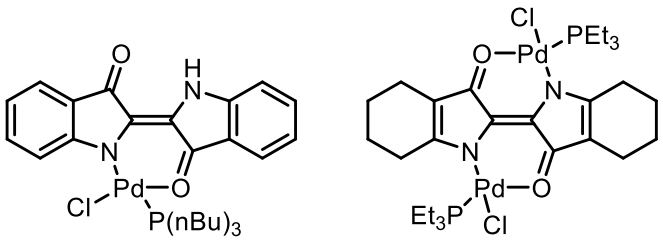

Figure 24. Indigo-Palladium complexes reported by Beck.[103]

In 2008, a trigonal prismatic hexametallic structure was reported which incorporated rhenium tricarbonyl linked by indigo and 2,4,6-tri-4-pyridyl-1,3,5- triazine (**Figure 25**).[104]

This was followed up by a report of the spectroscopic and electronic properties of this compound in 2012 by the same group.[105] The complex showed NIR absorption in the electronic spectrum in its neutral form.

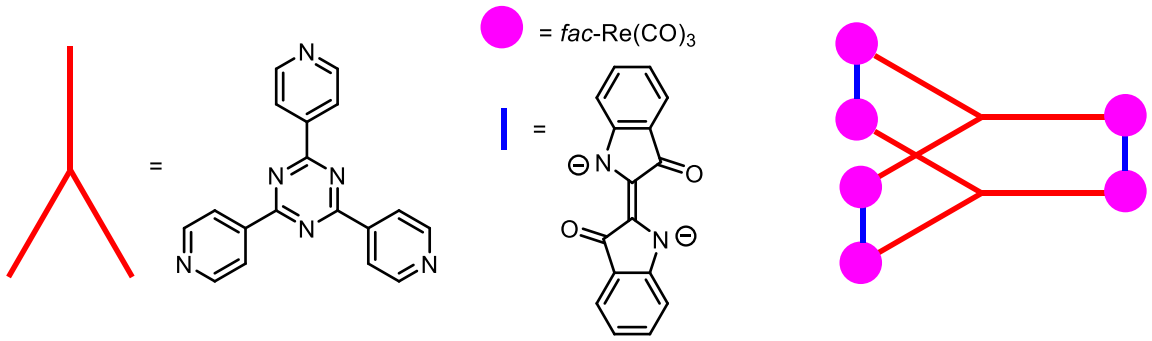

Figure 25. A Rhenium prism synthesized with indigo.[104]

A main group complex of indigo was reported in 2013 which incorporated a single boron-difluoride (BF_2) unit which was chelated by indigo (**Figure 26**).[106] The authors reported an absorption maximum between 620-660 nm (DCM). The ^{19}F and ^{11}B NMR spectra were unreported, so this work requires further investigation for validity.

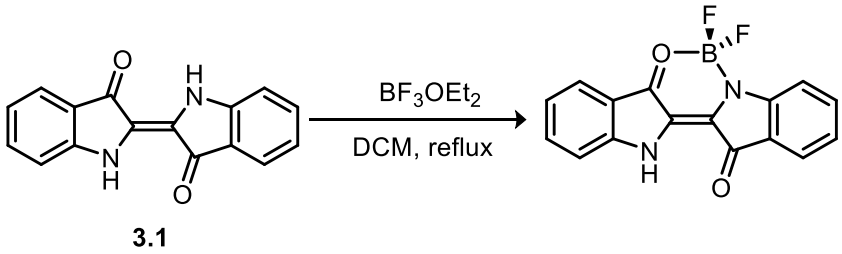

Figure 26. Synthesis of boron difluoride indigo complex.[106]

3.6 Conversion of indigo to Nindigo

In 2010, Hicks *et. al.* reported the diimine derivative of indigo (so called "Nindigo") which could be synthesized reproducibility and with good yields. In order for this transformation to occur, highly forcing conditions need to be used with a high boiling point solvent such as bromobenzene or *m*-xylene (**Scheme 23**). The conversion of indigo to its imine derivatives was achieved successfully for a wide variety of aryl substituents. These Nindigo compounds have improved solubility compared to indigo while maintaining the intense colour.[107]

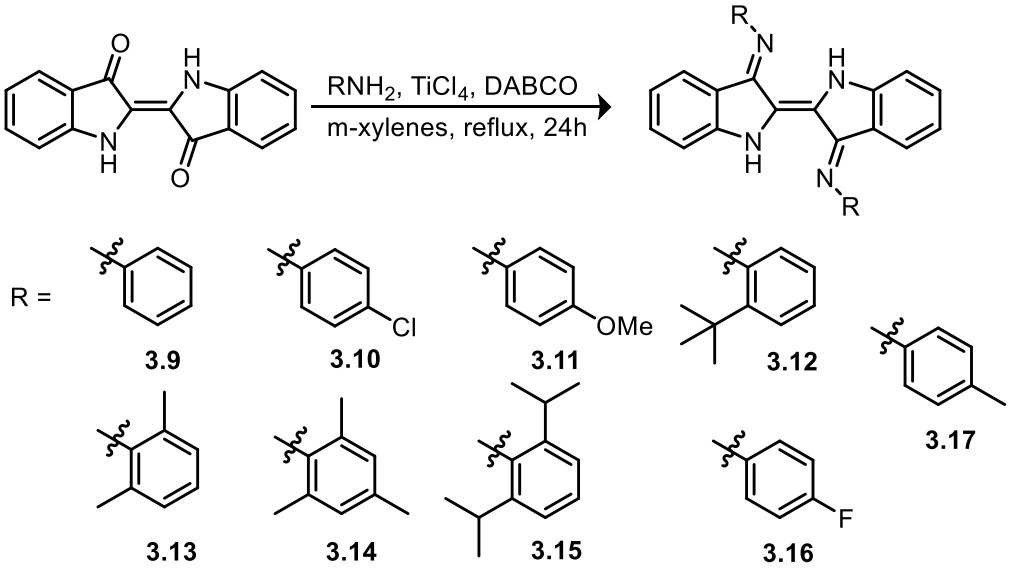

Scheme 23. Synthesis of the Nindigo ligand with a wide variety of aryl functionality.

Since the initial report of the synthesis in 2010, several co-ordination complexes have been reported from the Hicks group and others including: palladium, boron, mixed palladium-boron, cobalt, and ruthenium.[107-112] Some examples of the complexes

synthesized are shown in **Figure 27**. These complexes are of interest because they have a variety of properties which are attractive such as near infrared (NIR) absorption[107, 110-112] and a high degree of redox activity which is often ligand centred.[108-110, 113-115]

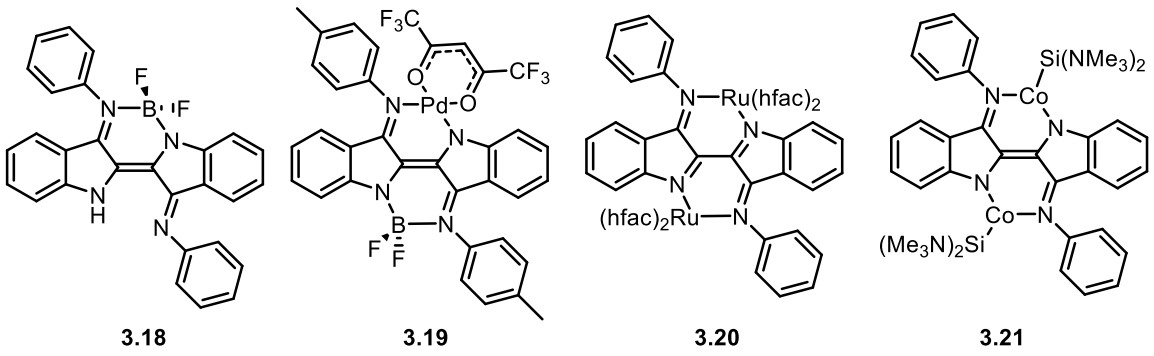

Figure 27. Examples of different Nindigo complexes reported in the recent literature.

3.7 Goals of this Research

The principle focus of Nindigo research by the Hicks group and others has been entirely focused on Nindigo's applications as a ligand. Up until this point, the non-metal chemistry or properties of Nindigo had not received any attention. The work in this thesis explores the avenues of the Nindigo research beyond the transition metal chemistry.

Chapter 4 of this thesis focuses on the synthesis of a new family of organic chromophores which are structurally modified from the indigo chromophore. This new family of chromophores was designed to address some stability concerns of the boron complexes of Nindigo.

Chapter 5 of this thesis focuses on the study Nindigo ligand itself using a variety of UV-Vis and NMR spectroscopic techniques in order to gain a better understanding of electronic

transitions in the UV-Vis that were previously not understood. In particular, this work focuses on the structural and spectroscopic characterization of Nindigo after treatment with a variety of strong acids and bases.

Chapter 4: Synthesis and Characterization of Perinaphthindigo and its Derivatives

4.1 Introduction

As described in Chapter 3, our group has developed a reliable synthesis for Nindigo.[107, 112] One of the pursuits undertaken by an earlier group member was to synthesize boron complexes of the Nindigo ligand. Synthetic protocols were developed to synthesize both the mono-BF_2 (**4.1**) and the bis-BF_2 (**4.2**) derivatives, respectively (**Scheme 24**).[110, 112] The visible spectra of the boron-Nindigo complexes exhibit bathchoromic shifts of their absorbance maxima relative to that of Nindigo with co-ordination of each BF_2 unit. The *bis*-boron derivatives absorb very close to the near-infrared region of the electromagnetic spectrum (**Figure 28**).[110]

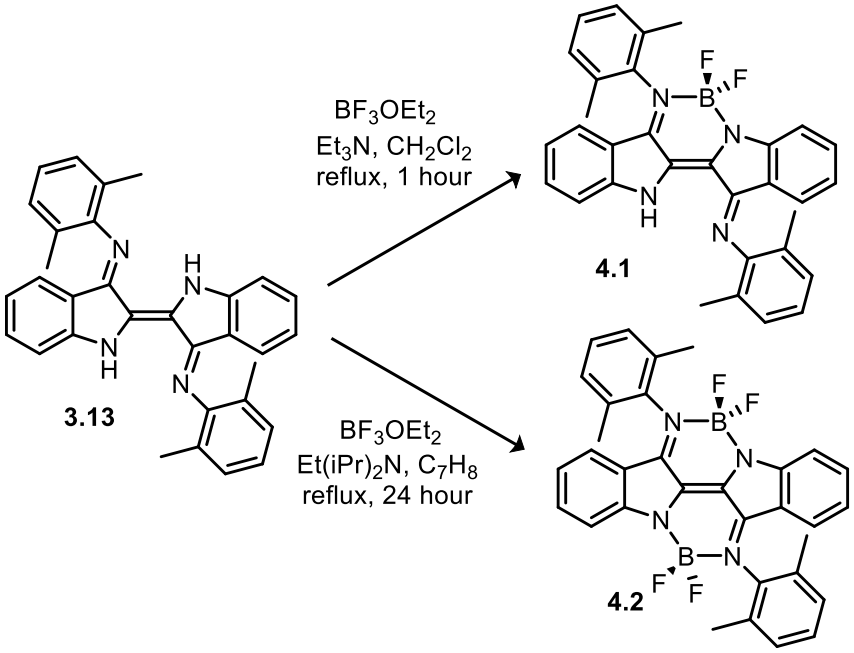

Scheme 24. Synthesis of the *mono*-boronNindigo **(4.1)** and *bis*-boronNindigo **(4.2)**.

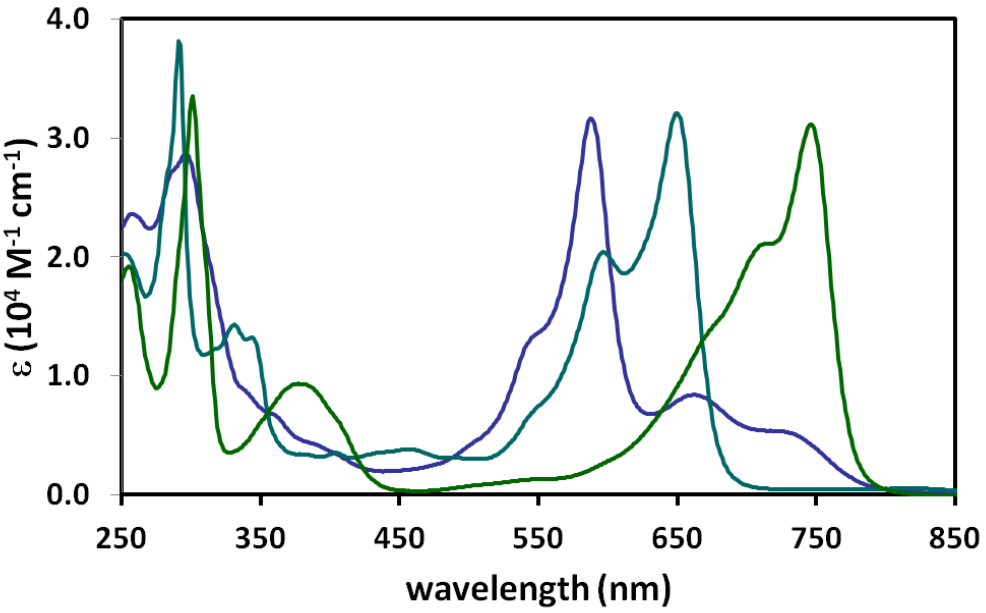

Figure 28. UV-Vis spectrum of **3.13 (**blue**), 4.1 (**teal**),** and **4.2 (**green**)** (CH_2Cl_2, 298K).

The Nindigo *mono* and *bis*-boron species were found to be weakly emissive in solution. Unfortunately, the *bis*-boron species are unstable in solution. Over a period of several hours to a few days (depending on the nature of the Nindigo aryl substituent) the *bis*-boron complexes decompose to their *mono*-boron counterparts (**Figure 29**).

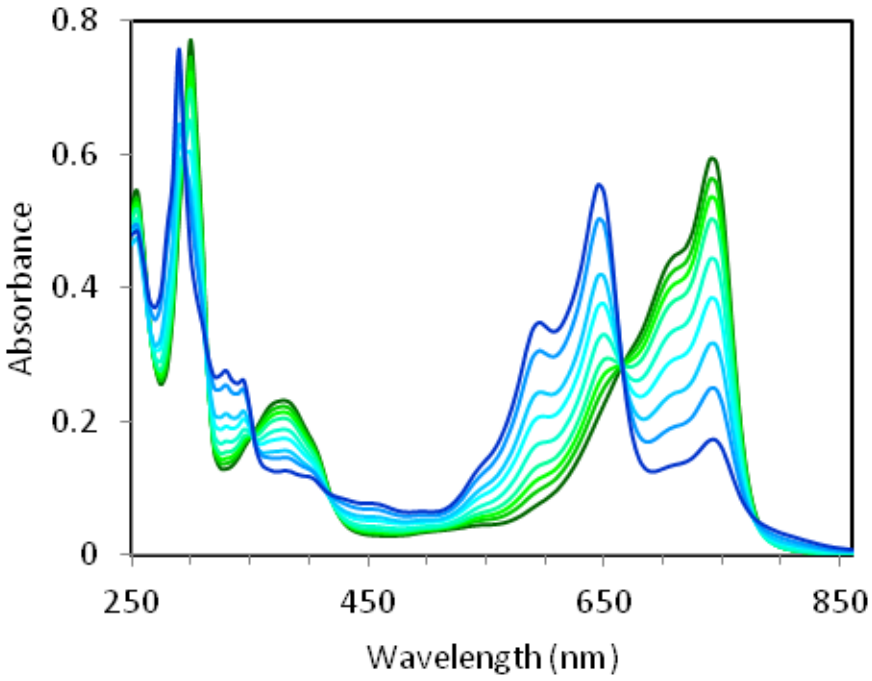

Figure 29. UV-Vis spectrum showing the decomposition of compound **4.2** (green) to compound **4.1** (blue) in dichloromethane over 96 hours[111] (awaiting permission from RSC publications).

The reason for this decomposition is believed to be structural. X-ray crystallographic data for free Nindigo derivatives show that N1 and N2 have an equal cavity distance of 2.804 Å (**Figure 30**) on both sides of the molecule. However, upon binding one BF_2 unit (**Figure 31**) the N31-N42 distance was reduced to 2.512 Å. The binding of the first BF_2 unit caused the other binding site of Nindigo to "open up" such that the distance between N41 and N32 increased to 3.020 Å. This larger cavity is not ideal for boron (a relatively small element) co-ordination, which leads to the lack of stability of the *bis*-boron complex with respect to the *mono*-boron analogue.

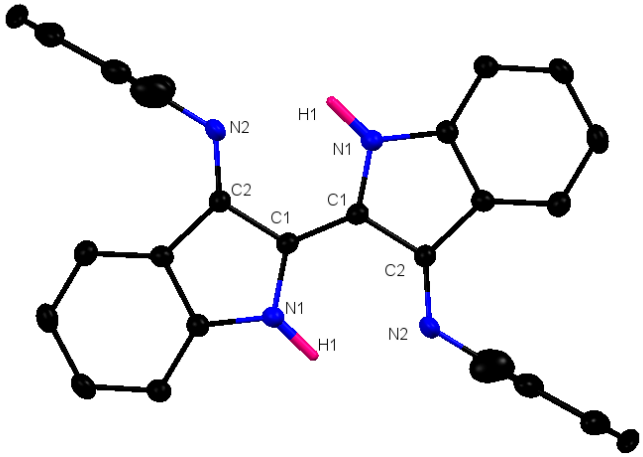

Figure 30. X-ray crystal structure of compound **3.13**. All hydrogen atoms except N-H's proton's removed for clarity. Thermal ellipsoids shown at the 50% probability level.

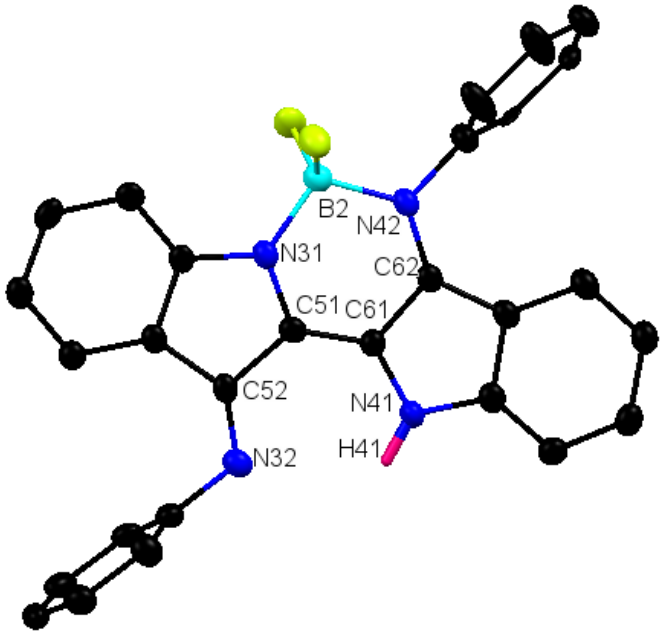

Figure 31. X-ray crystal structure of compound **3.18**. All hydrogen atoms except H41 removed for clarity. Thermal ellipsoids shown at the 50% probability level.

The structure of Nindigo is not well suited to small atom binding because the imine binding site is projected from a five-membered ring. Because the binding site is projected from the five-membered ring, the bite angle of the two binding sites is not ideal for small elements and this leads to structural distortion upon binding (**Figure 31**). By conceptually changing the backbone from a single aryl ring to a fused naphthalene backbone (compound **4.5**) the imine now projects from a six-membered ring which should improve the bite angle for boron co-ordination. The construction of this imine derivative can be imagined by working retrosynthetically from a carbonyl precursor (**Figure 32**), which we named perinaphthindigo (compound **4.4**, hereafter referred to as PNI). The objective of this work was to develop a synthesis of PNI (and some derivatives) and to explore the properties of these species.

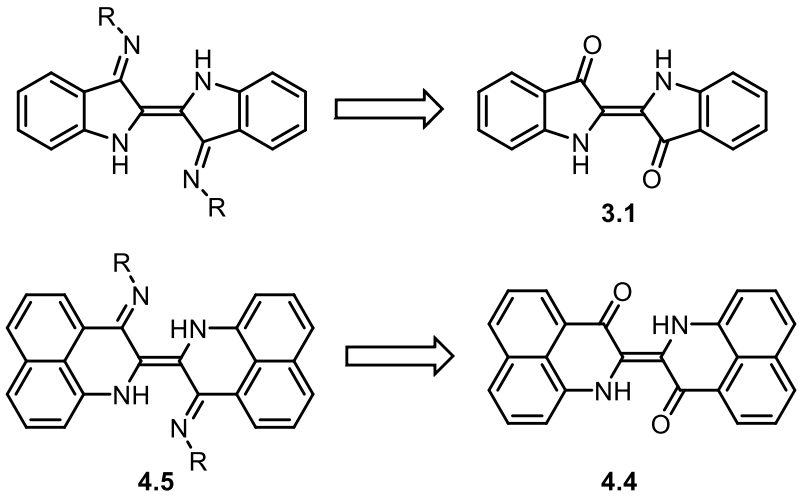

Figure 32. Retrosynthetic analysis of proposed new ligand system **4.5** from PNI (**4.4**).

4.2 Synthesis and characterization of perinaphthindigo

Perinaphthindigo bears a striking resemblance to the famous molecule indigo. However, PNI has only once been reported in the literature, in 1923, and has remained largely uncharacterized.[116] The original synthesis was four steps (shown in **Scheme 25**) starting from naphthastyril which was treated with potassium hydroxide and chloroacetic acid. The sodium salt prepared in the first step was treated sodium hydroxide in water and alcohol, the product of which was added to a mixture of dry sodium hydroxide and sodamide and then warmed. The solid product was boiled in aqueous sodium hyposulfite and then filtered. This solid was reported to be blue-green in sulfuric acid and was only sparingly soluble in aniline, nitrobenzene, and quinoline.[116] No other characterization data was reported.

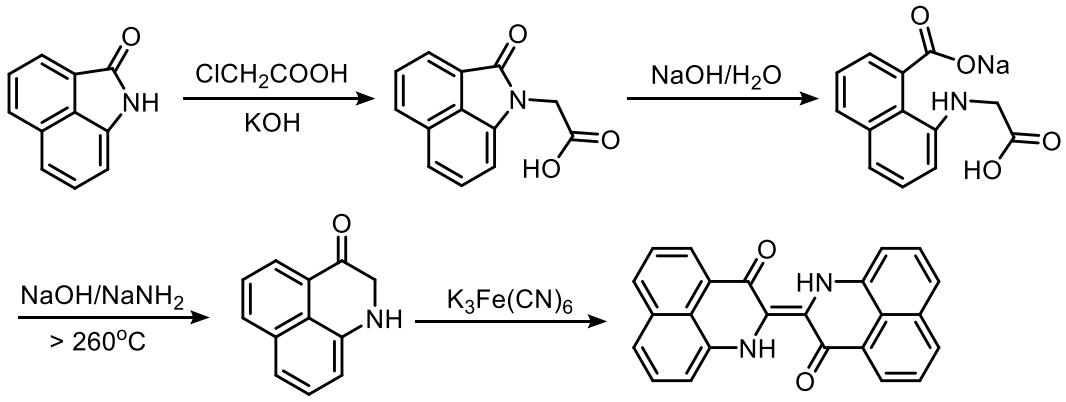

Scheme 25. Previously reported synthesis of perinaphthindigo.

Since perinaphthindigo was largely uncharacterized and the synthesis reported was arduous we set out to develop a different route to perinaphthindigo by adapting a well-known synthesis. The Baeyer-Drewson reaction involves treatment of *o*-

nitrobenzaldehyde with acetone and potassium hydroxide to yield indigo (**3.1**), albeit in poor yields (**Scheme 26**).[74, 77]

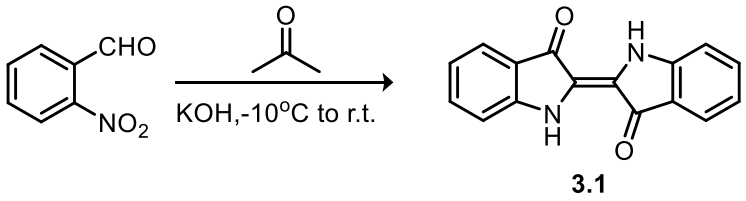

3.1

Scheme 26. Synthesis of indigo **(3.1)** by the Baeyer-Drewson reaction.

In order for the same chemistry to be utilized for perinaphthindigo, 1,8-nitronaphthaldehyde (compound **4.3a**) must first be synthesized. This could be easily achieved by standard electrophilic aromatic nitration conditions of 1-napthaldehyde which yielded an approximately 1:1 mixture of the 1,5-nitronaphthaldehyde (**4.3b**) and 1,8-nitronaphthaldehyde (**4.3a**) which were separated by column chromatography.[117] Absolute determination of regiochemistry was aided by X-ray crystallographic studies on **4.3a** (**Figure 33**). The 1,8-nitronaphthaldehyde was the subjected to Baeyer-Drewson conditions to lead to the cyclized perinaphthindigo (compound **4.4**, **Scheme 27**).[74, 77] The yield of this reaction was quite poor, but was improved by monitoring the temperature to ensure that it did not rise about 0^{o} C upon the addition of the 0.2 N potassium hydroxide and during the subsequent stirring. The yield was also improved by doing the reaction in relatively dilute concentrations.

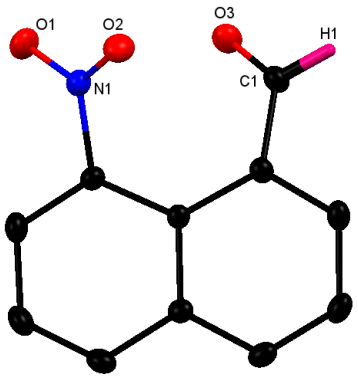

Figure 33. X-ray structure of compound **4.3a.** All hydrogen atoms with the exception of H1 removed for clarity. Thermal ellipsoids shown at 50% probability level.

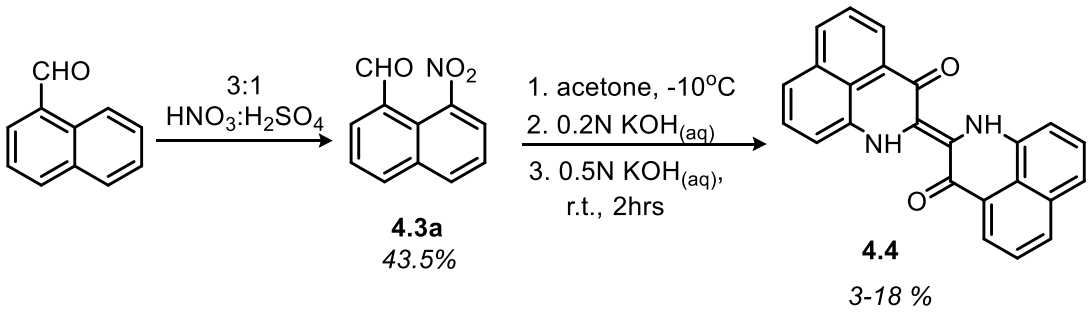

Scheme 27. Synthesis of perinaphthindigo (**4.4**).

Perinaphthindigo was green in solution (λ_{max} (DMSO) = 650 nm) which was bathochromically shifted with respect to indigo by approximately 50 nm. Since perinaphthindigo also suffered from poor solubility, spectra needed to be recorded in DMSO, shown in **Figure 36**. Compound **4.4** was also characterized by ^{1}H NMR (**Figure 34**) and ^{13}C NMR spectroscopy (**Figure 35**). The ^{1}H NMR spectrum for PNI showed aromatic hydrogen signals in the ratio that would be expected (that is, for twelve total aromatic hydrogen atoms). More importantly, there was a lack of an aldehyde signal at 10 ppm which indicated the consumption of the starting material **4.3a**. The ^{13}C NMR

spectrum of PNI was difficult to collect due to poor solubility. However, when run for 40 hours, a weak ^{13}C NMR spectrum was acquired. The inset shows 11 unique signals which is one less than would be expected from the chemical structure. It was likely that there are either overlapping signals as all carbon atoms are aromatic or one quaternary carbon centre is not observed which led to the difference in the predicted versus the observed number of carbon resonances. The infrared (IR) spectrum had two peaks of importance. The first is the amine N-H which appeared at 3298 cm^{-1} and the second is the carbonyl C=O which appeared at 1623 cm^{-1}. The carbonyl appears at a low stretching frequency due to the vinalogous amide which effects the carbon-oxygen bond order. The acquisition of accurate mass and elemental analysis results have proven difficult for compound **4.4**. However, low resolution mass spectral data was collected which showed that a solution of PNI with aqueous sodium hydroxide added has a peak for the anion and two sodium atoms in the positive ion mode.

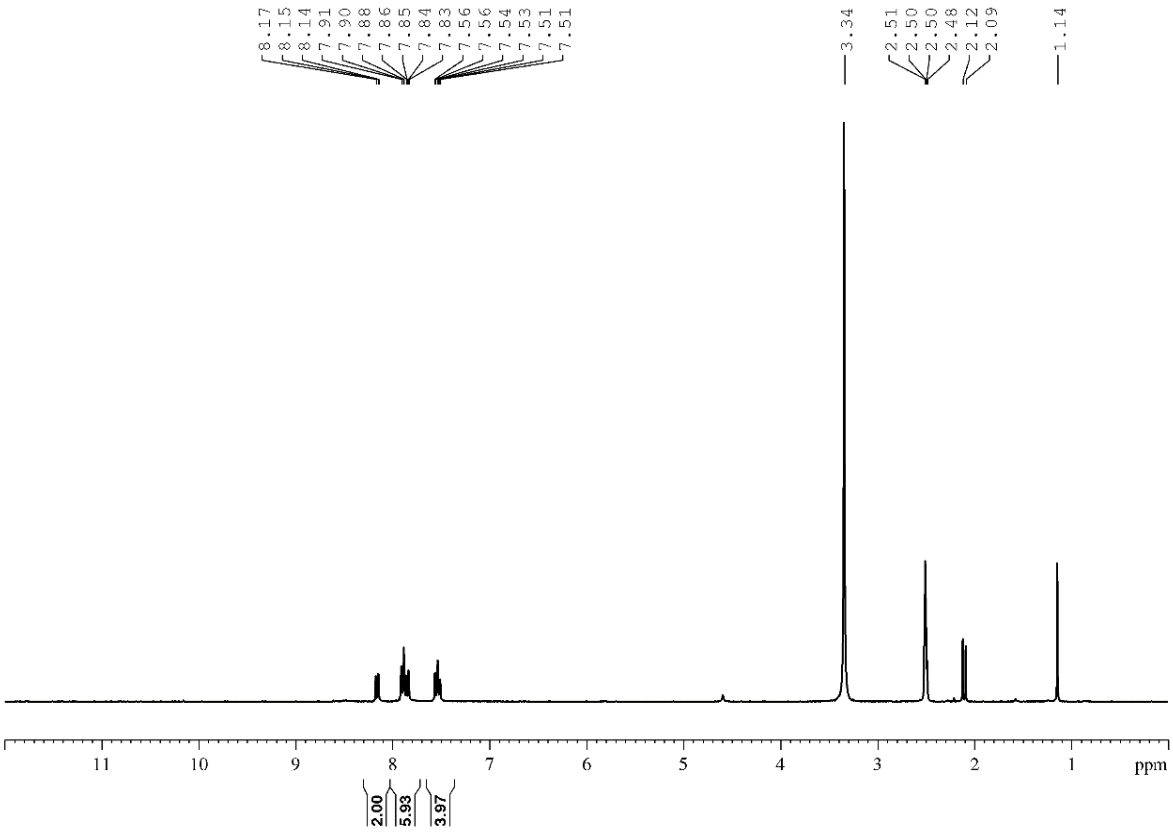

Figure 34. ^{1}H NMR of PNI in DMSO-d_6 (300 MHz, 298K).

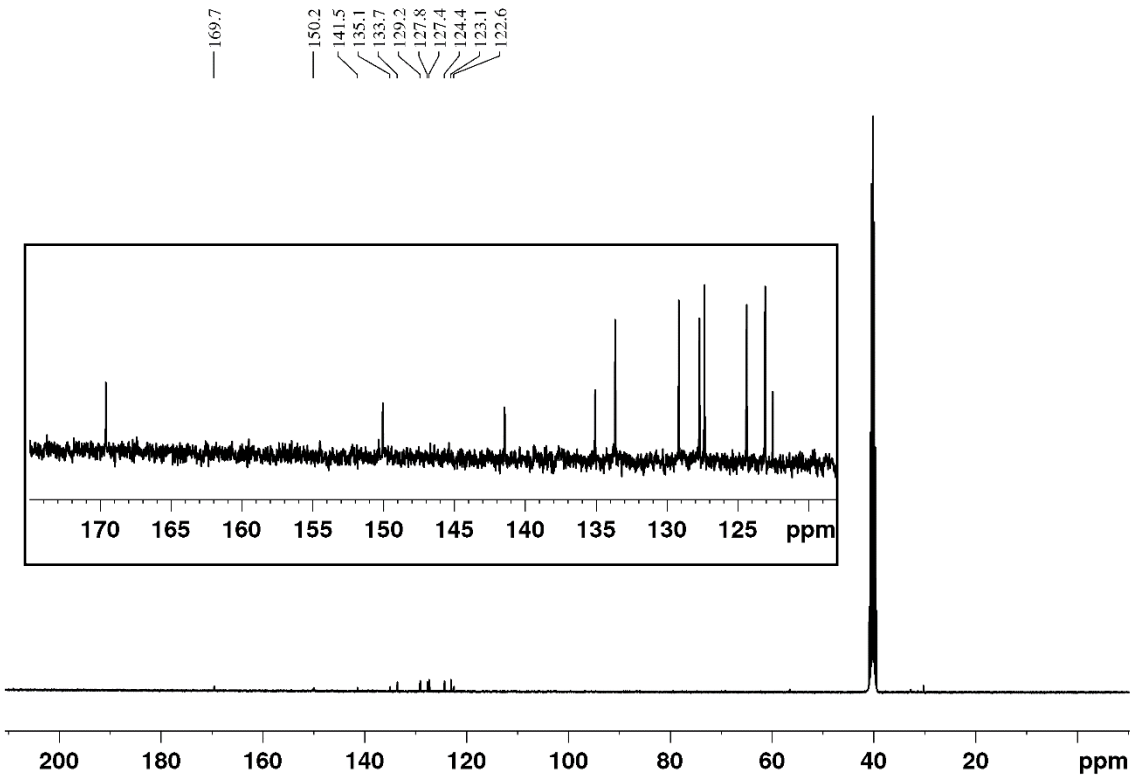

Figure 35. ^{13}C NMR spectrum of PNI in DMSO-d_6 (75.5 MHz, 298K).

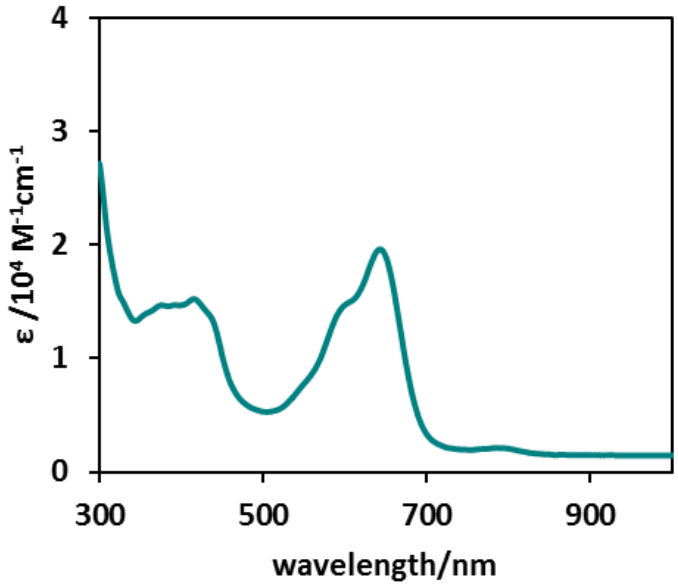

Figure 36. UV-Vis-NIR spectrum of PNI in DMSO (1 x 10^{-4} μM; 298K).

4.3 Alternative synthesis of perinaphthindigo

The low yield, even after condition optimization, for perinaphthindigo by Baeyer-Drewson conditions was a concern. The Baeyer-Drewson reaction is not the only known pathway to indigo, however. An alternative synthesis of indigo is outlined in **Scheme 28**. The first step was a Henry reaction - a modified aldol reaction - which uses nitromethane as both the solvent and the nucleophile. The intermediate sodium salt could be isolated as a yellow solid which was then dissolved in aqueous potassium hydroxide and sodium dithionite leading to immediate precipitation of indigo as a blue/purple solid.[118] The literature reports a yield of 80%; in our hands the yield was 64% (from *o*-nitrobenzaldehyde). This result was promising as this reaction presented us with an alternative to the Baeyer-Drewson reaction.

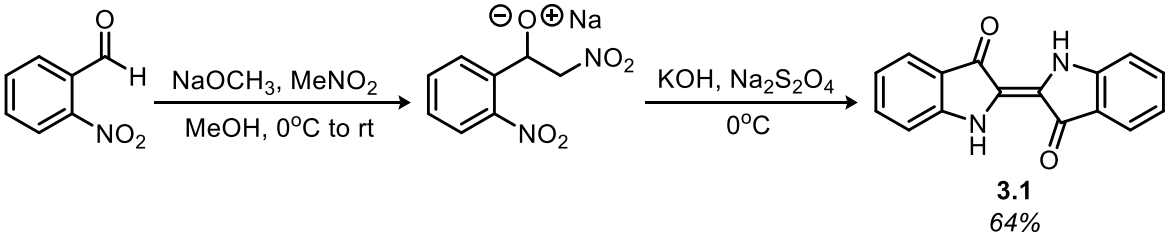

Scheme 28. Alternative synthesis of indigo (**3.1**).

The reaction of compound **4.3a** under the same Henry reaction conditions as described in **Scheme 28** led not to the desired product, but to a mixture of unidentifiable products, none of which were the desired compound (as determined by ^{1}H NMR) (**Scheme 29**, first reaction). In order to obtain the desired product, milder conditions were explored where sodium acetate was used as the base in a mixture of ethanol and nitromethane as the solvent.[119] At room temperature, no reaction occurred and only starting material was

recollected. By warming the reaction to 40 °C over two days, 60% conversion to the product was observed, with the remaining 40% being starting material (**Scheme 29**, second reaction). Refluxing this mixture for two days led to 90% conversion to the product (**Scheme 29**, third reaction). The remaining starting material could be separated from the desired compound by column chromatography**.**

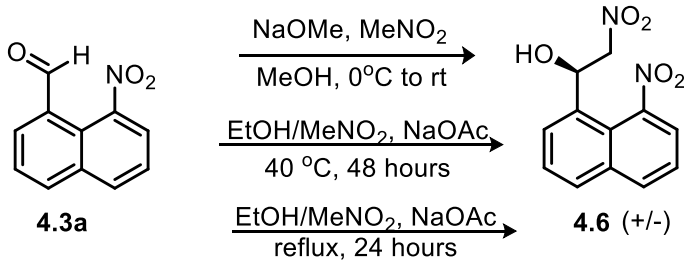

Scheme 29. Henry reaction with **4.3a** to synthesize compound **4.6**.

With this Henry reaction product (**4.6**) in hand, the synthesis of perinaphthindigo was attempted using the conditions described for the synthesis of indigo (**3.1**) (**Scheme 30**). Unlike indigo synthesis where there was an immediate precipitation of the blue product (indigo), the green precipitate that would have been expect for PNI was not observed. Instead the ^{1}H NMR revealed a mixture of compounds, none of which was the desired product.

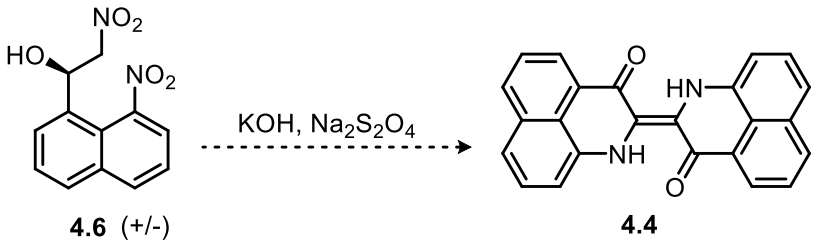

Scheme 30. Synthesis of PNI from compound **4.6**.

4.4 Synthesis of derivatives of perinaphthindigo

4.4.1 Synthesis of a more soluble derivative of perinaphthindigo

The first effort towards improving the solubility of perinaphthindigo was by introducing bulky alkyl groups at the periphery of the ring system. These alkyl groups were introduced at the outset of the synthesis using a Friedel-Crafts reaction on naphthalene (**Scheme 31**).[120] However, due to regioselectivity problems both the desired 2,7-di-*tert*-butylnaphthalene (**4.7b**) and its 2,6-isomer (not shown) compounds were produced in a 1:1 ratio. A protocol to separate similar compounds was found in the literature which used thiourea as a co-crystallization agent.[121] Refluxing the product mixture in ethanol with an excess of thiourea leads to the selective co-crystallization of the 2,6 isomer while the 2,7 isomer (**4.7b**) remains in the ethanol solution. This procedure needed to be repeated three to five times in order to give pure 2,7-di-*tert*-butylnaphthalene (**4.7b**) but it was effective in reasonable yields.

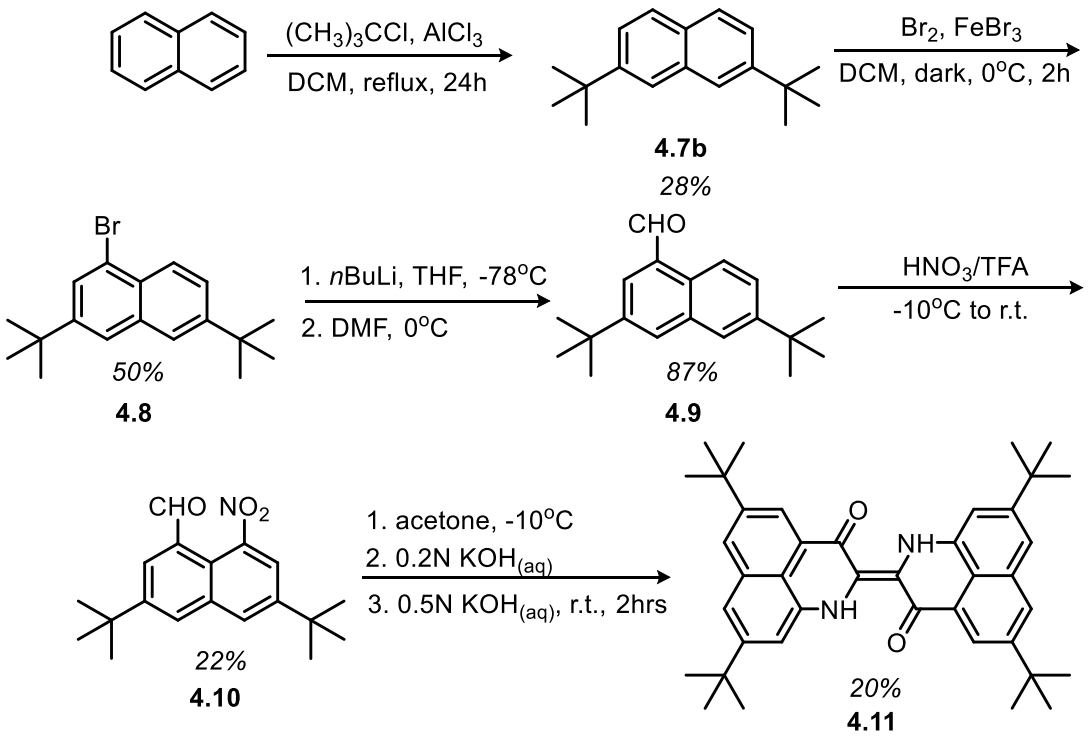

Scheme 31. Synthesis of 5,5',8,8'-tetra-tert-butylperinaphthindigo (**4.11**).

2,7-di-*tert*-butylnaphthalene (**4.7b**) was then brominated at the 4-position using standard bromination conditions that proceeded in good yields to produce compound **4.8**.[122] The bromine substituent was subsequently converted into an aldehyde group by lithium-halogen exchange followed by a dimethyl formamide quench, yielding compound **4.9**.[122] It is worth noting that a Vilsmayer-Haack reaction was attempted to synthesize **4.9** directly from **4.7b** but the conversion in this case was unreliable and often led to a mixture of compounds so the two-step procedure was used.

Finally, **4.9** was treated with the slow addition of concentrated nitric acid into a suspension of **4.9** in trifluoroacetic acid at -10 °C which nitrated almost exclusively at the 5-position (**4.10**) with a small amount of impurity from nitration occurring the 1-position

(10% by ^{1}H NMR). The Baeyer-Drewson cyclization conditions done on **4.10** afforded the 2,2',7,7'-tetra-*tert*-butylperinaphthindigo (compound **4.11**).

2,2',7,7'-tetra-*tert*-butylperinaphthindigo (compound **4.11**) is also green in solution with a λ_{max} (DCM) = 644 nm. The nearly identical absorption wavelength maxima of **4.11** and **4.4** was not unexpected because the electronics of the chromophore had not changed drastically by the introduction of the alkyl groups. The key IR data for **4.11** are similar to those of PNI with the NH stretch of the former at 3253 cm^{-1} and the C=O stretch at 1656 cm^{-1}. As anticipated, this compound was more soluble than its perinaphthindigo parent compound (**4.4**) due to the bulky alkyl groups. However, this improved solubility made the separation of the product from by-products of the Baeyer-Drewson reaction difficult thus obtaining a pure sample has been challenging. Like perinaphthindigo, accurate mass and elemental analysis results have not been acquired for the final compound **4.11.**

4.4.2 Synthesis of brominated perinaphthindigo

The next modification to the perinaphthindigo system that was explored was the introduction of bromine atoms at the 6- and the 7-position of the naphthalene ring. These bromine atoms were introduced because they open the door to cross-coupling reactions which would allow for the development of a library of compounds. This important intermediate could also allow for the extension of the π-system through introduction of substituents that are relevant to π-conjugated materials such as thiophene and other aromatic functionality. The synthesis of the two brominated PNI derivatives was accomplished by introducing the bromine atoms early in the synthesis.

The synthesis of 7,7'-dibromoPNI (**4.16**) is presented in **Scheme 32**. Bromination of 1-naphthoic acid at the 5-position generated compound **4.12**. The carboxylic acid function was first reduced to the primary alcohol (**4.13**) using dimethylsulfide stabilized borane[123] followed by oxidation with manganese dioxide to the corresponding aldehyde (**4.14**).[124] This aldehyde was then treated with 3:1 concentrated nitric acid and concentrated sulfuric acid to yield a 3:2 mixture of regioisomers with the nitro group at the 8- (**4.15a**) and the 2-positions, respectively, which were separated by column chromatography.[117] The desired isomer **4.15a** was then subjected to Baeyer-Drewson cyclization conditions to yield the final compound 7,7'-dibromoperinaphthindigo **4.16**.

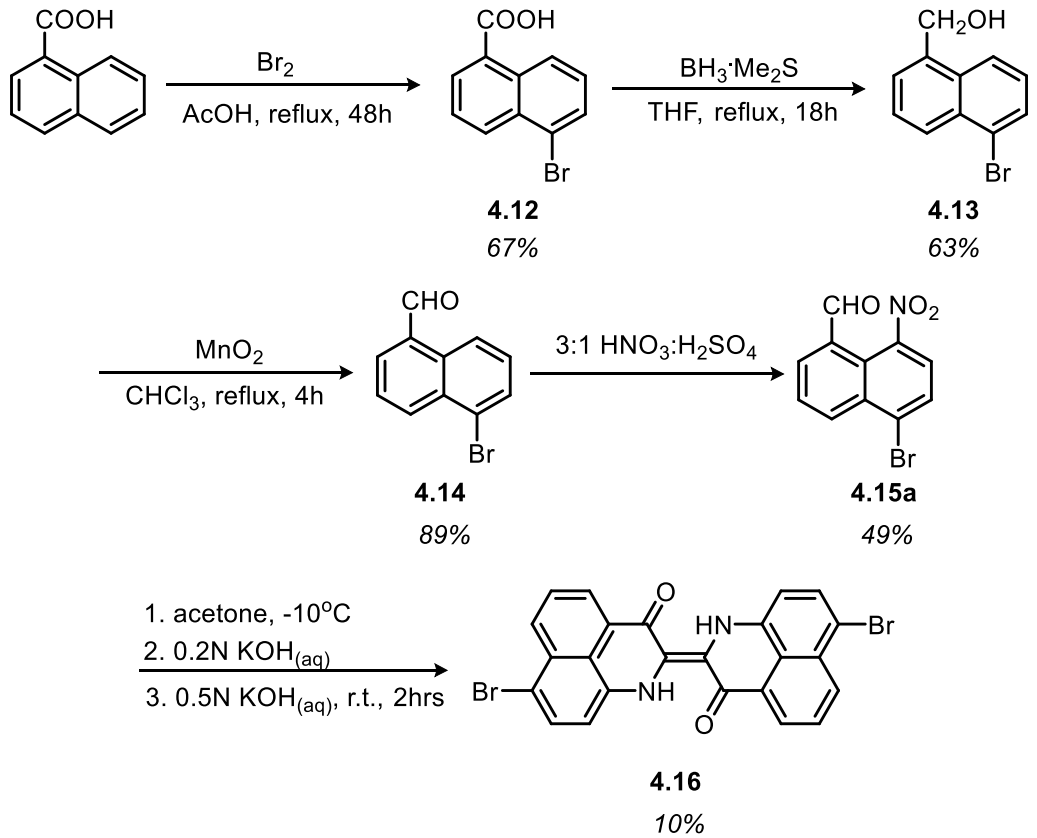

Scheme 32. Synthesis of 7,7'-dibromoperinaphthindigo (**4.16**).

The synthesis of the 6,6'-dibromoPNI derivative is presented in **Scheme 33**, 4-bromo-1-methyl-napthalene was treated with bromine and benzoyl peroxide (acting as a radical initiator) to generate compound **4.17**.[125] Compound **4.17** was then hydrolyzed in a basic ethanol/water mixture which generated the primary alcohol **4.18**.[126] From here, all subsequent procedures were analogous to the ones used for the 7,7'-dibromoPNI isomer shown in **Scheme 31.** Manganese dioxide was used as an oxidant to form the aldehyde function. Compound **4.19** was treated with standard electrophilic aromatic nitration conditions which generated the two regioisomers with the nitro group located at the 8-(**4.20a**) and the 5-poistions in a 1:1 mixture which was separated by column chromatography.[117] Compound **4.20a** was then cyclized using standard Baeyer-Drewson conditions to yield what is thought to be the final compound 6,6'-dibromoperinaphthindigo **4.21**.[74] Despite best efforts, suitable a ^{1}H NMR spectrum could not be obtained for **4.21**, due in part to the terrible yields of the final product and poor solubility, even in d_6-DMSO.

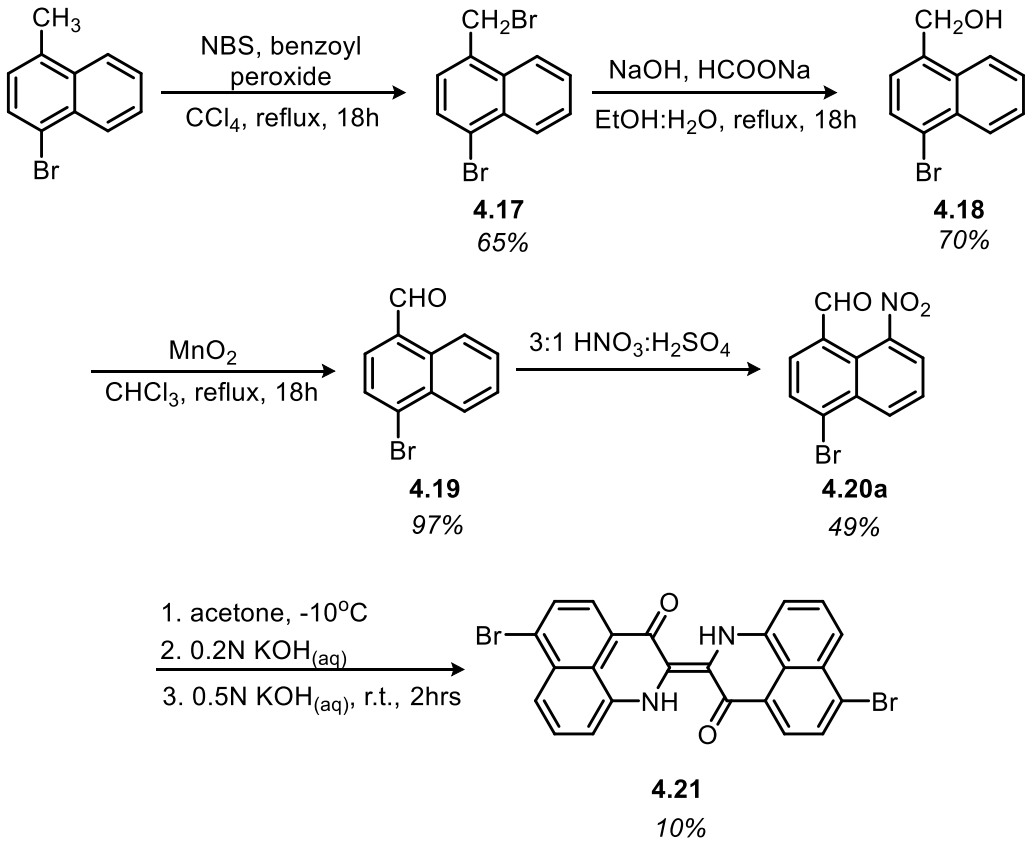

Scheme 33. Synthesis of 6,6'-dibromoperinaphthindigo (**4.21**).

7,7'-dibromoperinaphthindigo (**4.16**) was purple in solution (λ_{max} (DMSO) = 579 nm). The other brominated derivative, 6,6'-dibromoperinaphthindigo (**4.21**) was also hypsochromically shifted (but to a lesser degree) and had a λ_{max}(DMSO) = 608 nm. The hypsochromic shift of Tyrian purple (compound **3.5**) versus indigo is only 9 nm, whereas the shift of the 7,7-dibromoperinaphthindigo and 6,6'-dibromoperinaphthindigo compared to perinaphthindigo is 71 nm and 42 nm, respectively. This indicated that PNI may be more sensitive to perturbation than indigo. Changes to the periphery are certainly possible because the bromine atoms that have changed the electronics of the system can also serve

as a cross-coupling partner. Early work into the cross coupling chemistry using compound **4.15b** is outlined in section **4.5.**

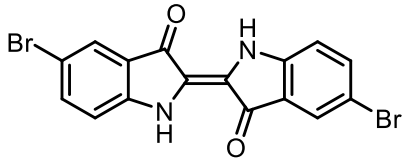

3.5

4.5 Early attempts at Cross-Coupling Chemistry

Brominated PNI compounds **4.16** and **4.20** were synthesized to ultimately do cross-coupling chemistry on. However, the Baeyer-Drewson reaction was so low yielding that it was proposed that installation of new functional groups through cross-coupling chemistry should be done earlier in the synthesis on either compound **4.15a** or compound **4.20a**. The conditions for a Suzuki coupling on compound **4.15a** reactions were screened by using *para*-tolylboronic acid, tetrakis(triphenylphosphine) palladium (0), cesium carbonate, and toluene as a high boiling point solvent heated under pressure to 110 ^{o}C (**Scheme 34**). Yields of 70-85% of **4.22** were achieved after optimization of reaction conditions.[127]

Once the coupling conditions were optimized for *para*-tolylboronic acid, the reaction was then attempted with synthesized 2-thienyl boronic acid **4.23** (selected as thiophenes are common components of π-conjugated materials because they are electron rich) with some minor reaction condition modifications. These conditions could also be used to couple the thiophene unit to compound **4.15a** in reasonable yields (60-75%) producing **4.24** (**Scheme 35**). These reaction served as proof of principle that cross-coupling

chemistry on these substrates could be used to generate a library of different compounds to investigate the effect of electron-donating groups and electron withdrawing groups on the periphery of the dye system.

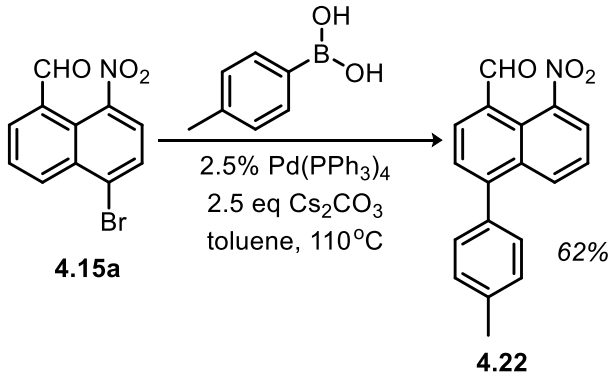

Scheme 34. Synthesis of **4.20** to optimize cross-coupling conditions.

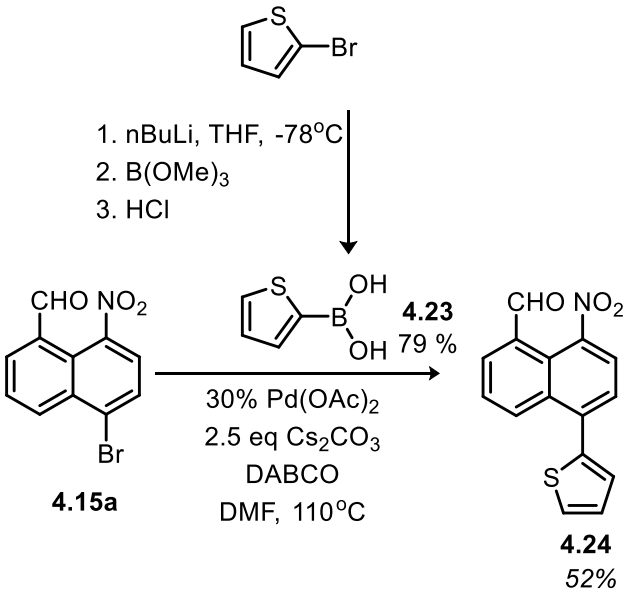

Scheme 35. Synthesis of **4.21** and **4.22**.

4.6 Summary

In order to address some solution stability concerns for the *bis*-boron Nindigo complexes, a new dye system was designed which could change the bite angle of the boron chelate. This change in the bite angle would hopefully serve to generate more stable boron complexes. However, the organic chromophore proposed, perinaphthindigo, had been reported only once in the literature and so the opportunity arose to synthesize and characterize perinaphthindigo as well as develop a synthesis of some derivatives. The synthesis of the organic precursors to different dye systems required optimization but was well developed. The Baeyer-Drewson cyclization is still a major concern as the yields are very poor. In order to address this concern, an alternative route was explored which started with a Henry reaction, followed by an oxidative coupling of two equivalents of the intermediate. The characterization of the target dyes also presented a problem as poor solution solubility made NMR spectroscopy beyond ^{1}H NMR a challenge. Poor volatility also made the acquisition of the mass spectroscopic results difficult.

4.7 Experimental Section

4.7.1 Method and Materials

All reactions and manipulations were carried out under an argon atmosphere using standard Schlenk or glovebox techniques unless otherwise stated. All reagents were purchased from Aldrich and used as received unless stated in which case they were purified or dried under appropriate conditions. NMR spectra were recorded on 300, 360 or 500 MHz instruments at room temperature unless stated otherwise. Electronic spectra were recorded on a Perkin-Elmer Lamda 1050 instrument in dichloromethane or dimethyl sulfoxide. Accurate mass determination was performed at the UVic Genome BC Proteomics Centre on a Thermo Scientific LTQ Velos Orbitrap instrument. Samples (mg/mL) were diluted by a factor of 10-100 and injected by liquid infusion through a nano ESI source. X-ray diffraction data was collected on a Bruker PLATFORM/SMART 1000 CCD with a graphite-monochromatacized Mo-Kα radiation ($\lambda = 0.71073$ Å) by Dr. Brian Patrick (University of British Columbia).

4.7.2 Experimental Data

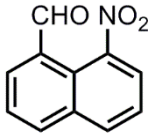

1,8-nitronaphthaldehyde (**4.3a**)

7.71g (0.0493 moles; 1eq) of 1-naphthaldehyde was added over 10 minutes to a 40 mL solution of 3:1 concentrated nitric acid:concentrated sulfuric acid cooled to 0ºC. This mixture was stirred for 3h at 0ºC before filtration to obtain **4.4** as a yellow solid. Column chromatography (silica gel, 30 cm, 2:1 dichloromethane:hexanes) yielded 8-nitro-1-napthaldehyde as a single regioisomer. Yield: 4.45 g (48.9%). ^{1}H NMR ($CDCl_3$, 298K, 300 MHz): δ 10.14 (singlet, 1*H*, C*H*O), 8.13 (m, 4*H*), 7.75 (dofd, 1*H* $^{3}J_{HH}$ = 7.3 Hz, $^{4}J_{HH}$ = 0.9 Hz), 7.65 (overlapping dofd, 1*H* ^{3}J = 8.0 Hz). ^{13}C NMR ($CDCl_3$, 298K, 75.6 MHz): δ 189.9, 134.88, 134.1, 133.9, 126.6, 125.9, 125.5. IR (thin film, dichloromethane, cm^{-1}): 3081, 1945, 2851, 1681, 1524, 1348, 1283, 1211, 833, 763.

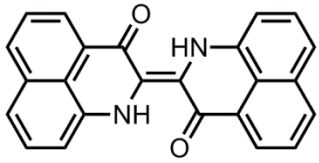

perinaphthindigo (**4.4**)

1.086g (0.00540 moles, 1 eq) of **4.3a** was dissolved in 15 mL acetone in a 100mL round bottom flask. This mixture was cooled to -10ºC and 2 mL of 0.2N potassium hydroxide was added by syringe. This mixture was stirred at -10ºC for a further 15 minutes before 20 mL of 0.5N potassium hydroxide was added over 10 minutes. This mixture was warmed gradually to room temperature and stirred overnight (19h). This was transferred to a 50 mL centrifuge tube and spun for 1 hour (RPM: 3250, room temperature). The liquid was decanted off and a solid was collected and allowed to dry. After extraction into dichloromethane, perinaphthindigo was collect as a dark green solid in a 57 mg (2.9%)

yield. ^{1}H NMR (DMSO-d_6, 298K, 300 MHz): 8.16 (d, 2*H*, ^{3}J = 8.3 Hz), 7.89 (doft, 4*H*, ^{3}J = 7.7 Hz, ^{4}J = 1.7 Hz), 7.84 (dofd, 2*H*, ^{3}J = 7.1 Hz, ^{4}J = 1.4 Hz), 7.53 (tofd, 4*H*, ^{3}J = 8.3 Hz, ^{4}J = 1.7 Hz). ^{13}C NMR (DMSO-d_6, 298K, 75.5 MHz): 169.7, 150.1, 141.5, 135.1, 135.1, 133.7, 129.2, 127.8, 127.4, 124.4, 123.1, 122.6. IR (KBr): 3295, 1632. UV-Vis (DMSO, 1x10^{-5}M, DMSO): 650 (20,000). LRMS: M-H^{+}+2Na^{+}: 407.

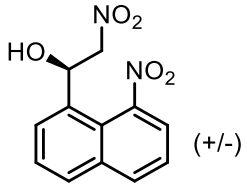

1-(2-nitro-1-ethanol)-8-nitronaphthalene (**4.6**)

0.746 g (37.1 mmoles; 1 eq) of **4.3a** was added to 30 mL of a 1:1 mixture of absolute ethanol:nitromethane. 0.541 g (65.9 mmoles; 1.8 eq) sodium acetate was added and this mixture was heated to 40^{o}C for 20 hours. After cooling to room temperature, this was quenched with 30 mL water and extracted into dichloromethane. After washing with 2 x 50 mL, the combined organic phases are dried over magnesium sulfate, filtered to remove the solid and the solvent was evaporated under reduced pressure to yield 0.650 g **4.6** as a yellow oil (66.7%). ^{1}H NMR ($CDCl_3$, 300 MHz, 298K): 8.36 (d, 1*H*, $^{3}J_{HH}$ = 8.8 Hz), 8.30 (d, 1*H*, $^{3}J_{HH}$ = 8.8 Hz), 8.09 (dofd, 1*H*, $^{3}J_{HH}$ = 7.7 Hz, $^{4}J_{HH}$ = 1.0 Hz), 7.84 (d, 1*H*, $^{3}J_{HH}$ = 7.2 Hz), 7.66 (dofd, 1*H*, $^{3}J_{HH}$ = 8.8 Hz, $^{3}J_{HH}$ = 7.7 Hz), 7.59 (dofd, 1*H*, $^{3}J_{HH}$ = 8.8 Hz, $^{3}J_{HH}$ = 7.7 Hz), 6.18 (dofd, 1*H*, $^{3}J_{HH}$ = 8.3 Hz, $^{3}J_{HH}$ = 3.4 Hz), 4.61 (overlapping doublets, 2*H*, $^{3}J_{HH}$ = 8.3 Hz, $^{3}J_{HH}$ = 3.4 Hz).

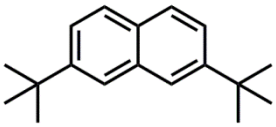

2,7-*di*-tert-*butylnaphthalene* (**4.7b**)

To a suspended solution of 11.450 g (0.0893 moles, 1 eq) naphthalene in 60mL dichloromethane cooled to 0ºC was added 2.776 g (23.3 mole %) aluminum trichloride. This mixture was stirred at 0ºC for 1.5 hours before 18.093 g (0.195 moles, 2.18 eq) 2-chloro-2-methylpropane was added dropwise from an addition funnel. This mixture was warmed gently to room temperature and heated to reflux overnight (10.5h). After cooling to room temperature the reaction was quenched with 80 mL 10% hydrochloric acid. The organic layer is separated and washed twice with 80 mL 10% hydrochloric acid and once with brine. The organic layer was dried over anhydrous magnesium sulfate and filtered to remove the solid. After concentration under reduced pressure, a 1:1 mixture of the 2,6-di-*tert*-butylnaphthalene and the 2,7-di-*tert*-butylnaphthalene was acquired. This mixture was taken up into 100 mL anhydrous ethanol and 16.093 g of thiourea is added. This mixture was heated to reflux for 2 hours and then cooled to room temperature. Once cooled, this mixture was filtered to remove the thiourea co-crystallized with the undesired regioisomer. This process is repeated a further two times before the desired regioisomer **4.7b** is collected as a white solid. Yield: 5.90 g (27.4%). ^{1}H NMR ($CDCl_3$, 298K, 300 MHz): δ 7.76 (d, 4*H*, $^{3}J_{HH}$ = 9.3 Hz), 7.53 (dofd, 2*H*, $^{3}J_{HH}$ = 8.6 Hz, $^{4}J_{HH}$ = 1.9 Hz), 1.44 (s, 18*H*). ^{13}C {^{1}H} NMR ($CDCl_3$, 298K, 75.50 MHz): δ 148.5, 127.8, 127.2, 124.4, 123.1, 31.5. IR (thin film): 2950, 2861, 1465, 1360, 1260, 1104, 960, 880.

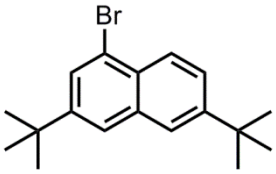

4-*bromo*-2,7-*di*-tert-*butylnaphthalene* (**4.8**)

1.280 g (0.00532 moles, 1 eq) **4.7a** was dissolved in 30 mL dichloromethane and cooled to 0ºC. To this mixture was added 1.089 g (0.00683 moles; 1.3 eq) bromine in 15 mL dichloromethane dropwise over 15 minutes. This mixture was stirred at 0ºC for 1 hour before warming to room temperature and continued to stir overnight (18h). This mixture was quenched with 30 mL 0.5N sodium hydroxide and the organic layer was separated and washed twice with 70 mL 0.5N sodium hydroxide and once with 70 mL brine. The organic layer was dried over magnesium sulfate and filtered to remove the solid. The solvent is removed under reduced pressure to yield **4.8** as a brown oil. Yield: 0.840 g (49.6%).^{1}H NMR ($CDCl_3$, 298K, 300 MHz): δ 8.08 (d, 1*H*, $^{3}J_{HH}$= 8.7 Hz), 7.78 (d, 1*H*, $^{3}J_{HH}$ = 2.6 Hz), 7.71 (m, 2*H*), 7.60 (dofd, 1*H*, $^{3}J_{HH}$ = 8.7 Hz, $^{4}J_{HH}$ = 1.9 Hz), 1.40 (s, 9*H*), 1.38 (s, 9*H*).^{13}C {^{1}H} NMR ($CDCl_3$, 298K, 75.5 MHz): δ 162.5, 149.5, 128.1, 126.4, 125.5, 123.3, 123.1, 122.6, 53.4, 31.2.IR (thin film): 2952, 2862, 1462, 1362, 1264, 1107, 965, 881, 816.

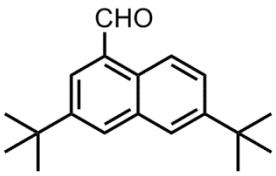

2,7-*di*-tert-*butyl*-4-*naphthaldehyde* (**4.9**)

0.898 g (2.82 mmoles, 1 eq) **4.8** was dissolved in 20mL tetrahydrofuran and cooled to -78ºC in a dry ice/acetone bath. To this was added 8.6 mL (excess, 6 eq) *n*BuLi dropwise via syringe over 20 minutes. This mixture was allowed to stir for a further two hours before the addition of 2.7 mL dimethylformamide (excess). This mixture was warmed to 0ºC and this mixture was allowed to stir for 2.5 hours. This mixture was quenched with brine and

extracted twice into 60mL ethyl acetate. The organic layers were combined and washed twice with 1.0M hydrochloric acid and once with brine. The combined organic layers were dried over magnesium sulfate and filtered to remove the solid. The solvent is removed under reduced pressure to yield crude **4.9** as a brown oil. Column chromatography was done on a silica column with benzene as the eluent. Yield: 0.66 g (87%).

^{1}H NMR ($CDCl_3$, 298K, 300 MHz): δ 10.41 (s, 1*H*), 8.02 (s, 1*H*), 7.83 (d, 1*H*, $^{4}J_{HH}$ = 2.0 Hz), 7.75 (m, 2*H*), 7.35 (s, 1*H*), 1.47 (s, 9*H*), 1.41 (s, 9*H*).^{13}C NMR ($CDCl_3$, 298K, 75.5 MHz): IR (thin film): 2960, 2868, 1692, 1462, 1363, 1258, 1211, 1075, 923, 900, 830, 738.

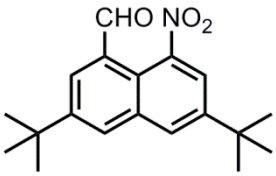

2,7-di-*tert-butyl*-5-*nitro*-4-*napthaldehyde* (**4.10**)

3.18 g (0.0114 moles; 1 eq) of **4.8** was added to a 15 mL solution of trifluoracetic acid and this mixture was cooled to -10^{o}C in a salt/ice bath. Slowly added was 4.1 mL (6.20g; 0.0984 g, 8.7 eq) nitric acid slowly over 15 minutes. This mixture was warmed to room temperature over one hour and is then quenched by 25mL of ice. The mixture was extracted into diethyl ether 3 x 60mL, the organic layers were combined and dried over magnesium sulfate. The mixture was filtered to remove the solid and the solvent was removed under reduced pressure to yield **4.10** as a mixture of regioisomers. Column chromatography was done with a gradient mixture of solvents from 2:1 dichloromethane:hexaens to 3:1 dichloromethane:hexanes to 100% dichloromethane. Fractions 7-9 are combined and the solvent was removed under reduced pressure to yield **4.10** as a yellow solid. Yield: 0.808 g (21.9%)^{1}H NMR ($CDCl_3$, 298K, 300 MHz): δ 10.11 (s, 1*H*), 8.11 (dofd, 2*H*, $^{3}J_{HH}$ = 6.2 Hz, $^{4}J_{HH}$ = 1.9 Hz), 8.01 (dofd, 2*H*, $^{3}J_{HH}$ = 4.0 Hz, $^{4}J_{HH}$

= 2.0 Hz), 1.45 (s, 9*H*), 1.42 (s, 9*H*). ^{13}C NMR ($CDCl_3$, 298K, 75.5 MHz): δ 190.2, 149.7, 149.4, 147.7, 135.4, 133.4, 132.4, 129.9, 129.1, 123.6, 35.1, 34.9, 30.9(4), 30.9(0). IR (thin film): 2963, 1697, 1540, 1468, 1362, 1348, 1264, 738. HRMS: calculated M+Na^+: 336.15700, found M+Na^+: 336.15702.

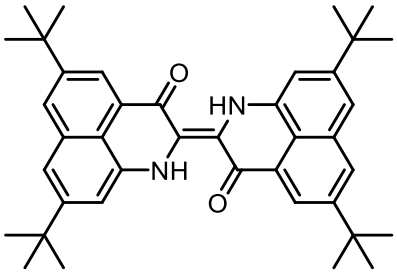

5,5',8,8'-tetra-tert-*butyl-perinaphthindigo* (**4.11**)

132 mg (0.393, 1 eq) of **4.10** was dissolved in 10 mL acetone in a 100mL round bottom flask. This mixture was cooled to -10°C and 1 mL of 0.2N potassium hydroxide was added by syringe. This mixture was stirred at -10°C for a further 15 minutes before 8 mL of 0.5N potassium hydroxide was added over 10 minutes. This mixture was warmed gradually to room temperature and stirred for 2 hours (19h). This was transferred to a 50 mL centrifuge tube and spun for 1 hour (RPM: 3250, room temperature). The liquid was decanted off and a solid was collected and allowed to dry. ^{1}H NMR (DMSO-d_6, 300 MHz, 298K): 7.71 (d, 2*H*, $^4J_{HH}$ = 2.1 Hz), 7.63, (d, 2*H*, $^4J_{HH}$ = 5.8 Hz), 7.53 (m, 2*H*), 7.48 (m, 2*H*), 1.40 (s, 18*H*), 1.30 (s, 18*H*). IR (thin film, air background, cm^{-1}): 3253, 1656, 1587,1530, 1350, 833. UV-Vis (DCM, 1x10^{-4}M, DMSO): 644 (16,000).

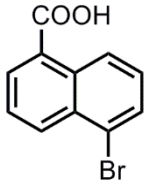

5-*bromo*-1-*naphthoic acid* (**4.12**)

To a suspension of 10.901 g (0.0633 moles, 1 eq) of **4.11** in 60 mL of glacial acetic acid was added 11.507 g (0.0722 moles, 1.14 eq) bromine dropwise by syringe. This mixture was heated to reflux for 38 hours. The mixture was cooled to room temperature before being filtered in air. The resulting solid was washed extensively with hexanes and dried. **4.12** acid was collected as a beige solid. Yield: 10.542g (66.6%). ^{1}H NMR (d_6-dmso, 298K, 300 MHz): δ 13.36 (broad s, 1*H*), 8.85 (d, 1*H*, $^{3}J_{HH}$ = 8.7 Hz), 8.38 (d, 1*H*, $^{3}J_{HH}$ = 8.5 Hz), 8.19 (dofd, 1*H*, $^{3}J_{HH}$ = 7.3 Hz, $^{4}J_{HH}$ =1.2 Hz), 7.97 (dofd, 1*H*, $^{3}J_{HH}$ = 7.6 Hz, $^{4}J_{HH}$ = 1.0 Hz), 7.75 (dofd, 1*H*, $^{3}J_{HH}$ = 8.7 Hz, $^{4}J_{HH}$ = 7.3 Hz), 7.55 (dofd, 1*H*, $^{3}J_{HH}$ = 8.7 Hz, $^{4}J_{HH}$ = 7.6 Hz).^{13}C NMR (d_6-dmso, 298K, 300 MHz): δ168.3, 131.9, 131.3, 130.9, 130.5, 130.3, 128.7, 128.1, 126.7, 125.7, 123.4.IR (thin film, cm^{-1}): 3070, 2913, 2716, 1667, 1297, 1146, 1018, 906, 777

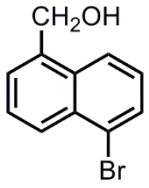

5-*bromo*-1-*naphthalenemethanol* (**4.13**)

To a suspension of 2.378g (9.51 mmoles; 1eq) **4.12** in 20 mL tetrahydrofuran cooled to 0^{o}C was added 3.8 mL (19.0 moles; 2 eqs) dimethyl sulfide stabilized borane dropwise by syringe. This mixture was warmed gradually to room temperature and stirred for 4 hours. This mixture was then warmed to reflux overnight (16h). The mixture was cooled to room temperature and quenched with brine. The aqueous layer was extracted twice with 50 mL dichloromethane. The organic layers were combined, washed once with brine, dried over

magnesium sulfate and filtered to remove the solid. The solvent was removed under reduced pressure to yield **4.13** as a beige solid. Yield: 1.419g (63.2%).^{1}H NMR (d_6-dmso, 298K, 300 MHz): δ 8.12 (d, 1*H*, $^{3}J_{HH}$ = 8.4 Hz), 8.08 (d, 1*H*, $^{3}J_{HH}$ = 8.4 Hz), 7.87 (dofd, 1*H*, $^{3}J_{HH}$ = 7.4 Hz, $^{4}J_{HH}$ = 0.8 Hz), 7.64 (m, 2*H*), 7.44 (d, 1*H*, $^{3}J_{HH}$ = 8.4 Hz, $^{3}J_{HH}$ = 7.4 Hz), 5.43 (t, 1*H*, $^{3}J_{HH}$ = 5.4 Hz), 4.99 (d, 2*H*, $^{3}J_{HH}$ = 5.4 Hz).^{13}C NMR (d_6-dmso, 298K, 75.5 MHz): δ 138.7m 131.2, 129.8, 127.3, 126.5, 125.6, 125.2, 124.1, 122.3, 61.0. IR (thin film, cm^{-1}): 3288, 2913, 2840, 1166, 1088, 1071, 1001, 774.

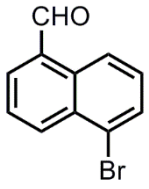

5-*bromo*-1-*naphthaldehyde* (**4.14**)

A suspension of 0.843g (3.57 mmoles; 1eq) **4.13** in 20 mL chloroform was heated to reflux. To this was added 2.07g (23.8 mmoles; 6.7eq) manganese dioxide (60-230 mesh, activated) and this mixture was refluxed overnight (19h). The mixture is cooled to room temperature and filtered over a fritted funnel with a layer of Celite. The solvent was removed under reduced pressure to yield **4.14** as a beige solid. Yield: 0.745g (89.1%).

^{1}H NMR ($CDCl_3$, 298K, 300 MHz): δ 10.37 (s, 1*H*), 9.23 (doft, 1*H*, $^{3}J_{HH}$ = 8.7 Hz, $^{4}J_{HH}$ = 0.8 Hz), 8.54 (dofd, 1*H*, $^{3}J_{HH}$ = 8.7 Hz, $^{4}J_{HH}$ = 0.8 Hz), 8.01 (dofd, 1*H*, $^{3}J_{HH}$ = 7.2 Hz, $^{4}J_{HH}$ = 1.2 Hz), 7.87 (dofd, 1*H*, $^{3}J_{HH}$ = 7.4 Hz, $^{4}J_{HH}$ = 0.8 Hz), 7.71 (dofd, 1*H*, $^{3}J_{HH}$ = 8.4 Hz, $^{3}J_{HH}$ = 7.2 Hz), 7.49 (dofd, 1*H*, $^{3}J_{HH}$ = 8.4 Hz, $^{3}J_{HH}$ = 7.4 Hz). ^{13}C NMR ($CDCl_3$, 298K, 75.5 MHz): δ 192.8, 137.1, 134.2, 132.2, 131.9, 131.6, 131.2, 126.2, 124.7, 123.4. IR (thin film, cm^{-1}): 2834, 1678, 1208, 1090, 1068, 777.

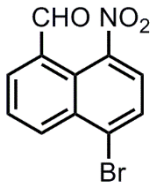

5-*bromo*-2-*nitro*-1-*naphthaldehyde* (**4.15a**)

0.745g (3.18 mmoles; 1eq) of **4.14** was added over 5 minutes to a 20 mL solution of 3:1 concentrated nitric acid:concentrated sulfuric acid cooled to 0°C. This mixture was stirred for 1.5 hours at 0°C before warming to room temperature for 2 hours. Filtration yielded a yellow solid as a mixture of regioisomers. Column chromatography (silica gel, 30 cm, 3:1 dichloromethane:hexanes) yielded **4.15a** as a single regioisomer. Yield: 0.174 g (48.9%).^{1}H NMR ($CDCl_3$, 298K, 300 MHz): δ 10.32 (s, 1*H*), 9.40 (d, 1*H*, $^{3}J_{HH}$ = 9.4 Hz), 8.71 (d, 1*H*, $^{3}J_{HH}$ = 8.7 Hz), 8.12 (dofd, 1*H*, $^{3}J_{HH}$ = 7.1 Hz, $^{4}J_{HH}$ = 1.0 Hz), 7.83 (overlapping d and dofd, 2*H*). ^{13}C NMR ($CDCl_3$, 298K, 75.5 MHz): δ 192.4, 149.5, 139.1, 132.7, 131.6, 128.3, 126.5, 123.3. IR (thin film, cm^{-1}): 3086, 2913, 2840, 1695, 1527, 1345, 1267, 1205, 1054. HRMS: calculated M+H^{+}: 279.96041, found M+H^{+}: 279.96045.

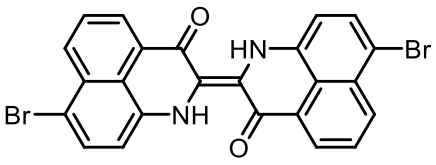

7,7'-dibromoperinaphthindigo (**4.16**)

125 mg (0.448 mmoles; 1 eq) of **4.15a** was dissolved in 10 mL acetone in a 50mL round bottom flask. This mixture was cooled to -10°C and 2 mL of 0.2N potassium hydroxide is added by syringe. This mixture was stirred at -10°C for a further 15 minutes before 9 mL of 0.5N potassium hydroxide was added over 5 minutes. This mixture was warmed gradually to room temperature and stirred overnight (19h). This was transferred to a 50 mL centrifuge tube and spun for 1 hour (RPM: 3250, room temperature). The liquid was decanted off and a solid is collected and allowed to dry. After extraction into

dichloromethane, **4.16** is collect as a dark purple solid in a 21 mg (10 %) yield. ^{1}H NMR (DMSO-d_6, 300 MHz, 298K): 8.40 (dofd, 2H, $^{3}J_{HH}$ = 7.9 Hz, $^{4}J_{HH}$ = 2.5 Hz), 7.98 (s, 2*H*), 7.57 (m, 6*H).* IR (KBr, air background): 3467, 3133, 2358, 2336, 1633, 1608, 1289, 1247, 1208. UV-Vis (DMSO, 1x10^{-5}M, DMSO): 579 (8,000).

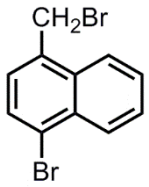

1-*bromo*-4-*bromomethyl*-*naphthalene* (**4.17**)

7.095 g (0.0321 moles; 1 eq) of **4.16** was suspended in 100mL carbon tetrachloride. At room temperature was added 6.296 g (0.0354 moles; 1.1 eq) N-bromosuccinamide and 0.282 g (3.29 mole %) benzoyl peroxide. This mixture was heated to reflux for 46 hours. After cooling to room temperature, the mixture was filtered over a fritted funnel to remove solid and the filtrate was concentrated under reduced pressure and **4.17** is collected as a pale yellow solid. Yield: 6.215 g (64.7%). ^{1}H NMR ($CDCl_3$, 298K, 300 MHz): δ 8.30 (m, 1*H*), 8.12 (m, 1*H*), 7.70 (d, 1*H*, $^{3}J_{HH}$ = 7.8 Hz), 7.63 (m, 3*H*), 4.89 (s, 2*H*). ^{13}C NMR ($CDCl_3$, 298K, 300 MHz): δ 133.4, 132.5, 132.1, 129.5, 128.1, 127.9, 127.6, 127.4, 124.6, 124.2, 30.8. IR (thin film, cm^{-1}): 2850, 2360, 1563, 1508, 1446, 1378, 1326, 1197, 1113, 915, 825, 755.

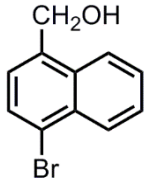

1-*bromo*-4-*naphthalenemethanol* (**4.18**)

1.294 g (0.00434 moles; 1 eq) of **4.16** is suspended in 100 mL of a 4:1 ethanol:water. To this was added 0.933 g (0.0137 moles; 3.2eqs) sodium formate. This mixture is heated to reflux for 19 hours. This mixture was cooled to room temperature and the ethanol was

removed under reduced pressure. To the water mixture was added 50 mL 2.5N sodium hydroxide solution. This mixture was placed in the freezer to induce crystallization. This was filtered to collect the solid which was recrystallized from water and filtered to collect **4.18** as a light brown solid. Yield: 0.723 g (70.3%). ^{1}H NMR ($CDCl_3$, 298K, 300 MHz): δ 8.14 (overlapping m, 2*H*), 7.85 (d, 1*H*, $^{3}J_{HH}$ = 7.6 Hz), 7.66 (overlapping dofdofd, 2*H*), 7.47 (d, 1*H*, $^{3}J_{HH}$ = 7.6 Hz), 5.42 (distorted t, 1*H*, $^{3}J_{HH}$ = ~4Hz), 5.94 (d, 2*H*, $^{3}J_{HH}$ = 3.4 Hz). ^{13}C NMR ($CDCl_3$, 298K, 75.5 MHz): δ 138.4, 131.9, 130.9, 129.5, 127.4, 126.9, 126.8, 124.8, 124.4, 120.7, 60.7. IR (thin film, cm^{-1}): 3411, 2918, 2815, 1264, 1088, 1006.

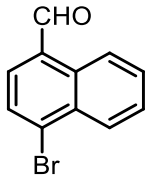

1-*bromo*-4-*naphthaldehyde* (**4.19**)

In a 100mL round bottom flask was suspended 6.729 g (0.0284 moles; 1.0 eq) **4.18** in 60 mL chloroform. To this was added 9.778 g (0.112 moles; 3.9 eq) manganese (IV) oxide and this mixture was warmed to reflux for 16 hours. After cooling this mixture to room temperature it was filtered over Celite on a fritted funnel to remove the excess manganese (IV) oxide. The solvent was removed under reduced pressure **4.19** as an off-white solid. Yield: 6.523 g (96.9%). ^{1}H NMR ($CDCl_3$, 298K, 300 MHz): δ 10.35 (s, 1*H*), 9.26 (m, 1*H*), 8.35 (m, 1*H*), 7.95 (d, 1*H*, $^{3}J_{HH}$ = 7.6 Hz), 7.79 (d, 1*H*, $^{3}J_{HH}$ = 7.6 Hz), 7.70 (overlapping dofdofd, 2*H*). ^{13}C NMR ($CDCl_3$, 298K, 75.5 MHz): δ 192.6, 136.0, 132.2, 131.5, 131.3, 131.0, 129.8, 129.4, 128.2, 127.7, 125.1. IR (thin film, cm^{-1}): 3064, 3036, 2862, 2767, 1684, 1558, 1507, 1222, 1155, 1054, 917, 816, 759.

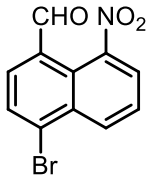

1-*bromo*-5-*nitro*-4-*naphthaldehyde* (**4.20a**)

1.415 g (6.02 mmoles; 1eq) of **4.19** was added over 5 minutes to a 20 mL solution of 3:1 concentrated nitric acid:concentrated sulfuric acid cooled to 0°C. This mixture was stirred for 1 hour at 0°C before warming to room temperature for 1 hour. Filtration yielded a yellow solid as a 1:1 mixture of regioisomers. Column chromatography (silica gel, 30 cm, 2:1 dichloromethane:hexanes) yielded **4.20a** as a single regioisomer. Yield: 0.565 g (48.9%). ^{1}H NMR ($CDCl_3$, 298K, 300 MHz): δ 10.35 (s, 1*H*), 9.57 (dofd, 1*H*, $^{3}J_{HH}$ = 8.7 Hz, $^{4}J_{HH}$ = 1.4 Hz), 8.14 (d, 1*H*, $^{3}J_{HH}$ = 7.8 Hz), 7.89 (d, 1*H*, $^{3}J_{HH}$ = 7.89 Hz), 7.85 (dofd, 1*H*, $^{3}J_{HH}$ = 7.6 Hz, $^{4}J_{HH}$ = 1.4 Hz), 7.74 (dofd, 1*H*, $^{3}J_{HH}$ = 8.7 Hz, $^{3}J_{HH}$ = 7.4 Hz). ^{13}C NMR ($CDCl_3$, 298K, 75.5 MHz): δ 192.0, 138.2, 137.1, 137.0, 134.5, 129.3, 128.9, 128.2, 127.7, 124.4. IR (thin film, cm^{-1}): 3086, 2907, 1686, 1555, 1527, 1493, 1351, 1230, 1197, 1169, 1124, 1102, 998. HRMS: calculated $M+H^{+}$: 279.96041, found: $M+H^{+}$: 279.96039.

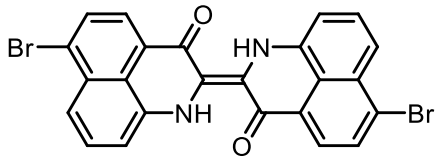

6,6'-dibromoperinaphthindigo (**4.21**)

232 mg (0.448 mmoles; 1 eq) of **4.20a** was dissolved in 10 mL acetone in a 50mL round bottom flask. This mixture was cooled to -10°C and 4 mL of 0.2N potassium hydroxide was added by syringe. This mixture was stirred at -10°C for a further 15 minutes before 9 mL of 0.5N potassium hydroxide was added over 5 minutes. This mixture was warmed gradually to room temperature and stirred overnight (19h). This was transferred to a 50 mL centrifuge tube and spun for 1 hour (RPM: 3250, room temperature). The liquid was decanted off and a solid is collected and allowed to dry. After extraction into

dichloromethane, **4.21** is collect as a dark purple solid in a 12 mg (2 %) yield. IR: 3467, 3133, 2358, 2336, 1633, 1608, 1289, 1247, 1208. UV-Vis (DMSO, $1x10^{-5}$M, DMSO): 608 (12,000).

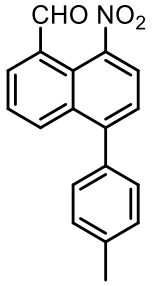

5-para-*tolyl-8-nitro-1-naphthaldehyde* (**4.22**)

100.9 mg (0.360 mmoles; 1 eq) **4.15a**, 41.9 mg (10 mol %) tetrakis(triphenylphosphine) palladium (0), 196.7 mg (1.42 mmoles; 3.6 eq) potassium carbonate, and 64.4 mg (0.474 mmoles; 1.3 eq) 4-tolylboronic acid was combined in a mixture of 6 mL toluene, 4 mL water, and 2 mL absolute ethanol. This mixture was heated to 95°C in an oil bath for 24 hours. After cooling to room temperature, the biphasic solution was quenched with a solution of saturated ammonium chloride before it was extracted into 2 x 20 mL dichloromethane. The organic layer was washed with 20 mL water and 20 mL saturated sodium carbonate. The organic layer was dried over sodium sulfate, filtered to remove the solid, and the solvent was removed under reduced pressure. Column chromatography (silica gel, 15 cm, 7:3 ethyl acetate: hexanes) yields 60 mg **4.22** as a tan solid (62 %). ^{1}H NMR ($CDCl_3$, 298K, 300 MHz): 10.09 (s, 1*H*), 8.08 (m, 5*H*), 7.67 (m, 3*H*), 7.25 (d, 1*H*, $^{3}J_{HH}$ = 8.4 Hz). ^{13}C NMR ($CDCl_3$, 298K, 75.5 MHz): 189.9, 146.8, 138.6, 134.4, 133.0, 132.6, 132.2, 132.0, 129.8, 129.4, 128.6, 128.4, 126.7, 126.3, 125.0, 21.2.

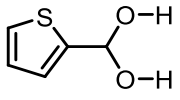

2-thienyl boronic acid (**4.23**)

8.240 g (0.0516 moles; 1 eq) 2-bromothiophene was suspended in 100 mL THF and this solution was cooled to -78^{o}C in a dry/ice acetone bath. 40.0 mL (0.064 moles: 1.25 eq) n-butyl lithium solution (1.6M) was added dropwise over 30 minutes via syringe. This mixture was stirred at -78^{o}C for 2.5 hours before the addition of 7.456 g (0.0718 moles; 1.4 eq) trimethylborate. This mixture was warmed to room temperature and stirred for 18 hours. The reaction was quenched with 100 mL of 1M aqueous HCl. This mixture was extracted into 250 mL ether and washed 2 x 100 mL aqueous HCl and 2 x 100 mL brine. The organic layer was dried over magnesium sulfate, filtered to remove the solid and the solvent was removed under reduced pressure to yield **4.23** a white solid. Yield: 6.52 g (79.1%) ^{1}H NMR (MeOD, 300 MHz, 298K): 7.61 (broad singlet, 2*H*), 7.16 (broad singlet, 1*H*). BO*H* not observed. ^{13}C NMR (MeOD, 75.5 MHz, 298K): 132.3, 128.84.

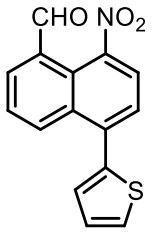

8-nitro-5-thienyl-1-naphthaldehyde (**4.24**)

287 mg (1.03 mmoles; 1 eq) **4.15a**, 157 mg (1.23 mmoles; 1.2 eq) 2-thienyl boronic acid, 556 mg (4.96 mmoles; 4.8 eq) DABCO, 656 mg (2.01 mmoles; 2.0 eq) cesium carbonate, and 68.6 mg (30 mol %) palladium acetate was combined a 20 mL DMF in a 100 mL round bottom flask and heated to 110^{o}C for 20 hours. After cooling to room temperature the reaction mixture was quenched with water, extracted 2 x 50 mL DCM. The combined organic layers were dried over magnesium sulfate and filtered to remove the solid. After the solvent was removed under reduced pressure, **4.24** was is collected as a brown solid

which is purified by column chromatography with 2:1 dichloromethane:hexanes as an eluent. Yield: 150 mg (52%). ^{1}H NMR ($CDCl_3$, 300 MHz, 298K): 10.15 (s, 1*H*), 8.51 (dofd, 1*H*, $^{3}J_{HH}$ = 8.7 Hz, $^{4}J_{HH}$ = 1.3 Hz), 8.16 (d, 1*H*, $^{3}J_{HH}$ = 7.9 Hz), 8.13 (dofd, 2*H*, $^{3}J_{HH}$ = 7.3 Hz, $^{4}J_{HH}$ = 1.3 Hz), 7.72 (m, 3*H*), 7.54 (dofd, $^{3}J_{HH}$ = 4.9 Hz, $^{3}J_{HH}$ = 1.4 Hz). ^{13}C NMR ($CDCl_3$, 75.5 MHz, 298 K): 190.1. 134.5, 132.1, 127.8, 127.7, 126.8, 124.7.

Chapter 5: Investigation of the Spectroscopic Properties and Acid/Base Chemistry of Nindigo

5.1 Introduction

Nindigo has exhibited tremendous versatility and potential as a ligand for the co-ordination of transition metal and main group atoms.[107-111, 113-115] However, Nindigo itself could also, in principle, be utilized for advanced technological applications such as organic field effect transistors, dye-sensitized solar cells and biomedical imaging. In order to be considered for these applications, the physical properties of Nindigo need to be fully understood. Many derivatives of Nindigo have been synthesized, but there remained some unexplained results in the UV-Vis spectroscopy: in particular, two peaks which are red-shifted from the proposed π-to-π transition (586 nm) found at 657 nm and 741 nm (DCM) (**Figure 37**, spectrum of Nindigo shown in purple). These two peaks show dependence on a variety of variables including the nature of the aryl substituent, concentration, and solvent. Computational studies predicted a single electronic transition between 580-590 nm.[110] When Nindigo is compared with indigo (run at the same concentration, **Figure 37**, spectrum of indigo shown in blue), an analogous electronic transition for indigo is observed at 599 nm (DCM), without red-shifted peaks. This chapter presents the results of spectroscopic studies to try to better understand the visible spectroscopy of Nindigo. Also presented in this chapter is the discovery that Nindigo can be readily protonated and that the act of protonation induces an isomerization of the central carbon-carbon double bond of Nindigo from *trans* to *cis*.

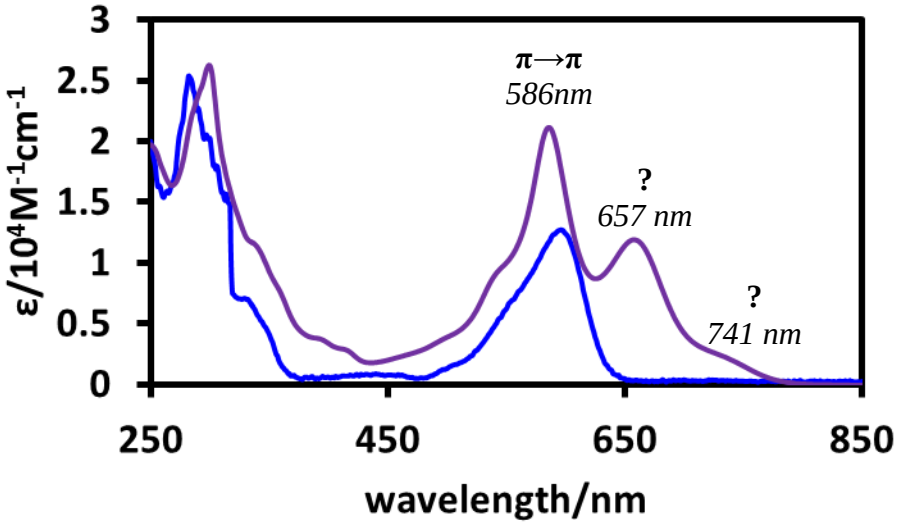

Figure 37. UV-Vis spectrum of Nindigo **3.13** (purple, CH_2Cl_2, 5μM, 298K) and indigo (**3.1**, blue, CH_2Cl_2 5μM, 298K).

5.2 Protonation of Nindigo, monoimine indigo, and indigo

5.2.1 Protonation of Nindigo

In unpublished work by Dr. Graeme Nawn, it was observed that treatment of Nindigo with strong acids led to a stable, intense green solution. The product of these reactions were studied by ^{1}H NMR spectroscopy and UV-Vis spectroscopy. This led us to treat Nindigo with a series of strong acids such as trifluoroacectic acid, trifluoromethane sulfonic acid, hydrochloric acid, and acetic acid all of which gave green solutions. This chemistry can be done preparatively in high yields (**Scheme 36**). A weaker acid such as benzoic acid did not induce this colour change. The UV-Vis of the resulting protonated compound is shown in **Figure 38** with a λ_{max} (DCM) = 655 nm. The ^{1}H NMR spectrum collected (**Figure 39**) was inconsistent with structure **5.1b**. Downfield, two peaks appear

at 16.15 ppm and 13.01 ppm which reliably integrate 1:2, respectively. This observation is inconsistent with structure **5.1b** in which all the N-H peaks are chemically inequivalent and would appear as three separate resonances, each integrating to one. Perhaps even more compelling is the lone methyl group resonance at 2.15 ppm which integrates to 12 hydrogen atoms. Again, if the product was compound **5.1b** then two methyl group resonances would be expected. The ^{1}H NMR evidence supports a more symmetric structure than **5.1b**, possibly **5.1a**. The hypothesized structure which was in better agreement with the NMR spectrum is structure **5.1a** which was eventually confirmed through X-ray crystallography. This study revealed that the central carbon-carbon olefin has undergone *trans* to *cis* isomerization about the central carbon-carbon double bond (**Figure 40**, **Table 6**).

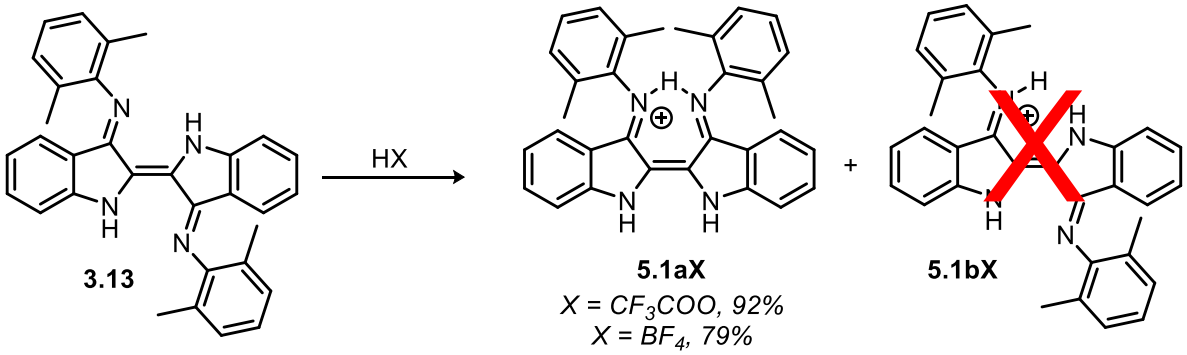

Scheme 36. Protonation of compound **3.13** with a strong acid.

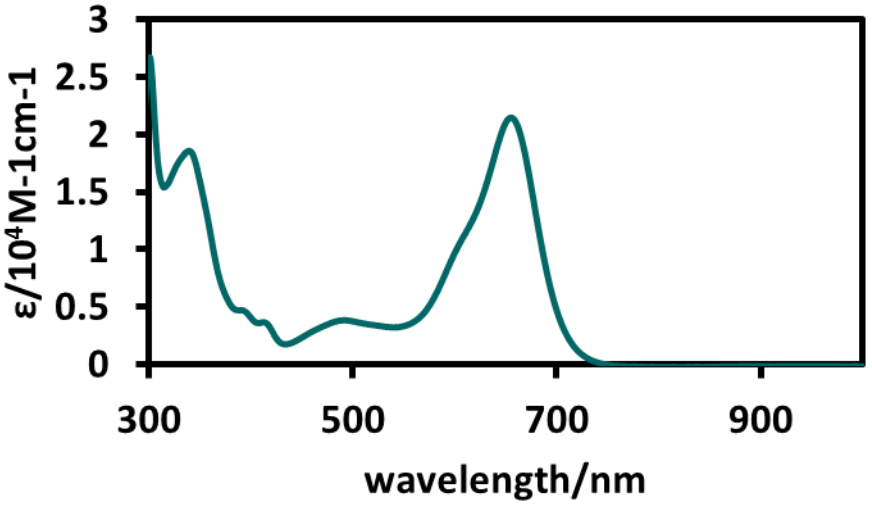

Figure 38. UV-Vis spectrum of **5.1aCF$_3$COO** (CH_2Cl_2, 25μM, 298K).

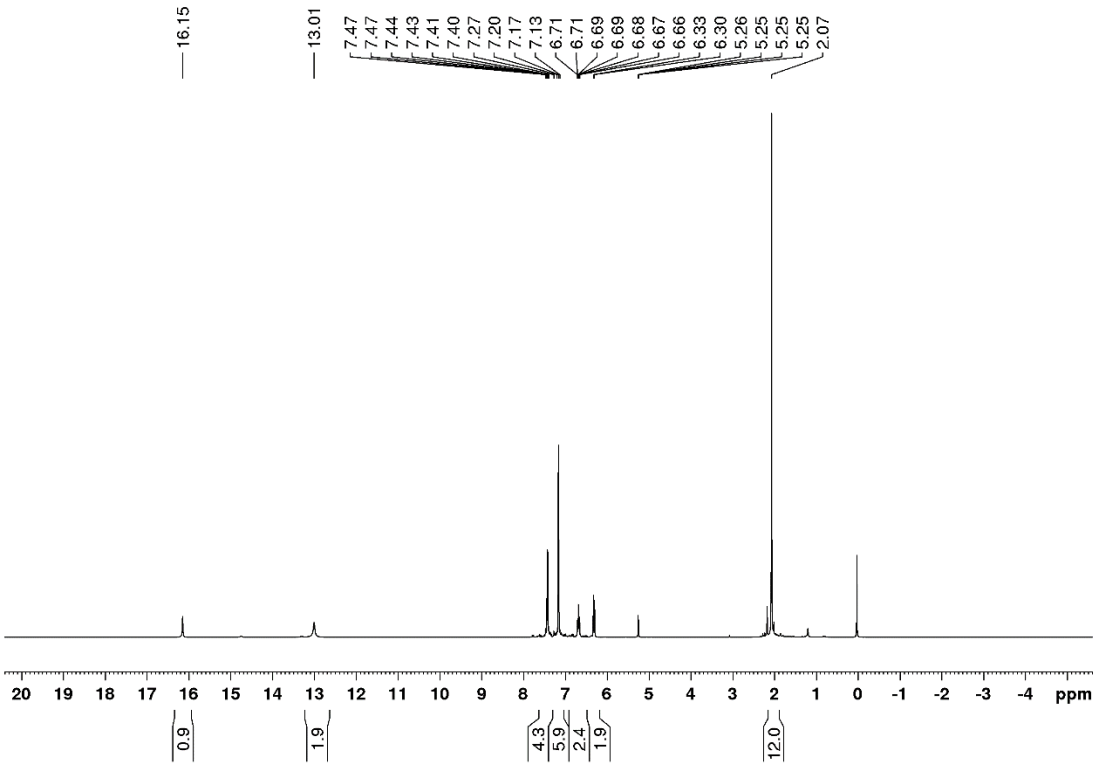

Figure 39. ^{1}H NMR spectrum of compound **5.1aCF$_3$COO** in CD_2Cl_2.

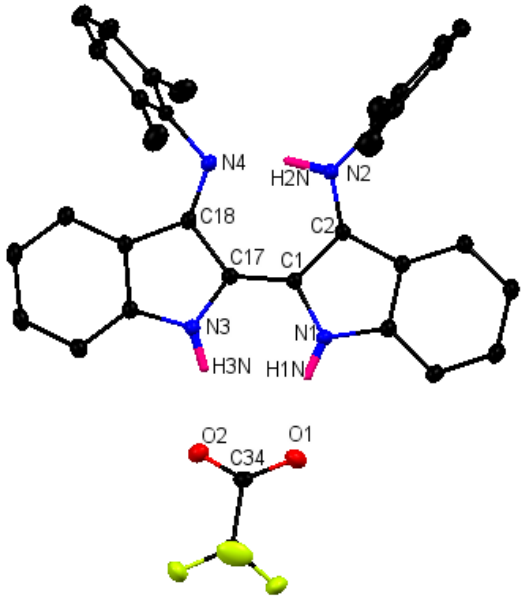

Figure 40. X-ray crystal structure of compound **5.1aCF$_3$COO.** All hydrogen atoms with the exception of the N-H protons removed for clarity. Thermal ellipsoids shown at the 50% probability level.

Bond	Bond Length (Å)
N4-C18	1.3007(14)
C18-C17	1.4838(14)
C17-C1	1.3852(14)
C1-C2	1.4678(14)
C2-N2	1.3153(13)
N2-H2N	0.93(3)
C17-N3	1.3695(13)
C1-N1	1.3807(13)
N3-H3N	0.894(19)
N1-H1N	0.912(19)
H3N-O2	1.847
H1N-O1	1.872
O2-C34	1.2449(14)
O1-C34	1.2399(14)

Table 6. Selected bond lengths for compound **5.1aCF$_3$COO**.

Although protonated Nindigo **5.1aCF$_3$COO** has pseudo-C_{2v} symmetry in solution, the solid state structure of **5.1aCF$_3$COO** does not possess this symmetry. For instance, the N4-

C18 bond length is slightly shorter than the C2-N2 bond. Another site of bond length asymmetry are between C17-N3 and C1-N1. The trifluoroacetate counterion serves as a good hydrogen bond partner for H3N and H1N with close contact distances of 1.847Å and 1.872Å, respectively. These hydrogen bonds appear to be present in solution, based on the downfield ^{1}H NMR chemical shifts for H3N and H1N of 13.01 ppm.

This isomerization was unexpected and we were interested in the mechanism. As discussed in Chapter 3, indigo does not undergo *cis-trans* isomerization due to an intramolecular hydrogen bond between the hydrogen atom on the indole nitrogen atom and the carbonyl oxygen atom. In contrast, thioindigo lacks these hydrogen bonds and can isomerize photochemically. Because Nindigo, like indigo, has hydrogen atoms on the indole nitrogen atoms, we initially assumed that light-driven isomerization was unlikely. This assumption was tested in the protonation experiments by performing the protonation in the absence of light, this time using tetrafluoroboric acid to produce **5.1aBF$_4$**. Reaction of Nindigo with tetrafluoroboric acid in the dark gave the analogous to **5.1aCF$_3$COO** product **5.1BF$_4$** which also consisted of an isomerized protonated Nindigo. Since the tetrafluoroborate counterion is a poorer hydrogen bond partner than trifluoroacetate, the chemical shift of the hydrogen atoms bound to the indole rings in **5.1BF$_4$** are significantly upfield (9.71 ppm) relative to the chemical shift in **5.1aCF$_3$COO** (13.01 ppm). Compound **5.1aBF$_4$** was also characterized by X-ray crystallography (**Figure 41**, **Table 7**). The bond length analysis for **5.1aBF$_4$** was very similar than for **5.1aCF$_3$COO** where the bond lengths are not perfectly centrosymmetric, especially within the core the molecule. The tetrafluoborate counterion in **5.1aBF$_4$** has longer contact distances between H3N and H1N

and F1 than H3N and H1N with O1 and O2, respectively for **5.1aCF$_3$COO**. This is consistent with the solution ^{1}H NMR data.

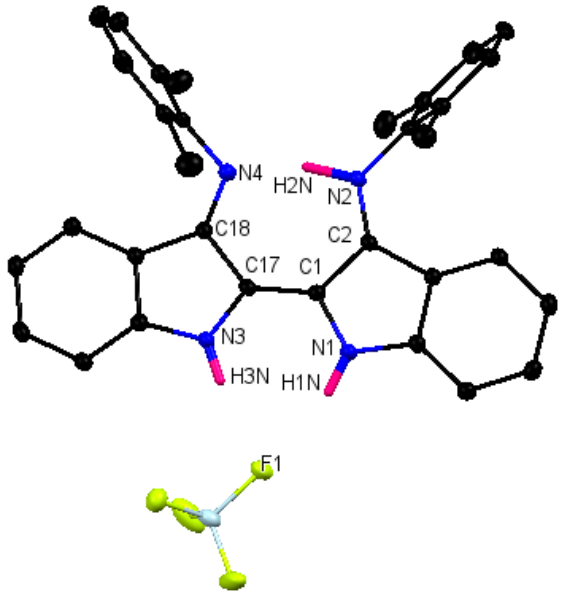

Figure 41. X-ray crystal structure of compound **5.1aBF$_4$**. All hydrogen atoms except N-H protons removed for clarity. Thermal ellipsoids shown at the 50% probability level.

Bond	**Bond Length (Å)**
N4-C18	1.2974(15)
C18-C17	1.4836(15)
C17-C1	1.3800(15)
C1-C2	1.4649(15)
C2-N2	1.3142(14)
N2-H2N	1.05(2)
C17-N3	1.316(15)
C1-N1	1.3881(14)
N3-H3N	0.861(18)
N1-H1N	0.890(18)
H3N-F1	1.980
H1N-F1	2.060

Table 7. Selected bond lengths for compound **5.1aBF$_4$**.

The question of the mechanism of isomerization accompanying protonation is an interesting one. There are two possible isomerization pathways, shown in **Scheme 37**. The first possibility is that there was a rapid equilibrium between the *cis* and *trans* forms of the neutral Nindigo and the *cis* form was more basic so it was isolated upon protonation. The alternative is that the protonation occurred first and this was followed by isomerization to the final product, protonated Nindigo **5.1a**.

We hoped to observe an intermediate that would allow us to differentiate between the two mechanisms, and for this we turned to UV-Vis spectroscopy. Initially, an experiment was performed where one equivalent of acid was added to a solution of Nindigo and a visible spectrum was obtained immediately. However, the reaction was complete in within the "mixing time" of the experiment, so we resorted a stopped-flow experiment which can be performed on a faster time scale.

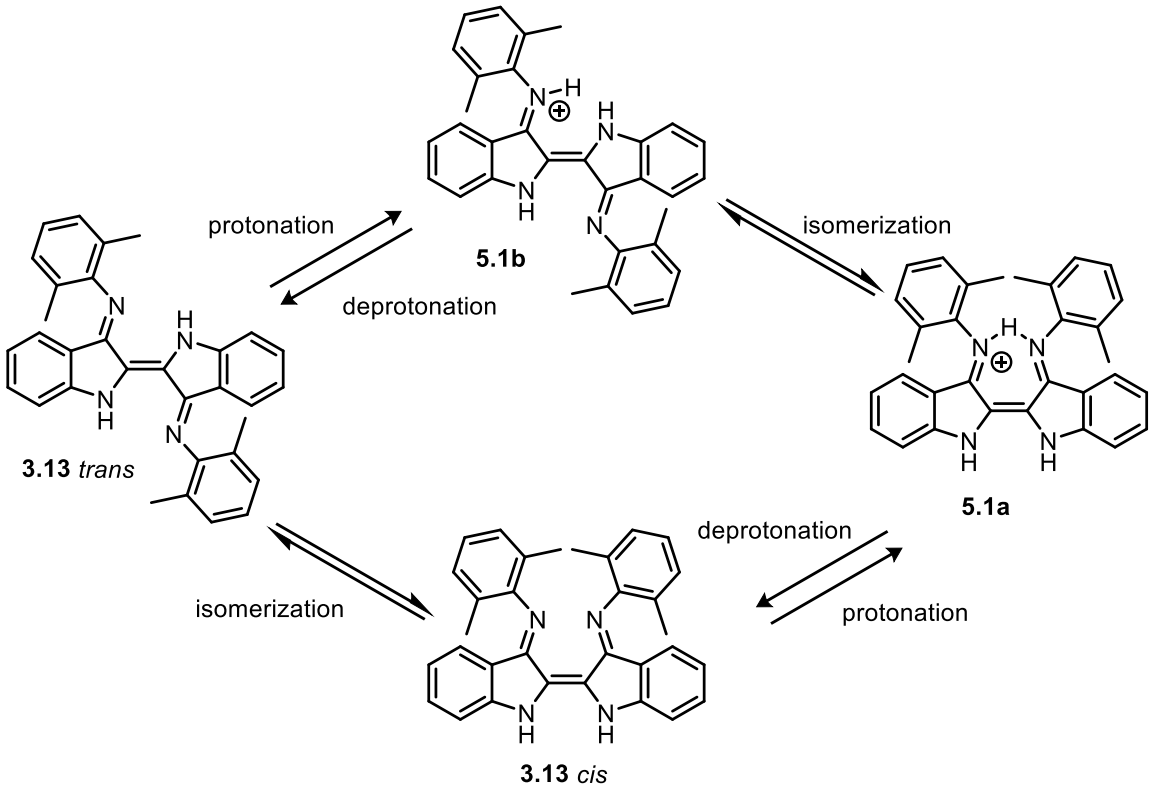

Scheme 37. Possible pathways from compound **3.13** (*trans*) to compound **5.1a**.

Stopped-flow UV-Vis experiments were performed in which a solution of compound **3.13** in methanol and a solution of acetic acid (at varying concentrations) in methanol were mixed. These experiments were designed to observe the protonated species at 635 nm (this wavelength was selected as the protonated species absorbs at 655 nm but a mercury-xenon lamp was used which has a sharp emission at 635 nm so selection of this wavelength will maximize the output). The absorbance intensity was monitored at 635nm as a function of time. The time frame observed was 0.5s, but it is clear that the reaction is over within the first 10% of this time (**Figure 42**, **Figure 43**).

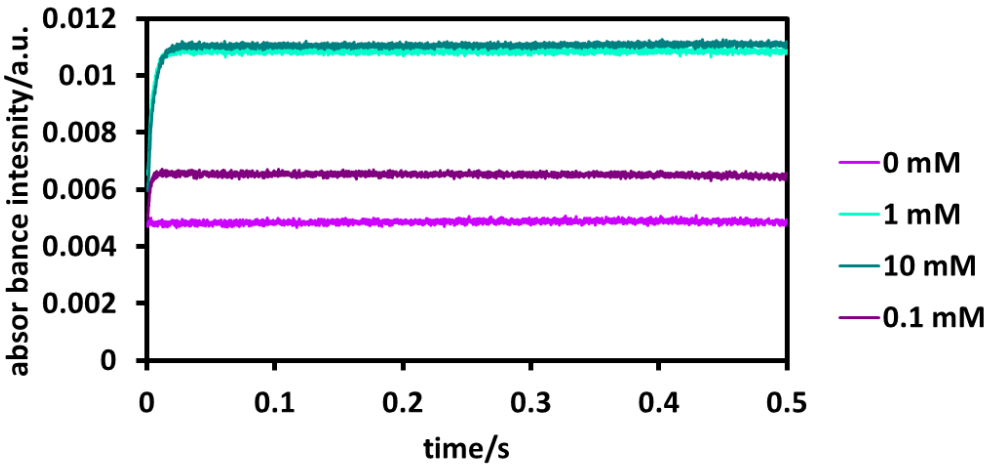

Figure 42. Stopped-flow studies of compound **3.13** (MeOH, 0.1mM, 298K, 0.5s) and varying concentrations of acetic acid (see legend).

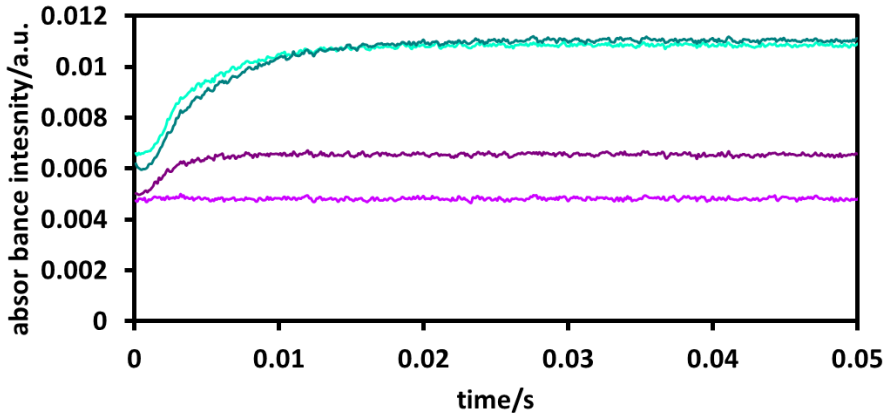

Figure 43. Stopped-flow studies of compound **3.13** (MeOH, 0.1mM, 298K, 0.05s) and varying concentrations of acetic acid (see legend in **Figure 43**).

Two different observations can be made from the stopped-flow results. The first was that the slope of the increasing absorbance intensity is similar regardless of the acid concentration. This indicated that the process that is being observed is the isomerization of the internal double bond as it showed no acid dependence. The second observation from

the stopped-flow experiment is that t = 0 for all concentrations of acid started at approximately the same location on the absorbance intensity axis. If the transformation of compound **3.13***trans* to **5.1a** proceeded first through the protonated species followed by the isomerization, the absorbance intensity would vary with different concentrations of acid. This allowed us to infer the other pathway (passing through a *cis*, neutral intermediate) was more likely.

5.2.2 Protonation of indigo monoimine

The indigo monoimine (compounds **5.2** and **5.3**) can be accessed by using the same reaction conditions as the Nindigo synthesis with the exception of the solvent which was switched from *m*-xylene to the lower boiling point toluene (**Scheme 38**).[115] Careful selection of one-to-one stoichiometry of the aniline to indigo leads to the monoimine product. The UV-Vis spectrum of indigo monoimine **5.3** is shown below in **Figure 44** and has an absorption maximum of 592 nm (DCM).

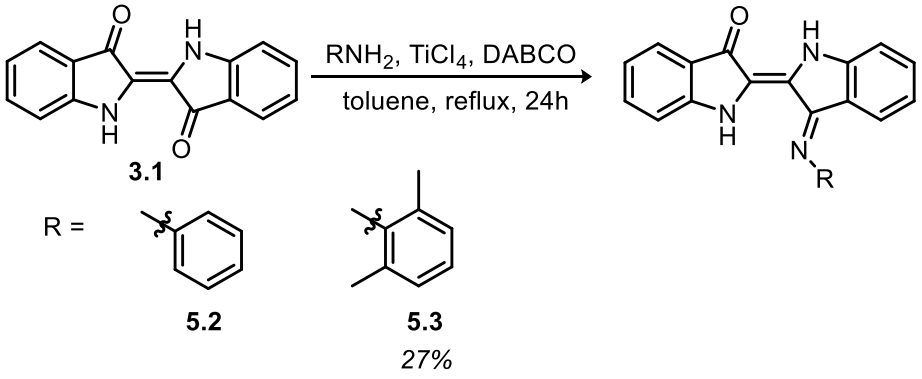

Scheme 38. Synthesis of indigo mono imines **5.2** and **5.3** from indigo (**3.1**).

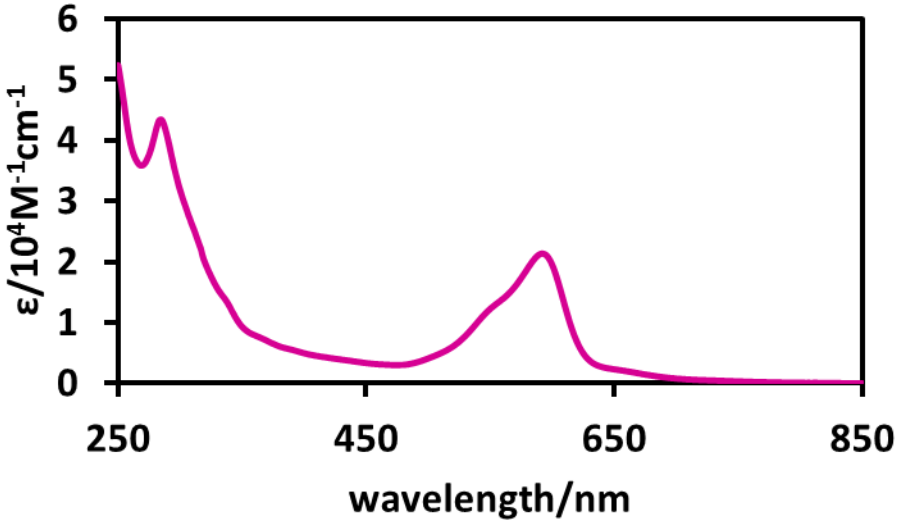

Figure 44. UV-Vis spectrum of compound monoimine **5.3** (CH_2Cl_2, 25μM, 298K).

Indigo monoimine **5.3** can also be protonated by the same series of strong acids that were used in the Nindigo chemistry (**Scheme 39**). Upon addition of the strong acid to a solution of compound **5.3**, the colour changed immediately from purple to green. The UV-Vis spectrum of the protonated product is shown in **Figure 45** and has a λ_{max} (DCM) = 661 nm. Here, the NMR spectrum (shown in **Figure 46**) of the protonated indigo monoimine does not provide much insight into whether or not the *cis* (**5.4a**) or *trans* (**5.4b**) orientation of the protonated species is formed because both species have the same symmetry (or lack-thereof), as observed by the ^{1}H NMR.

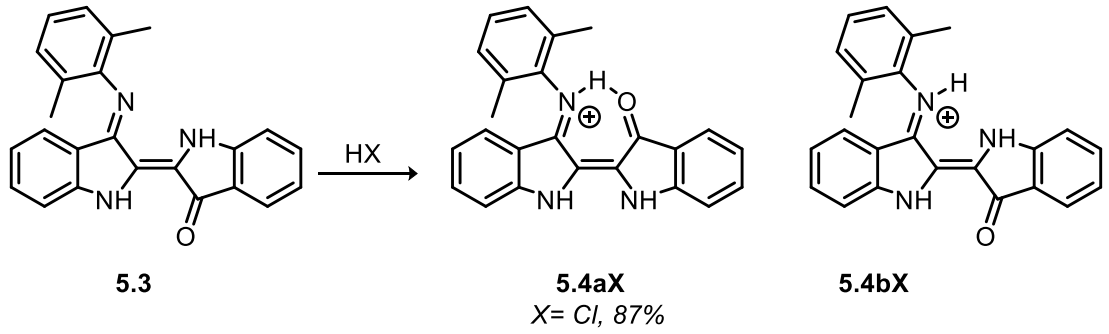

Scheme 39. Protonation of compound **5.3** with a strong acid.

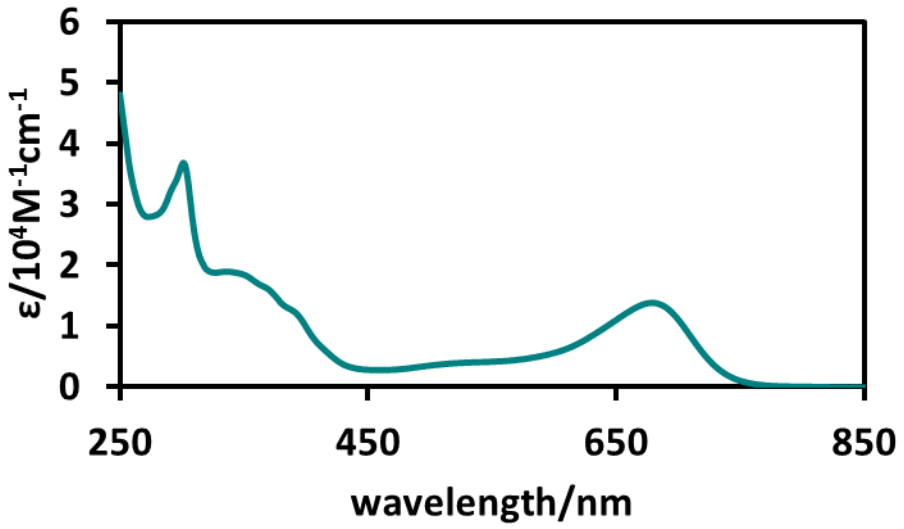

Figure 45. UV-Vis spectrum of protonated monoimine **5.4aCl** (CH_2Cl_2, 25 μM, 298K).

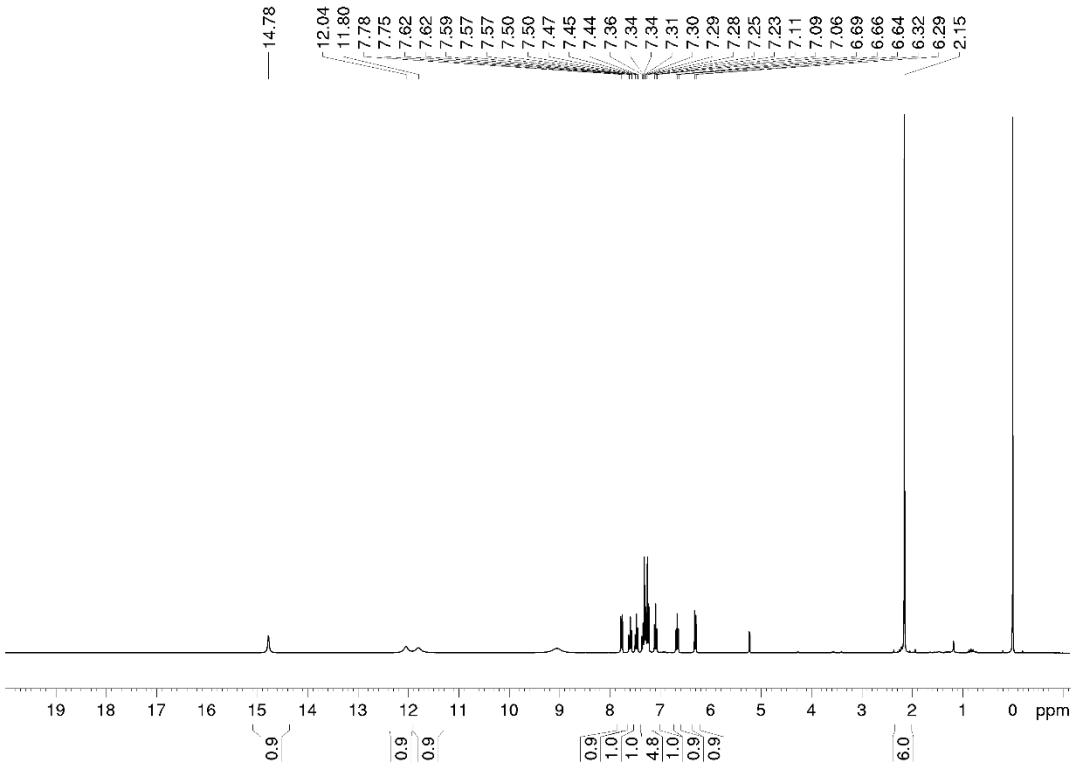

Figure 46. ^{1}H NMR of compound protonated monoimine **5.4aCl** in CD_2Cl_2.

X-ray crystallography (**Figure 47**, **Table 8**) provided definitive evidence for the *cis* structure **5.4a**. The chloride counterion in the structure solution is an artifact of the 1.0M aqueous hydrogen chloride work-up after the reaction has gone to completion with treatment with trifluoroacetic acid. In order to confirm that the product is the same with treatment with hydrochloric acid, the protonation of **5.3** was performed using an excess of concentrated hydrochloric acid. The ^{1}H NMR spectrum of the product is analogous to the one prepared using trifluoroacetic acid.

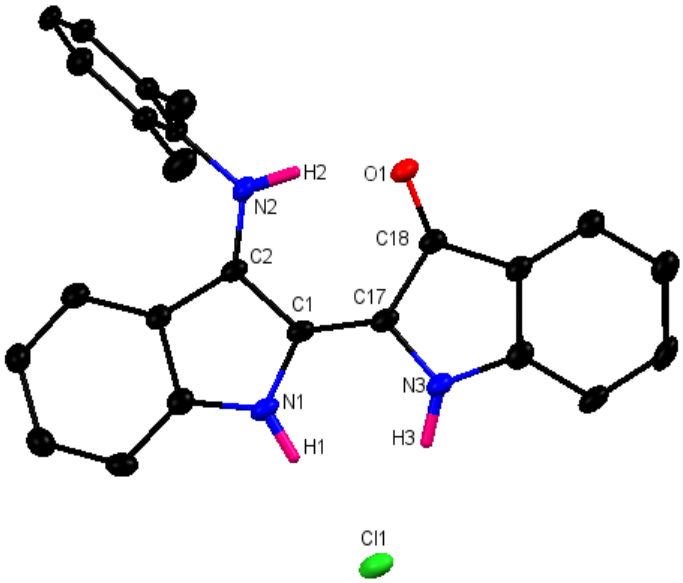

Figure 47. X-Ray Crystallographic of compound **5.4a**. All hydrogen atoms with the exception of the N-H protons removed for clarity. Thermal ellipsoids shown at the 50% probability level.

Bond	Bond Distance (Å)
N2-H2	0.86(3)
N2-C2	1.323(3)
C2-C1	1.454(3)
C1-N1	1.378(3)
N1-H1	0.90(3)
C1-C17	1.377(3)
C17-C18	1.502(3)
C18-O1	1.231(3)
C17-N3	1.366(3)
N3-H3	0.96(3)
H1-Cl1	2.206
H3-Cl1	2.166

Table 8. Selected bond lengths for compound **5.4aCl**.

5.2.3 Protonation of indigo

The protonation of Nindigo and indigo monoimine raised the question of whether or not indigo would have the same reactivity when treated with strong acids. When studied,

indigo proved to be far less basic than Nindigo. Although indigo is poorly soluble in organic solvents, is could be dissolved in chloroform with a solubility of approximately 0.1 mM. Trifluoroacetic acid – which easily protonated Nindigo and indigo monoimine – did not invoke any colour change at all in the indigo solution (which would be indicative of protonation). The only acids that showed any colour change at all were concentrated sulfuric acid and trifluoromethane sulfonic acid. The protonation-induced colour change was observed using UV-Vis spectroscopy. Indigo has an absorption at 599 nm ($CHCl_3$) and upon treatment with excess sulfuric acid a broad absorption is observed with a $\lambda_{max}(CHCl_3)$ = 623 nm (**Figure 48**). The broadness of the absorption was likely because the reaction had not gone to completion and some indigo remains unreacted. When treated with excess trifluoromethanesulfonic acid the λ_{max} ($CHCl_3$) = 642 nm and the absorption was less broad.

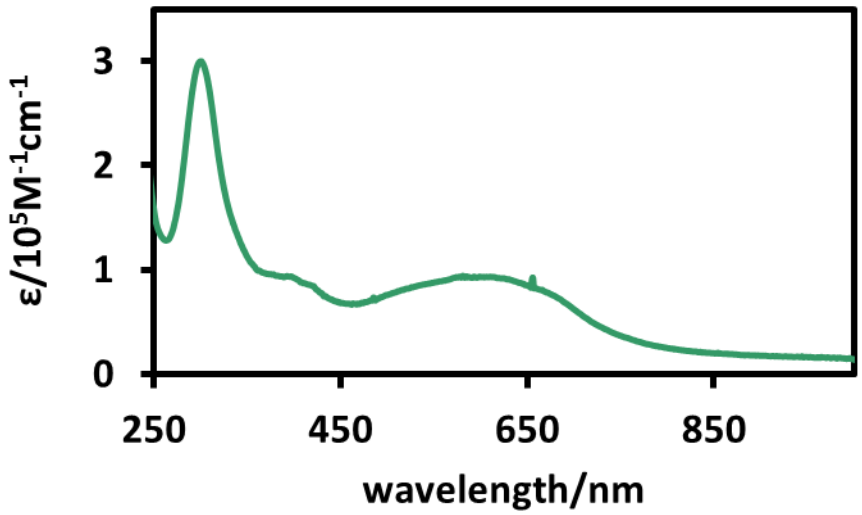

Figure 48. UV-Vis of protonated indigo (with H_2SO_4, $CHCl_3$, 5 μM, 298K).

When a solution of indigo in chloroform was treated with concentrated sulfuric acid the colour change was immediate from blue to green. If left to stand at room temperature, the green colour faded and a solid precipitate formed at the bottom of the vial. This precipitate was not soluble in chloroform but was soluble in water – a similar property to indigo carmine (**3.6**), a water soluble indigo derivative. It seems likely that the eventual product of indigo with sulfuric acid is one in which indigo has been sulfonated to some degree.[128] The green intermediate was not long lived enough to permit determination of its structure.

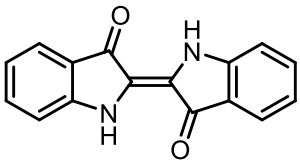

3.1

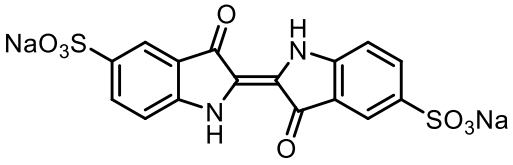

3.6

A 0.1 mM solution of indigo treated with excess trifluoromethane sulfonic acid produced the same immediate colour change from dark blue to green. Similar to the sulfuric acid reaction, the green solution generated with triflic acid reverted back to blue within minutes open to air, but with no formation of a precipitate. The fact that the blue compound remains in solution is consistent with it being indigo itself and not the sulfonated analogue. The decomposition back to indigo was confirmed using UV-Vis spectroscopy.

Protonated indigo can in principle adopt the *trans* configuration without any steric congestion between NH and OH protons (highlighted in blue in **Scheme 40**). This makes the *trans* protonated species of indigo more likely than it was in the Nindigo and indigo monoimine case.

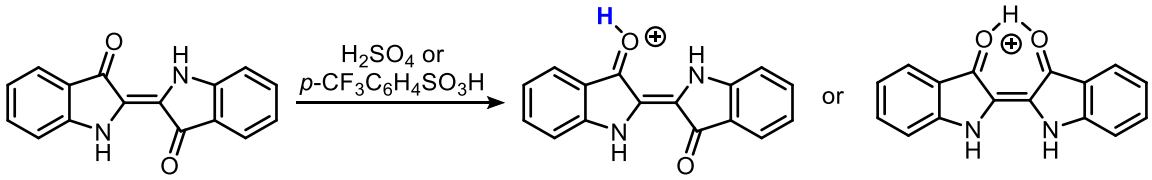

Scheme 40. Protonation of indigo (**3.1**) leading to either *cis* or *trans* protonated indigo.

Unfortunately, NMR spectroscopy did not allow assignment of the structure of the protonated indigo. The main challenge was the poor solubility of indigo in solution. To overcome the solubility concerns, DMSO-d_6 was selected as a potential NMR solvent, but upon addition of the strong acids (sulfuric acid or trifluomethane sulfonic acid) the NMR solution became warm with no colour change – likely due to the sulfoxide oxygen of the DMSO becoming protonated preferentially over the carbonyl oxygen of indigo.

A final attempt to study this system was undertaken by selecting deuterated sulfuric acid as the added acid. The use of deuterated acid prevented excess acid from "swamping" the proton signal while still being able to add excess acid to observe a colour change. The asymmetry or symmetry (in the case of *trans* and *cis*, respectively) of the aromatic backbone in principle could be used to determine if the same isomerization had occurred. The NMR spectrum for this reaction was unhelpful as peaks were broadened and a large amount of water in the NMR solvents made any assignments impossible.

5.3 UV-Vis titrations

The preparative chemistry for the protonated Nindigo species revealed that the synthetically prepared cation provided a very good spectral match in the UV-Vis spectrum

for the first red shifted peak at 657 nm. One possible explanation for the origin of the two red shifted peaks at 657 nm and 741 nm in the neutral Nindigo UV-Vis spectrum was an autoionization process, as proposed in the thesis by Nawn (**Figure 49**).[115] To study this further, and to further investigate the origin of the peak at 741 nm, UV-Vis titrations were performed.

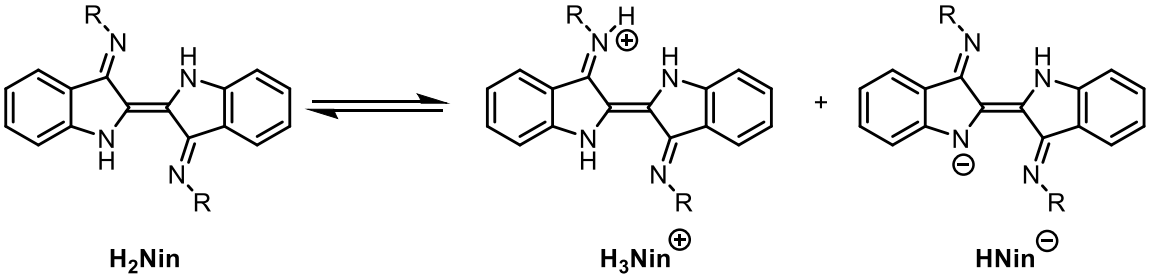

Figure 49. Proposed autoionization of Nindigo.

UV-Vis titrations were performed using dichloromethane as a solvent and using trifluoroacetic acid and triflic acid as proton sources. As acid was added, the peaks at 586 nm and 741 nm decreased and the peak at 641 nm increased (**Figure 50**).

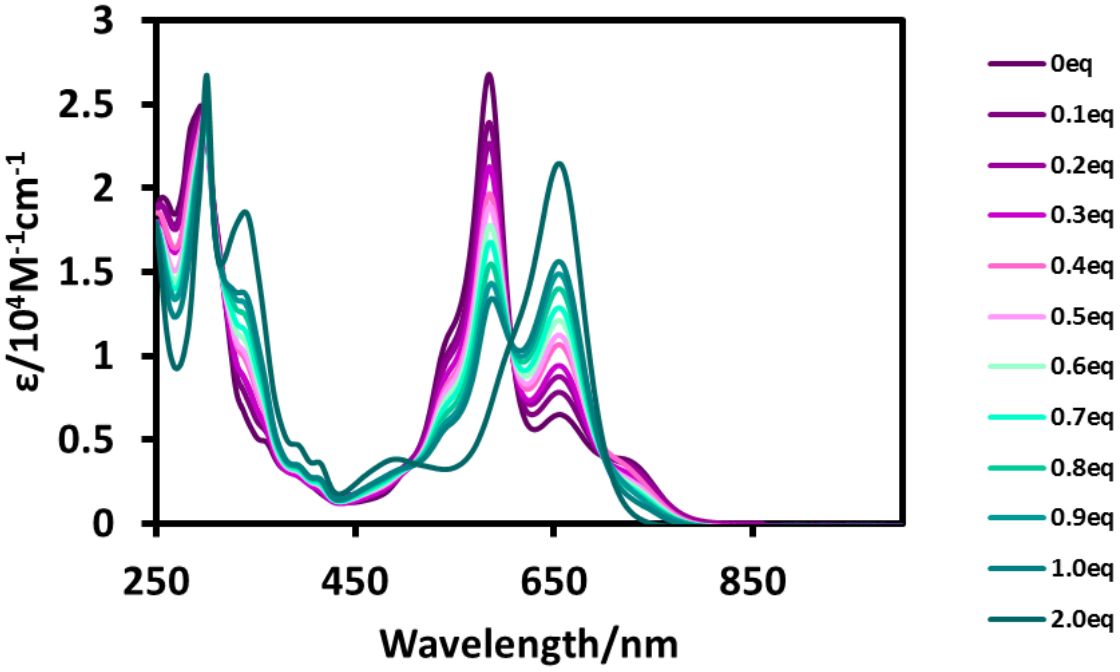

Figure 50. UV-Vis titration of **3.13** with trifluoroacetic acid (CH_2Cl_2, 25μM **3.13**, 298K).

Back titrations were done to demonstrate the reversibility of the protonation process. A variety of mild bases can be used such as triethylamine, 1,8-diazabicyclo[5.4.0]undec-7-ene (DBU) and pyridine; all of which show clean conversion back to the neutral species. However, at high base loadings (greater than three equivalents of base), the peaks at 657 nm and 741 nm are still present (**Figure 51**). In fact, when the spectrum of Nindigo was run in pyridine (purified by distillation and passing the solvent through basic alumina), these two peaks were still present (**Figure 52**). This was one of the first indications that a simple autoionization argument was not sufficient to explain these peaks in the UV-Vis-NIR spectrum.

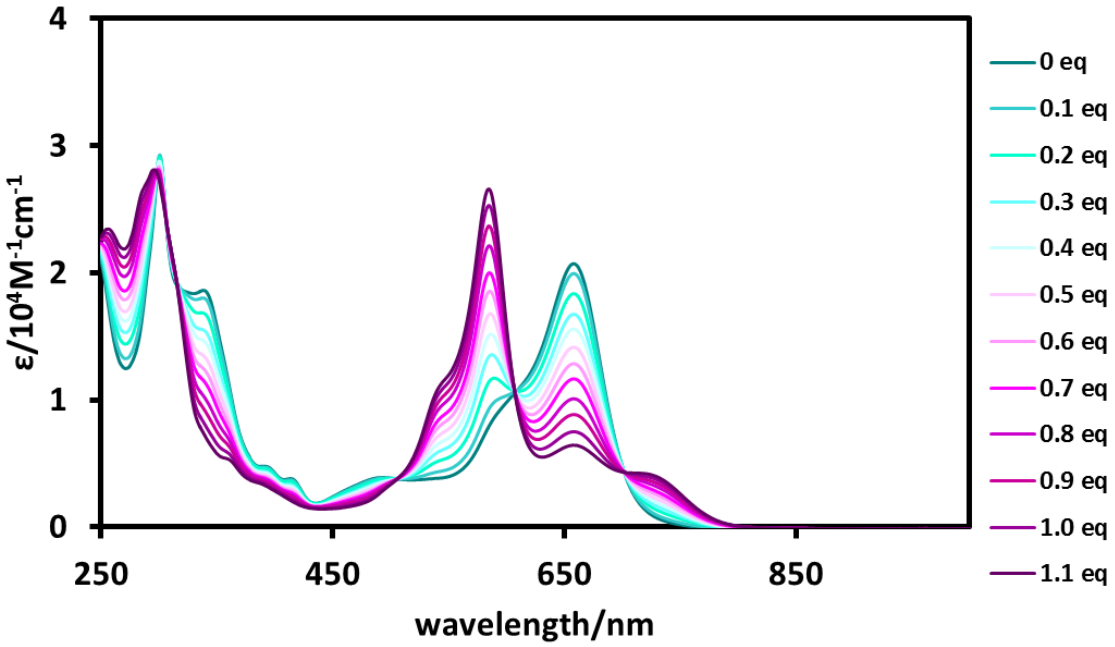

Figure 51. Back titration of **5.1aCF$_3$COO** with Et_3N (CH_2Cl_2, 25μM, 298K).

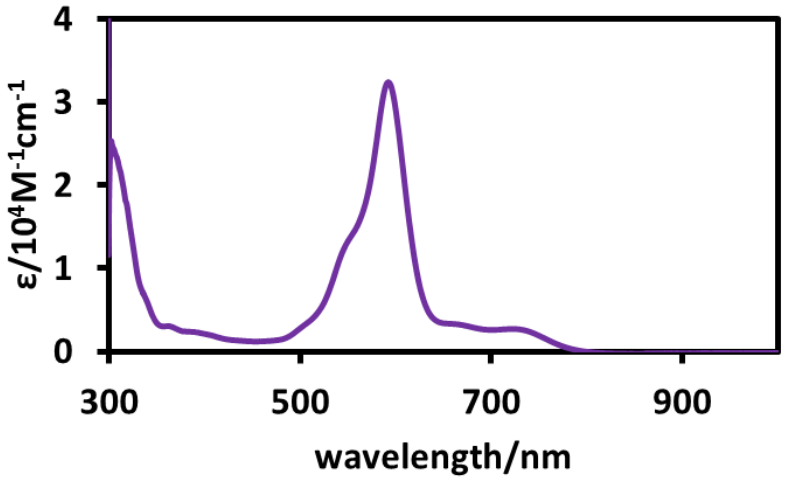

Figure 52. Spectrum of compound **3.13** (pyridine, 36μM, 298K).

5.4 Nindigo deprotonation

The protonation studies of Nindigo, especially the acid titration studies, provided a reasonable explanation for the peak at 657 nm in the UV-Vis spectrum of Nindigo. If this peak is the protonated species, then the peak 741 nm could be a result of autoionization of Nindigo into its acidic and basic forms, although this was not in good agreement with some results from the titration experiments. To probe this hypothesis further, the deprotonated species was synthesized and studied spectroscopically.

Nindigo could be deprotonated (**Scheme 41**) using 2.5 equivalents of a lithium hexamethyldisilazane diethyl etherate dimer – an air stable, solid base that was synthesized "in house" – in freshly distilled THF with freshly distilled 12-crown-4. The colour changed gradually over approximately 10 minutes from purple to dark green to generate doubly deprotonated **5.5** which was air and moisture sensitive. The ^{1}H NMR (**Figure 53**) spectrum recorded shows the loss of the indole N-H proton signals and a single methyl resonance – indicative of a symmetrical system which was consistent with the addition of excess base. Isolation of the mono-deprotonated species proved futile and resulted in a mixture of many species as determined by ^{1}H NMR.

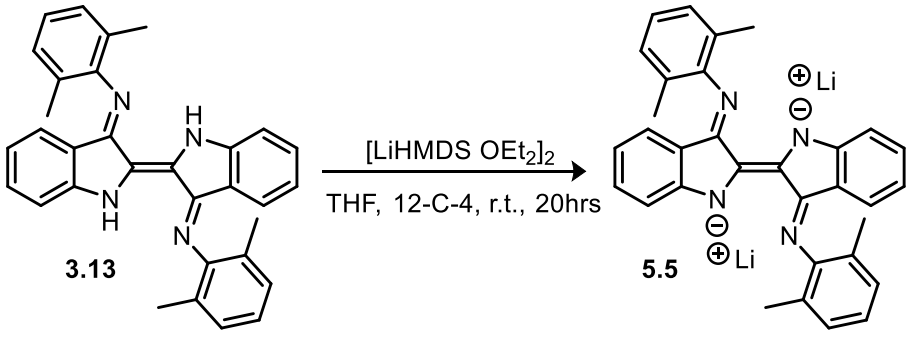

Scheme 41. Synthesis of compound **5.5**.

In addition to the ^{1}H NMR spectrum recorded, ^{7}Li NMR (**Figure 54**) and ^{13}C NMR spectra were also collected. The ^{7}Li NMR had two resonances, one for the starting material at -0.90 ppm and one assigned to the lithium co-ordinated to the anion at 1.03 ppm. The ^{13}C NMR spectrum was not particularly informative as it merely confirmed the symmetry indicated by the ^{1}H NMR. The UV-Vis spectrum for this species had an absorption maximum at 768 nm in THF (**Figure 55**). Growth of crystals suitable for X-ray diffraction proved difficult partially because of the solubility and crystallinity of the salt (only soluble in THF, DMSO; small cation and large anion leads to poor crystallinity) as well as the moisture and air sensitivity of the complex. Efforts were undertaken to do a cation exchange reaction to a larger cation such as tetraethylammonium and cobaltocenium or ferrocenium, but attempts at crystal growth of these systems also proved difficult.

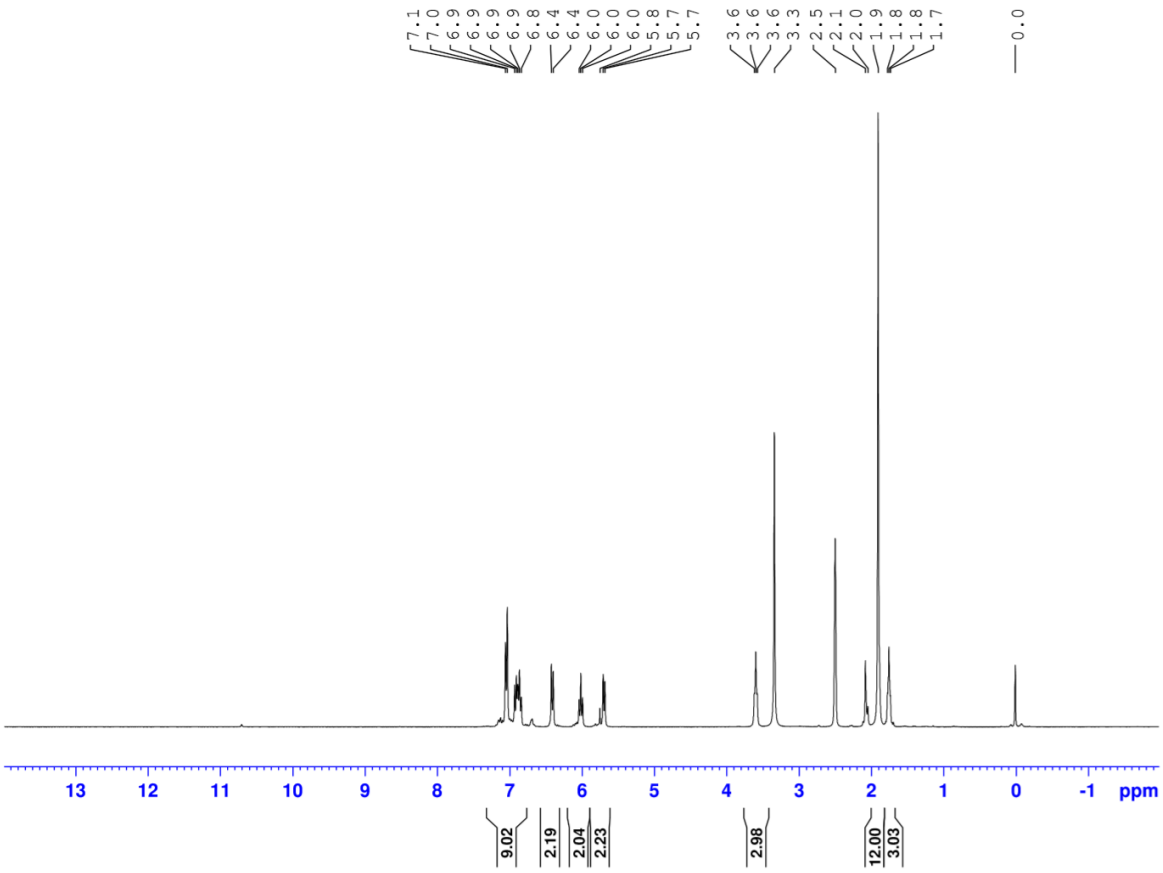

Figure 53. ^{1}H NMR of **5.5** (DMSO-d_6, 300 MHz, 298K).

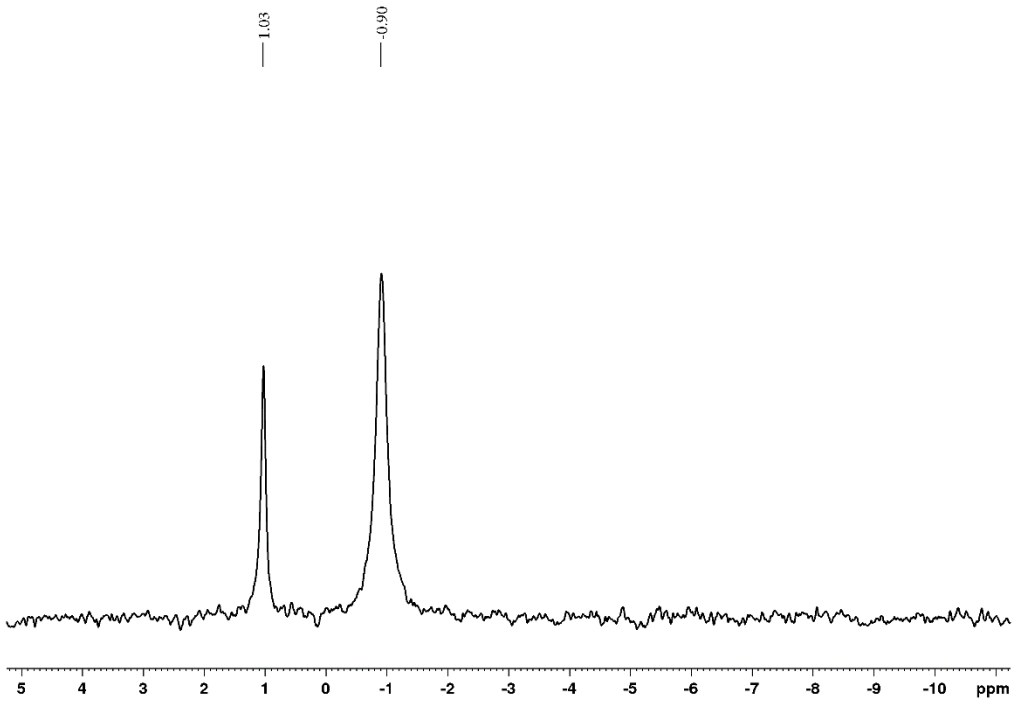

Figure 54. ^{7}Li NMR of **5.5** (DMSO-d_6, 140 MHz, 298K).

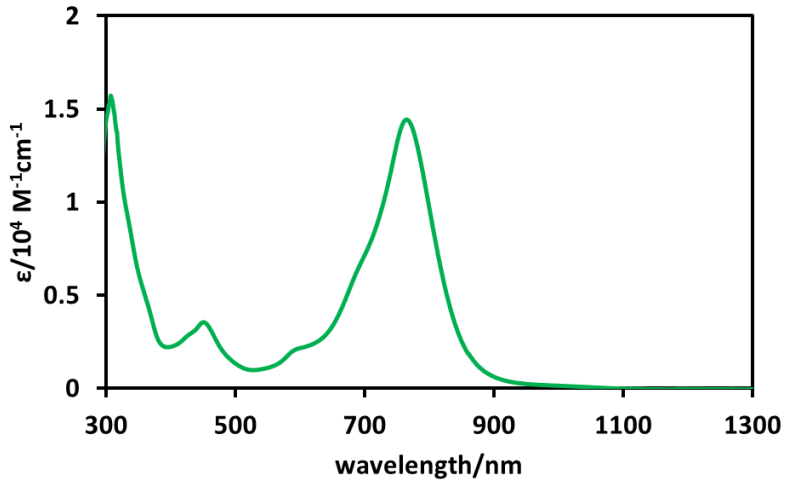

Figure 55. UV-Vis spectrum of compound **5.5** (THF, 25μM, 298K).

5.5 Aggregation studies of Nindigo

The phenomena of dye aggregation is exhibited in indigo. At low concentrations (less than ten micromolar), the visible spectrum of indigo consists of a single transition near 600 nm attributed to a π-to-π transition. However, at higher concentrations (100 micromolar), a second peak appears which is red-shifted from the original transition at 700 nm. The temperature dependence of the spectrum of indigo is consistent with an equilibrium between a monomer and dimer. Quantitative analysis of the temperature dependence of the electronic spectra produced an equilibrium constant for formation of the dimer at 298K is (1.2 +/- 0.2) x 10^4 dm^3mol^{-1}.[85]

Because the Nindigo red shifted peaks were the most prominent in dichloromethane, our concentrations studies were first done in this solvent (**Figure 56**). The spectra shown in **Figure 56** are normalized to set the largest absorption at 586 nm equal to one to illustrate the concentration dependence. The peak at 741 nm was largely unaffected by the change in concentration. The most pronounced difference was the ratio between the peak at 586 nm and the peak at 657 nm. As the concentration decreased, the species at 657 nm grew in relative to the species at 586 nm. This was the opposite of what is observed in the indigo case and would actually be consistent with the theory that the peak at 586 nm (which was previously assigned to a π-to-π transition) is some sort of aggregate.

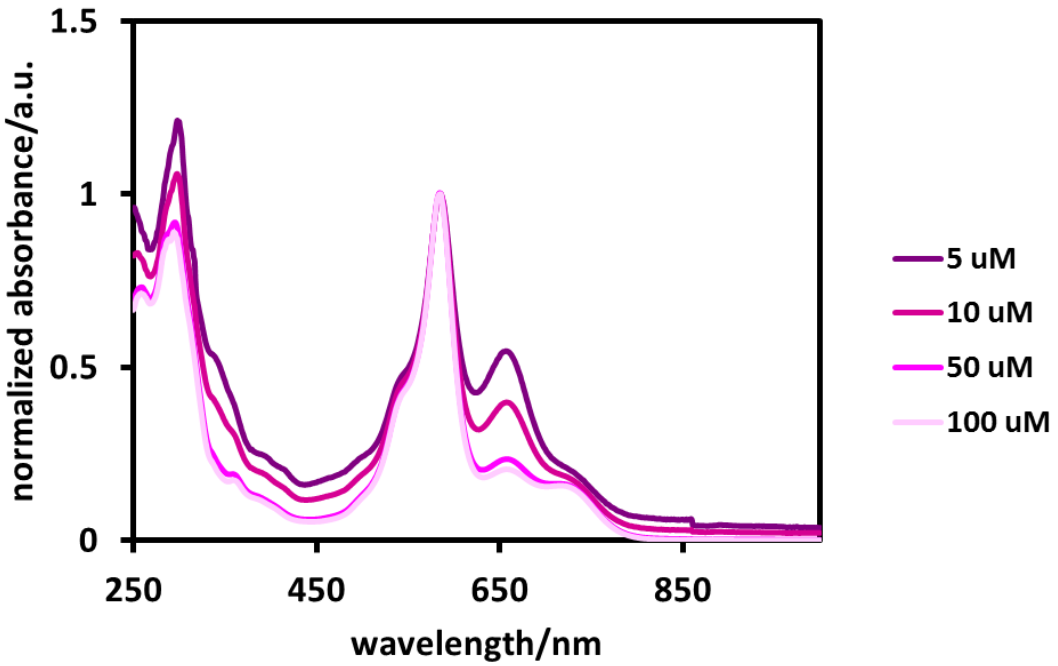

Figure 56. Aggregation studies of compound **3.13** (CH_2Cl_2, 298K).

In different solvents (acetone, acetonitrile), the aggregation behaviour was also seen but was far less pronounced. We postulated that the difference between the dichloromethane and the other organic solvents used could be due to acid content from acid stabilizers commonly found in chlorinated solvents. UV-Vis studies with dichloromethane at various purities were run to see if there was a change in spectral shape:

1. dichloromethane from the bottle
2. dichloromethane from the still which is pre-treated with a sulfuric acid wash and stored over calcium hydride
3. dichloromethane from the still which is pre-treated with a sulfuric acid wash and stored over calcium hydride which was then passed through basic alumina and stored over 4 Å molecular sieves

The selection of the solvent made no difference to the spectral shape which means that the acid stabilizer had nothing to do with the uniqueness of the dichloromethane as a solvent.

5.6 Variable temperature studies of Nindigo spectra

Another experiment to test the working hypothesis of autoionization was variable temperature NMR spectroscopy to see whether the cationic or anionic species could be observed at low temperatures. Two different NMR solvents were used: deuterated dichloromethane and deuterated ethanol. Deuterated dichloromethane was first selected because the unusual spectral changes as observed in the UV-Vis-NIR spectrum and due to the low freezing point. The ^{1}H NMR spectra remained the same from ambient temperature down to 183K (except for broadening of the signals as a result of the increased viscosity of the solvent as a result of cooling). Even at the freezing point of ethanol (148K) there was still no evidence for either the protonated or deprotonated Nindigo species in the ^{1}H NMR. The ^{13}C NMR spectrum could not be collected due to poor solubility of Nindigo at low temperatures.

Variable temperature UV-Vis-NIR spectroscopy was also explored. Dichloromethane was used for lower temperature experiments (due to the low freezing point) as well as the higher temperature experiments. Since dichloromethane has a low boiling point, acetonitrile was also used for higher temperature studies.

As the temperature was decreased, the ratio of the 590 nm/650nm peaks increased (**Figure 57** and **Figure 58**). This result was consistent with the concentration-dependent studies which suggested that the species at 586 nm is an aggregate.

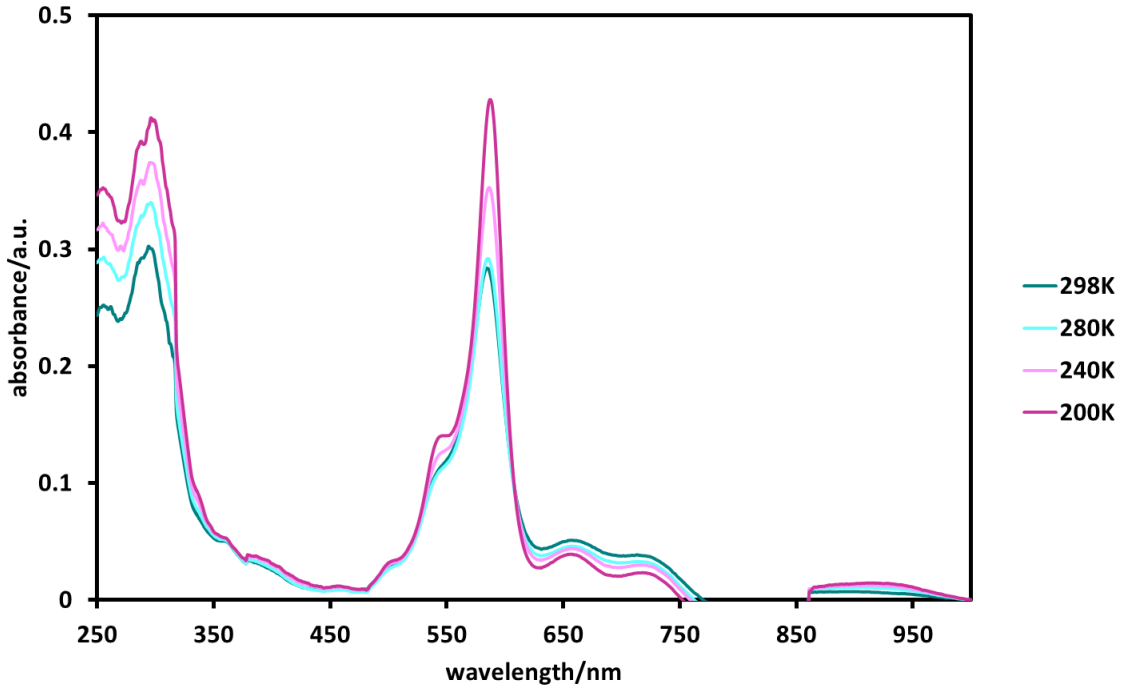

Figure 57. Spectrum of species **3.13** (CH_2Cl_2, 10 mM, 298K (teal), 280K (aqua), 240K (light pink), 200K (dark pink)).

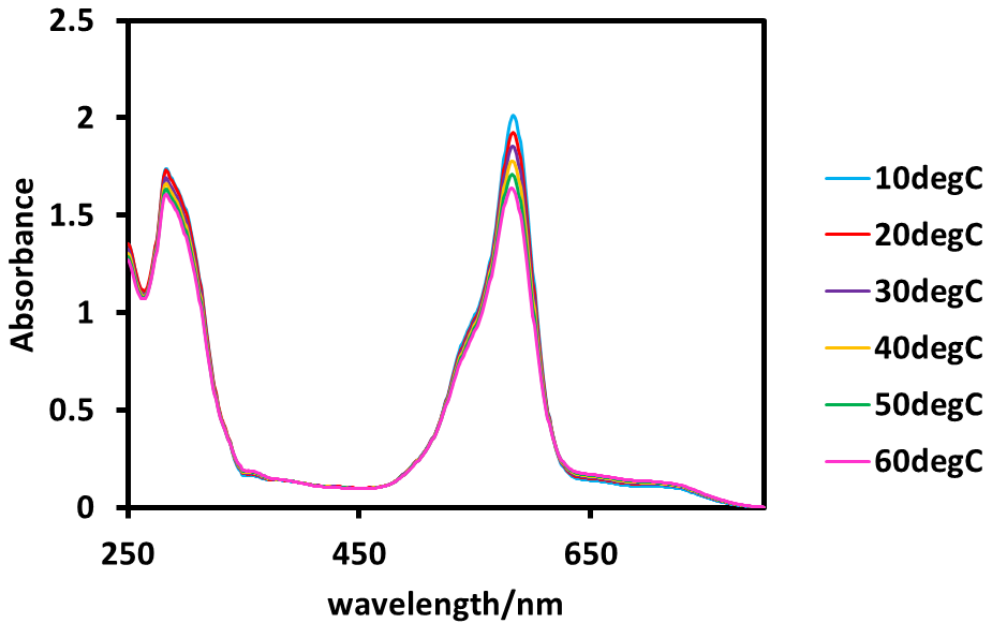

Figure 58. Spectrum of compound **3.13** (CH_3CN, 100μM, 283K (blue), 293K (red), 303K (purple), 313K (yellow), 323K (green), 333K (pink)).

5.7 Summary

The two red-shifted peaks in the visible spectrum of neutral Nindigo have been a mystery since the first report Nindigo in the literature. Nawn originally postulated that these peaks were a function of the autoionization of Nindigo in solution.[115] The possibility of either autoionization and/or aggregation of Nindigo was investigated by a variety of methods including concentration studies, titrations, and variable temperature studies. These studies have enhanced our understanding of Nindigo in solution, but have not led to a definitive explanation of the additional peaks in the absorption spectrum. Acidic titrations in tandem with preparative chemistry reveal that the first red shifted peak at 657 nm is the result of the cation in solution. However, the identity of the species at 741 nm remains unclear but it unlikely to be a consequence of simple autoionization or aggregation.

An unexpected and interesting observation was the "protoisomerization" of Nindigo under acidic conditions which led to olefin isomerization to form a stable salt. This isomerization was characterized by a number of spectroscopic methods, and definitive proof of isomerization was provided with X-ray crystallographic results. This protonated species is a new and interesting compound itself and the pH dependent isomerization of olefins is actually quite rare. Olefin isomerization is normally achieved through photochemical means or by catalysis with transition metals or acid.[129-132] To our knowledge, there is only one other report of pH dependent isomerization reported in *JACS* in 2005 for the natural product Norbadione A.[133] Future work will focus on the potential utility of this protonated species as a proton delivery source.

5.8 Experimental Section

5.8.1 Methods and Materials

All reactions and manipulations were carried out under an argon atmosphere using standard Schlenk or glovebox techniques unless otherwise stated. All reagents were purchased from Aldrich and used as received unless stated in which case they were purified or dried under appropriate conditions. NMR spectra were recorded on 300, 360 or 500 MHz instruments at room temperature unless stated otherwise. Electronic spectra were recorded on a Perkin-Elmer Lamda 1050 instrument in dichloromethane or dimethyl sulfoxide. A Varian Cary-100 UV-Vis spectrophotometer was used for the high temperature experiments with dichloromethane or acetonitrile as a solvent. An applied photophysics SX20 stopped-flow system was used for the UV-Vis stopped-flow studies in methanol. Accurate mass determination was performed at the UVic Genome BC Proteomics Centre on a Thermo Scientific LTQ Velos Orbitrap instrument. Samples (mg/mL) were diluted by a factor of 10-100 and injected by liquid infusion through a nano ESI source. X-ray diffraction data was collected on a Bruker PLATFORM/SMART 1000 CCD with a graphite-monochromatacized Mo-Kα radiation ($\lambda = 0.71073$ Å) by Dr. Brian Patrick (University of British Columbia).

5.8.2 Experimental Details

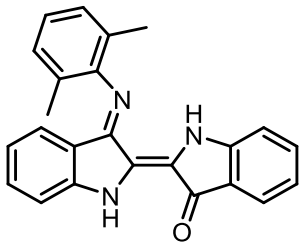

indigo mono(2,6-methylphenylimine) (**5.3**)

A 1.0 M toluene solution of $TiCl_4$ (9.8 mL; 9.80 mmoles; 1.8 eq) was added dropwise to a 1,4-dioxane solution containing DABDO (1.00 g; 8.92 mmoles; 1.7 eq) and 2,6-dimethylaniline (1.63 g; 13.4 mmoles; 2.5 eq), immediately generating a white vapour and a green precipitate. After fuming had subsided, indigo (1.40 g; 5.33 mmoles; 1 eq) was added. The dark blue mixture was warmed to reflux overnight (19h). The resulting solution was filtered while warm and the solid was washed with diethyl ether until the washing were colourless. The filtrate was concentrated to dryness to yield 1.12 g of a compound **5.3** as a purple powder (26.7 %). ^{1}H NMR (300 MHz, CD_2Cl_2, 298 K): δ 9.59 (broad singlet, 1*H*), 9.28 (singlet, 1*H*), 7.67 (d, 1*H*, $^3J_{HH}$ = 7.9 Hz), 7.38 (tofd, 1*H*, $^3J_{HH}$ = 7.7 Hz, $^3J_{HH}$ = 1.2 Hz), 7.24 (tofd, 1*H*, $^3J_{HH}$ = 7.7 Hz, $^3J_{HH}$ = 1.2 Hz), 7.09 (d, 2*H*, $^3J_{HH}$ = 7.7 Hz), 7.00 (m, 3*H*), 6.88 (tofd, 1*H*, $^3J_{HH}$ = 7.5 Hz, $^3J_{HH}$ = 0.9 Hz), 6.57 (tofd, 1*H*, $^3J_{HH}$ = 7.8 Hz, $^3J_{HH}$ = 0.9 Hz), 6.38 (d, 1*H*, $^3J_{HH}$ = 7.8 Hz). ^{13}C NMR (75 MHz, CD_2Cl_2, 298 K): δ 184.6, 160.1, 149.5, 147.6, 147.1, 133.9, 132.7, 131.7, 127.5, 124.1, 123.6, 119.3, 118.4, 118.1, 110.6, 109.9, 16.3, 16.2. UV-Vis (CH_2Cl_2, λ (ε)): 592 (21350). HRMS: Calcd for $C_{24}H_{19}N_3O + H^+$ *m/z* = 366.16011, found *m/z* = 366.16005.

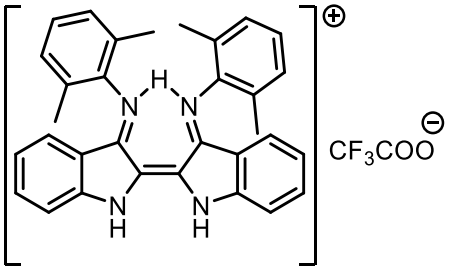

indigo bis(2,6-dimethylphenyliminium) trifluoroacetate (**5.1aCF$_3$COO**)

Excess trifluoroacetic acid was added to a solution of **3.13** (77 mg; 164.4 mmoles; 1eq). The resulting solution was stirred at room temperature for 30 minutes. The teal solution was washed with 1M HCl solution (2 x 100 mL), dried over magnesium sulfate, filtered, and the solvent was removed at reduced pressure to yield 88 mg of a dark black-green powder (92.0 %). X-Ray quality crystals were grown from slow evaporation of a saturated dichloromethane solution. ^{1}H NMR (CD_2Cl_2, 300 MHz, 298 K): δ 16.02 (s, 1*H*), 13.07 (s, 2*H*), 7.41 (m, 4*H*), 7.16 (s, 6*H*), 6.68 (t, 2*H*, $^3J_{HH}$ = 7.6 Hz), 6.31 (d, 2*H*, $^3J_{HH}$ = 8.1 Hz). ^{13}C NMR (CD_2Cl_2, 75.5 MHz, 298K): δ 158.5, 148.7, 140.9, 135.9, 130.9, 129.5, 127.9, 125.8, 122.1, 117.3, 113.7, 18.2. IR (thin film, cm^{-1}): 3269, 2913, 2851, 1613. UV-Vis (CH_2Cl_2; λ_{max} (nm) (ε ($M^{-1}cm^{-1}$))): 650 (22, 000). HRMS: Calcd for $C_{32}H_{29}N_4$ *m/z* = 469.23922, found *m/z* = 469.23830.

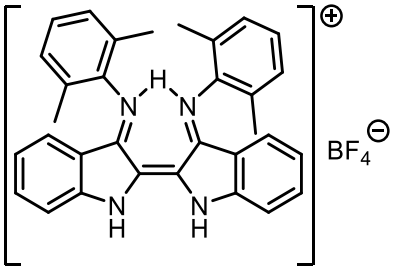

indigo bis(2,6-dimethylphenyliminium) tetrafluoroborate (**5.1aBF$_4$**)

Excess tetrafluoroboric acid was added to a solution of DmPNindigo (93 mg; 0.198 mmoles; 1 eq) in 20 mL dichloromethane with an immediate colour change from purple to teal with the exclusion of light. The resulting solution is stirred at room temperature for 30 minutes. The teal solution was washed with 1M HCl solution (2x 100 mL), dried over magnesium sulfate, filtered and evaporated in vacuo to yield 87 mg of a dark black-green powder (79.2%). X-Ray quality crystals were grown from slow evaporation of a saturated solution in dichloromethane. ^{1}H NMR (300 MHz, CD_2Cl_2, 298 K): δ 16.47 (s, 1*H*), 9.71 (s, 2*H*), 7.49 (t, 2*H*, $^3J_{HH}$ = 7.8 Hz), 7.38 (d, 2*H*, $^3J_{HH}$ = 8.3 Hz), 7.18 (m, 6*H*), 6.74 (t, 2*H*, $^3J_{HH}$ =7.8 Hz), 6.35 (d, 2*H*, $^3J_{HH}$ = 8.3 Hz). ^{13}C NMR (75 MHz, CD_2Cl_2, 298 K): δ 159.3, 148.6, 140.5, 136.6, 130.6, 130.0, 129.6, 128.2, 125.9, 122.9, 117.4, 113.9, 18.2.

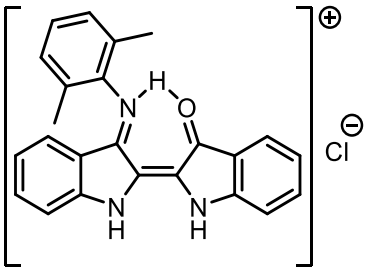

indigo mono(2,6-dimethylphenyliminium) chloride(**5.4aCl**)

An excess of concentrated hydrochloric acid was added to a solution of monoDmPNindigo (38 mg; 0.104 mmoles; 1 eq) in 20 mL dichloromethane with an

immediate colour change from purple to teal. The resulting solution was stirred at room temperature overnight. The teal solution was washed with 1M HCl solution (2 x 100 mL), dried over magnesium sulfate, filtered, and the solvent was removed under reduced pressure to yield 33 mg of a dark black-green powder (86.8%). X-Ray quality crystals were grown from slow evaporation of a solution of **5.4aCl** in dichloromethane/acetone. ^{1}H NMR (300 MHz, CD_2Cl_2, 298 K): δ 14.64 (s, 1*H*), 13.05 (s, 1*H*), 12.79 (s, 1*H*), 7.77 (d, 1*H*, $^{3}J_{HH}$ = 8.1 Hz), 7.58 (t of d, 1*H*, $^{3}J_{HH}$ = 8.3 Hz, $^{4}J_{HH}$ = 1.1 Hz) 7.45 (t of d, 1*H*, $^{3}J_{HH}$ = 7.4 Hz, $^{4}J_{HH}$ = 1.1 Hz), 7.28 (m, 5*H*), 7.11 (m, 2*H*), 6.65 (t, 1H, $^{3}J_{HH}$ = 7.4 Hz), 6.31 (d, 1*H*, $^{3}J_{HH}$ = 8.1 Hz), 2.17 (s, 6*H*). ^{13}C NMR (75 MHz, CD_2Cl_2, 298 K): δ 186.0, 150.2, 148.3, 147.8, 142.2, 133.8, 132.5, 127.5, 127.3, 124.8, 124.8, 123.3, 123.0, 120.7, 120.0, 118.8, 116.8, 111.4, 110.7, 16.5. IR: UV-Vis (CH_2Cl_2; λ_{max} (nm) (ε ($M^{-1}cm^{-1}$))): 659 (13,800).

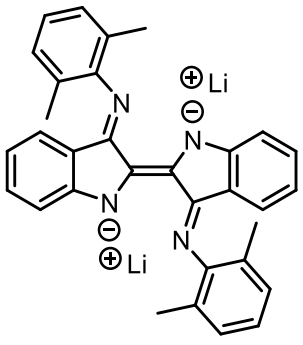

(**5.5**)

116 mg (0.251 mmoles; 1 eq) of **3.13** was added to a stirring solution of 160 mg (0.487 mmoles; 1.9 eq) lithium bis(trimethylsilyl) amide in 25 mL tetrahydrofuran. There was an immediate colour change from purple to dark green. This mixture was stirred overnight (19 hours) before the solvent is removed under reduced pressure. The solid was taken up in a suspension of hexanes and filtered under nitrogen. This green solid was washed

3x10mL hexanes before being dried under vacuum for two hours before being brought into the glovebox. Collected in the glove box was 102 mg (87.9%) of a dark green solid. To prepare the NMR samples, dmso-d_6 was vacuum distilled over calcium hydride and was taken through three freeze-pump-thaw cycles and was stored over 4Å molecular sieves before being brought into the glovebox. NMR samples were prepared in the glovebox and put in a J-young tube before being removed from the glovebox to record spectra. ^{1}H NMR (300 MHz, $(CD_3)_2SO$, 298 K): δ 7.01 (m, 8*H*), 6.55 (d, 2*H*, $^{3}J_{HH}$ = 8.1 Hz), 5.90 (d, 2*H*, $^{3}J_{HH}$ = 8.1 Hz), 5.72 (d, 2*H*, $^{3}J_{HH}$ = 8.1 Hz), 1.91 (s, 12*H*). ^{13}C NMR (75 MHz, $(CD_3)_2SO$, 298K): δ 150.5, 137.8, 134.1, 129.4, 128.3, 126.3, 125.8, 124.4, 123.3, 123.0, 121.1, 119.5, 116.8, 114.8, 21.5. ^{7}Li (140 MHz, $(CD_3)_2SO$, 298 K): δ 1.03. UV-Vis (THF, 298 K, $1x10^{-4}$ M^{-1}): 768 nm (15,000 $mol^{-1}Lcm^{-1}$).

UV-Vis titration experiments:

*Protonation of **3.13** with trifluoracetic acid*

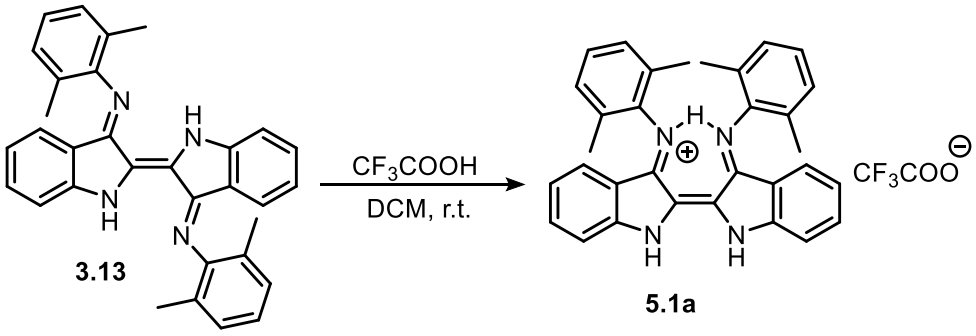

A 100 mL $1x10^{-4}$ M^{-1} solution of compound **3.13** in dichloromethane was prepared and transferred to an oven dried 100 mL Erlenmeyer flask equipped with a stir bar and covered with a watchglass. A 100 mL $1x10^{-2}$ M^{-1} solution of trifluoroacetic acid in dichloromethane

was prepared. The solution of **3.13** was stirred at room temperature and 0.1 equivalent aliquots of acid were added using volumetric pipette. After each addition of acid, the solution was stirred for 5 minutes before a sample was removed for UV-Vis spectroscopy. After each spectrum was collected, the sample was transferred back to the Erlenmeyer flask and the next aliquot of acid was added. Aliquots of acid were added until there was no change in the spectrum.

*Deprotonation of **5.1a** with DBU*

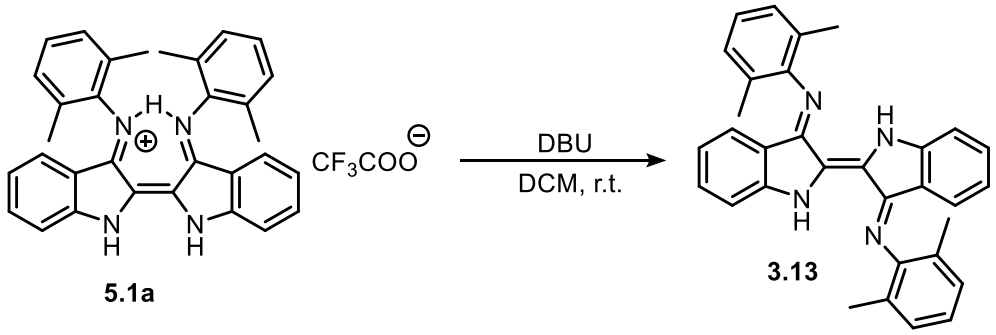

5.1a **3.13**

A 100 mL $1x10^{-4}$ M^{-1} solution of compound **5.1a** in dichloromethane was prepared and transferred to an oven dried 100 mL Erlenmeyer flask equipped with a stir bar and covered with a watchglass. A 100 mL $1x10^{-2}$ M^{-1} solution of DBU in dichloromethane was prepared. The solution of **5.1a** was stirred at room temperature and 0.1 equivalent aliquots of base were added using volumetric pipette. After each addition of base, the solution was stirred for 5 minutes before a sample was removed for UV-Vis spectroscopy. After each spectrum was collected, the sample was transferred back to the Erlenmeyer flask and the next aliquot of base was added. Aliquots of base were added until there was no change in the spectrum.

Variable Temperature UV-Vis Experiments:

Low temperature Experiments:

The lower temperature experiments require a set-up with a cryostat running to a Perkin-Elmer UV-Vis-NIR spectrometer which allows for controlled cooling of the sample. The sample holder requires a short path cell so the solutions were made at ten times the concentration that were usually prepared in order to have the absorbance in the range of 0-1 a.u. which leads to optimal accuracy.

A $2.5x10^{-3}$ M^{-1} solution of compound **3.13** was prepared in dichloromethane and was deoxygenated by bubbling nitrogen through the solution for 20 minutes. This was then transferred to a 1mm pathlength quartz cell and placed in the cryostat. The sample was cooled and the temperature was allowed to equilibrate for 30 minutes before the spectrum was recorded.

High temperature Experiments:

A $1x10^{-4}$ solution of **3.13** was prepared in acetonitrile. This was then transferred to a 1 cm pathlength quartz cell and placed in the warm water bath. This sample was warmed at 5ºC increments and was allowed to equilibrate for 10 minutes before a spectrum was recorded. A spectrum at room temperature was recorded after the sample had been cooled down after the heating experiment to ensure that no decomposition had occurred.

Stopped-Flow Studies:

Stopped-flow studies were performed by preparing a 100 μM solution of **3.13** in methanol which was pretreated with calcium hydride and stored over 4Å molecular sieves before use. Acidic solutions were prepared of the concentrations 10 mM, 1 mM, and 0.1 mM of acetic acid in the same pretreated methanol. The wavelength of observation was 635 nm.

Chapter 6: Suggested Future Work

6.1 Future work of the lanthanide-scorpionate co-ordination chemistry

After the development of a tolerant synthesis for a wide variety of scorpionate ligands some lanthanide metal complexes were synthesized. An X-ray crystal structure of what was initially thought to be the *tris*(pyrazolyl)borate-ytterbium complex **2.27** was actually revealed to be the complex **2.28** where there are two *bis*(pyrazolyl)borate ligands bound to a ytterbium metal centre (both compounds shown in **Figure 59**). Investigation of the bond lengths of this compound led us to believe that the pyridine substituent that was being used as an additional chelation site was too far away from the metal centre to have a stable complex over a long time-frame.

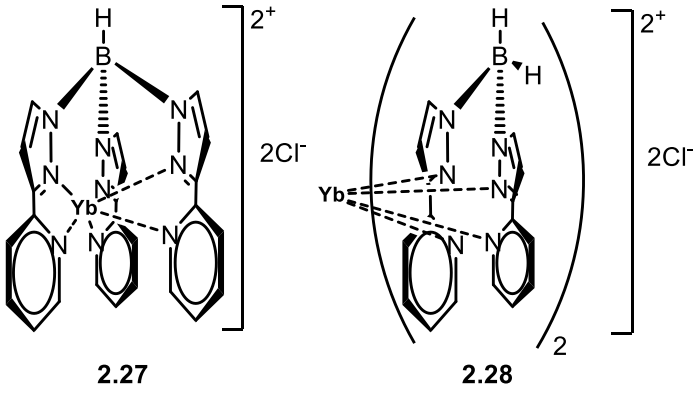

Figure 59. Molecular structure of compound **2.27** and compound **2.28**.

Future work should focus on ligand design where the additional chelation site on the *tris*(pyrazolyl)borate ligand or *tris*(triazolyl)borate ligand should not be contained within a

ring (as was the case with the pyridine ring in compound **2.11c**). Instead, the placement of the additional chelation site is likely best projected from an aromatic backbone.

Another avenue of interest would be to introduce some flexibility into the scorpionate ligand in the form of an alkyl chain. This could be accessed by opening the lactone ring in compound **2.18c** by base hydrolysis (shown in **Scheme 42**).[134]

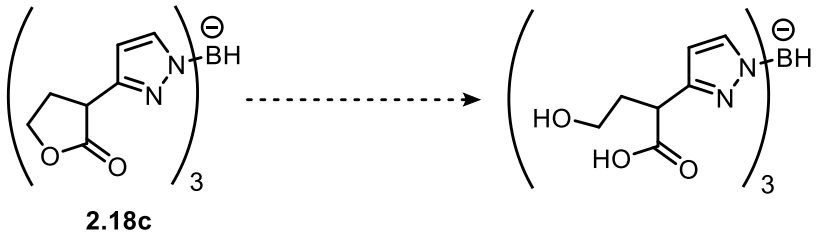

2.18c

Scheme 42. Proposed ring opening of the lactone substrate **2.18c**.

The physical parameters that need to be measured to determine if a complex is a good candidate for PARACEST applications included exchange rates of the ligand, hydration number, and stability constant. The exchange rate of the ligand in solution can be observed using mass spectroscopy as previously reported by the group.[29]

6.2 Future work in the synthesis of perinaphthindigo and its derivatives

The synthesis of perinaphthindigo and some derivatives was reported and these compounds showed some preliminary data that indicate these chromophores are sensitive to different substitution. However, there still exists a major bottleneck step in this chemistry – the Baeyer-Drewson cyclization reaction to make the final product. This reaction is a concern because of the low yields – especially when five or more steps are

required to make the organic precursor to this cyclization. The Henry reaction chemistry described in section 4.3 shows potential to improve these yields as was done with indigo. However, in order for this to be a better route to PNI, the last step (the cyclization) needs to explored and optimized. The proof of principle for the palladium cross-coupling chemistry was described in section 4.6. The coupling chemistry in tandem with the improved yields from the Henry reaction could serve synthesize appreciable quantities of compounds that extend the π-conjugation of the chromophore on which further chemistry can be done.

As described in Chapter 4, Nindigo did not form stable *bis*-boron complexes. The synthesis of perinaphthindigo was achieved but poor yields made further chemistry difficult. The hypothesis of perinaphthindigo as a better chelate for boron needs to be probed. This synthesis would likely require a high boiling point to solubilize perinaphthindigo but otherwise the synthetic methodology for similar chemistry could be used (**Scheme 43**).

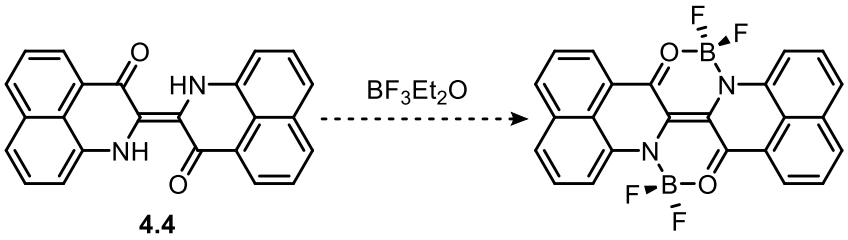

4.4

Scheme 43. Proposed synthesis of boron complexes of compound **4.4**.

Another aspect of this chemistry that could be explored is the conversion of the carbonyl moieties to imine functional groups as an extension of the Nindigo chemistry.

Since the imine functionality improved the solubility of indigo, the same should be true for perinaphthindigo (**Scheme 44**).

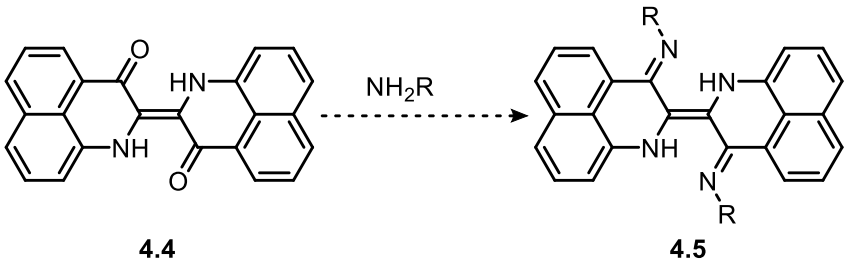

4.4 **4.5**

Scheme 44. Conversion of PNI to its imine analogue.

6.3 Future work for Nindigo

Investigation into the two red shifted peaks in the UV-Vis spectrum of Nindigo led us to the conclusion that the peak at 657 nm is the result of the protonated species of Nindigo. However, the origin of the second red-shifted peak at 741 nm remains unknown. Since the simple answer of solely aggregation or autoionization does not explain this peak at 741 nm, it is likely that this peak is a result of some kind of combined process. Further experiments include the back titration of the protonated species with a strong base such as the lithium (trimethylsilyl)amide used for the deprotonation in Chapter 5 to see if there is a point in the titration where only the peak at 586 nm is present. Another experiment is the treatment of the deprotonated species (which has only one electronic transition) with water to see if the resulting compound will exhibit the two red shifted peaks. This will probe if the peaks at 657 nm and 741 nm arise from the synthesis of Nindigo or if they are an artefact of solution behavior.

The protoisomerization of Nindigo was unexpected and resulted in compounds that are interesting in their own right. These stable salts could be utilized as a Brønsted acid (or

proton shuttle) in a variety of organic transformations including the Diels-Alder reaction or the Mannich reaction. While we recognize that protonated Nindigo could be suitable for such chemistry, normally more mundane Brønsted acids (hydrochloric acid, *para*-tolylsulfonic acid) are effective. There has been recent interest in the use of chiral organocatalytic Brønsted acids for asymmetric transformations. Two key examples of these chiral Brønsted acids include proline and BINOL derived phosphoric acids.[135-136] Like these examples, it is possible for protonated Nindigo to be chiral. This can be achieved by having a substituent at the 2-position only of the aryl ring (**Scheme 45**). Before protonation, this species will be prochiral. However, upon pronation and isomerization we propose the substituents will face on the opposite face of the planar benzannulated rings inducing chirality (as a racemic mixture) (**Scheme 45**). These enantiomers will need to be separated, likely by using a chiral proton source to generate the protonated Nindigo, such as camphor sulfonic acid. Once separated, the chiral Brønsted acid could be used as a co-catalyst for one of these organic transformations to assess the viability of these chiral proton sources.[137-140]

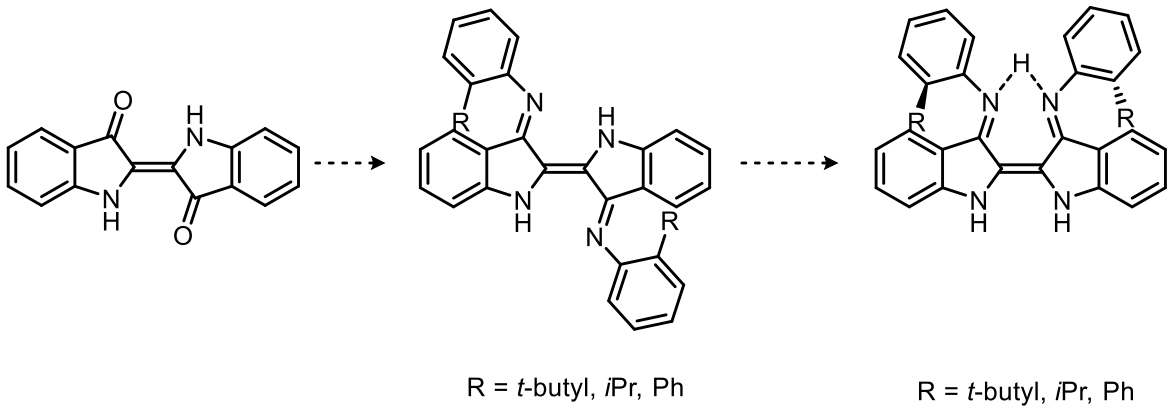

Scheme 45. Synthesis of the chiral protonated Nindigo.

Literature precedent exists for using structurally similar (to the protonated Nindigo) chiral Brønsted acids for reactions such as the Aza-Henry reaction (**Figure 60**).[141-142] The authors consider this a model reaction for many carbon-carbon bond-forming reactions catalyzed by enzymes. The authors also suggest that using this ionic hydrogen bond in asymmetric catalysis may also be a viable "green" chemistry approach to single-enantiomer organic compounds. Similar chemistry could be attempted with our substrates to see if we get comparable enantiomeric excess.

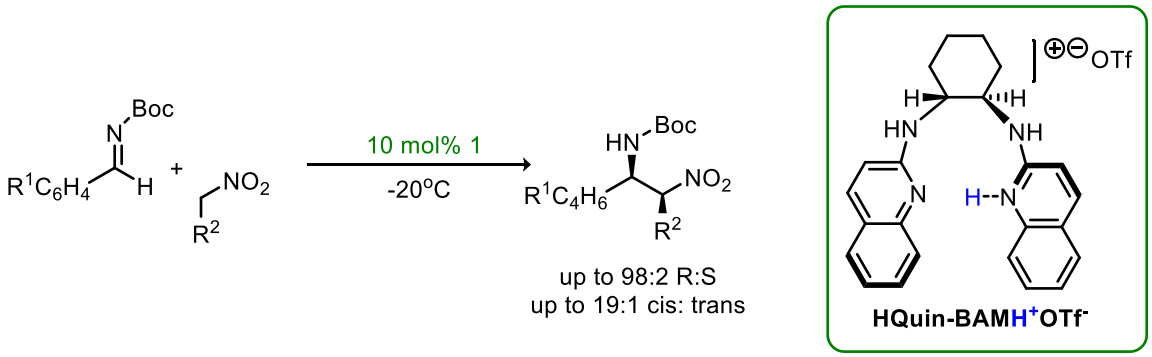

Figure 60. Example of a chiral proton source for an Aza-Henry reaction.[142]

Bibliography

1. Bergamo, A.; Gaiddon, C.; Schellens, J. H. M.; Beijnen, J. H.; Sava, G. *Journal of Inorganic Biochemistry* **2012,** *106* (1), 90-99.
2. Wang, K.; Gao, E. *Anti-Cancer Agents Medicinal Chemistry* **2014,** *14* (1), 147-169.
3. Mukherjee, A.; Sadler, P. J. In *Metals in medicine: therapeutic agents*, John Wiley & Sons, Inc.: 2009; pp 80-126.
4. Salas, P. F.; Herrmann, C.; Cawthray, J. F.; Nimphius, C.; Kenkel, A.; Chen, J.; de Kock, C.; Smith, P. J.; Patrick, B. O.; Adam, M. J.; Orvig, C. *Journal of Medicinal Chemistry* **2013,** *56* (4), 1596-1613.
5. Sekhon, B. S.; Bimal, N. *Journal of Pharmaceutical Educational Research* **2012,** *3* (2), 52-63.
6. Caravan, P., *Wiley Encyclopedia of Chemical Biology*. John Wiley & Sons, Inc.: 2008.
7. Terreno, E.; Castelli, D. D.; Aime, S. *Contrast Media Molecular Imaging* **2010,** *5* (2), 78-98.
8. Woods, M., Woessner, D.E., Sherry, A.D. *Chemical Societiy Reviews* **2006,** *35*, 500-511.
9. Beyer, T.; Townsend, D. W.; Brun, T.; Kinahan, P. E.; Charron, M.; Roddy, R.; Jerin, J.; Young, J.; Byars, L.; Nutt, R. *Journal of Nuclear Medicine* **2000,** *41* (8), 1369-79.
10. Ward, K. M.; Aletras, A. H.; Balaban, R. S. *Journal of Magnetic Resonance* **2000,** *143* (1), 79-87.
11. Lauterbur, P. C. *Nature* **1973,** *242* (5394), 190-191.
12. Caravan, P.; Ellison, J. J.; McMurry, T. J.; Lauffer, R. B. *Chemistry Reviews* **1999,** *99* (9), 2293-2352.
13. Taddei, M.; Ricci, A. *Synthesis* **1986,** (8), 633-5.
14. Pierre, V. C.; Allen, M. J.; Caravan, P. *JBIC, Journal of Biological Inorganic Chemistry* **2014,** *19* (2), 127-131.
15. Canada, H. Whole Body Imaging: CT or MRI.
16. Sadowski, E. A.; Bennett, L. K.; Chan, M. R.; Wentland, A. L.; Garrett, A. L.; Garrett, R. W.; Djamali, A. *Radiology* **2007,** *243* (1), 148-157.
17. Sadowski, E. A.; Djamali, A. *Radiology* **2007,** *244* (3), 931-932.
18. Nelson, J. H., *Nuclear Magnetic Resonance Spectroscopy*. Peason Education Inc: 2003.
19. Viswanathan, S.; Kovacs, Z.; Green, K. N.; Ratnakar, S. J.; Sherry, A. D. *Chemistry Reviews (Washington, DC, U. S.)* **2010,** *110* (5), 2960-3018.
20. Woods, M.; Woessner, D. E.; Sherry, A. D. *Chemical Society Reviews* **2006,** *35* (6), 500-511.
21. Fernando, S. K.; Chao, P.; Kiefer, G. E.; Wu, Y.; Sherry, D. A. In *Breaking the slow water exchange barrier in the design of functional PARACEST agents for MRI*, American Chemical Society: 2013; pp SWRM-234.

22. Fernando, W. S. K.; Zhao, P.; Kiefer, G. E.; Wu, Y.; Sherry, A. D. In *Optimization of water exchange in PARACEST agents for in vivo imaging*, American Chemical Society: 2014; pp INOR-562.
23. Ratnakar, S. J.; Soesbe, T. C.; Lumata, L. L.; Do, Q. N.; Viswanathan, S.; Lin, C.-Y.; Sherry, A. D.; Kovacs, Z. *Journal of the American Chemical Society* **2013,** *135* (40), 14904-14907.
24. Wang, X.; Wu, Y.; Zhao, P.; Sherry, A. D. In *Development of a new PARACEST agent for in vivo pH imaging*, American Chemical Society: 2014; pp INOR-575.
25. Datta, A.; Raymond, K. N. *Acc. Chem. Res.* **2009,** *42* (7), 938-947.
26. Raymond, K. N.; Pierre, V. C. *Bioconjugate Chemistry* **2005,** *16* (1), 3-8.
27. Werner, E. J.; Datta, A.; Jocher, C. J.; Raymond, K. N. *Angewandte Chemie, International Edition* **2008,** *47* (45), 8568-8580.
28. Klaui, W.; Lenders, B.; Hessner, B.; Evertz, K. *Organometallics* **1988,** *7* (6), 1357-1363.
29. Allen, K. J. H.; Nicholls-Allison, E. C.; Johnson, K. R. D.; Nirwan, R. S.; Berg, D. J.; Wester, D.; Twamley, B. *Inorganic Chemistry* **2012,** *51* (22), 12436-12443.
30. Trofimenko, S. *Polyhedron* **2004,** *23* (2-3), 197-203.
31. Bieller, S.; Haghiri, A.; Bolte, M.; Bats, J. W.; Wagner, M.; Lerner, H.-W. *Inorganica Chimica Acta* **2006,** *359* (5), 1559-1572.
32. Burzlaff, N.; Hegelmann, I.; Weibert, B. *Journal of Organometallic Chemistry* **2001,** *626* (1–2), 16-23.
33. Cowley, R. E.; Bontchev, R. P.; Duesler, E. N.; Smith, J. M. *Inorganic Chemistry* **2006,** *45* (24), 9771-9779.
34. Crawford, D.; Hofer, A. K.; Edler, K. L.; Ferrence, G. M. *Acta Crystallography, Section E: Structure Reports Online* **2011,** *67* (4), m496.
35. Litlaboe, R.; Saliu, K.; Ferguson, M. J.; McDonald, R.; Takats, J.; Anwander, R. *Organometallics* **2009,** *28* (23), 6750-6754.
36. Owen, G. R.; Tsoureas, N.; Hope, R. F.; Kuo, Y.-Y.; Haddow, M. F. *Dalton Transactions* **2011,** *40* (22), 5906-5915.
37. Roppe, J.; Smith, N. D.; Huang, D.; Tehrani, L.; Wang, B.; Anderson, J.; Brodkin, J.; Chung, J.; Jiang, X.; King, C.; Munoz, B.; Varney, M. A.; Prasit, P.; Cosford, N. D. P. *Journal of Medicinal Chemistry* **2004,** *47* (19), 4645-4648.
38. Roy, B. N.; Singh, G. P.; George, S. K.; Lathi, P. S.; Agrawal, M. K.; Trivedi, A.; Mishra, M.; Singh, G. *Indian Journal of Chemistry, Section B: Organic Chemistry including Medicinal Chemistry.* **2014,** *53B* (5), 610-618.
39. Moleele, S. S.; Michael, J. P.; De Koning, C. B. *Tetrahedron* **2006,** *62* (12), 2831-2844.
40. Jernigan, F. E., 3rd; Sieracki, N. A.; Taylor, M. T.; Jenkins, A. S.; Engel, S. E.; Rowe, B. W.; Jove, F. A.; Yap, G. P. A.; Papish, E. T.; Ferrence, G. M. *Inorganic Chemistry* **2007,** *46* (2), 360-2.
41. Al-Mousawi, S. M.; Moustafa, M. S.; Elnagdi, M. H. *Green Chemistry Letters and Reviews* **2011,** *4* (2), 185-193.
42. Zheng, R.-L.; Zeng, X.-X.; He, H.-Y.; He, J.; Yang, S.-Y.; Yu, L.-T.; Yang, L. *Synthetic Communications* **2012,** *42* (10), 1521-1531.
43. Lin, Y. I.; Jennings, M. N.; Sliskovic, D. R.; Fields, T. L.; Lang, S. A., Jr. *Synthesis* **1984,** (11), 946-7.

44. Ospina, C. A.; Rodriguez, A. D.; Sanchez, J. A.; Ortega-Barria, E.; Capson, T. L.; Mayer, A. M. S. *Journal Natural Products* **2005,** *68* (10), 1519-1526.
45. Webster, C. E.; Hall, M. B. *Inorganica Chimica Acta* **2002,** *330*, 268-282.
46. McOmie, J. F. W.; Watts, M. L.; West, D. E. *Tetrahedron* **1968,** *24* (5), 2289-92.
47. Node, M.; Nishide, K.; Sai, M.; Ichikawa, K.; Fuji, K.; Fujita, E. *Chemistry Letters* **1979,** (1), 97-8.
48. Yadav, J. S.; Ganganna, B.; Bhunia, D. C.; Srihari, P. *Tetrahedron Letters* **2009,** *50* (30), 4318-4320.
49. Cha, K. H.; Kang, T. W.; Cho, D. O.; Lee, H.-W.; Shin, J.; Jin, K. Y.; Kim, K.-W.; Kim, J.-W.; Hong, C.-I. *Synthetic Communications* **1999,** *29* (20), 3533-3540.
50. Gevorgyan, V.; Rubin, M.; Benson, S.; Liu, J.-X.; Yamamoto, Y. *Journal of Organic Chemistry* **2000,** *65* (19), 6179-6186.
51. Chakraborti, A. K.; Sharma, L.; Nayak, M. K. *Journal of Organic Chemistry* **2002,** *67* (18), 6406-6414.
52. Pignataro, L.; Boghi, M.; Civera, M.; Carboni, S.; Piarulli, U.; Gennari, C. *Chemistry, a European Journal* **2012,** *18* (5), 1383-1400, S1383/1-S1383/113.
53. Sefkow, M.; Kaatz, H. *Tetrahedron Letters* **1999,** *40* (36), 6561-6562.
54. Choi, P. J.; Rathwell, D. C. K.; Brimble, M. A. *Tetrahedron Letters* **2009,** *50* (26), 3245-3248.
55. Li, T.-S.; Li, A.-X. *Journal of the Chemical Society: Perkin Transactions 1* **1998,** (12), 1913-1918.
56. Hart, L. S.; Waddington, C. R. *Journal of the Chemical Society: Perkin Transactions 2* **1985,** (10), 1607-12.
57. Zhang, F.; Jin, J.; Zhong, X.; Li, S.; Niu, J.; Li, R.; Ma, J. *Green Chemistry* **2011,** *13* (5), 1238-1243.
58. Allen, C. F. H.; Van Allan, J. *Organic Synthesis* **1942,** *22*, 9-12.
59. Fox, B. A.; Threlfall, T. L. *Organic Synthesis* **1964,** *44*, 34-9.
60. Singh, G., *Chemistry of Lanthanides and Actinides*. Discovery Publishing House.
61. Fossheim, S.; Johansson, C.; Fahlvik, A. K.; Grace, D.; Klaveness, J. *Magnetic Resonance Medicine* **1996,** *35* (2), 201-6.
62. Shannon, R. D. *Acta Crystallography, Section A* **1976,** *A32* (5), 751-67.
63. Saliu, K. O.; Takats, J.; Ferguson, M. J. *Acta Crystallography, Section E: Structural Report Online* **2009,** *65* (6), m643-m644.
64. Fabian, J.; Nakazumi, H.; Matsuoka, M. *Chemistry Reviews* **1992,** *92* (6), 1197-1226.
65. Fabian, J.; Zahradník, R. *Angewandte Chemie International Edition in English* **1989,** *28* (6), 677-694.
66. Qian, G.; Wang, Z. Y. *Chemistry an Asian Journal* **2010,** *5* (5), 1006-1029.
67. Ciardelli, F.; Bertoldo, M.; Bronco, S.; Pucci, A.; Ruggeri, G.; Signori, F. *Polymer International* **2013,** *62* (1), 22-32.
68. Filichev, V. V. *Chemistry in New Zealand* **2010,** *74* (1), 24-31.
69. Hales, J. M.; Barlow, S.; Kim, H.; Mukhopadhyay, S.; Bredas, J.-L.; Perry, J. W.; Marder, S. R. *Chemistry of Materials* **2014,** *26* (1), 549-560.
70. *General Introduction to the Chemsitry of Dyes*. IARC Monographs: Vol. 99.
71. Elsawy, W.; Lee, C.-L.; Cho, S.; Oh, S.-H.; Moon, S.-H.; Elbarbary, A.; Lee, J.-S. *Physical Chemistry Chemical Physics* **2013,** *15* (36), 15193-15203.

72. Yang, M.; Chen, X.; Zou, Y.; Pan, C.; Liu, B.; Zhong, H. *Journal of Materials Science* **2013,** *48* (3), 1014-1020.
73. Glowacki, E. D.; Voss, G.; Sariciftci, N. S. *Advanced Materials (Weinheim, Ger.)* **2013,** *25* (47), 6783-6800.
74. *Indigo and Indigo Colourants*. Ullman Encyclopedia: 2004.
75. Littma, E., *Maya blue - further perspective & the possible use of indigo as the colourant*. American Antiquity: 1982.
76. In *Chemistry of Blue Jeans: Indigo Synthesis and Dyeing*.
77. von Baeyer, A. *Berichte der deutschen chemischen Gesellschaft* **1882,** *15* (2).
78. Seixas de Melo, J. S.; Rondao, R.; Burrows, H. D.; Melo, M. J.; Navaratnam, S.; Edge, R.; Voss, G. *ChemPhysChem: of Chemical Physics and Physical Chemistry* **2006,** *7* (11), 2303-2311.
79. Serrano-Andres, L.; Roos, B. O. *Chemistry, a European Journal* **1997,** *3* (5), 717-725.
80. Wille, E.; Luettke, W. *Angewandte Chemie, Internation Edition in English* **1971,** *10* (11), 803-4.
81. Bauer, H.; Kowski, K.; Kuhn, H.; Luttke, W.; Rademacher, P. *Journal of Molecular Structure* **1998,** *445* (1-3), 277-286.
82. Wille, E.; Luettke, W. *Liebigs Annalen der Chemie* **1980,** (12), 2039-54.
83. Dittmann, M.; Graupner, F. F.; Maerz, B.; Oesterling, S.; de Vivie-Riedle, R.; Zinth, W.; Engelhard, M.; Luettke, W. *Angewandte Chemie International Edition* **2014,** *53* (2), 591-594.
84. Kobayashi, T., Rentzepis, P.M. *Journal of Chemical Physics* **1979,** 70.
85. Miliani, C.; Romani, A.; Favaro, G. *Spectrochemica Acta, Part A* **1998,** *54A* (4), 581-588.
86. Rondao, R.; Seixas de Melo, J.; Schaberle, F. A.; Voss, G. *Physical Chemistry Chemical Physics* **2012,** *14* (5), 1778-1783.
87. Irimia-Vladu, M.; Glowacki, E. D.; Troshin, P. A.; Schwabegger, G.; Leonat, L.; Susarova, D. K.; Krystal, O.; Ullah, M.; Kanbur, Y.; Bodea, M. A.; Razumov, V. F.; Sitter, H.; Bauer, S.; Sariciftci, N. S. *Advanced Materials (Weinheim, Ger.)* **2012,** *24* (3), 375-380.
88. Pouliquen, J.; Wintgens, V.; Toscano, V.; Kossanyi, J. *Dyes and Pigments* **1985,** *6* (3), 163-75.
89. Schanze, K. S.; Lee, L. Y. C.; Giannotti, C.; Whitten, D. G. *Journal of the American Chemical Society* **1986,** *108* (10), 2646-55.
90. Jung, E. H.; Jo, W. H. *Energy and Environmental Science* **2014,** *7* (2), 650-654.
91. Stalder, R.; Mei, J.; Reynolds, J. R. *Macromolecules (Washington, DC, U. S.)* **2010,** *43* (20), 8348-8352.
92. Tsuji, S.; Nakano, M.; Furukawa, M.; Yoshii, K.; Tonogai, Y. *Shokuhin Eiseigaku Zasshi* **2005,** *46* (3), 116-120.
93. Miwa, T.; Maruo, Y. Y.; Akaoka, K.; Kunioka, T.; Nakamura, J. *J. Air Waste Management Association* **2009,** *59* (7), 801-808.
94. Bergman, J.; Eklund, N. *Chem. Scr.* **1982,** *19* (5), 193-204.
95. Smith, B. D.; Alonso, D. E.; Bien, J. T.; Metzler, E. C.; Shang, M.; Roosenberg, J. M., II. *Journal of Organic Chemistry* **1994,** *59* (26), 8011-14.

96. Sukari, M. A.; Vernon, J. M. *Journal of the Chemistry Society: Perkin Transactions 1* **1983,** (9), 2219-23.
97. Giuliano, C. R., Hess, L.D., Margerum, J.D. *Journal of the American Chemical Society* **1967,** *90*.
98. Weinstein, J., Wyrnan, G.M. *Journal of Organic Chemistry* **1956,** *78*, 4007.
99. Wyman, G. M. *Chemistry Reviews (Washington, DC, U. S.)* **1955,** *55*.
100. Corval, A.; Trommsdorff, H. P. *The Journal of Physical Chemistry* **1987,** *91* (6), 1317-1324.
101. Karstens, T.; Kobs, K.; Memming, R.; Schröppel, F. *Chemical Physics Letters* **1977,** *48* (3), 540-544.
102. Klages, C. P.; Kobs, K.; Memming, R. *Chemical Physics Letters* **1982,** *90* (1), 51-54.
103. Beck, W.; Schmidt, C.; Wienold, R.; Steimann, M.; Wagner, B. *Angewandte Chemie* **1989,** *101* (11), 1532-4.
104. Wu, J.-Y.; Chang, C.-H.; Thanasekaran, P.; Tsai, C.-C.; Tseng, T.-W.; Lee, G.-H.; Peng, S.-M.; Lu, K.-L. *Dalton Transactions* **2008,** (44), 6110-6112.
105. Bhattacharya, D.; Chang, C.-H.; Cheng, Y.-H.; Lai, L.-L.; Lu, H.-Y.; Lin, C.-Y.; Lu, K.-L. *Chemistry, a European Journal* **2012,** *18* (17), 5275-5283, S5275/1-S5275/15.
106. Wang, S. J.; Zhao, Y. L.; Zhao, C. X.; Liu, L.; Yu, S. J. *Journal of Fluorine Chemistry* **2013,** *156*, 236-239.
107. Oakley, S. R.; Nawn, G.; Waldie, K. M.; MacInnis, T. D.; Patrick, B. O.; Hicks, R. G. *Chemical Communications* **2010,** *46* (36), 6753-6755.
108. Mondal, P.; Ehret, F.; Bubrin, M.; Das, A.; Mobin, S. M.; Kaim, W.; Lahiri, G. K. *Inorganic Chemistry* **2013,** *52* (15), 8467-8475.
109. Mondal, P.; Plebst, S.; Ray, R.; Mobin, S. M.; Kaim, W.; Lahiri, G. K. *Inorganic Chemistry* **2014,** *53* (17), 9348-9356.
110. Nawn, G.; McDonald, R.; Hicks, R. G. *Inorganic Chemistry* **2013,** *52* (19), 10912-10919.
111. Nawn, G.; Oakley, S. R.; Majewski, M. B.; McDonald, R.; Patrick, B. O.; Hicks, R. G. *Chemical Science* **2013,** *4* (2), 612-621.
112. Nawn, G.; Waldie, K. M.; Oakley, S. R.; Peters, B. D.; Mandel, D.; Patrick, B. O.; McDonad, R.; Hicks, R. G. *Inorganic Chemistry* **2011,** *50* (20), 9826-9837.
113. Fortier, S.; Gonzalez-del Moral, O.; Chen, C.-H.; Pink, M.; Le Roy, J. J.; Murugesu, M.; Mindiola, D. J.; Caulton, K. G. *Chemical Communications (Cambridge, U. K.)* **2012,** *48* (90), 11082-11084.
114. Fortier, S.; Le Roy, J. J.; Chen, C.-H.; Vieru, V.; Murugesu, M.; Chibotaru, L. F.; Mindiola, D. J.; Caulton, K. G.*Journal fo the American Chemistry Society* **2013,** *135* (39), 14670-14678.
115. Nawn, G. Synthesis, Redox and Spectroscopic Properties of Nindigo and a Variety of Nindigo Coordination Compounds. University of Victoria, Victoria, BC, 2013.
116. Dutt, S. *Journal of the Chemistry Society, Transactions* **1923,** *123*, 224-5.
117. Sainz-Diaz, C. I. *Monatshefte fur Chemie* **2002,** *133* (1), 9-22.
118. Wolk, J. L.; Frimer, A. A. *Molecules* **2010,** *15*, 5561-5580.
119. Oriyama, T.; Aoyagi, M.; Iwanami, K. *Chemistry Letters* **2007,** *36* (5), 612-613.

120. Quast, H.; Nudling, W.; Klemm, G.; Kirschfeld, A.; Neuhaus, P.; Sander, W.; Hrovat, D. A.; Borden, W. T. *Journal of Organic Chemistry* **2008,** *73* (13), 4956-4961.
121. McCandless, F. P. *Industrial & Engineering Chemistry Product Research and Development* **1982,** *21* (3), 483-488.
122. Goto, K.; Kubo, T.; Yamamoto, K.; Nakasuji, K.; Sato, K.; Shiomi, D.; Takui, T.; Kubota, M.; Kobayashi, T.; Yakusi, K.; Ouyang, J. *Journal of the American Chemistry Society* **1999,** *121* (7), 1619-1620.
123. Repine, J. T.; Johnson, D. S.; White, A. D.; Favor, D. A.; Stier, M. A.; Yip, J.; Rankin, T.; Ding, Q.; Maiti, S. N. *Tetrahedron Letters* **2007,** *48* (31), 5539-5541.
124. Carme Pampin, M.; Estevez, J. C.; Estevez, R. J.; Maestro, M.; Castedo, L. *Tetrahedron* **2003,** *59* (36), 7231-7243.
125. Chen, H.; Luzy, J.-P.; Gresh, N.; Garbay, C. *European Journal of Organic Chemistry* **2006,** (10), 2329-2335.
126. Wipf, P.; Lynch, S. M. *Organic Letters* **2003,** *5* (7), 1155-1158.
127. Stokes, B. J.; Jovanovic, B.; Dong, H.; Richert, K. J.; Riell, R. D.; Driver, T. G. *Journal of Organic Chemistry* **2009,** *74* (8), 3225-3228.
128. Bailey, J. E., Jr.; Travis, J. *Dyes and Pigments* **1985,** *6* (2), 135-54.
129. Arai, T.; Tokumaru, K. *Chemistry Reviews* **1993,** *93* (1), 23-39.
130. Cramer, R.; Lindsey, R. V. *Journal of the American Chemical Society* **1966,** *88* (15), 3534-3544.
131. Gibson, T. W.; Strassburger, P. *The Journal of Organic Chemistry* **1976,** *41* (5), 791-793.
132. Hammond, G. S.; Saltiel, J.; Lamola, A. A.; Turro, N. J.; Bradshaw, J. S.; Cowan, D. O.; Counsell, R. C.; Vogt, V.; Dalton, C. *Journal of the American Chemistry Society* **1964,** *86* (16), 3197-3217.
133. Kuad, P.; Borkovec, M.; Desage-El Murr, M.; Le Gall, T.; Mioskowski, C.; Spiess, B. *Journal of the American Chemistry Society* **2005,** *127* (4), 1323-1333.
134. Gómez-Bombarelli, R.; Calle, E.; Casado, J. *The Journal of Organic Chemistry* **2013,** *78* (14), 6868-6879.
135. Toda, Y.; Pink, M.; Johnston, J. N. *Journal of the American Chemistry Society* **2014,** *136* (42), 14734-14737.
136. MacMillan, D. W. C. *Nature (London, U. K.)* **2008,** *455* (7211), 304-308.
137. Mutyala, A. K.; Patil, N. T. *Organic Chemistry Fronteirs* **2014,** *1* (5), 582-586.
138. Rono, L. J.; Yayla, H. G.; Wang, D. Y.; Armstrong, M. F.; Knowles, R. R. *Journal of the American Chemistry Society* **2013,** *135* (47), 17735-17738.
139. Rueping, M.; Raja, S. *Beilstein Journal of Organic Chemistry* **2012,** *8*, 1819-1824, No. 208.
140. Tian, X.; Hofmann, N.; Melchiorre, P. *Angew. Chem., Int. Ed.* **2014,** *53* (11), 2997-3000.
141. Hodgson, P.; Lloyd-Jones, G. C.; Murray, M.; Peakman, T. M.; Woodward, R. L. *Chemistry – A European Journal* **2000,** *6* (24), 4451-4460.
142. Nugent, B. M.; Yoder, R. A.; Johnston, J. N. *Journal of the American Chemical Society* **2004,** *126* (11), 3418-3419.

Appendix A: Crystallographic Parameters

	2.28	**4.3a**	**3.13**
Formula	$C_{40}H_{44}B_2ClN_{12}O_2Yb$	$C_{11}H_7NO_3$	$C_{32}H_{28}N_4$
Formula weight	954.98	201.18	468.58
Crystal dimensions (mm)	0.05 x 0.03 x 0.01	0.35 x 0.14 x 0.08	0.20 x 0.27 x 0.42
Crystal system	Monoclinic	Monoclinic	Monoclinic
Space group	$P2_1/n$	$P2_1/n$	$P\ 2_1/c$ (#14)
a (Å)	10.2500(16)	7.1131(15)	8.567(4)
b (Å)	28.602(5)	15.601(3)	10.568(2)
c (Å)	14.348(2)	8.0408(16)	13.198(4)
α (deg)	90	90	90
β (deg)	101.423(2)	95.920(5)	92.01(3)
γ (deg)	90	90	90
V (Å3)	4123.0(11)	887.5(3)	1194.2(7)
Z	4	4	2
*r*calcd (gcm^{-3})	1.538	1.506	1.303
μ (mm^{-1})	2.860	0.112	0.78
Temperature (K)	150(2)	90	100(2)
Data collection 2*q* limit (deg)	28.99	60.148	
Total data collected	45315	10315	15127
Independent reflections	8415	2592	2973
Data/restraints/parameters	8415/4/535	2592/0/136	2973/226/13.15
*R*1 [Fo2^{3}2s(Fo2)]	0.0597	0.0616	0.052
wR2 [all data]	0.1204	0.1561	0.150

$R1 = \Sigma \, ||Fo| - |Fc|| \, / \, \Sigma \, |Fo|$

$wR2 = [\, \Sigma \, (\, w \, (Fo^2 - Fc^2)^2 \,) / \, \Sigma \, w(Fo^2)^2]^{1/2}$

	3.18	**5.1aCF_3COO**	**5.1aBF_4**
Formula	$C_{28}H_{19}N_4BF_2$	$C_{34}H_{29}N_4O_2F_3$	$C_{32}H_{29}N_4BF_4$
Formula weight	460.28	582.61	556.40
Crystal dimensions (mm)	0.02 x 0.10 x 0.18	0.22 x 0.25 x 0.75	0.40 x 0.40 x 0.40
Crystal system	Monoclinic	Monoclinic	Monoclinic
Space group	*P* $2_1/c$	*P* – 1	*P* $2_1/c$
a (Å)	9.7307(9)	10.7480(5)	12.746(2)
b (Å)	36.653(3)	11.7990(5)	9.883(2)
c (Å)	13.0299(13)	12.2207(6)	22.461(4)
α (deg)	90	76.828	90
β (deg)	111.108	73.111(1)	106.476(4)
γ (deg)	90	87.926(1)	90
V (Å3)	4364.0(7)	1443.2(1)	2713.2(7)
Z	8	2	4
*r*calcd (gcm^{-3})	1.401	1.341	1.362
μ (mm^{-1})	0.96	0.98	1.00
Temperature (K)	90	90	90
Data collection 2*q* limit (deg)	50.5	60.2	60.1
Total data collected	8016	8479	7934
Independent reflections	632	409	386
Data/restraints/parameters	8016/632/13	8479/409/21	7934/386/21
*R*1 [Fo2^{3}2s(Fo2)]	0.061	0.056	0.058
wR2 [all data]	0.128	0.111	0.108

$R1 = \Sigma \, ||Fo| - |Fc|| \, / \, \Sigma \, |Fo|$

$wR2 = [\Sigma (w (Fo^2 - Fc^2)^2) / \Sigma \, w(Fo^2)^2]^{1/2}$

	5.4aCl
Formula	$C_{24}H_{20}ClN_3O$
Formula weight	401.88
Crystal dimensions (mm)	0.04 x 0.06 x 0.06
Crystal system	Triclinic
Space group	*P*-1
a (Å)	7.956(3)
b (Å)	9.421(4)
c (Å)	13.978(6)
α (deg)	107.481(8)
2β (deg)	96.743(8)
Γ1. (deg)	100.430(8)
V (Å3)	966.1(7)
Z	2
*r*calcd (gcm^{-3})	1.381
μ (mm^{-1})	2.19
Temperature (K)	90
Data collection 2*q* limit (deg)	52.2
Total data collected	3800
Independent reflections	276
Data/restraints/parameters	3800/276/14
*R*1 [Fo2^{3}2s(Fo2)]	0.075
wR2 [all data]	0.113

$R1 = \Sigma \, ||Fo| - |Fc|| \, / \, \Sigma \, |Fo|$

$wR2 = [\Sigma (w (Fo^2 - Fc^2)^2) / \Sigma \, w(Fo^2)^2]^{1/2}$

Appendix B: Complete Listing of Bond Lengths and Angles

Figure B-1: ORTEP diagram of **2.28** with all hydrogen atoms removed for clarity and thermal ellipsoids shown at the 50% probability level

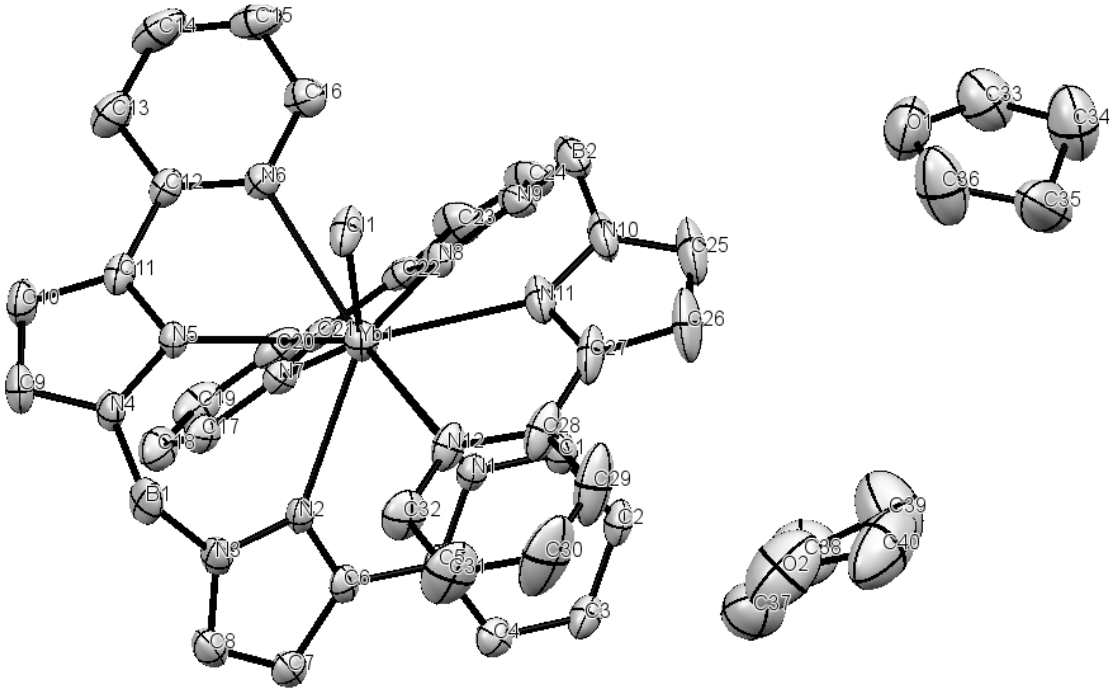

Table B-1: Bond Lengths (Å) and angles (º) for **2.28**

Yb1	N2	2.550(4)	C4	C5	1.379(7)
Yb1	N8	2.559(4)	C5	C6	1.466(7)
Yb1	N11	2.588(4)	C6	C7	1.399(7)
Yb1	N5	2.610(4)	C7	C8	1.369(8)
Yb1	N12	2.673(4)	C9	C10	1.349(9)
Yb1	N1	2.674(4)	C10	C11	1.400(7)
Yb1	N7	2.675(4)	C11	C12	1.450(7)
Yb1	N6	2.696(4)	C12	C13	1.397(7)
Yb1	Cl1	2.7056(14)	C13	C14	1.375(9)
N1	C5	1.348(7)	C14	C15	1.366(10)
N1	C1	1.350(7)	C15	C16	1.379(8)
N2	C6	1.344(7)	C17	C18	1.376(7)
N2	N3	1.366(6)	C18	C19	1.388(9)
N3	C8	1.346(7)	C19	C20	1.357(9)

N3	B1	1.544(8)	C20	C21	1.404(8)
N4	C9	1.355(7)	C21	C22	1.451(8)
N4	N5	1.363(6)	C22	C23	1.393(8)
N4	B1	1.541(8)	C23	C24	1.358(10)
N5	C11	1.342(6)	C25	C26	1.351(12)
N6	C16	1.342(7)	C26	C27	1.400(9)
N6	C12	1.344(7)	C27	C28	1.454(9)
N7	C17	1.344(7)	C28	C29	1.395(9)
N7	C21	1.348(6)	C29	C30	1.363(13)
N8	C22	1.355(7)	C30	C31	1.378(12)
N8	N9	1.359(6)	C31	C32	1.392(8)
N9	C24	1.341(8)	O1	C36	1.415(10)
N9	B2	1.544(10)	C33	C34	1.458(12)
N10	C25	1.345(8)	C34	C35	1.477(14)
N10	N11	1.354(7)	C35	C36	1.459(14)
N10	B2	1.518(11)	O2	C40	1.416(14)
N11	C27	1.342(8)	O2	C37	1.419(12)
N12	C32	1.328(8)	C37	C38	1.473(13)
N12	C28	1.349(7)	C38	C39	1.486(14)
C1	C2	1.379(8)	C39	C40	1.449(16)
C2	C3	1.374(8)	O1	C33	1.383(10)
C3	C4	1.387(8)			

N2	Yb1	N8	123.30(13)	C27	N11	N10	107.0(5)
N2	Yb1	N11	121.54(14)	C27	N11	Yb1	120.2(4)
N8	Yb1	N11	70.71(15)	N10	N11	Yb1	132.2(4)
N2	Yb1	N5	70.96(13)	C32	N12	C28	117.3(5)
N8	Yb1	N5	119.50(13)	C32	N12	Yb1	123.8(4)
N11	Yb1	N5	158.15(14)	C28	N12	Yb1	118.9(4)
N2	Yb1	N12	68.51(14)	N1	C1	C2	123.2(5)
N8	Yb1	N12	127.84(14)	C3	C2	C1	119.1(5)
N11	Yb1	N12	63.00(15)	C2	C3	C4	118.4(5)
N5	Yb1	N12	112.34(13)	C5	C4	C3	119.7(5)
N2	Yb1	N1	63.19(13)	N1	C5	C4	122.3(5)
N8	Yb1	N1	71.84(13)	N1	C5	C6	116.4(5)
N11	Yb1	N1	72.47(14)	C4	C5	C6	121.3(5)
N5	Yb1	N1	128.05(13)	N2	C6	C7	110.1(5)
N12	Yb1	N1	72.47(13)	N2	C6	C5	119.9(5)
N2	Yb1	N7	71.51(12)	C7	C6	C5	130.0(5)

N8	Yb1	N7	63.19(13)	C8	C7	C6	104.8(5)
N11	Yb1	N7	128.56(14)	N3	C8	C7	109.2(5)
N5	Yb1	N7	70.79(13)	C10	C9	N4	109.0(5)
N12	Yb1	N7	135.47(14)	C9	C10	C11	105.2(5)
N1	Yb1	N7	72.61(12)	N5	C11	C10	110.3(5)
N2	Yb1	N6	126.87(13)	N5	C11	C12	119.3(4)
N8	Yb1	N6	68.51(13)	C10	C11	C12	130.4(5)
N11	Yb1	N6	111.30(15)	N6	C12	C13	122.4(5)
N5	Yb1	N6	61.26(13)	N6	C12	C11	116.4(4)
N12	Yb1	N6	150.66(14)	C13	C12	C11	121.2(5)
N1	Yb1	N6	135.48(13)	C14	C13	C12	118.4(6)
N7	Yb1	N6	72.03(13)	C15	C14	C13	119.4(6)
N2	Yb1	Cl1	120.07(10)	C14	C15	C16	119.3(6)
N8	Yb1	Cl1	116.63(10)	N6	C16	C15	122.7(6)
N11	Yb1	Cl1	77.34(11)	N7	C17	C18	124.1(5)
N5	Yb1	Cl1	80.84(10)	C17	C18	C19	118.5(6)
N12	Yb1	Cl1	75.82(11)	C20	C19	C18	118.9(5)
N1	Yb1	Cl1	143.49(9)	C19	C20	C21	119.6(5)
N7	Yb1	Cl1	143.83(9)	N7	C21	C20	122.2(5)
N6	Yb1	Cl1	74.88(10)	N7	C21	C22	116.6(5)
C5	N1	C1	117.3(5)	C20	C21	C22	121.1(5)
C5	N1	Yb1	118.6(3)	N8	C22	C23	109.6(5)
C1	N1	Yb1	124.0(4)	N8	C22	C21	120.5(4)
C6	N2	N3	106.5(4)	C23	C22	C21	129.9(5)
C6	N2	Yb1	121.0(3)	C24	C23	C22	105.1(6)
N3	N2	Yb1	131.9(3)	N9	C24	C23	109.6(5)
C8	N3	N2	109.4(4)	N10	C25	C26	109.2(6)
C8	N3	B1	128.2(5)	C25	C26	C27	105.5(7)
N2	N3	B1	122.5(4)	N11	C27	C26	109.1(7)
C9	N4	N5	109.5(4)	N11	C27	C28	120.5(5)
C9	N4	B1	129.5(5)	C26	C27	C28	130.4(7)
N5	N4	B1	120.9(4)	N12	C28	C29	122.3(7)
C11	N5	N4	106.0(4)	N12	C28	C27	117.1(5)
C11	N5	Yb1	120.2(3)	C29	C28	C27	120.7(6)
N4	N5	Yb1	131.1(3)	C30	C29	C28	118.9(7)
C16	N6	C12	117.6(5)	C29	C30	C31	120.0(7)
C16	N6	Yb1	123.1(4)	C30	C31	C32	117.5(7)
C12	N6	Yb1	118.9(3)	N12	C32	C31	123.9(6)
C17	N7	C21	116.7(4)	N4	B1	N3	107.5(5)
C17	N7	Yb1	124.4(3)	N10	B2	N9	110.4(5)
C21	N7	Yb1	118.9(3)	C33	O1	C36	109.1(6)
C22	N8	N9	106.3(4)	O1	C33	C34	107.2(8)

C22	N8	Yb1	120.7(3)	C33	C34	C35	103.2(8)
N9	N8	Yb1	132.9(3)	C36	C35	C34	102.8(8)
C24	N9	N8	109.4(5)	O1	C36	C35	106.8(8)
C24	N9	B2	127.4(5)	C40	O2	C37	102.9(8)
N8	N9	B2	122.6(5)	O2	C37	C38	105.6(8)
C25	N10	N11	109.2(6)	C37	C38	C39	104.3(9)
C25	N10	B2	127.7(6)	C40	C39	C38	104.6(9)
N11	N10	B2	122.9(5)	O2	C40	C39	106.2(8)

Figure B-2: ORTEP diagram of **4.3a** will all hydrogen atoms with the exception of H1 removed for clarity and thermal ellipsoids shown at the 50% probability level

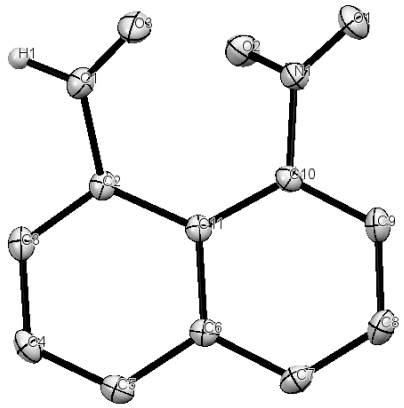

Table B-2: Bond Lengths (Å) and angles (º) for **4.3a**

C1	C2	1.4803(19)	C6	C11	1.4304(18)
C1	O3	1.2180(18)	C7	C8	1.368(2)
C2	C3	1.3779(19)	C8	C9	1.410(2)
C2	C11	1.4370(18)	C9	C10	1.3765(19)
C3	C4	1.410(2)	C10	C11	1.4192(18)
C4	C5	1.366(2)	C10	N1	1.4774(18)
C5	C6	1.4250(19)	N1	O1	1.2301(16)
C6	C7	1.4204(19)	N1	O2	1.2316(16)

O3	C1	C2	125.60(13)	C7	C8	C9	119.43(13)
C3	C2	C1	113.86(12)	C10	C9	C8	119.93(13)
C3	C2	C11	120.03(12)	C9	C10	C11	123.05(12)
C11	C2	C1	125.08(12)	C9	C10	N1	114.94(12)
C2	C3	C4	121.74(13)	C11	C10	N1	121.30(12)
C5	C4	C3	119.34(13)	C6	C11	C2	117.58(12)
C4	C5	C6	121.14(12)	C10	C11	C2	126.70(12)
C5	C6	C11	119.68(12)	C10	C11	C6	115.72(12)
C7	C6	C5	119.77(12)	O1	N1	C10	118.50(12)
C7	C6	C11	120.50(12)	O1	N1	O2	123.73(12)
C8	C7	C6	121.16(13)	O2	N1	C10	117.66(11)

Figure B-3: ORTEP diagram of **3.13** with all hydrogen atoms with the exception of the N-H's removed for clarity and thermal ellipsoids shown at the 50% probability level

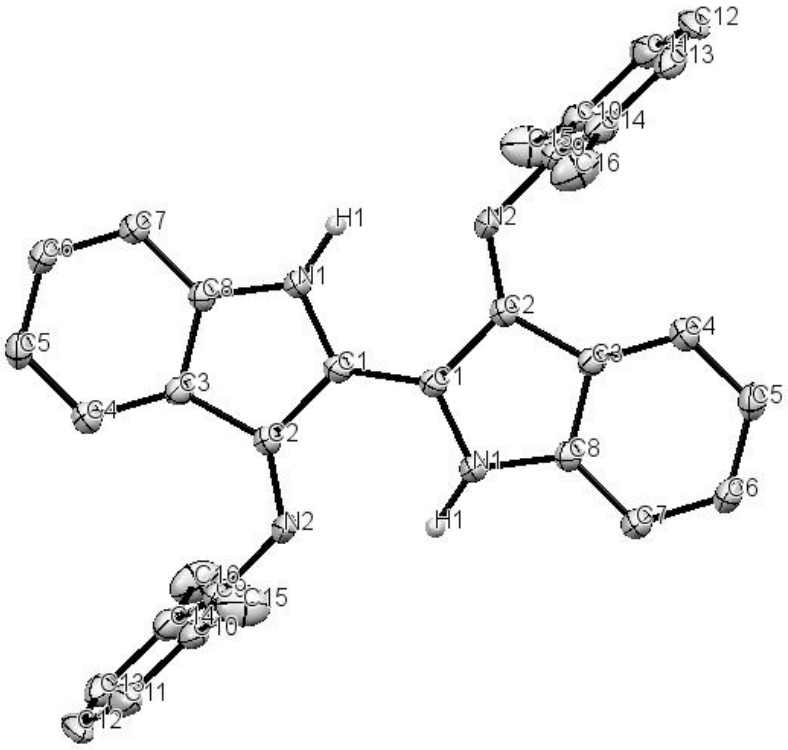

Table B-3 Bond Lengths (Å) and angles (°) for **3.13**

N1	C1	1.3618(18)	C14	1.3900	
N1	C8	1.3902(18)	C11	1.3900	
N2	C2	1.296(11)	C15	1.514(3)	
N2	C9	1.385(11)	C12	1.3900	
N2B	C2	1.36(2)	C13	1.3900	
N2B	C9B	1.50(2)	C14	1.3900	
C1	C1[1]	1.402(3)	C16	1.512(4)	
C1	C2	1.4566(18)	C10B	1.3900	
C2	C3	1.463(2)	C14B	1.3900	
C3	C4	1.401(2)	C11B	1.3900	
C3	C8	1.412(2)	C15B	1.495(9)	
C4	C5	1.382(2)	C12B	1.3900	
C5	C6	1.401(2)	C13B	1.3900	
C6	C7	1.390(2)	C14B	1.3900	
C7	C8	1.388(2)	C16B	1.506(8)	
C9	C10	1.3900			

C1	N1	C8	107.82(11)	C10	C9	C14	120.0
C2	N2	C9	124.6(9)	C11	C10	C9	120.0
C2	N2B	C9B	111.7(18)	C11	C10	C15	118.80(18)
N1	C1	C1[1]	123.93(16)	C9	C10	C15	121.20(19)
N1	C1	C2	110.19(12)	C10	C11	C12	120.0
C1[1]	C1	C2	125.87(16)	C13	C12	C11	120.0
N2	C2	C1	124.8(5)	C12	C13	C14	120.0
N2B	C2	C1	118.7(11)	C13	C14	C9	120.0
N2	C2	C3	130.0(5)	C13	C14	C16	120.2(2)
N2B	C2	C3	136.0(11)	C9	C14	C16	119.8(2)
C1	C2	C3	105.14(11)	C10B	C9B	C14B	120.0
C4	C3	C8	120.00(13)	C10B	C9B	N2B	130.2(14)
C4	C3	C2	134.36(13)	C14B	C9B	N2B	109.5(14)
C8	C3	C2	105.63(12)	C11B	C10B	C9B	120.0
C5	C4	C3	118.83(14)	C11B	C10B	C15B	118.6(6)
C4	C5	C6	120.55(13)	C9B	C10B	C15B	121.4(6)
C7	C6	C5	121.47(14)	C10B	C11B	C12B	120.0
C8	C7	C6	118.03(14)	C13B	C12B	C11B	120.0
C7	C8	N1	127.67(13)	C12B	C13B	C14B	120.0
C7	C8	C3	121.10(13)	C13B	C14B	C9B	120.0

N1	C8	C3	111.22(12)	C13B	C14B	C16B	118.8(5)
N2	C9	C10	114.7(7)	C9B	C14B	C16B	121.2(5)
N2	C9	C14	125.2(7)				

Figure B-4: ORTEP diagram of **3.18** with all hydrogen atoms removed for clarity and thermal ellipsoids shown at the 50% probability level

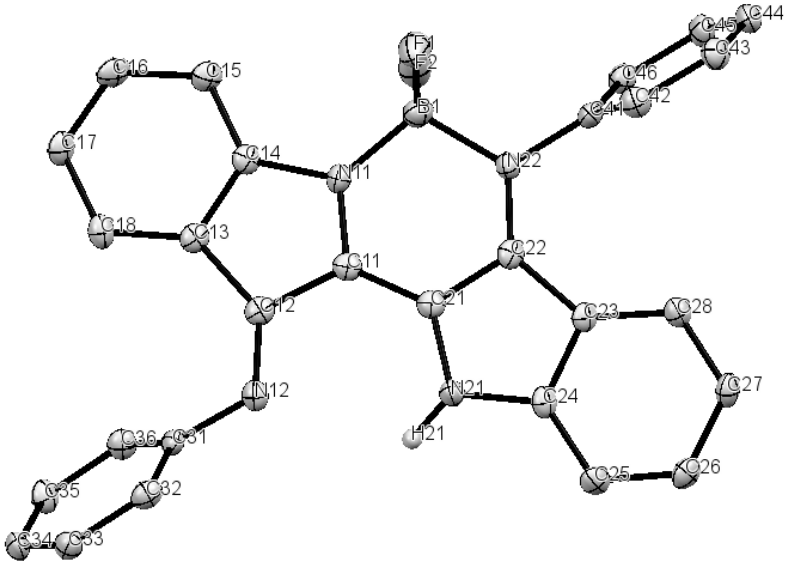

Table B-4: Bond Lengths (Å) and angles (º) for **3.18**

C11	N11	1.352(3)	C54	N31	1.408(4)
C11	C21	1.377(4)	C55	C56	1.389(4)
C11	C12	1.459(4)	C56	C57	1.397(4)
C12	N12	1.293(4)	C57	C58	1.383(4)
C12	C13	1.474(4)	C61	N41	1.378(4)
C13	C18	1.396(4)	C61	C62	1.434(4)
C13	C14	1.410(4)	C62	N42	1.339(4)
C14	C15	1.384(4)	C62	C63	1.436(4)
C14	N11	1.416(3)	C63	C68	1.407(4)
C15	C16	1.390(4)	C63	C64	1.421(4)

C16	C17	1.393(4)	C64	N41	1.374(4)
C17	C18	1.384(4)	C64	C65	1.389(4)
C21	N21	1.382(4)	C65	C66	1.382(4)
C21	C22	1.414(4)	C66	C67	1.399(4)
C22	N22	1.339(3)	C67	C68	1.372(4)
C22	C23	1.449(4)	C71	C76	1.385(4)
C23	C28	1.398(4)	C71	C72	1.394(4)
C23	C24	1.420(4)	C71	N32	1.422(4)
C24	N21	1.380(4)	C72	C73	1.377(4)
C24	C25	1.391(4)	C73	C74	1.384(4)
C25	C26	1.373(4)	C74	C75	1.385(4)
C26	C27	1.398(4)	C75	C76	1.388(4)
C27	C28	1.382(4)	C81	C82	1.3900
C31	C32	1.390(4)	C81	C86	1.3900
C31	C36	1.395(4)	C81	N42	1.443(4)
C31	N12	1.415(3)	C82	C83	1.3900
C32	C33	1.388(4)	C83	C84	1.3900
C33	C34	1.386(4)	C84	C85	1.3900
C34	C35	1.388(4)	C85	C86	1.3900
C35	C36	1.383(4)	C81A	C82A	1.3900
C41	C46	1.384(4)	C81A	C86A	1.3900
C41	C42	1.390(4)	C81A	N42	1.452(7)
C41	N22	1.437(4)	C82A	C83A	1.3900
C42	C43	1.389(4)	C83A	C84A	1.3900
C43	C44	1.384(4)	C84A	C85A	1.3900
C44	C45	1.384(4)	C85A	C86A	1.3900
C45	C46	1.386(4)	B1	F1	1.392(4)
C51	N31	1.358(4)	B1	F2	1.397(4)
C51	C61	1.365(4)	B1	N11	1.533(4)
C51	C52	1.483(4)	B1	N22	1.560(4)
C52	N32	1.291(4)	B2	F3	1.393(4)
C52	C53	1.476(4)	B2	F4	1.398(4)
C53	C58	1.394(4)	B2	N31	1.539(4)
C53	C54	1.411(4)	B2	N42	1.557(4)
C54	C55	1.372(4)			

N11	C11	C21	120.2(3)	N42	C62	C61	120.2(3)
N11	C11	C12	111.2(2)	N42	C62	C63	133.6(3)

C21	C11	C12	128.5(3)	C61	C62	C63	106.3(3)
N12	C12	C11	119.5(2)	C68	C63	C64	118.7(3)
N12	C12	C13	135.9(3)	C68	C63	C62	134.7(3)
C11	C12	C13	104.6(2)	C64	C63	C62	106.5(2)
C18	C13	C14	119.4(3)	N41	C64	C65	128.6(3)
C18	C13	C12	134.3(3)	N41	C64	C63	109.3(3)
C14	C13	C12	106.0(2)	C65	C64	C63	122.1(3)
C15	C14	C13	122.0(3)	C66	C65	C64	117.5(3)
C15	C14	N11	127.1(3)	C65	C66	C67	121.3(3)
C13	C14	N11	110.8(2)	C68	C67	C66	121.5(3)
C14	C15	C16	117.1(3)	C67	C68	C63	118.8(3)
C15	C16	C17	122.1(3)	C76	C71	C72	119.0(3)
C18	C17	C16	120.3(3)	C76	C71	N32	121.2(3)
C17	C18	C13	119.1(3)	C72	C71	N32	119.8(3)
C11	C21	N21	127.8(3)	C73	C72	C71	120.7(3)
C11	C21	C22	122.1(3)	C72	C73	C74	120.2(3)
N21	C21	C22	109.9(2)	C73	C74	C75	119.5(3)
N22	C22	C21	121.0(2)	C74	C75	C76	120.4(3)
N22	C22	C23	132.4(3)	C71	C76	C75	120.1(3)
C21	C22	C23	106.5(2)	C82	C81	C86	120.0
C28	C23	C24	119.4(3)	C82	C81	N42	121.4(7)
C28	C23	C22	134.9(3)	C86	C81	N42	118.5(7)
C24	C23	C22	105.5(2)	C81	C82	C83	120.0
N21	C24	C25	128.3(3)	C84	C83	C82	120.0
N21	C24	C23	110.2(2)	C83	C84	C85	120.0
C25	C24	C23	121.4(3)	C86	C85	C84	120.0
C26	C25	C24	117.6(3)	C85	C86	C81	120.0
C25	C26	C27	122.1(3)	C82A	C81A	C86A	120.0
C28	C27	C26	120.7(3)	C82A	C81A	N42	120.2(15)
C27	C28	C23	118.8(3)	C86A	C81A	N42	119.7(15)
C32	C31	C36	119.9(3)	C83A	C82A	C81A	120.0
C32	C31	N12	118.6(2)	C84A	C83A	C82A	120.0
C36	C31	N12	121.3(2)	C85A	C84A	C83A	120.0
C33	C32	C31	119.8(3)	C84A	C85A	C86A	120.0
C34	C33	C32	120.3(3)	C85A	C86A	C81A	120.0
C33	C34	C35	119.7(3)	F1	B1	F2	108.3(3)
C36	C35	C34	120.4(3)	F1	B1	N11	111.2(3)
C35	C36	C31	119.8(3)	F2	B1	N11	109.7(2)
C46	C41	C42	120.8(3)	F1	B1	N22	108.4(2)
C46	C41	N22	120.4(2)	F2	B1	N22	109.8(3)
C42	C41	N22	118.8(3)	N11	B1	N22	109.3(2)
C43	C42	C41	119.5(3)	F3	B2	F4	108.0(3)

C44	C43	C42	119.7(3)	F3	B2	N31	110.4(3)
C43	C44	C45	120.4(3)	F4	B2	N31	110.5(2)
C44	C45	C46	120.3(3)	F3	B2	N42	109.7(2)
C41	C46	C45	119.3(3)	F4	B2	N42	109.8(3)
N31	C51	C61	120.7(3)	N31	B2	N42	108.4(2)
N31	C51	C52	110.1(2)	C11	N11	C14	107.3(2)
C61	C51	C52	129.2(3)	C11	N11	B1	124.2(2)
N32	C52	C53	135.3(3)	C14	N11	B1	128.2(2)
N32	C52	C51	120.5(3)	C12	N12	C31	121.1(2)
C53	C52	C51	104.1(2)	C24	N21	C21	107.8(2)
C58	C53	C54	119.2(3)	C22	N22	C41	119.2(2)
C58	C53	C52	134.1(3)	C22	N22	B1	122.6(2)
C54	C53	C52	106.7(2)	C41	N22	B1	117.8(2)
C55	C54	N31	127.7(3)	C51	N31	C54	108.6(2)
C55	C54	C53	121.9(3)	C51	N31	B2	124.7(2)
N31	C54	C53	110.4(3)	C54	N31	B2	126.7(3)
C54	C55	C56	118.0(3)	C52	N32	C71	117.3(3)
C55	C56	C57	121.2(3)	C64	N41	C61	109.1(2)
C58	C57	C56	120.4(3)	C62	N42	C81	118.5(4)
C57	C58	C53	119.2(3)	C62	N42	C81A	118.4(8)
C51	C61	N41	129.4(3)	C62	N42	B2	124.1(2)
C51	C61	C62	121.9(3)	C81	N42	B2	117.4(4)
N41	C61	C62	108.7(2)	C81A	N42	B2	117.3(8)

Figure B-5: ORTEP diagram of **5.1aCF$_3$COO** with all hydrogen atoms with the exception of N-H's removed for clarity and thermal ellipsoids shown at the 50% probability level

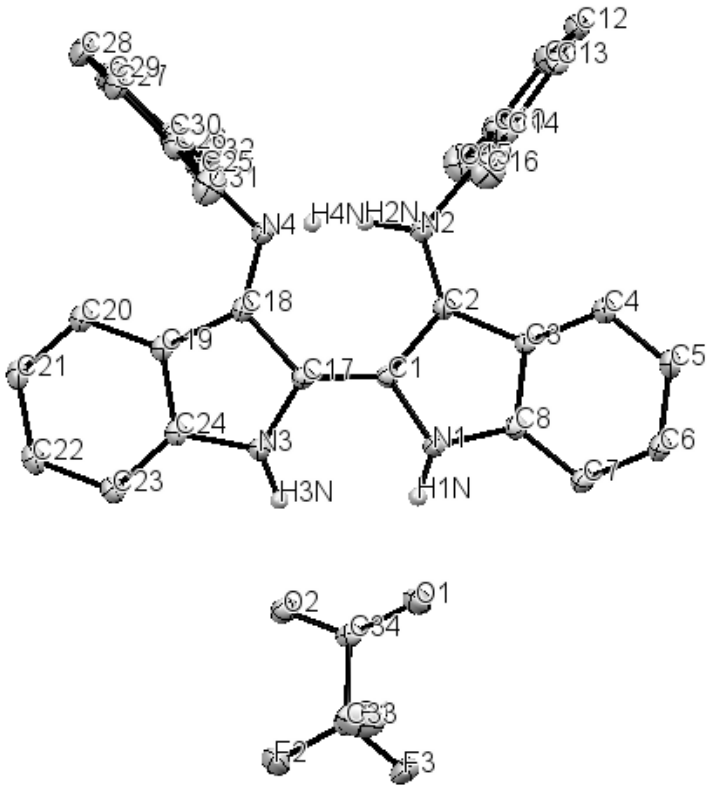

Table B-5: Bond Lengths (Å) and angles (º) for **5.1aCF$_3$COO**

F1	C33	1.3350(14)	C10	C11	1.3957(16)
F2	C33	1.3328(13)	C10	C15	1.5060(18)
F3	C33	1.3436(13)	C11	C12	1.381(2)
O1	C34	1.2399(14)	C12	C13	1.384(2)
O2	C34	1.2449(14)	C13	C14	1.3940(17)
N1	C8	1.3787(13)	C14	C16	1.5039(17)
N1	C1	1.3807(13)	C17	C18	1.4838(14)
N2	C2	1.3153(13)	C18	C19	1.4640(14)
N2	C9	1.4337(13)	C19	C24	1.4033(15)
N3	C17	1.3695(13)	C19	C20	1.4039(15)
N3	C24	1.3843(13)	C20	C21	1.3870(16)
N4	C18	1.3007(14)	C21	C22	1.3990(17)

N4	C25	1.4276(14)	C22	C23	1.3887(16)
C1	C17	1.3852(14)	C23	C24	1.3938(15)
C1	C2	1.4678(14)	C25	C26	1.3974(16)
C2	C3	1.4463(14)	C25	C30	1.3992(15)
C3	C4	1.4061(15)	C26	C27	1.3979(16)
C3	C8	1.4104(15)	C26	C31	1.5015(17)
C4	C5	1.3846(16)	C27	C28	1.3782(19)
C5	C6	1.4084(17)	C28	C29	1.387(2)
C6	C7	1.3856(16)	C29	C30	1.3898(17)
C7	C8	1.3960(15)	C30	C32	1.5054(18)
C9	C10	1.4001(15)	C33	C34	1.5525(15)
C9	C14	1.4002(16)			

C8	N1	C1	109.83(9)	N4	C18	C19	130.37(10)
C2	N2	C9	123.96(9)	N4	C18	C17	123.70(10)
C17	N3	C24	110.49(9)	C19	C18	C17	105.92(9)
C18	N4	C25	119.96(9)	C24	C19	C20	119.79(10)
N1	C1	C17	122.39(9)	C24	C19	C18	106.14(9)
N1	C1	C2	107.19(9)	C20	C19	C18	133.98(10)
C17	C1	C2	130.41(9)	C21	C20	C19	118.26(10)
N2	C2	C3	129.45(10)	C20	C21	C22	120.94(10)
N2	C2	C1	124.05(9)	C23	C22	C21	121.85(10)
C3	C2	C1	106.50(9)	C22	C23	C24	116.90(10)
C4	C3	C8	119.78(10)	N3	C24	C23	127.33(10)
C4	C3	C2	133.98(10)	N3	C24	C19	110.38(9)
C8	C3	C2	106.21(9)	C23	C24	C19	122.25(10)
C5	C4	C3	118.14(10)	C26	C25	C30	122.37(10)
C4	C5	C6	121.24(11)	C26	C25	N4	119.18(10)
C7	C6	C5	121.52(11)	C30	C25	N4	118.42(10)
C6	C7	C8	117.18(10)	C25	C26	C27	117.81(11)
N1	C8	C7	127.70(10)	C25	C26	C31	121.25(10)
N1	C8	C3	110.23(9)	C27	C26	C31	120.94(11)
C7	C8	C3	122.07(10)	C28	C27	C26	120.73(12)
C10	C9	C14	122.52(10)	C27	C28	C29	120.32(11)
C10	C9	N2	119.10(10)	C28	C29	C30	121.03(12)
C14	C9	N2	118.26(10)	C29	C30	C25	117.63(11)
C11	C10	C9	117.52(11)	C29	C30	C32	121.29(11)
C11	C10	C15	120.97(11)	C25	C30	C32	121.08(10)
C9	C10	C15	121.50(11)	F2	C33	F1	107.00(10)

C12	C11	C10	121.08(11)	F2	C33	F3	106.44(9)
C11	C12	C13	120.23(11)	F1	C33	F3	107.16(10)
C12	C13	C14	121.07(12)	F2	C33	C34	114.02(9)
C13	C14	C9	117.54(11)	F1	C33	C34	111.16(10)
C13	C14	C16	121.13(12)	F3	C33	C34	110.70(9)
C9	C14	C16	121.33(11)	O1	C34	O2	129.75(10)
N3	C17	C1	122.31(9)	O1	C34	C33	114.38(10)
N3	C17	C18	107.03(9)	O2	C34	C33	115.87(10)
C1	C17	C18	130.61(9)				

Figure B-6 ORTEP diagram of **5.1aBF$_4$** with all hydrogen atoms with the exception of N-H's removed for clarity and thermal ellipsoids shown at the 50% probability level

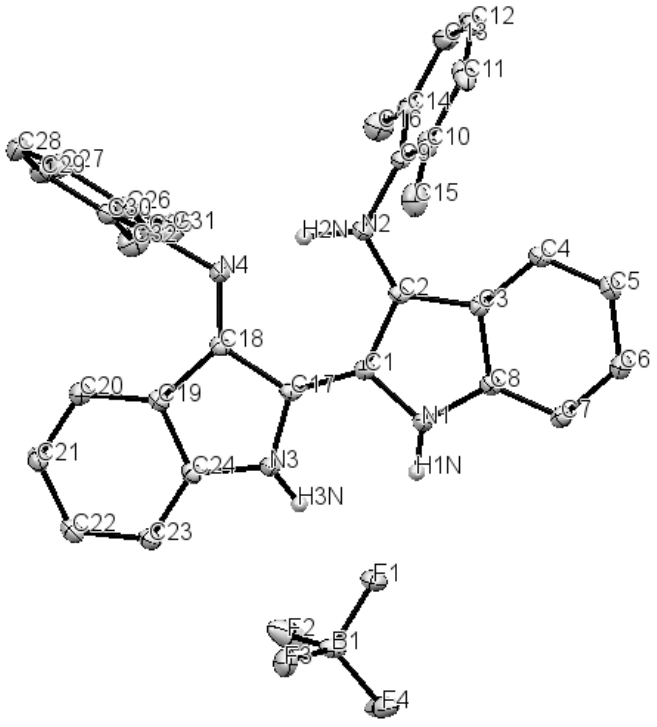

Table B-6: Bond Lengths (Å) and angles (°) for **5.1aBF$_4$**

C1	C17	1.3800(15)	C18	N4	1.2974(15)
C1	N1	1.3881(14)	C18	C19	1.4628(16)
C1	C2	1.4649(15)	C19	C24	1.4025(16)
C2	N2	1.3142(14)	C19	C20	1.4063(16)
C2	C3	1.4526(15)	C20	C21	1.3861(17)
C3	C4	1.4052(15)	C21	C22	1.3973(17)
C3	C8	1.4077(16)	C22	C23	1.3900(16)
C4	C5	1.3849(16)	C23	C24	1.3882(16)
C5	C6	1.4010(17)	C24	N3	1.3927(14)
C6	C7	1.3857(17)	C25	C30	1.3984(17)
C7	C8	1.3939(15)	C25	C26	1.4005(16)
C8	N1	1.3822(14)	C25	N4	1.4350(14)
C9	C14	1.3945(17)	C26	C27	1.3960(16)
C9	C10	1.3985(17)	C26	C31	1.5003(18)
C9	N2	1.4385(15)	C27	C28	1.3832(19)
C10	C11	1.3926(18)	C28	C29	1.3879(19)
C10	C15	1.5024(18)	C29	C30	1.3957(17)
C11	C12	1.385(2)	C30	C32	1.5089(18)
C12	C13	1.384(2)	B1	F4	1.3742(16)
C13	C14	1.3911(17)	B1	F2	1.3822(17)
C14	C16	1.5012(18)	B1	F3	1.3958(16)
C17	N3	1.3716(15)	B1	F1	1.4249(15)
C17	C18	1.4836(15)			

C17	C1	N1	122.22(10)	C19	C18	C17	105.87(10)
C17	C1	C2	130.77(10)	C24	C19	C20	119.61(10)
N1	C1	C2	106.97(9)	C24	C19	C18	106.69(9)
N2	C2	C3	129.24(10)	C20	C19	C18	133.70(11)
N2	C2	C1	124.35(10)	C21	C20	C19	118.06(11)
C3	C2	C1	106.38(9)	C20	C21	C22	121.23(11)
C4	C3	C8	119.87(10)	C23	C22	C21	121.63(11)
C4	C3	C2	133.32(10)	C24	C23	C22	116.91(11)
C8	C3	C2	106.72(9)	C23	C24	N3	127.64(11)
C5	C4	C3	118.03(11)	C23	C24	C19	122.55(10)
C4	C5	C6	121.02(11)	N3	C24	C19	109.80(10)
C7	C6	C5	122.10(11)	C30	C25	C26	122.44(10)

C6	C7	C8	116.71(11)	C30	C25	N4	118.82(10)
N1	C8	C7	128.08(11)	C26	C25	N4	118.68(10)
N1	C8	C3	109.71(10)	C27	C26	C25	117.70(11)
C7	C8	C3	122.21(10)	C27	C26	C31	121.21(11)
C14	C9	C10	122.72(11)	C25	C26	C31	121.07(10)
C14	C9	N2	119.51(11)	C28	C27	C26	120.98(12)
C10	C9	N2	117.75(10)	C27	C28	C29	120.24(11)
C11	C10	C9	117.68(12)	C28	C29	C30	120.85(12)
C11	C10	C15	121.25(12)	C29	C30	C25	117.78(11)
C9	C10	C15	121.05(11)	C29	C30	C32	121.17(12)
C12	C11	C10	120.60(12)	C25	C30	C32	121.04(11)
C13	C12	C11	120.50(12)	F4	B1	F2	111.81(11)
C12	C13	C14	120.85(12)	F4	B1	F3	110.38(11)
C13	C14	C9	117.64(12)	F2	B1	F3	108.99(11)
C13	C14	C16	121.31(12)	F4	B1	F1	109.61(11)
C9	C14	C16	121.05(11)	F2	B1	F1	108.13(10)
N3	C17	C1	122.03(10)	F3	B1	F1	107.81(10)
N3	C17	C18	107.01(9)	C8	N1	C1	110.17(10)
C1	C17	C18	130.94(10)	C2	N2	C9	122.62(10)
N4	C18	C19	130.94(10)	C17	N3	C24	110.62(10)
N4	C18	C17	123.19(10)	C18	N4	C25	120.68(10)

Figure B-7: ORTEP diagram of **5.4aCl** with all hydrogen atoms with the exception of N-H's removed for clarity and thermal ellipsoids shown at the 50% probability level

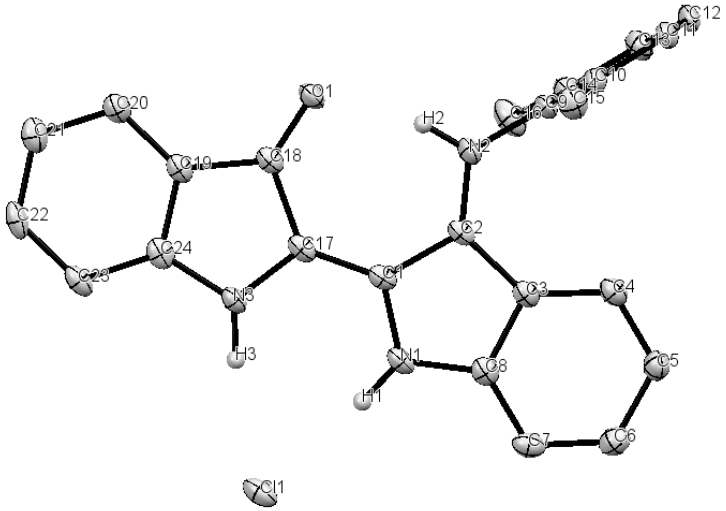

Table B-7: Bond Lengths (Å) and angles (º) for **5.4aCl**

O1	C18	1.231(3)	C9	C10	1.394(3)
N1	C8	1.366(3)	C9	C14	1.401(3)
N1	C1	1.378(3)	C10	C11	1.399(3)
N2	C2	1.323(3)	C10	C15	1.506(3)
N2	C9	1.438(3)	C11	C12	1.389(3)
N3	C17	1.366(3)	C12	C13	1.377(3)
N3	C24	1.396(3)	C13	C14	1.394(3)
C1	C17	1.377(3)	C14	C16	1.500(3)
C1	C2	1.454(3)	C17	C18	1.502(3)
C2	C3	1.437(3)	C18	C19	1.457(3)
C3	C4	1.405(3)	C19	C20	1.390(3)
C3	C8	1.411(3)	C19	C24	1.393(3)
C4	C5	1.375(3)	C20	C21	1.389(3)
C5	C6	1.407(3)	C21	C22	1.389(3)
C6	C7	1.377(3)	C22	C23	1.388(3)
C7	C8	1.390(3)	C23	C24	1.386(3)

C8	N1	C1	109.92(19)	C11	C10	C15	121.1(2)
C2	N2	C9	123.4(2)	C12	C11	C10	121.1(2)
C17	N3	C24	110.37(19)	C13	C12	C11	120.2(2)
C17	C1	N1	122.4(2)	C12	C13	C14	121.1(2)
C17	C1	C2	130.4(2)	C13	C14	C9	117.5(2)
N1	C1	C2	107.18(19)	C13	C14	C16	121.8(2)
N2	C2	C3	128.1(2)	C9	C14	C16	120.7(2)
N2	C2	C1	125.2(2)	N3	C17	C1	122.9(2)
C3	C2	C1	106.74(19)	N3	C17	C18	107.32(19)
C4	C3	C8	119.3(2)	C1	C17	C18	129.6(2)
C4	C3	C2	134.6(2)	O1	C18	C19	128.1(2)
C8	C3	C2	106.06(18)	O1	C18	C17	127.0(2)
C5	C4	C3	118.6(2)	C19	C18	C17	104.74(19)
C4	C5	C6	121.0(2)	C20	C19	C24	121.2(2)
C7	C6	C5	121.5(2)	C20	C19	C18	131.1(2)
C6	C7	C8	117.4(2)	C24	C19	C18	107.7(2)
N1	C8	C7	127.9(2)	C21	C20	C19	118.3(2)
N1	C8	C3	110.1(2)	C20	C21	C22	119.7(2)
C7	C8	C3	122.0(2)	C23	C22	C21	122.7(2)
C10	C9	C14	122.9(2)	C24	C23	C22	117.1(2)
C10	C9	N2	119.69(19)	C23	C24	C19	121.0(2)
C14	C9	N2	117.32(19)	C23	C24	N3	129.2(2)
C9	C10	C11	117.2(2)	C19	C24	N3	109.80(19)
C9	C10	C15	121.7(2)				

Appendix C: UV-Vis Spectra

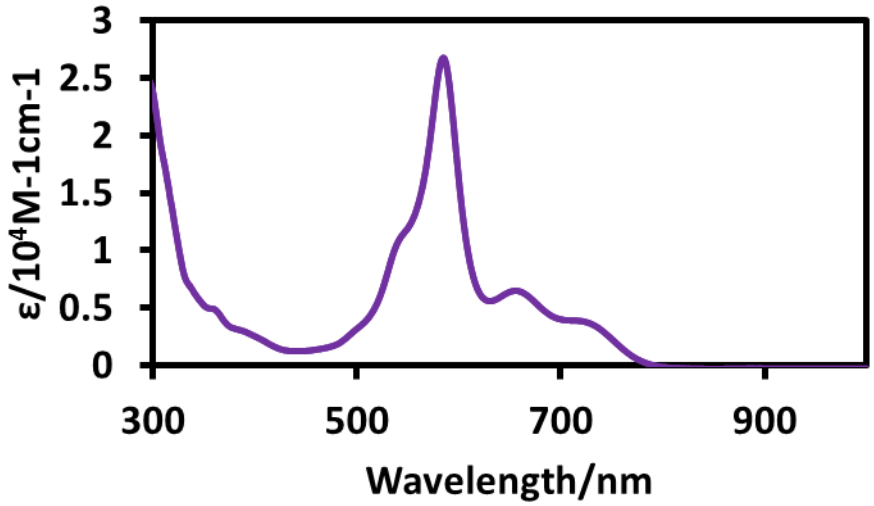

Figure C-1: 3.13, DCM, 25μM

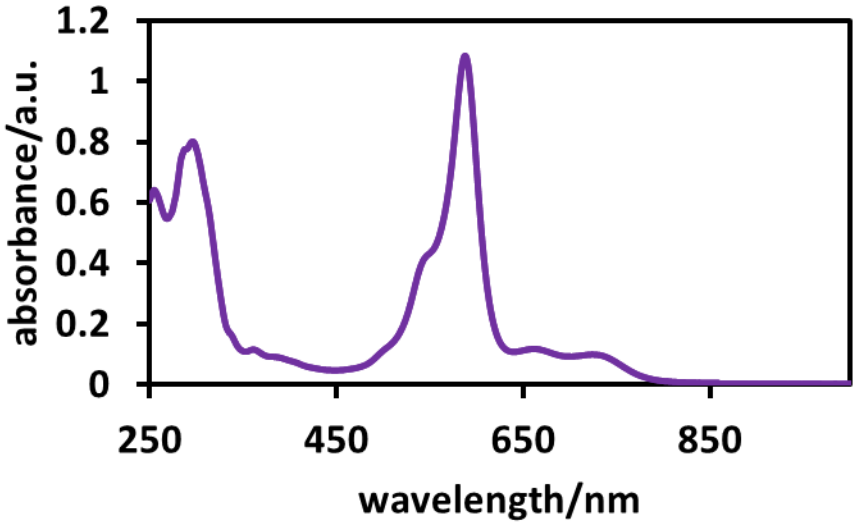

Figure C-2: 3.13, THF, 25μM

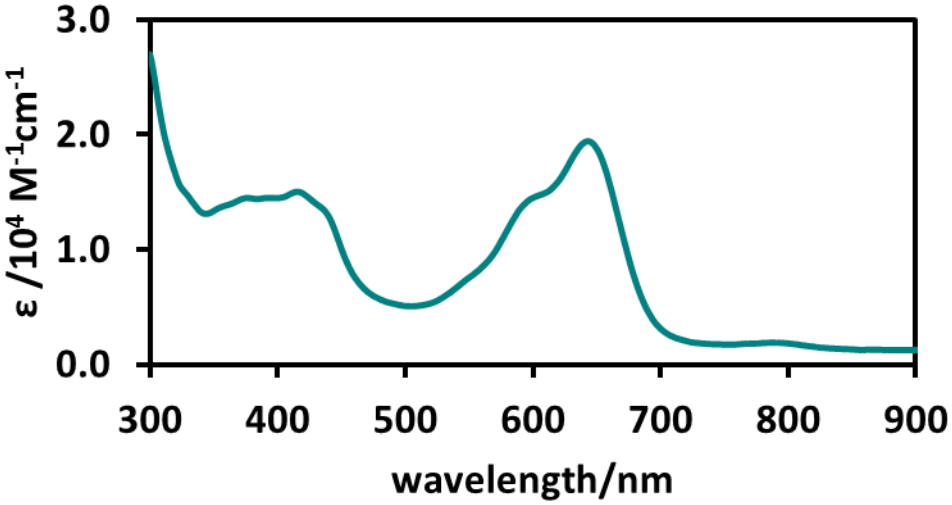

Figure C-3: 4.4, DMSO, 50μM

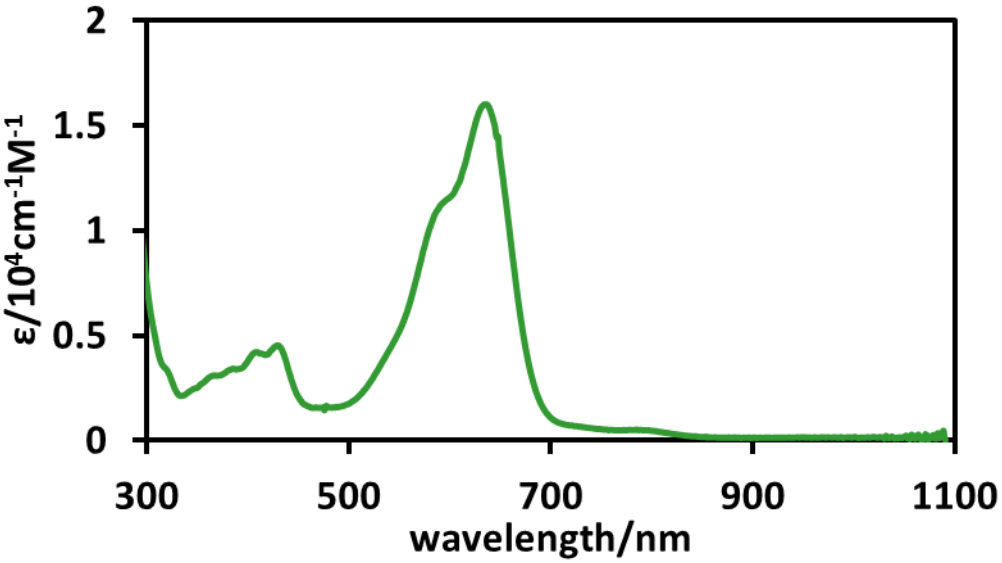

Figure C-4: 4.11, DMSO, 50 μM

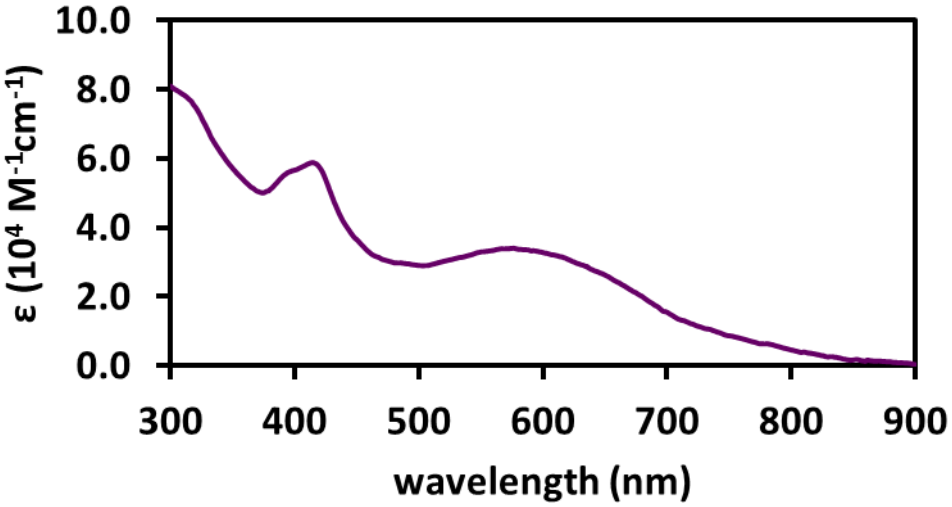

Figure C-5: 4.16, DMSO, 50μM

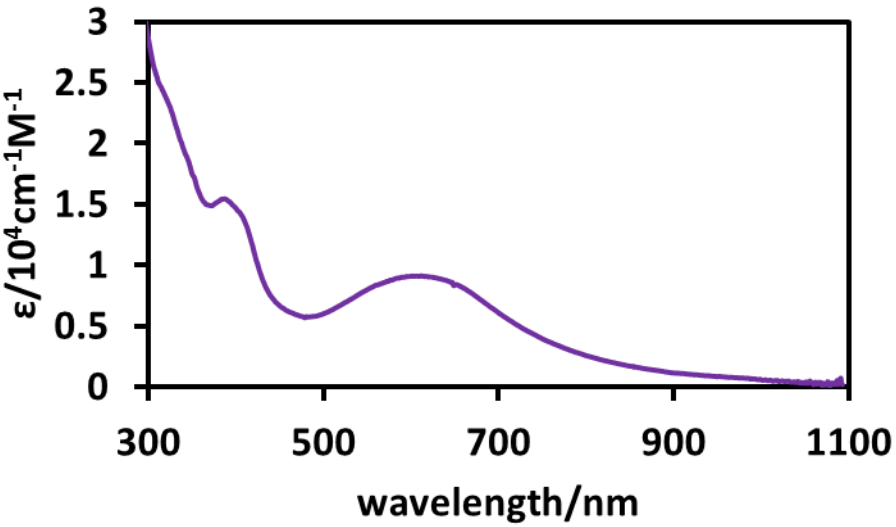

Figure C-6: 4.20, DMSO, 50μM

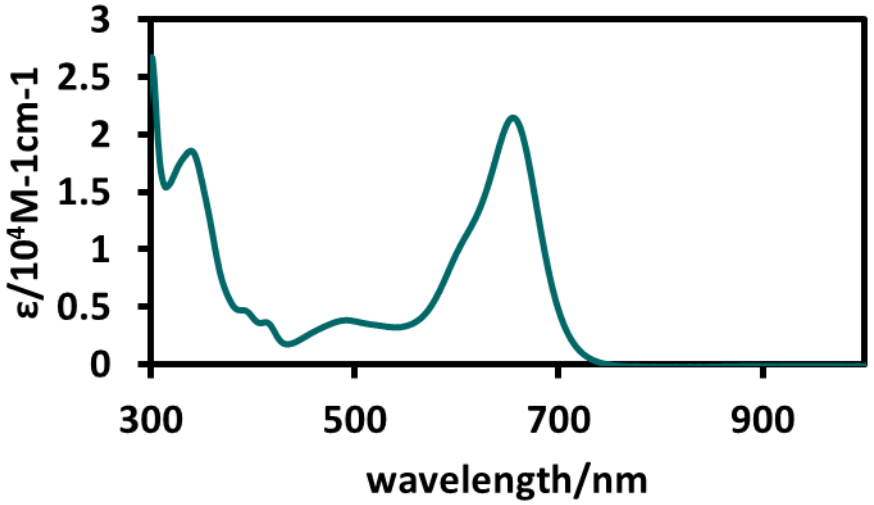

Figure C-7: 5.1aCF_3COO, DCM, 25μM

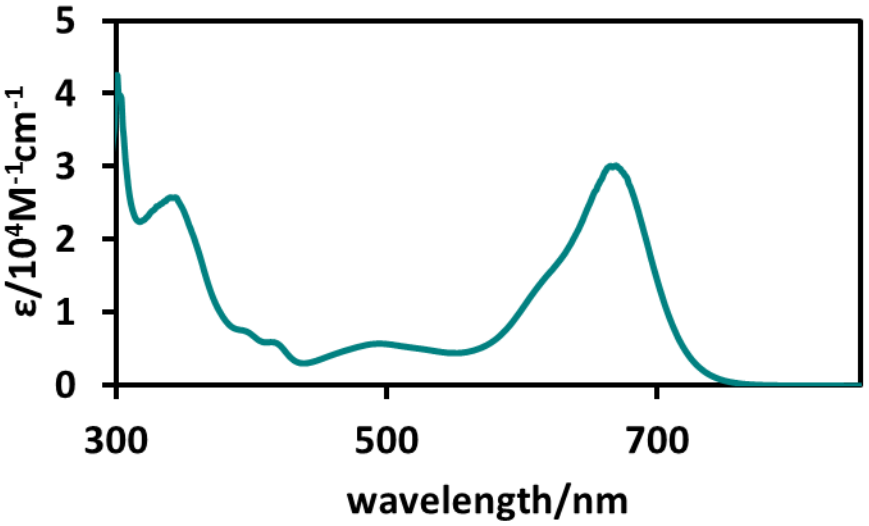

Figure C-8: 5.1aBF_4, THF, 100μM

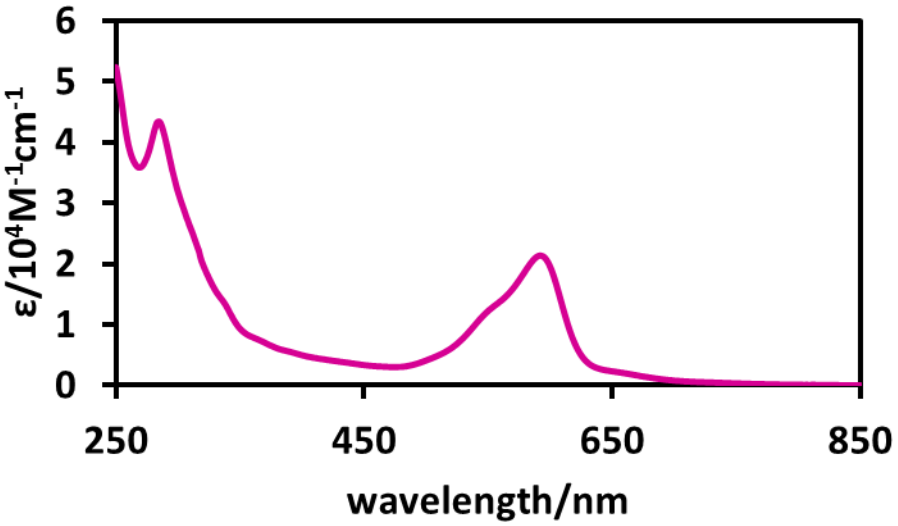

Figure C-9: 5.3, DCM, 25μM

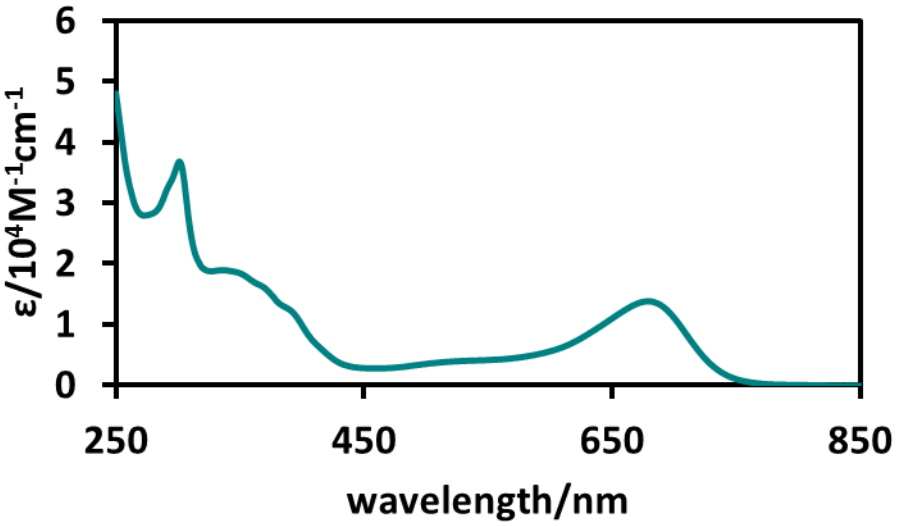

Figure C-10: 5.4aCl, DCM, 25μM

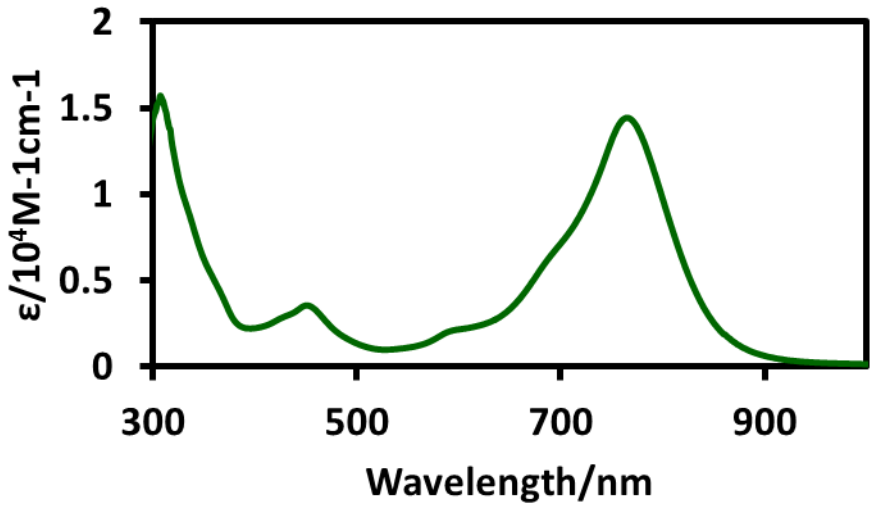

Figure C-11: 5.5, THF, 25μM

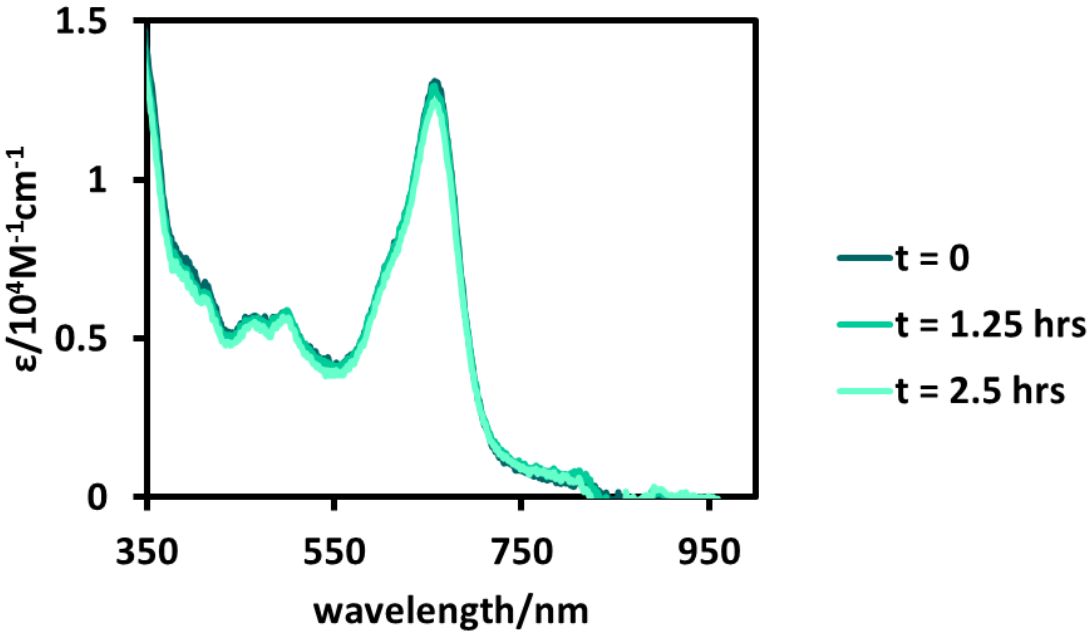

Figure C-12: Protonation of **3.13** with acetic acid, time points on legend, DCM, 1μM

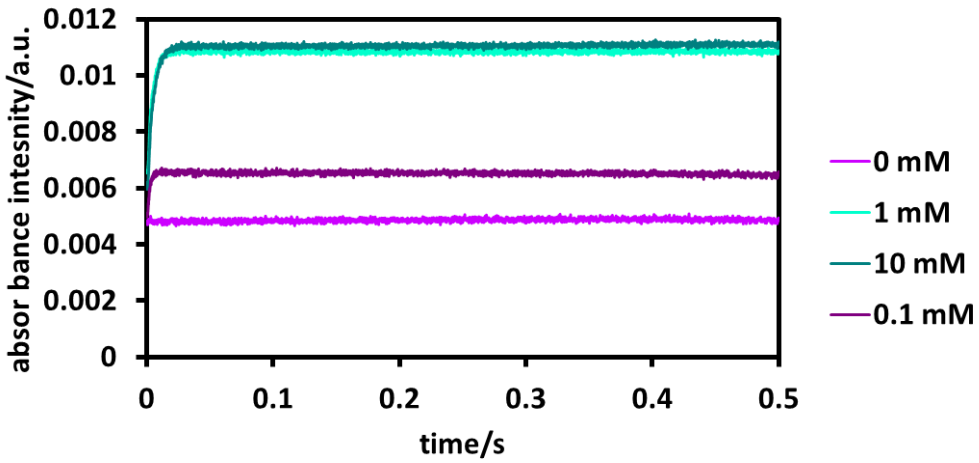

Figure C-13: Stopped-flow results of 100 μM **3.13** in MeOH with acetic acid at varying concentrations (see legend), t = 0.5s

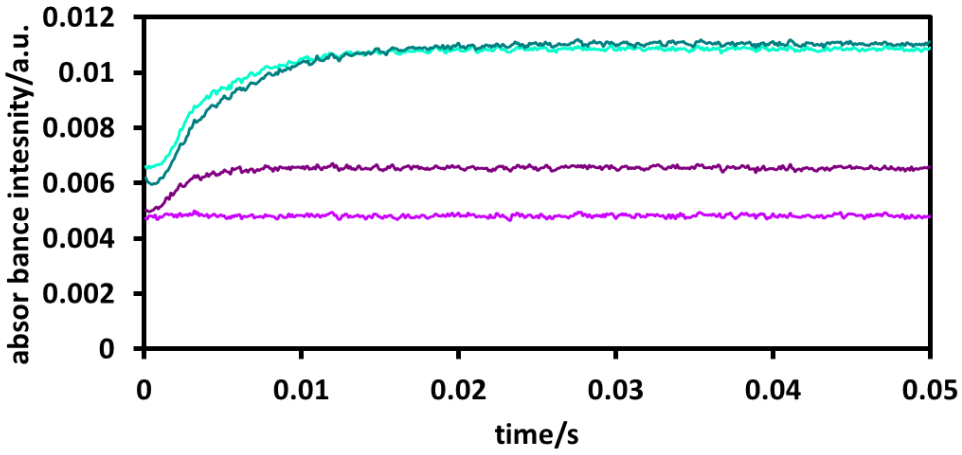

Figure C-14: Stopped flow results of 100 uM **3.13** in MeOH with acetic acid at varying concentrations (see legend in **Figure C-13**), t = 0.05

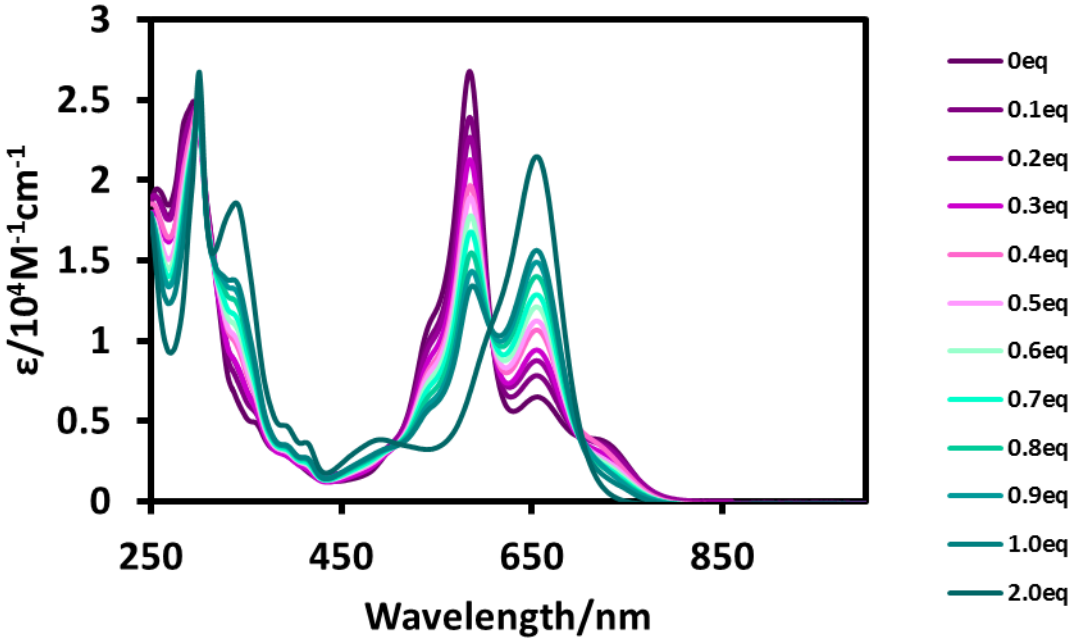

Figure C-15: Titration of **3.13** with trifluoroacetic acid, DCM, 25μM **3.13**

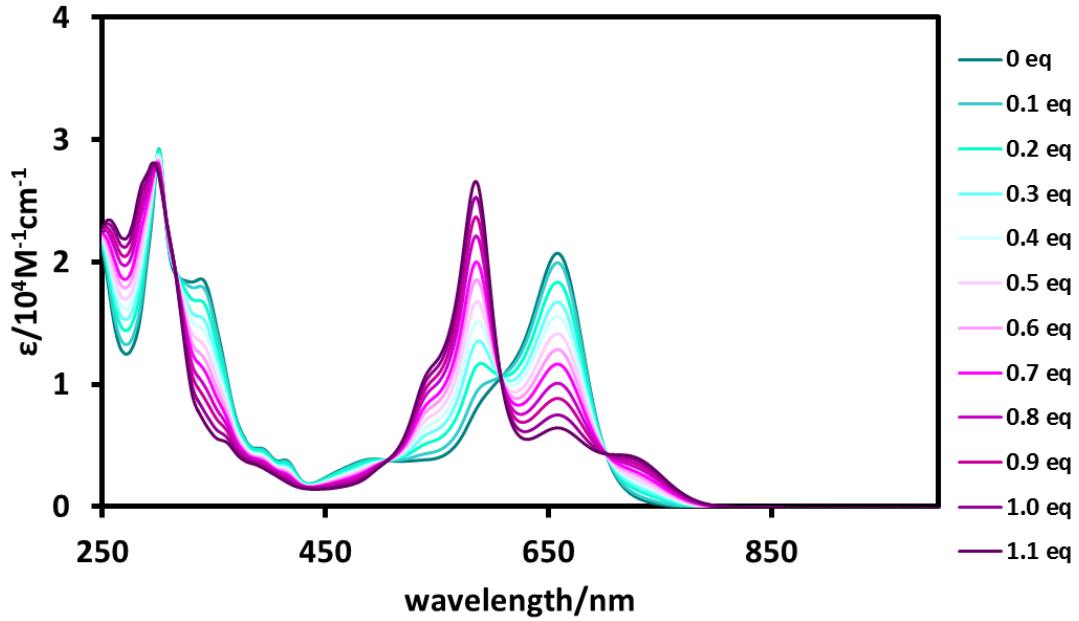

Figure C-16: Titration of **5.1aCF$_3$COO** with Et$_3$N, DCM, 25μM **5.1aCF$_3$COO**

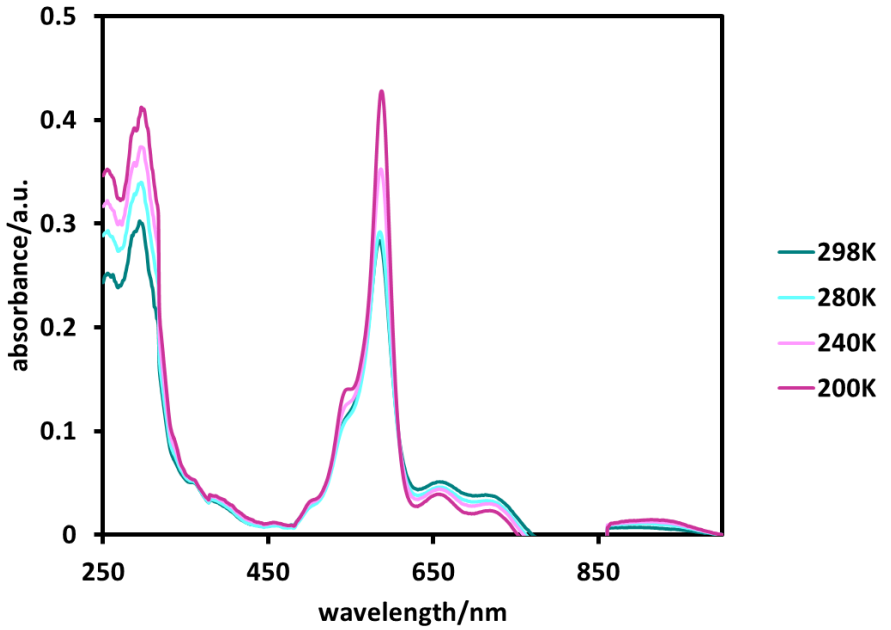

Figure C-17: Variable temperature of **3.13,** 250μM, DCM, see legend for temperature

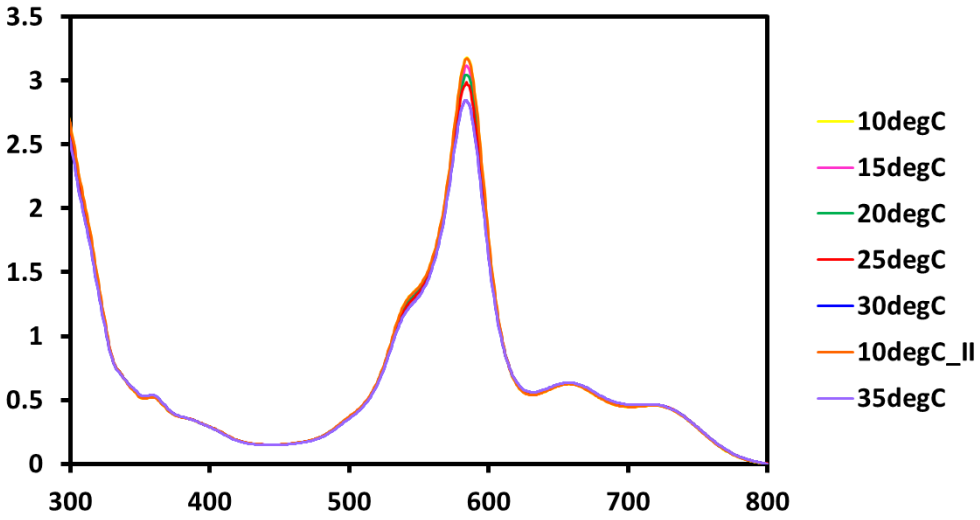

Figure C-18: Variable temperature of **3.13,** 100μM, DCM, see legend for temperature

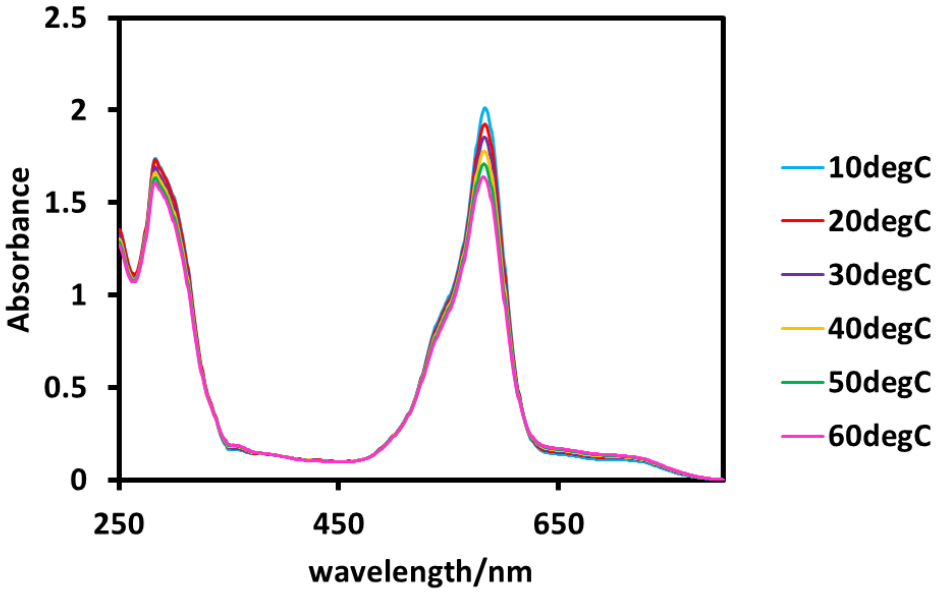

Figure C-19: Variable temperature of **3.13**, 100μM, ACN, see legend for temperature

Appendix D: Variable Temperature NMR Data

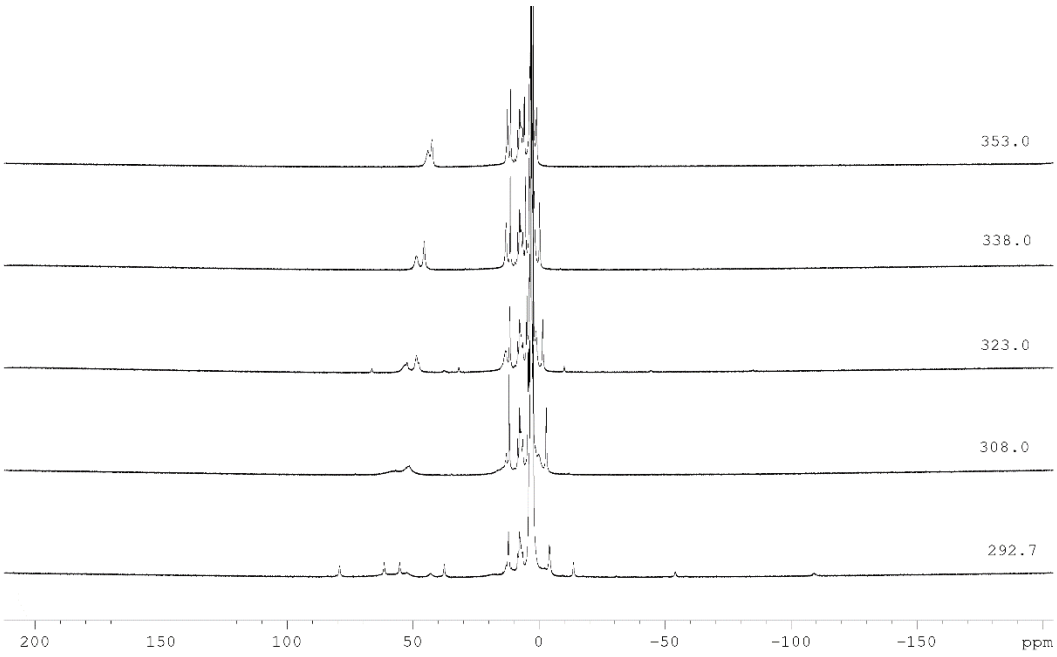

Figure D-1: Variable temperature NMR of **2.27**, DMSO-d_6

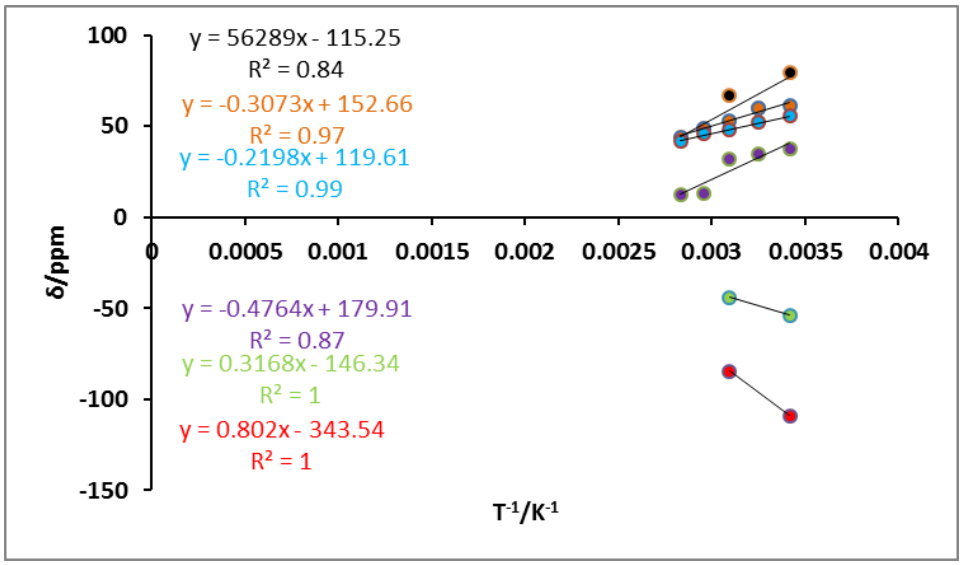

Figure D-2: Curie-Weiss Plot for **2.27**

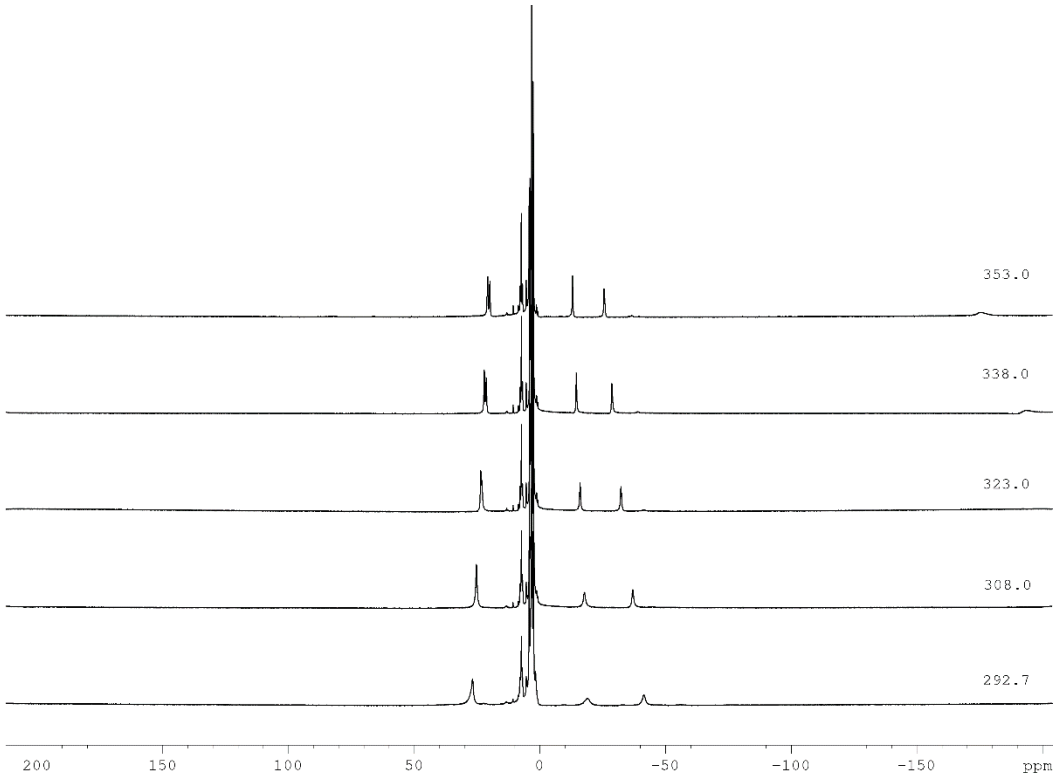

Figure D-3: Variable temperature NMR of **2.32**, DMSO-d_6

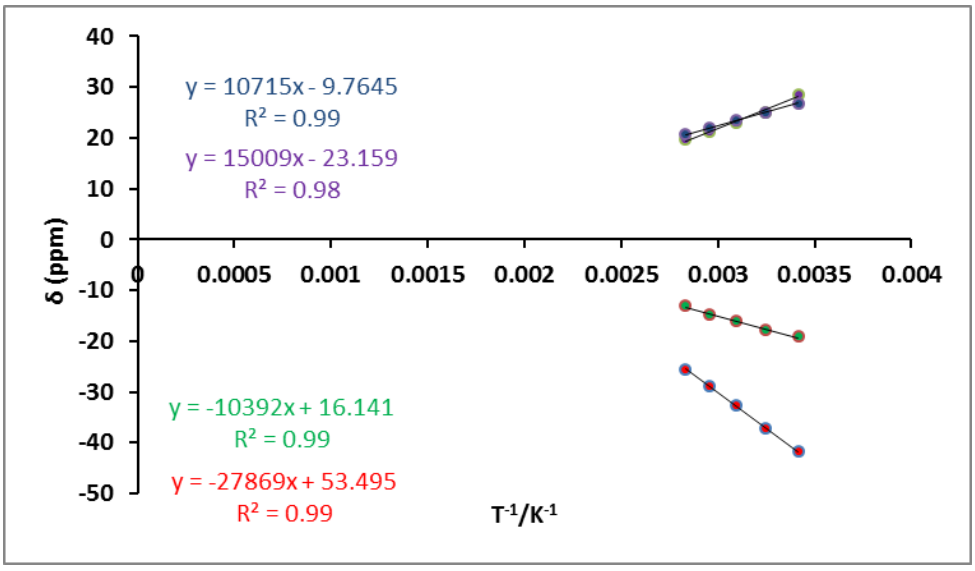

Figure D-4: Curie-Weiss Plot for **2.32**

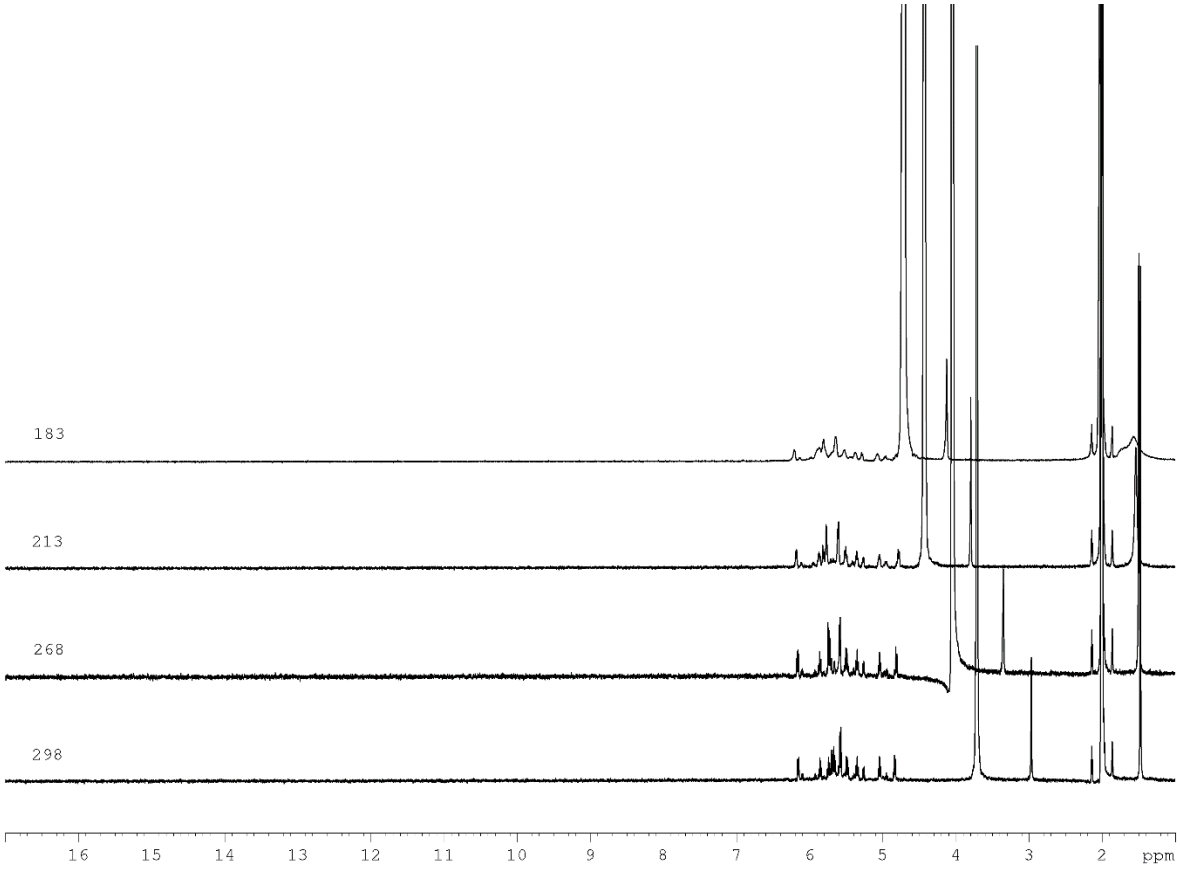

Figure D-5: ^{1}H Variable temperature, **3.13**, 500 MHz, d_6-ethanol

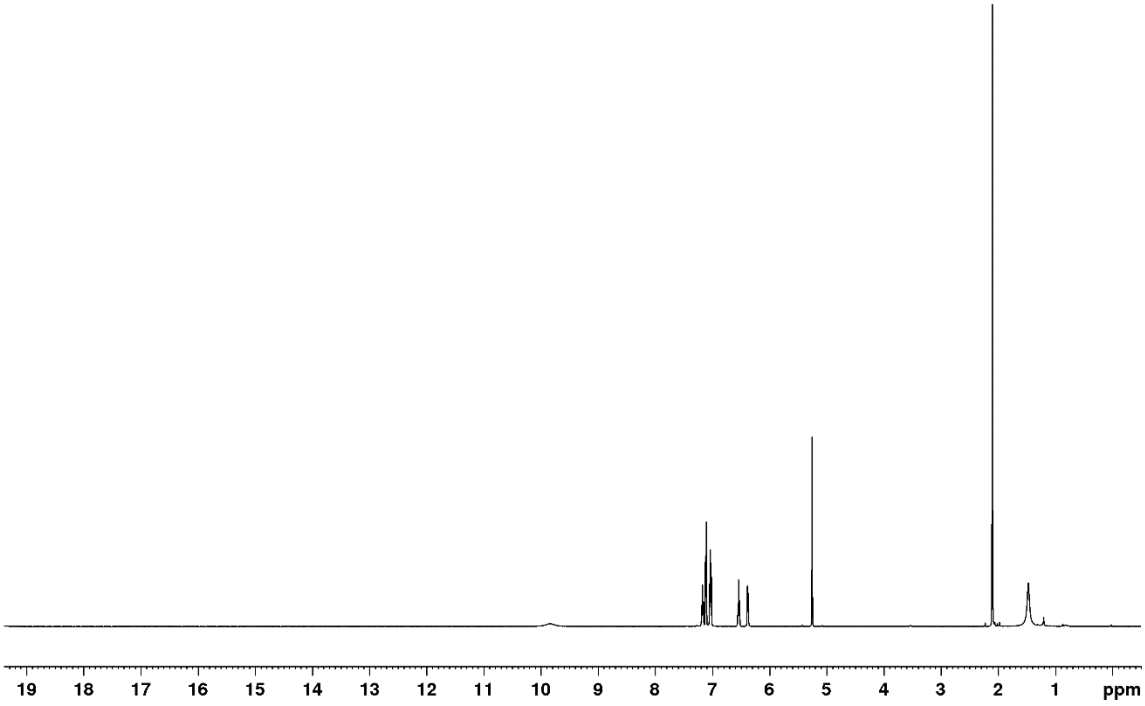

Figure D-6: ^{1}H, **3.13**, 500 MHz, CD_2Cl_2, 183 K